Chair of Mining Engineering and Mineral Economics

Doctoral Thesis

A Methodology for Dynamic Belt Simulation

Dipl.-Ing. Eric Fimbinger

September 2021

MONTANUNIVERSITÄT LEOBEN
www.unileoben.ac.at

AFFIDAVIT

I declare on oath that I wrote this thesis independently, did not use other than the specified sources and aids, and did not otherwise use any unauthorized aids.

I declare that I have read, understood, and complied with the guidelines of the senate of the Montanuniversität Leoben for "Good Scientific Practice".

Furthermore, I declare that the electronic and printed version of the submitted thesis are identical, both, formally and with regard to content.

Date 09.09.2021

Signature Author
Eric Fimbinger

Title: A Methodology for Dynamic Belt Simulation

Author: Eric Fimbinger

Year / Place: 2021 / Leoben, Austria

DOI: https://doi.org/10.34901/mul.pub.2021.3

A dissertation submitted to the
Chair of Mining Engineering and Mineral Economics –
Conveying Technology and Design Methods at the
University of Leoben (Montanuniversität Leoben).

Submitted by
Dipl.-Ing. Eric Fimbinger

Supervisor:
Univ.-Prof. Dipl.-Ing. Dr.mont. Nikolaus August Sifferlinger

Co-Supervisor:
Univ.-Prof. Dipl.-Ing. Dr.mont. Thomas Antretter

Copyright Declaration

Abstract

This thesis presents a methodology that enables the modelling and simulation of dynamically interacting belt models in Discrete Element Method (DEM) simulations.

In conventional DEM simulation setups, belt models are typically modelled as rigid surfaces, which are further applied with a contact model that induces a movement into bulk material particles that contact with these belt-representing surfaces. Accordingly, such rigid belt models are not able to depict dynamic interactions – neither with bulk material particles conveyed on the belt nor with system components that further interact with the belt, such as idlers and pulleys. Particularly for the numerical simulation of conveyor systems comprising belts that significantly influence system characteristics due to dynamic belt behaviour, however, the consideration of belts as dynamically interacting objects is required. Such systems are, for example, sandwich or pipe conveyors. Furthermore, such dynamically interacting belt models are also required for simulations in which the analysis of particular effects are of interest, such as belt deformation/deflection effects.

The belt simulation methodology developed and presented in this thesis explicitly addressed the simulation of such complex systems where dynamic belt behaviour is inevitable. This methodology is generally based on using a bonded-particle belt model (BP belt), which is furthermore initialised with a specific geometrical shape, more specifically relating to belt initialisation in almost-final state. These two areas – the general setup of a BP belt and its initialisation in almost-final state – form the major parts of the methodology.

The general setup of a BP belt is defined fundamentally to show a single layer of rectangularly arranged/bonded cuboidal particles. The bondings that connect those

belt particles are further defined by an enhanced bonding model, which is explicitly extended to enable the representation of belt-typical flexibility characteristics.

The essential method with which such a BP belt is initialised is introduced as belt initialisation in almost-final state. This method comprises the computation of a BP belt with a specific complex shape approximating an assembled belt within a specific belt system. Therefore, an algorithm was developed that enables the conversion of such a given belt geometry, provided as a CAD model, into a corresponding BP belt. This developed conversion algorithm was also implemented into a software tool (BeltConverter), allowing convenient use via a GUI. As a further enhancing feature, initial belt velocity can be applied to the converted BP belt, thus allowing the initialisation of an already running BP belt. Especially noteworthy in terms of using this initialisation principle is the significantly reduced pre-simulation effort required for assembling such a belt model, which is generally reduced to imperceptible levels.

Illustrations of applying the presented methodology on several different exemplary industry-relating applications highlight the various benefits of the methodology, such as in terms of computational efforts required, and ultimately reveal the methodology's favourable suitability for DEM simulations comprising dynamically interacting belt models.

Table of Contents

Version date: 30th September 2021

Chapter 1

Introduction

This thesis resides principally in the field of computational mechanics. In terms of application, this thesis relates primarily to bulk material handling, and in particular to belt conveying technology and numerical simulation by means of the Discrete Element Method (DEM).

The methodology developed and described within this thesis presents a technique for modelling conveyor belts or similar structures in non-rigid form for the use in DEM simulations to enable their consideration as components with dynamically deformable behaviour. The application of this methodology is specifically suitable for DEM simulations of systems in which belts or similar structures significantly influence the analysed processes due to effects resulting from such behaviour.

In the following context, the application of the developed methodology is mainly focused on belt conveyor technologies, but it is also transferable to other fields of application. In principle, any object with dynamically deformable behaviour is conceivable. Typical examples of such flexible objects are ropes, fibres, nets, fabrics/textiles, and similar.

1.1 Motivation

The initial background of the methodology's development lies in its necessity for the development process of complex or novel types of belt conveyor systems.

Proper consideration of the behaviour of belts and resulting influences on the total conveyor system is of utmost importance for the evaluation of the functionality and the suitability of belt conveyor systems in development. This applies especially to early phases of the development process, such as conception, design and dimensioning. For novel belt conveyor developments, and also for a lot of already existing complex belt conveyor types, e.g. pouched belt conveyors, an estimation of the belt behaviour based on existing knowledge or analytical methods is usually not possible or at least very limited. In general, the use of numerical simulation as a supporting tool for engineering work is useful to allow the analysis of belt conveyor systems. However, the simulation of complex belt conveyor systems for bulk material transportation with consideration of belts as dynamically deformable objects in an application-orientated, engineering-friendly and efficient way proves to be very challenging.

DEM simulations (numerical simulations based on the DEM) are widely used and established for digital examinations of all kinds of bulk material processes. The DEM can consequently be chosen as a basic computation method for the simulation of belt conveyors transporting bulk materials. But, as conventional DEM only allows the modelling of conveyor belts as rigid surfaces, further methods are necessary to enable the consideration of belts as flexible and dynamically deformable objects. These methods, which are explained in detail within the course of this thesis, constitute the basis of the developed methodology for the simulation of dynamically deformable conveyor belts using the DEM.

Also, the development, the implementation/realisation, and the applicational testing of the developed methods revealed further potential adaptations/extensions and supplementary approaches that complement the methodology. These concern, for example, enhancements in usability and thus efficiency, expansions to further areas of application, and additional features that extend the scope of the developed methodology.

1.2 Objectives

The general objective pursued within the context of this thesis is to provide approaches and methods in the form of a consistent methodology for the consideration of conveyor belts and similar belt-like objects in DEM simulations as dynamically deformable/interacting structures.

A primary purpose is to set the focus on application-oriented and especially application-scale use in engineering practice. Therefore, the application on industry-related systems and, moreover, keeping additional efforts within reasonable limits is of interest. In that respect, the belts are set up as idealised digital models with a sufficient level of detail, whereby dynamically deformable belt behaviour is depictable with adequate approximation. This affects the computational effort required. Another emphasis lies on the ease of use regarding the preparation and the requirements to set up the basics for performing a simulation. Therefore, the use of a single simulation environment is preferred instead of complex software coupling with additional simulation environments that also needs further linking via additional coupling interfaces. Also, no disproportionate additional knowledge, such as in programming, manual modelling techniques, etc., is assumed.

One major benefit for practical application of the developed methodology is the implementation of methods, or more precisely, the implementation of developed algorithms, into software programs. Such programs are then able to be used as supporting tools for users in engineering practice. Applicational demonstrations of DEM simulations of various exemplary systems with deformable belt models, such as specific and also unconventional belt conveyors, are additionally presented to illustrate the practice-oriented application of the methodology and of the respective developments, such as to prove the use of the developed techniques, methods and software tools.

Regarding the overall efficiency for performing DEM simulations, especially of systems with deformable belt models, enhancements are feasible on three basic levels: modelling/preparation, pre-simulation and actual simulation. It is a general intention to keep the necessary efforts at all three of these levels relatively low. Moreover, in terms of computational power, it is ideally intended to enable an effective and purposeful use of typical hardware, commercially available for numerical simulations.

The methodology focuses on digital aspects and methods to enable virtual numerical simulation of belt conveyor systems with consideration of deformable belt behaviour. Therefore, specific material parameter determinations are not dealt with in detail within the course of this thesis.

The objectives set out above relate in particular to issues pertaining to the current state of the art in this field of numerical simulation, which principally covers methods for setting up belt objects as deformable objects – on the one hand, on a rather small-scale level and generally for relatively simple applications only – and on the other hand, with requiring a considerable amount of effort, in terms of preparation as well as computation (and typically also analysis).

In summary, the addressed objectives concern:

- enabling belt-like objects in DEM simulations as dynamically deformable/interacting models;
- supporting application-scaled usage, also of application-oriented (relatively complex) systems;
- keeping the efforts – in terms of modelling/preparation and simulation – within reasonable limits, especially regarding required pre-simulation efforts; thus, keeping required resources within limits, i.e.:
    - in software-related terms (with omitting software/solver coupling and associated efforts)
    - in hardware-related terms (with using typical/commercially available hardware systems; relating to computational efforts)
    - in modelling/preparation-related terms (with providing adequate techniques/methods and also additional supporting (software) tools)

1.3 Contents of the methodology

The developed methodology comprises several methods and approaches. Thereby, the two fundamental subjects concern the structural setup of belt models and the initialisation of belt models with a specific geometrical shape.

The structural belt model setup describes how dynamically deformable belt models are composed according to this methodology and how such belt models are defined in detail for use in DEM simulations. This includes basics, such as regarding the linking of particles (discrete elements) via bonding elements, as well as specific setup details, such as for the modelling of anisotropic belt behaviour.

An essential key element of the methodology is the belt initialisation method. It allows the initialisation of a belt, according to the structural setup principles, as a deformable belt model with a specific geometrical shape, thus ready to be used in the DEM simulation of a given belt conveyor system. For this purpose, the initialisation method, presented in the form of an algorithm, which was also implemented in a software program, enables the conversion of CAD[1] belt models into DEM belt models. Existing belt conditions due to local belt deformations are thereby taken into account. Due to the resulting substantial reduction of the necessary modelling and pre-simulation efforts, this initialisation method is primarily responsible for significant efficiency enhancements of the overall simulation process.

Additionally, an enhancing method for the initialisation of smooth cylindrical parts in DEM simulation setups is also presented. This enhancing method addresses the use of numerically smooth cylinders (as mathematical primitive shapes) instead of DEM-typical triangulated cylindrical parts. This method is especially intended to be used for idlers and drums, which form essential (cylindrically-shaped) system components as interacting with the belt (accordingly modelled and initialised following the two major subjects outlined above).

[1] computer-aided design

1.4 Thesis outline

The following description provides an overview of the general structure and the contents presented in this thesis.

The following Chapter 2 contains relevant basics – on the one hand regarding the DEM in general (Chapter 2.1), and on the other hand, regarding belt conveying technology (Chapter 2.2), where after a general system/component description, the focus is set towards the simulation of such systems, and therefore especially regarding considering belts in DEM simulations. Furthermore, specific belt (conveyor) systems are presented, which in particular relate to dynamic belt behaviour, and which are consequently relevant to dynamic belt simulation, as further dealt with in this thesis.

Chapter 3 presents approaches and methods for the modelling and also for the initialisation of dynamically deformable belts in DEM simulations.

In terms of deformable belt modelling (Chapter 3.1), two fundamental approaches are explained (as relating to the systematics with which a belt is modelled): FEM[2]-based and DEM-based belt modelling. This section generally presents a reappraisal of the state-of-the-art concerning methods allowing the modelling of deformable/flexible (especially but not exclusively belt-like) objects for use in DEM simulation.

Regarding belt initialisation (Chapter 3.2), two approaches are introduced: state-of-rest initialisation and almost-final state initialisation, basically relating to the geometrical shape with which a specific belt is initialised in a DEM simulation setup.

The approaches that are set to form the basis of the developed methodology are furthermore concludingly summarised in approach evaluations: DEM-based belt modelling, i.e. using a bonded-particle belt model (BP belt) and almost-final state belt initialisation, according to which a BP belt is initialised based on a geometry provided as a CAD model.

[2] Finite Element Method

In Chapter 4, the developed methodology for dynamic belt simulation is presented. Thereby, the two major parts of the methodology – structural belt setup and belt initialisation – are described in detail, and an additional methodology-extending method for using smooth-surfaced cylinders is also introduced.

The structural belt setup (Chapter 4.1) regards the modelling of a BP belt in general as consisting of a systematically arranged network of bonded particles, forming a surface-like deformable object. This subject regards specific modelling details, on the one hand, relating to the BP-belt-forming particles, and on the other hand, to the BP-belt-forming bondings; especially to allow belt-typical behaviour, such as flexibility characteristics (deviating bending/tension behaviour) or anisotropic characteristics (deviating belt behaviour in longitudinal and transverse belt directions).

The belt initialisation (Chapter 4.2) explicitly presents the method for almost-final state initialisation. This method forms an essential part of the methodology, as it allows the initialisation of a BP belt (according to the modelling principles from the previously outlined chapter) with a particular geometry – based on a provided CAD model. By providing this CAD belt geometry closely approximated to the intended geometry of the belt in its operating state, pre-simulation efforts can be reduced to almost a minimum, as the initialisation of a pre-deformed/pre-tensioned BP belt is enabled. Even already running BP belts can be simulated by applying initial belt velocity. Therefore, the provided CAD belt model (containing the belt geometry) is converted into a BP belt model (DEM data) via the developed algorithm. This algorithm is implemented into a software tool (BeltConverter; explained in Chapter 4.2.5) for convenient use. Especially for the purpose to allow reproduction and implementation, this algorithm is explained in close detail, including all relevant numerics. The application of the developed algorithm/software tool is furthermore illustrated on various belt-representing geometries, which demonstrate and furthermore prove its use (Chapter 4.3).

The additional method regarding smooth-surfaced cylinders (Chapter 4.4) presents an extension that allows the initialisation of numerically smooth cylinders – such as to represent idlers and pulleys in belt (conveyor) systems – instead of triangulated parts as commonly used in DEM simulation. In this context, a supportive software tool (PartConverter; explained in Chapter 4.4.3) is presented, which (in similar form

to the BeltConverter) allows convenient conversion of CAD data containing cylindrical geometries into such smooth-surfaced cylinders.

In Chapter 5, the application of the developed methodology is illustrated with practice-oriented case studies. These examples are given explicitly to indicate characteristics and capabilities that stand in context with applying the developed methodology for dynamic belt simulation.

The final chapters, Chapter 6 and Chapter 7, provide an outlook on further potentials and a conclusion on the topics dealt with in the presented methodology.

1.5 Prior Publications

Several contents of this thesis have previously been published, especially in conference papers and corresponding presentations, such as in the course of the following conferences and congresses: (starting from the most recent event)

- 14th WCCM&ECCOMAS[3] 2020 (2021), Virtual Congress [100]
- 13th ICBMH[4], 2019, in Gold Coast, Australia [86, 98]
- NAFEMS[5] World Congress 2019, in Quebec City, Canada [88, 97]
- REMA TIP TOP International Sales Meeting, 2019, in Munich, Germany [89]
- 15th Conference on Belt Conveyors and their Components, 2019, in Essen, Germany (15. Fachtagung Gurtförderer und deren Elemente) [87, 96]
- 23th Conference on Bulk Material Handling 2018, in Garching (Munich), Germany (23. Fachtagung Schüttgutfördertechnik 2018) [82, 93]
- 8th Colloquium on Conveying Technology in Mining, 2018, in Clausthal, Germany (8. Kolloquium Fördertechnik im Bergbau) [84, 92]

[3] World Congress on Computational Mechanics & European Congress on Computational Methods in Applied Sciences and Engineering

[4] International Conference on Bulk Materials Storage, Handling and Transportation

[5] International Association for the Engineering Modelling, Analysis and Simulation Community

Further contents have also been published in papers/articles, abstracts, and posters, such as published in:

- BHM (ASMET Research GmbH, BVÖ; Springer) Vol. 166, 2021 [91]
- SimuLand 2020 (Hochschule Düsseldorf), 2020 [90]
- Schüttgut (Vogel Communications Group) Nr. 6, 2018 [83].

The contents of this present thesis include topics, which have already been discussed, illustrated or mentioned in these previous publications. In the following, various contents, referencing to these publications, are discussed again and described in more detail. In this respect, general reference is made to these publications at this point.

The first official public releases of the developed software tools (BeltConverter [94] and PartConverter [95]; presented in Chapter 4.2.5 and Chapter 4.4.3) were launched and published in 2019 on GitHub [107].

Chapter 2

DEM & Belt Conveying Technology

In the development of bulk material handling systems, it is vital to take the bulk material flows and the resultant effects on the systems into account in order to design those systems properly. This requires the understanding of bulk material physics, especially of the interaction effects related to the bulk materials. These interactions occur as effects inside of bulk materials, and also as interactions of bulk materials interacting with various other system components, such as floors, walls, chutes, etc. Both, material-internal and also interactional effects with system components, are depending on a large variety of influencing factors, mainly of material- and structure-related nature, such as bulk material composition, material densities, frictional properties due to particle geometries or surface properties, etc.

When analysing conveyor systems, it is also important to consider that bulk material handling processes are always evoked by external influences on the handled bulk materials. Some examples herefore are shovel movements in excavators, rotating screws in screw conveyors, or even gravity effects in chutes. In these examples, the resulting influences on the bulk materials are furthermore fundamentally responsible for the general movement of the bulk material. In order to enhance and to optimise a bulk material system or process, it is of great interest to respectively design those parts and to tune those system parameters that are responsible for such influences on the handled bulk materials.

For a lot of bulk material systems, especially beyond a certain level of complexity, detailed analytical examinations are not possible in a reasonable manner. In such

cases, computer-aided engineering (CAE), and more specifically using the Discrete Element Method (DEM; also Distinct Element Method), provides the possibility to replicate physical systems as digital prototypes for virtual testing and analysis, especially at an early stage of the development process. In comparison to conventional prototyping, the use of such digital prototypes provides testing without the need for physical prototypes and their related efforts. Also, digital design studies and virtual insights into systems, such as bulk material flow analyses, are made possible, as well as iterative optimisations. Further advantages are that adaptions and adjustments are easy to implement on virtual system models, and that critical system parameters and operating states can be tested without risking physical and cost-intense damage.

The DEM is based on numerical approaches and methods that are able to depict bulk material physics in approximated form. These physics include, as abovementioned, the bulk material interactions and also further effects related to influences on the bulk materials. As a particle-based method, the DEM is a well-established tool in the bulk material conveying technology. Some common examples for its usage in this technology are, for example, for analyses of material flows (e.g. at transfer points), for design studies (e.g. of chutes), for material observations (e.g. wear or impact evaluations), etc. As in these cases, the analyses of calculated simulation results relate to various criteria, such as design suitability (e.g. bulk guidance in chutes), dimensional aspects (shape and size of components), performance-related parameters (efficiency), or bulk material behaviour (fracture, mixing or segregation). In the following Chapter 2.1, further relevant basics of the DEM, in particular in terms of the developed methodology for the simulation of conveyor belts, are given.

In belt conveyor systems, which are of particular interest for this thesis, the moving conveyor belts are the central parts of those systems. They are primarily responsible for the handling of the bulk materials, and therefore, when analysing such systems, their decisive influences on the conveying processes and further on the entire systems need to be taken into account accordingly. In order to describe evolutionary developments in conveyor belt analysis, and to clarify the usage of the DEM for belt conveyor simulation, a transition from basic conventional approaches for the analysis of conveyor belts, such as with the help of various standards, up to numerical DEM simulation is given in Chapter 2.2. Especially for belt conveyor systems in which the dynamic effects and the deformational behaviour of the belts have significant influences on the analysed processes or systems, it is necessary to consider the belts as

flexible, deformable objects. This aspect is in contrast to conventional approaches for DEM simulations of belt conveyors, where the belts are typically defined as rigid surfaces (see also Chapter 2.2.3). In Chapter 3.1, a general overview and an evaluative comparison are given on several basic approaches that principally allow a consideration of conveyor belts as dynamically deformable objects to be used in DEM bulk material simulations. According to a promising basic approach, such a belt model can be set up within the DEM environment by connecting particles via bonding elements to a net-like structure (bonded-particle belt or BP belt). The developed methodology, as described in Chapter 4, and as also used in the subsequent chapters, builds on this general approach of using such a BP belt model.

2.1 Basics of the DEM

The fundamentals of the Discrete Element Method (DEM) were initially set by Cundall and Strack (1979) [43] to depict the behaviour of granular media. In general, it is an explicit, mesh-free, particle-based numerical method for the digital modelling and simulation of bulk solids and similar material setups. Cundall and Hart (1992) [42] later also set the term Distinct Element Method, which is also widely used in technical literature alongside the term Discrete Element Method.

The basics of the DEM are related to the principles of Molecular Dynamics (MD), such as described by Alder and Wainwright (1959) [4], with which systems of atoms or molecules are analysed for use in chemical physics etc. Further related to the DEM is the method of Smoothed-Particle Hydrodynamics (SPH), initialised by Gingold and Monaghan (1977) [106] and Lucy (1977) [164]. This method, also based on a mesh-free approach using particles to represent continuum media, is particularly suitable for the numerical simulation of fluids, whereas the conventional DEM is typically related to applications with bulk solids.

In the following, a short introduction regarding the fields of application for using the DEM is given. Further on, the focus is set on aspects that are of major relevance in the context of this thesis, which proposes a methodology for the numerical modelling

of deformable objects based on the DEM; therefore, comprising relevant basics in terms of general DEM modelling as well as computation.

As this thesis focuses on general numerical modelling techniques (as highlighted), details regarding specific material parameter values, such as typically concerning a particular application with a certain and specifically defined material type, are not explicitly covered in the context of this thesis (ref. material calibration). Details on this specific topic of DEM calibration can be found in pertinent literature, such as also in (or further concluding from) references given in the following subchapters (or also within the general course of this thesis, e.g. in Chapter 3.1.2, as specifically regarding bonded particle structures).

Additional DEM-related details can further be found in corresponding references and in pertinent literature, to name representatives, such as in "Discrete Element Methods: Basics and Applications in Engineering" by Wriggers and Avci [257], or "Discrete element method to model 3D continuous materials" by Jebahi, et al. [134].

2.1.1 Fields of application for using the DEM

As state of the art, the DEM became an established tool in various areas of application in which large numbers of interacting particles, or comparable material setups, need to be analysed. Thereby, such represented bulk solids typically range from fine powders to coarse boulders. Some major ones of various areas of application are listed in the following, including also some corresponding representative examples of goods that can be handled/characterised as a bulk material. For additional illustration purposes, some examples of those bulk solids or granular media materials are also shown in Figure 2-1.

- Mining and rock technology (ore, coal, potash…)
- Soil and sand handling (gravel, limestone…)
- Food industry (fruits, vegetables, grains, nuts, cereals, sweets, chips, sugar…)
- Agriculture (crops, seeds, wood chips, fertilisers…)
- Pharmaceutical and chemical industry (pills, tablets…)
- Waste management (plastic waste, glass sand, scrap metal…)
- Mass products handling (nuts, bolts, screws, washers etc., toys parts…)

- Manufacturing (powder metallurgy materials, plastic granulates…)
- Various powder handling applications (cement, ash…)

Figure 2-1: Various examples for bulk solids/granular media; e.g. dry stones (top right), wood chips (bottom left), hay/straw (top left), coffee beans (below hay/straw) [204]

Regarding the overall purpose of applying DEM simulation/analysation, Becker (2020) [15] describes the general use of the DEM for engineers and academics as follows:

- Reduce the need for physical prototypes
- Troubleshoot operational problems
- Expedite product development
- Indicate possible problems during the design process
- Obtain information on bulk and particle-scale behaviour that cannot be measured easily
- Investigate the effects of changes to process machinery and operating conditions

In that respect, the purpose of simulations/analyses using the DEM is often in context with the bulk material flow and corresponding resulting effects, such as comparing the flow behaviour in various setups using design or parameter studies, or predicting loads on system components for dimensioning purposes. But also further effects, such as surface wear, particle loads, coating or temperature effects, as well as even more complex effects, for example particle breakage, are able to be analysed using appropriately configured DEM simulations.

A few selected applications for typical use of the DEM are, for example, in bulk materials handling/transportation (e.g. for chute design analyses, as by Katterfeld, et al. [141]), in soil/rock mechanics (e.g. geotechnical investigations, such as stability

assessments, as by Donze, et al. [57]), or in process engineering (e.g. for screening/sieving analyses, as by Peng, et al. [197]). Further applications can also be found within the contents of references given in the following chapters, describing especially more belt-simulation related application of the DEM. Much more applications can be found in respective literature, even unusual or unconventional applications, for example, the analysis of relatively complex phenomena, such as of snow, as by Hagenmuller, et al. [113], to perform studies on avalanches.

2.1.2 Respective basics for setting up DEM simulations

A primary intention behind conventional DEM bulk material simulation/analysation for bulk solids is to represent not every single particle of a bulk material precisely as it appears in reality (with its exact shape, size, roughness etc.) but to digitally represent the behaviour of a large number of those particles in sum. This means that a certain amount of DEM particles is used to represent the behaviour of bulk material as a whole.

Such a digital bulk material model is defined by using specific simplifications and modelling techniques with the aim to approximate the behaviour of physical bulk material in a specific system setup. In the following subchapters, general DEM fundamentals for this modelling of bulk material systems are described. In that regard, the focus is also set on those DEM aspects that are of significant relevance to this thesis, such as the connection of particles by using bonding elements. Subsequently, concise insights into the DEM computation process is given in the next Chapter 2.1.3.

2.1.2.1 DEM particles

Typical in conventional DEM simulation is the digital modelling of discrete elements (DE), referred to as particles, with an ideal-spherical geometry as particle shape and specific contact models to define characteristics regarding their interacting behaviour. A digital bulk material model consisting of a multitude of such particles is then used to approximate the behaviour of physical bulk material, even with not ideally round-shaped physical particles. Such a multitude of spherical particles representing a bulk material poured through a cone and onto a plane using LS-DYNA [160] is shown in Figure 2-2.

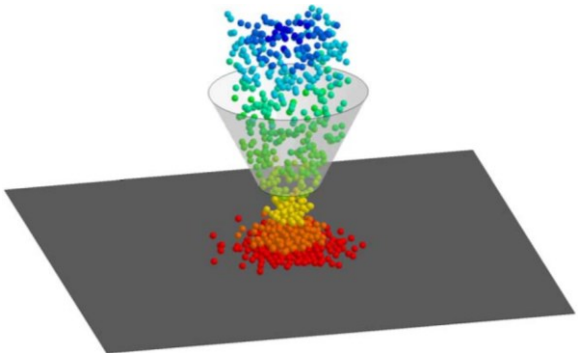

Figure 2-2: Simple example of a DEM simulation; pouring multiple spherical particles through a cone and onto a plane [136]

As the simplest three-dimensional volume geometry to be described mathematically and to be handled in computation, spherical-shaped particles are preferred for common DEM applications. Although, other types of particle geometries can be defined as well. Therefore, various approaches for the modelling of non-spherical particles exist, including multi-spherical setups (multispheres, clumps), primitive geometrical shapes (primitives), compound particles (by combining multiple primitives), or even defining complex-shaped particle geometries as three-dimensional meshed/triangulated objects. On that topic, Becker describes more details in the user guide [13] (and further also shows related use cases in the examples overview [11]) for the use of complex particles in ThreeParticle/CAE [17]. For further illustration of the mentioned approaches, Figure 2-3 exemplarily shows several different particle geometries for the use in DEM simulations:

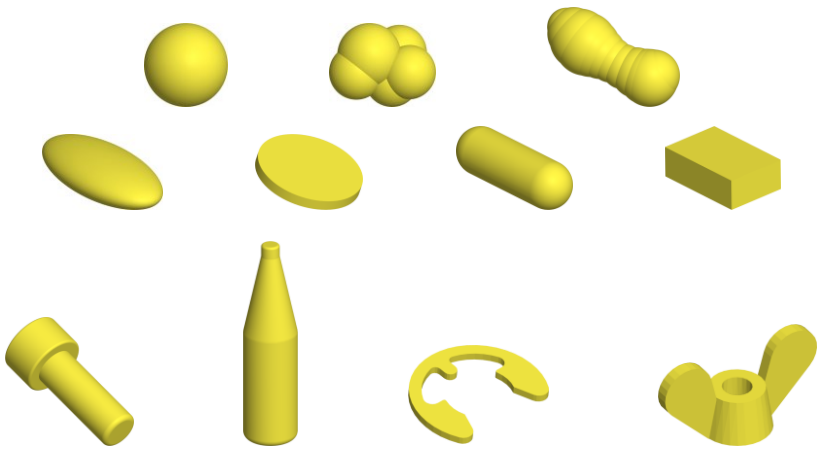

Figure 2-3: Some representative examples for possible particle geometries; simple sphere and multispheres (top), primitives (middle), and complex shapes (bottom)

- Sphere and sphere-based (multipsheres): (top, from left to right)
    - typical sphere (common particle shape)
    - multi-sphere; stone-representing shape consisting of five spheres
    - multi-sphere; peanut shape consisting of a dozen spheres
- Single primitives: (middle, from left to right)
    - ellipsoid
    - cylinder (relatively flat)
    - capsule
    - cuboid
- More-complex particle shape setups: (bottom, from left to right)
    - compound of cylinders, representing a socket head bolt (cf. DIN EN ISO 4762 [56])
    - compound of cylinders and a cone, representing a bottle
    - complex meshed shape of an external circlip (cf. DIN 6799 [55])
    - complex meshed shape of a wing nut (cf. DIN 315 [54])

Similar to a simplified particle shape, the particle sizes may also differ between a digital model and a physical bulk material, resulting in the typical simplification that a single particle size in the DEM model is often used to represent a physical particle size distribution. The modelling of a bulk material mixture consisting of particles of more than one size is possible, but if applied typically done by representing a size distribution with a few different particle sizes (e.g. two different particle sizes representing a complex bulk material size distribution).

Furthermore, especially to enhance the level of efficiency related to the required computation effort in applications with very large numbers of particles, a reduction of the amount of particles by increasing their individual size is feasible and reasonably common. This upscaling technique, also known as coarse-graining, requires adjustments with regard to the resulting effects of oversized particles on the overall bulk material behaviour. For more details, this technique is proposed, described, and applied, for example, by Kuwagi, et al., using the term similar particle assembly [152], by Bierwisch, as described in the course of his PhD thesis [26], and in further related work on coarse grain modelling, such as by Sakai and Koshizuka (2009) [219], etc.

Such particles are generally rigid objects. In some specific cases, complex particle behaviour may be required (e.g. allowing flexible or breakable abilities for deformable fibres or breakable agglomerates, etc.). For that purpose, advanced modelling techniques can be applied, such as using bondings to set up bonded-particle structures to represent complex-behaving particles. Some of these setups are covered in Chapter 2.1.2.6.1.

2.1.2.2 Material properties

For the material definition, main properties such as the density, the shear modulus and the Poisson's ratio need to be set.

When defining the solid density of particles, the deviation from this density to the desired bulk density must be considered. This is also in close connection to the shape of the particles and, if applied, to the particle size distribution used. To obtain a specific bulk density, the density of particles is correspondingly adjusted (which generally refers to density calibration, cf. [212] (by Aldrich (ed.), regarding Rocky [76]).

Furthermore, adaptations on the shear modulus may be applied in order to enhance the computational efficiency of DEM simulations. This topic was discussed by Lommen, et al. (2014) [161], analysing stiffness effects on bulk material behaviour in terms of a DEM speedup approach. Using this approach by lowering the stiffness of particles can significantly enhance a DEM simulation process without notably affecting the macroscopic behaviour of the bulk material in total.

2.1.2.3 Contact handling

Contact models are responsible for interactional behaviour, such as when particles collide with each other. The classical DEM is in general based on a soft contact approach, which means that particles are able to overlap and therefore penetrate each other during contact. In contrast to that, hard contact basically corresponds to conventional impact kinetics. Furthermore, particles do not deform during contact, as it is the case according to the FDEM (Finite-Discrete Element Method) approach, which is also further outlined in Chapter 3.1.1.3.

In Figure 2-4, a simple illustration shows two contacting particles with their overlap distinctive in the contact area between them; referring to the soft contact approach. The symbolic contact model between those two particles represents a specific approach (as an algorithm), defining the contact handling that further results in specific forces/torques on those particles.

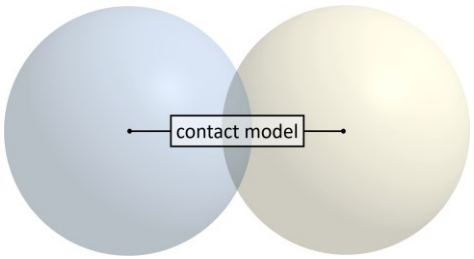

Figure 2-4: Two overlapping particles with a symbolic contact model that is representing the handling of contact effects between these two particles

The exact details behind such contact models are defining specific interactional behaviour and are therefore decisive for the behaviour of a digital bulk model in total. A common and widely used DEM contact model is the Hertz-Mindlin contact model (based on the Hertzian contact theory by Hertz (1882) [117] for normal, and on work by Mindlin (1949) [176] / Mindlin and Deresiewicz (1953) [177] for tangential contact), as further described with respective numerics in the course of the contact force calculation in Chapter 2.1.3.2. Also, further models, for example, as given by Di Renzo and Di Maio (2005) [52], are advanced versions, principally based on the Hertz-Mindlin contact model. Such a typical Hertz-Mindlin contact model can be defined with frictional coefficients (static, dynamic and rolling friction) and a damping factor (restitution), as, for example, to be used in the DEM software environment of ThreeParticle/CAE [17]. Further examples for basic contact models, as also implemented in ThreeParticle/CAE and accordingly described in the User Guide by Becker [13], are corresponding to a Hooke, a Linear Spring, or an Elasto-Plastic approach. In Figure 2-5, a classificational overview of various particle interaction models is shown by Yeom, et al. [260], also describing further contact model details.

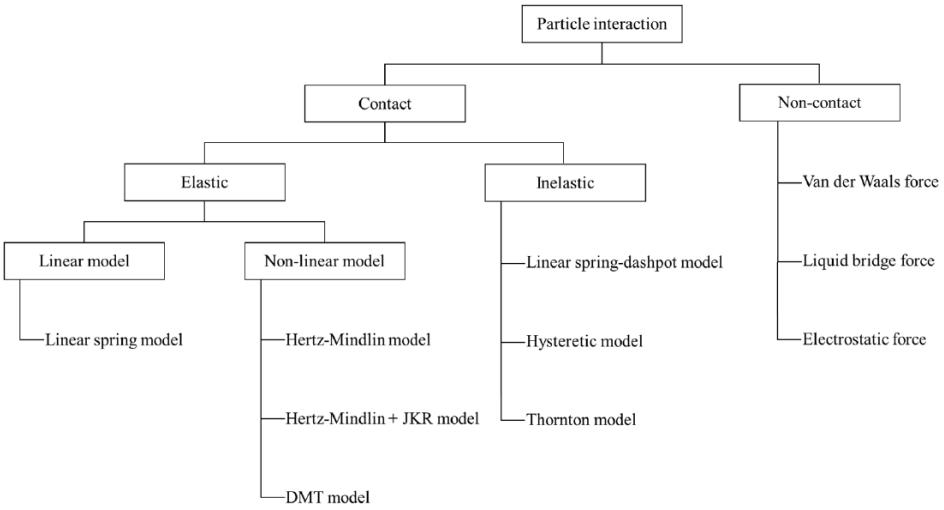

Figure 2-5: Categorised overview of various particle interaction models [260]

These principles regarding the handling of interactions as described, apply accordingly to interactions between particles and other system components, such as surfaces of parts (particle-wall-contacts).

Further details, especially related to the numerics of contact handling mechanisms, are described in Chapter 2.1.3.2, in the respective contact force section.

Furthermore, as it is possible to lock particles in their ability to rotate individually, this locking, when enabled, needs to be considered in the interactional behaviour, as such particles are incapable of spatial rotation. In that matter, it needs to be considered that this locking option is unsuitable when angular particle movements are essential, such as for complex particle shapes, complex contact models or applications with (beam-based) bonded particle structures (bondings see Chapter 2.1.2.6.1; bonded particle structures see Chapter 3.1.2).

2.1.2.4 Particle generation/initialisation

There are several ways to create particles in a DEM environment, which can, in general, be in the form of a single positioning or an ongoing generation of particles. Furthermore, such a creation can be based on random distribution approaches or predetermined initialisation.

For simulations with bulk material flows, as typical in a lot of applications for DEM simulations, an ongoing generation of particles is useful. Therefore, the use of a kind

of source is common, with which a particle flow is continuously generated. This source can be modelled, for example, as a plane (generator plane) with specific dimensions on which particles are generated in a defined way, such as with a given mass flow rate, or an initial velocity. Further contents herefore can also be found in several DEM simulation software applications, such as ThreeParticle/CAE [17], EDEM [51], or Rocky [76], etc.

Furthermore, as for example also supported by ThreeParticle/CAE, filling of specific volumes with particles is also possible. Accordingly, a volume, such as a given box, can be filled up with particles, either randomly but also precisely defined, such as in a grid-type arrangement.

For the initialisation of particles in a precise predetermined way, it is necessary to set the respective parameters herefore, which are:

- general particle type information (corresponding to a defined particle type; with shape, size, material, etc.)
- position and alignment (as coordinates and spatial orientation)
- time (when does a particle should be added to the simulation)
- velocities (translatory and rotatory)
- further definitions (such as particle ID)

Especially to set up specific bonded-particle structures in the form of bonded particle assemblies (as explained in more detail in the approaches for DEM-based belt modelling in Chapter 3.1.2; and as used for the belt initialisation in almost-final state, described in Chapter 4.2) this initialisation by positioning particles in a precisely defined way is of great importance.

2.1.2.5 System environment

In this context, the system environment is seen as the virtual setup, in which particles are handled during a DEM simulation. This setup comprises general conditions, such as gravity and system limits, and also system components as parts, in particular those, that are responsible for the handling of the bulk material.

Gravity

The definition of gravity is an essential global environment setting, as it acts on each particle in the simulation and results in the corresponding mass-related forces.

Domain

A three-dimensional domain is used as a virtual space, in which particles are able to be handled. Typically, a domain can be determined with specific limits, such as in the three main axes (x, y, z) and if a particle gets outside of this defined domain, it is removed from the simulation. Thus, exceeding of domain limits can be useful to delete particles in the form of a particle sink, which in principle corresponds to the opposite of particle generation (using a generator plane as a particle source), as described in the previous Chapter 2.1.2.4.

Another useful way of treating the domain can be the use of periodic boundaries. As also explained in an illustrative application by Wang, et al. (2017) [250], a periodic boundary condition enables the simulation of a form of infinite space by connecting opposite sides of a finite domain with each other. If a particle exits one side of the domain, it is accordingly reentered on the opposite side.

Parts

For most applications, the use of various system components in the form of parts is substantial to perform a DEM simulation. Therefore, floors, walls, pipes, but above all also geometrically complex components, such as conveyor screws, sieves, mixing arms, etc., are represented as three-dimensional objects that are able to interact with particles (accordingly similar to the principles of contact handling between particles, as described in the previous Chapter 2.1.2.3). Such parts are typically modelled as rigid surfaces, as later also described in the rigid belt modelling technique in Chapter 2.2.3, in a triangulated form. Triangulation means that any general surface is approximated with multiple triangular surfaces (see Figure 2-6, left), which is also common for some forms of 3D model data, such as in STL format (originally documented by 3D Systems, Inc. (1988 and 1989) [1, 2]). Thus, respective surface triangulation techniques, and also using such triangulated (STL) model data for the import of parts are relatively common in applications of DEM simulations.

Beyond that, modern DEM software, such as ThreeParticle/CAE, also supports the modelling of selected parts, specifically of such with mathematically primitive shapes, in non-triangulated form. Since the surface of such simple-shaped parts, for example cylinders, can accordingly be represented as ideally-smooth surfaces instead of approximations consisting of multiple triangles, advantages regarding the simulation accuracy, as well as regarding computational aspects (due to minimising the number of surface elements and correspondingly their edges and vertices) can be gained. A simple illustration of such a primitive part in comparison to a triangulated model is shown in Figure 2-6, where the same cylindrical part is once modelled in a typical triangulated form (on the left; with 16-edge polynomials for the base circles) and as a smooth primitive part (on the right). Further insights into this topic, especially regarding the use of such primitives for the modelling of smooth-surfaced cylindrical parts to represent idlers and pulleys in conveyor belt applications, are also given in Chapter 4.4.

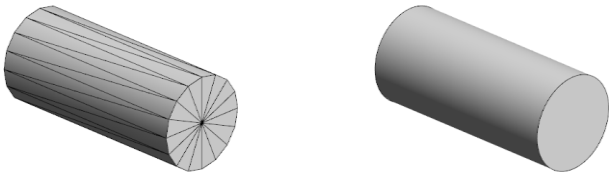

Figure 2-6: A cylindrical part, modelled in triangulated form (left) and as a primitive (smooth) cylinder (right)

In addition to parts that are able to interact with particles, the modelling of virtual (non-interacting) parts is also possible. Such virtual parts can be useful to enhance the comprehensibility of systems by visualising entire system structures and surroundings.

2.1.2.6 Extending models and methods

The above-described aspects comprising the basics of DEM particles, materials, contacts, particle generation/initialisation and environmental definitions are the fundamental basis of a general DEM simulation. In addition to that, many other specific methods, modelling techniques, and extensions are available for different kinds of simulation applications, whereby their usage is strongly depending on individual purposes.

With particular reference to the contents of this thesis, the methods listed below are outlined in more detail in the next subchapters:

- Bondings
- Movements

Further methods, techniques and extensions also refer (amongst others) to those as listed in the following (including corresponding examples/references):

- Advanced contact models, e.g. as:
    - Cohesive/adhesive models (e.g. based on the Johnson-Kendall-Roberts model of elastic contact (JKR) [138])
    - Capillary (or pendular liquid) bridge models (e.g. cf. Weigert and Ripperger [253], Mikami, et al. [175], or Lambert, et al. [154] (improving Rabinovich, et al. [207]))
- Loads and fields (individual forces/torques and velocity/force fields)
- Wear (part and particle wear)
- Processes (e.g. coating, drying)
- Thermal characteristics (e.g. thermal conductivity)
- Electrical characteristics
- Chemical characteristics

2.1.2.6.1 Bondings

A bonding element (bonding; bond; joint) is referring to a defined type of virtual connection between two particles. Therefore, bondings can technically be categorised as a specific type of contact model, as it defines the interactional behaviour between two (bonded) particles. In ThreeParticle/CAE [17], for example, bondings are implemented as slave contact models, which means, that they are defined in addition to a master contact model, which is defining general contact interactions between particles, as described in Chapter 2.1.2.3. The additional bonding model is then applied in superposition principle to the master contact model, resulting in a specific linking of two particles in the form of a beam-like connection. The purpose of the bonding is to define this connection in a specific way. Therefore, such bondings are typically represented as virtual connection models without surface, volume

or mass (just like other general contact models; also explained in various references, such as by André, et al. (2012) [5]).

In general, bonding mechanisms can be useful to depict complex behaviour in DEM simulations, not only regarding particle modelling, to set up particles that are consisting of several bonded sub-particles, but also regarding the modelling of entire structures (as system components) with multiple bonded particles. Therefore, bondings considerably extend the range of possibilities for DEM simulation, for example, to allow the modelling of flexible or breakable bonded particle setups (cf. bonded-particle model; BPM). As relevant to this thesis, further details on complex bonded-particle structures, especially regarding belt modelling, are also given in Chapter 3.1.2.

The fundamental idea behind the mechanics of a bonding element is related to the mechanical approach of a (one-dimensional) beam element (which is generally also related to approaches as in the FEM; as further described in Chapter 3.1.2, and as addressed in relation to the DEM in Chapter 3.1.1). Similar to classical contact models, also a large variety of different variants and adaptions of bonding models can be found in the literature or also implemented in software. In the following, some general bonding approaches and corresponding basics are outlined. Early applications reach back to Lorig and Cundall (1989) [163], applying bonding for the modelling of reinforced concrete.

Longitudinal-only bondings

Simple longitudinal-only bondings can be used to handle and further transmit only longitudinal loads, such as tension or compression. The stress-strain relation of such bondings can be considered, for example, in a linear form by using a Youngs's modulus and a cross-sectional bonding area. A very simple type of such a longitudinal-only bonding can be a connection between two particles at a fixed distance, which relates to an absolute rigid beam. In contrast to a multi-spherical particle compound, such bonded particles are accordingly allowed to rotate individually, as no loads, except for longitudinal forces, are transmittable.

Beam-theory-based bondings

In order to handle and transmit general load cases via bondings, it is necessary to consider a complex load system that includes tension/compression, shear, torsion, and bending. Such a general load system at a bonding between two bonded particles is illustrated in Figure 2-7.

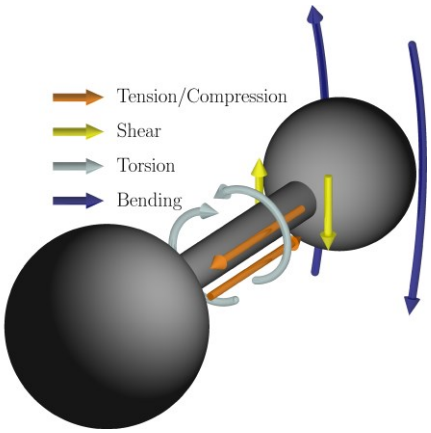

Figure 2-7: Bonding model between two bonded particles that allows the consideration of different types of loads [252]

This figure also shows the fact that a bonding is typically modelled as a homogenous one-dimensional beam element with a constant circular cross-section. This is common for bonding models, as a circular cross-section does not require an additional orientation, which is in particular beneficial for the handling of shear and bending effects.

For the consideration of such load cases via bondings, the use of beam theory approaches, such as based on the Timoshenko (also Timoshenko-Ehrenfest [73]) beam theory [240, 241], has been proven to be suitable in DEM bonding applications. A scientific comparison of linear beam theories, including Euler-Bernoulli, Timoshenko and two-dimensional elasticity, is further given by Labuschagne, et al. (2009) [153] (from a basic, not explicitly DEM-related point of view). In the literature, various specific beam-theory based bonding models and corresponding applications can be found. For example, a cohesive beam bond model is presented by André, et al. (2012) [5], showing the relaxation state in comparison to the loading state of a correspondingly beam-theory-based bonding, as illustrated in Figure 2-8.

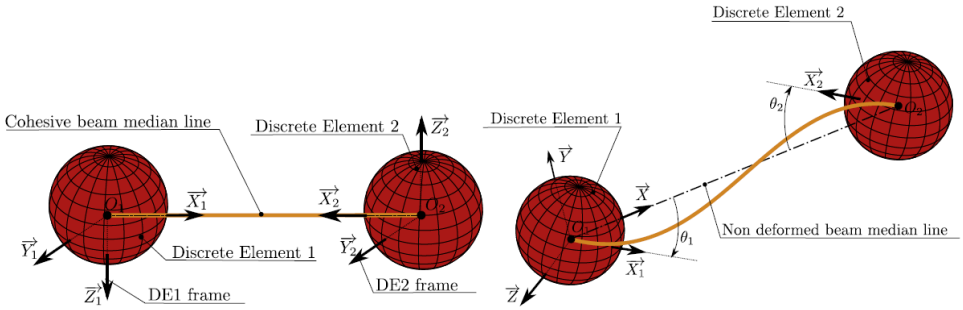

Figure 2-8: Bonding as a virtual beam element between two particles, in the relaxed (left) and in a loaded state (right) [5]

As another representative example, an adapted Timoshenko beam bond model (TBBM) for cementitious materials and deformable structures is given by Brown, et al. (2014) [28]. In this context, Brown is also insightfully describing the basics of the Timoshenko beam approach, and further explaining the implementation of this model in a DEM software (EDEM [51]) in a subsequent publication (Brown, et al. (2015) [29]). Further relevant reference regarding to beam-theory-based bonding techniques can also be made to Obermayr, et al. (2013) [189].

To further enhance the capabilities and the behaviour of bondings, advancements and specific adaptions were developed for various purposes, as also described in the following:

Breakage and further stress-strain related behaviour

Breakage is a very common capability of bonding models. It allows the fracture of continuous structures that are modelled as a multitude of bonded-particles. Deleting of a bonding between two particles, if a certain criterion applies, corresponds to such a breakage. For these criteria, various stress hypotheses can typically be useful, such as based on the von Mises yield criterion (introduced by von Mises (1913) [247]). In lots of applications with bonded-particles, breakage is a central aspect, such as also in the work of the previously mentioned authors, Lorig and Cundall (1989) [163], Potyondy and Cundall (2004) [203], Brown, et al. (2014) [28], etc.

Further bonding model adaptions can also apply to specific stress-strain behaviour, such as hysteretic stress-strain effects, or to represent complex effects, such as accumulated or specific damage/failure mechanisms (e.g. as in work by Dau, et al. (2016) [45] or Tavares, et al. (2020) [233]).

Inhomogeneous bonding model (bonding reduction factor)

A specific bonding model adaption, which is forming an essential part of this methodology (as already described by Fimbinger in corresponding publications, see Chapter 1.5), was developed and further implemented to be used in the DEM simulation software ThreeParticle/CAE in exclusive cooperation with Becker 3D (cf. [16]).

In general, this model adaption extends the capabilities of a typical bonding (with a circular cross-section, as indicated in Figure 2-7) to behave like an inhomogeneous beam. Even though this inhomogeneous bonding model still consists of a single and uniform connection element only, it can be used to represent complex inhomogeneous characteristics. Therefore, an additional (bonding) reduction factor is introduced, which defines this specific behaviour. As this type of bonding is essential for the modelling of inhomogeneous material behaviour of bonded particle structures (see Chapter 3.1.2), such as conveyor belts modelled according to the developed methodology, further details and specifically the use of this bonding model are given within the methodology's description in Chapter 4.1.2. In particular, the implementation of the reduction factor is shown in this course (see Eq. (24)-(27)), as proposed in collaboration with Becker (Becker and Fimbinger [16]; collaborative development study in early 2017 with bonding numerics based on work by Obermayr, et al. (2013) [189]) and in this form initially implemented in an early release of ThreeParticle/CAE (R1.1, released March 19, 2017) as an undocumented feature, intended for testing and evaluation purposes. After a successful evaluation phase, this advanced bonding model was officially released in the following software versions, initially as a simple documented keyword option (R1.3, released on June 12, 2017) and later also as an available embedded model option, accessible within the software's graphical user interface (GUI) (R3.1, released July 19, 2018).

Besides conveyor belts and belt-like structures, further practical applications of this inhomogenous bonding model refer to structures which are typically flexible in bending while stiff regarding tension, such as ropes, wires, steel cords, or textiles, etc. Vice versa, the modelling of structures with lower resistance in tension/compression than in bending is also conceivable in principle, but there are fewer practical examples for models that require this type of behaviour compared to soft-bending structures.

Bond modelling with more complex bonding elements

To even further increase the complexity of bonding models, advanced bonding structures are conceivable, such as by using specific (non-circular) bonding cross-sections. It should be noted that the use of such complex bonding structures requires correspondingly high demands of computing power. A representative example for a complex bonding structure is the flat-joint contact model by Potyondy (2012) [202], developed for the modelling of structures in complex rock mechanics. Therefore, this model is using a cross-sectional bonding area that is sub-divided in individual sub-bondings, as schematically illustrated in Figure 2-9. In contrast to using a simple (single) circular cross-section, as earlier indicated in Figure 2-7, this setup allows the definition of various advanced effects, for example, the breakage of only a few sub-bondings instead of the whole connection.

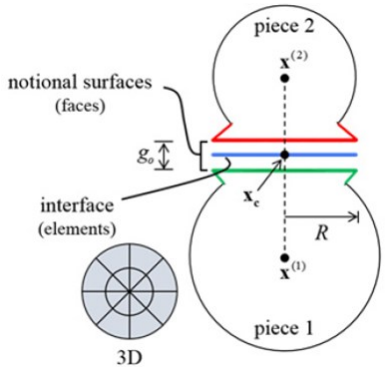

Figure 2-9: Scheme of a flat-joint model as a complex bonding structure [30] (based on Potyondy [202]; illustration referred to Itasca [128])

Further bonding-related techniques are specifically shown and referenced in Chapter 3.1.2 on bonded particle models (structures comprising multiple bonded particles).

2.1.2.6.2 Movements

Typically, modern DEM software allows the modelling of parts, as described within Chapter 2.1.2.5, as objects with the advanced ability to be movable, which allows the simulation of dynamic systems with moving components. Thereby, translatory and rotatory part movements are possible, as well as a combination of both. In general, part movements in DEM simulations can be seen in two major forms: in the form of

a specifically defined movement, or in the form of a resulting movement that is induced and influenced by various interactions. Furthermore, multibody dynamics can be useful to define complex movement behaviour of parts.

More details regarding these methods for part movements, as also addressed in the following subsections, are further given in the user guide and in respective tutorials by Becker [11, 13] especially to be used in the DEM software ThreeParticle/CAE [17].

Specific movement definition

A specifically defined movement of a part, such as with a certain speed in a certain direction, is not affected by retroactive effects. Therefore, there is no need to define further mass-related part characteristics, such as part mass or moments of inertia, when moving a part in this specifically defined form. The definition of a drive pulley of a belt conveyor (described in Chapter 2.2.2) with a certain rotational speed around the pulley's axis corresponds to such a defined movement. Furthermore, complex velocity amplitudes, such as to perform a soft start-up or a sinusoidal movement, or complex path definitions, such as the guidance of a part along a specific route, are typically possible.

In some modern DEM codes, such as in ThreeParticle/CAE, it is also possible to define specific particle movements in the same manner as described above for parts. This option allows several possibilities towards complex DEM simulation, as for custom applications in which defining specific particle movements are more convenient (and exact) than using moving parts (which are further moving the desired particles via contacts); as in particular regarding the movements of bonded particle structures (which are representing parts but are consisting of a multitude of particles).

Another movement type, which is by now relatively common in DEM software programs, is the definition of a virtual movement. This virtual movement can be used to induce certain effects in particles that get in contact with a virtual moving part (or more specifically: with this part's surface). Thereby, the relevant part is actually not moving, but contacting particles react as if it does. An illustrative and typical application example herefore is the use of a virtual moving plane to represent a moving

conveyor belt. This application is in more detail explained in the rigid belt modelling technique in Chapter 2.2.3.

Six degrees of freedom

A simple way that allows a part to be moved by influencing effects is the movement definition based on the part's six degrees of freedom (6DoF). This 6DoF correspond to the three translatory and the three rotatory degrees of freedom (DoF) of the part's local coordinate system (three-dimensional (3D); x, y, z). Each DoF can be individually locked or unlocked to define a moveability of a part in a specific way, whereby unlocking a certain DoF enables a corresponding movement of the part. As such an unlocked part is then moved by influencing effects, such as by impacting particles, the part needs to be defined with mass-related properties, such as mass and moment of inertia, to act accordingly. Furthermore, the definition of damping behaviour could be useful. An illustrative example herefore could be a bucket wheel, such as in the form of a conventional water wheel, which is allowed to rotate when a particle flow is turning the wheel. Therefore, the rotational DoF of this wheel in reference to its main centre axis (e.g. rotatory z) is unlocked. All the other DoFs are locked to keep the wheel in position (translatory x, y, z) and to prevent the wheel from tilting sideways (rotatory x, y). Similarly, rotatable idlers of belt conveyor systems (see Chapter 2.2.2) can be defined, as in some exemplary applications of BP belt simulations of belt conveyors later described in Chapter 5.

Principally, a combination of part movements with specifically defined movements and also 6DoF is conceivable under certain circumstances. Both movements must be defined in respect to each other so that they do not interfere with each other. Such a combination would then allow a part, which is primarily moving with a defined movement (e.g. fixed translatory movement), to react to some influencing effects additionally (e.g. resulting rotation around an axis).

Multibody dynamics

Using enhanced movement definitions, as basically categorised in the field of multibody dynamics (MBD), can be useful to enable the definition of highly complex movement behaviour, which is not possible to be depicted with the relatively simple methods of specifically defined movements or 6DoF. This enhancement of the DEM

with MBD capabilities also relates to a type of multi-physics simulation (later described in Chapter 3.1.1.3).

Generally, MBD in this use case allows the linking of multiple parts to a dynamic system by using various types of linking joints. Simple types of such joints are, for example, revolute joints or ball joints, and more complex types are, for example, spring-damper connections or even angular or linear actuators. More details regarding such joints, and for example, specifically their use in ThreeParticle/CAE, are further given in the respective User Guide by Becker (2019) [13].

In Chapter 5.6, MBD is used to set up a complex system of moveable idlers in the DEM simulation of a round hay baler. This general application is also described in Chapter 2.2.5.5, where the principles of this system are also explained. For the simulation of this complex (belt/idler) system, methods of the MBD module are used, such as to define rotating and even pre-tensioned arms on which several (and again rotating) idlers are mounted.

2.1.3 The DEM computation scheme

The overall computation process of a DEM simulation can be exemplified as a repetitive loop, according to which a series of subordinate system modules are computed iteratively. This loop, simplified to the two major core fundamentals that are forming the computation process, is shown in Figure 2-10 by Itasca [129].

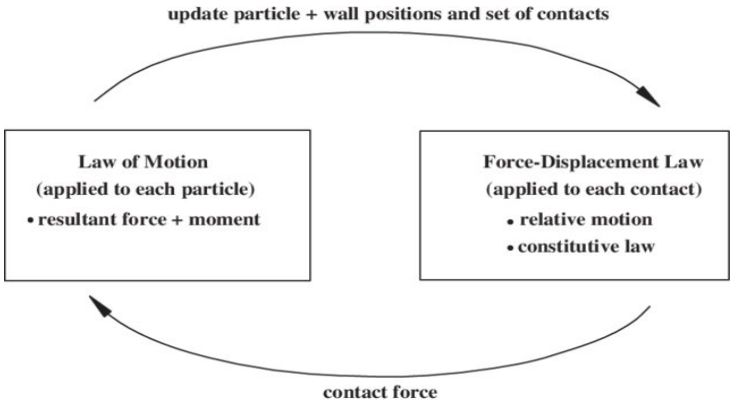

Figure 2-10: Simplified schematics of a basic DEM simulation loop [129]

These two fundamentals (law of motion (Newton's second law) and force-displacement law (contact mechanics)) regard the basic handling of particle-related effects

during the ongoing (dynamic) changes in a numerical particle conglomeration, typically consisting of a large number of particles (discrete elements), under consideration for DEM computation. Thereby, the changes of particle positions result in changes of their respective contact conditions, and consequently in changing of resulting contact forces/moments – and vice versa.

2.1.3.1 Time handling

The dynamic computation process is typically performed in an explicit form (in contrast to implicit approaches, as, for example, implicit Finite Element Method (FEM) simulations, in which multiple iterations for a single time step are computed until a convergency criterion is met). Therefore, the simulated time is discretised into multiple time steps, a series of successive time increments. As indicated in the scheme provided by O'Sullivan (2011) [192] and given in Figure 2-11, after each computation loop, the current simulation time (t) gets increased by a time step (Δt), which results in moving one step further in computed time. In addition to this time dependency, the illustrated computation loop again shows the above-addressed force/displacement calculation steps, similar to the basic procedure as already described by means of Figure 2-10. Typically, the simulation is finished when a defined time to stop the simulation (t_{end}) is reached/exceeded. [168, 192]

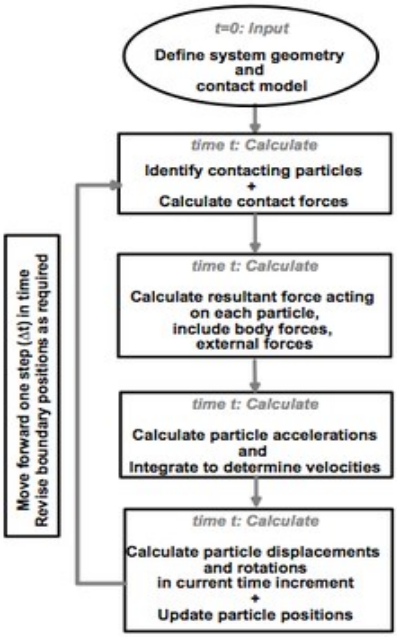

Figure 2-11: DEM Computation cycle overview indicating time dependency [192]

Itasca [133] describes the time incrementation scheme as follows: *"The dynamic behaviour is represented numerically using a time-stepping algorithm in which it is assumed that the velocities and accelerations are constant within each time step. The solution scheme is identical to that used by the explicit finite-difference method for continuum analysis. The DEM is based upon the idea that the time step chosen may be so small that during a single time step, disturbances cannot propagate further from any particle than its immediate neighbours. Then the forces acting on any particle are determined exclusively at all times by its interaction with the particles with which it is in contact."*

The size of the time step (Δt) has a significant influence when performing a DEM simulation, and can be seen as a compromise between stability and accuracy aspects on the one side, and computational efficiency on the other side. Therefore, on the one hand, the time step must be small enough so that numerical instabilities are avoided. Such instabilities may occur from too large time steps, as those can lead to large particle displacements, which may further lead to large particle overlaps and probably unstable force/moment effects as a consequence. But on the other hand, smaller time steps require higher computational effort, as more (smaller) time steps need to be computed to reach a specific simulation time. Consequently, performing DEM simulations with too small time steps can require relatively long computation time, corresponding to a negative aspect regarding the overall simulation efficiency.

Especially for determining a suitable time step, the Rayleigh time step ($T_{Rayleigh}$) (referencing to Rayleigh wave propagation, based on work by Rayleigh (1885) [208]) is commonly used to represent a critical and comparable reference value, typically applicable for simple DEM applications, e.g. with spherical particles and common conditions. The given Equation (1) (e.g. as by Becker [14] embedded in ThreeParticle/CAE [17], or by Marigo and Stitt (2015) [166] regarding EDEM [51]) shows the Rayleigh time step dependence to major simulation model parameters (particle radius (R), density (ρ), shear modulus (G), Poisson's ratio (υ)). Thus, by indicating direct/indirect influence on this reference time step, the equation also explains the resulting advantages of enlarging radii (see coarse-graining, Chapter 2.1.2.1) or of common approaches that use shear moduli reduction to enhance computational efficiency (see Chapter 2.1.2.2).

$$T_{Rayleigh} = \frac{\pi R \sqrt{\frac{\rho}{G}}}{0.1631\,\upsilon + 0.8766} \quad (1)$$

Further work relating to the general topic of time dependency in DEM, such as to find critical or further suitable (stable) time step sizes, is dealt with in continuative literature, for example by O'Sullivan and Bray (2004) [191].

In general, it can also be stated that in addition to the typical parameters mentioned above, especially in complex DEM simulation setups, much more aspects influence the critical or suitable time step sizes. This concerns, for example, when using complex-shaped particle geometries or complex bonding models, which is thus of importance in the context of this thesis, as it regards the belt modelling technique further described in Chapter 4.

2.1.3.2 Basic computation modules

Looking at Figure Figure 2-11, the fundamental steps of the basic computation loop can further be described as follows.

Contact detection

The contact identification step (also termed contact or collision detection) finds each contact pair of two contacting particles (or respectively particle contact with walls). Various algorithms can principally be used for that purpose, reaching from simple brute-force approaches (checking all particle-particle combinations for possible contacts), to typical cell-based contact detection methods (subdividing the domain (Chapter 2.1.2.5) into a grid of cells and checking only potential particles within a smaller cell-based area), up to more complex collision detection algorithms. A closer look into that topic in general is further given by Kockara, et al. (2009) [145]. Regarding the computational effort required, O'Sullivan (2011) [192] also notes that in general DEM codes, these contact detection steps can account for a significant (eventually even a predominant) amount of computational effort.

Contact forces (shown on a typical contact model)

The subsequently executed contact force calculation is linked to the general topic of contact handling, as already described in Chapter 2.1.2.3. In numerical context, the forces (and torques) resulting in each contact pair, detected in the previous step, are calculated using the particle overlap (δ) as the primary parameter. (Refers accordingly to the common soft contact approach.)

As addressed also in Chapter 2.1.2.3, Hertz-Mindlin-based contact models are common standards and thus often available as default contact models in many DEM codes. Therefore, the basic numerics of such a simple Hertz-Mindlin contact model are shown in the following, representing typical contact force calculation of two overlapping particles (with spherical geometry). Figure 2-12 (as an extension of Figure 2-4) visualises a schematic diagram of the contact handling mechanism, specifically for this Hertz-Mindlin contact model. The components indicate stiffness (k), damping (γ), and friction (μ_s); and also show the affiliation in normal (index n) and tangential (index t) direction.

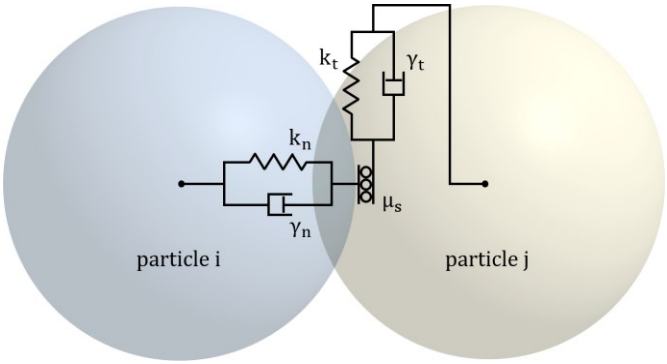

Figure 2-12: Contact model schematics (ref. Hertz-Mindlin (no slip))

Initially, equivalent parameter values (indicated with *; e.g. Y^*) are calculated by merging the respective properties of the two contacting particles (particle i and particle j; where the affiliations are each indicated with index i and j), as according to Equations (2)-(5), concerning these (particle) parameters: Young's modulus (Y), shear modulus (G), radius (R), and mass (m). (Note: The relation between Young's modulus (Y) and shear modulus (G) via the Poisson's ratio (υ) is known with: $Y = 2\,(1 + \upsilon)\,G$.)

$$\frac{1}{Y^*} = \frac{1 - \upsilon_i^2}{Y_i} + \frac{1 - \upsilon_j^2}{Y_j} \tag{2}$$

$$\frac{1}{G^*} = \frac{2 - \upsilon_i^2}{G_i} + \frac{2 - \upsilon_j^2}{G_j} \tag{3}$$

$$\frac{1}{R^*} = \frac{1}{R_i} + \frac{1}{R_j} \tag{4}$$

$$\frac{1}{m^*} = \frac{1}{m_i} + \frac{1}{m_j} \tag{5}$$

In general, the contact force ($\mathbf{F}_{\text{contact}}$) acting between the two contacting particles is composed of two main parts: the force in the normal direction and the force in the tangential direction. (With directions respecting the particle-particle contact, where the centre-centre direction represents normal.) According to Equation (6), the component in the normal direction is formed by a normal force ($\mathbf{F}_n$; Eq. (7)) and a normal damping force ($\mathbf{F}_{n,d}$; Eq. (12)). Similarly, the component in the tangential direction is formed by a tangential force ($\mathbf{F}_t$; Eq. (10)) and a tangential damping force ($\mathbf{F}_{t,d}$; Eq. (14)), with the supplement that the tangential force is typically considered using a "history effect" (further described subsequently).

$$\mathbf{F}_{\text{contact}} = \left(\mathbf{F}_n - \mathbf{F}_{n,d}\right) + \left(\mathbf{F}_t - \mathbf{F}_{t,d}\right) \tag{6}$$

Equation (7) explains the normal force ($\mathbf{F}_n$) as a function of the normal overlap (δ_n), with the elastic constant for normal contact (k_n) and the contact normal vector ($\mathbf{n}$). The numerical details of the elastic constant (k_n) are further given in Equation (8) (acc. Hertzian contact theory, Hertz (1882) [117]). For comprehensibility, the normal overlap (δ_n) is explained in Equation (9) as a function of the distance of the centres (d) of the two contacting particles with their radii (see also Figure 2-12).

$$\mathbf{F}_n = k_n \, \delta_n \, \mathbf{n} \tag{7}$$

with

$$k_n = \frac{4}{3} Y^* \sqrt{R^* \delta_n} \tag{8}$$

and

$$\delta_n = R_i + R_j - d \tag{9}$$

In similar form, the tangential force ($\mathbf{F}_t$) is calculated, according to Equation (10), as a function of the tangential overlap ($\boldsymbol{\delta}_t$), with the elastic constant for tangential contact (k_t) expressed in Equation (11) (acc. work by Mindlin (1949) [176] / Mindlin and Deresiewicz (1953) [177]). Earlier addressed as "history effect", the tangential overlap ($\boldsymbol{\delta}_t$), more specifically the tangential displacement vector between the two contacting particles, is computed with respect to the duration of the contact. For that purpose, previous time steps are taken into account for the computation (if enabled; otherwise set to zero). In that regard, Becker [14] (concerning ThreeParticle/CAE [17]), for example, describes two methods, termed "single-step" and "multi-step".

$$\mathbf{F}_t = k_t \boldsymbol{\delta}_t \tag{10}$$

with

$$k_t = 8 G^* \sqrt{R^* \delta_n} \tag{11}$$

The normal damping force ($\mathbf{F}_{n,d}$) and the tangential damping force ($\mathbf{F}_{t,d}$) are calculated according to Equations (12) and (14), as functions of the relative velocities, respectively in the normal and in the tangential direction ($\mathbf{v}_{n,rel}$ and $\mathbf{v}_{t,rel}$). The viscoelastic damping constants for normal and tangential contact (γ_n and γ_t) are further given in Equations (13) and (15) (e.g. ref. work by Tsuji (1992) [242]).

$$\mathbf{F}_{n,d} = \gamma_n \mathbf{v}_{n,rel} \tag{12}$$

with

$$\gamma_n = -2 \sqrt{\frac{5}{6}} \beta \sqrt{S_n m^*} \geq 0 \tag{13}$$

and

$$\mathbf{F}_{t,d} = \gamma_t \mathbf{v}_{t,rel} \tag{14}$$

with

$$\gamma_t = -2\sqrt{\frac{5}{6}}\,\beta\sqrt{S_t\, m^*} \geq 0 \tag{15}$$

Equations (16) and (17) further express the normal stiffness (S_n) and the tangential stiffness (S_t), and the constant value for damping (β) is calculated according to Equation (18) from the coefficient of restitution (ε).

$$S_n = 2\,Y^*\sqrt{R^*\,\delta_n} \tag{16}$$

$$S_t = 8\,G^*\sqrt{R^*\,\delta_n} \tag{17}$$

$$\beta = \frac{\ln(\varepsilon)}{\sqrt{\ln^2(\varepsilon) + \pi^2}} \tag{18}$$

In addition, a tangential limitation is set, based on simple Coulomb friction, as according to Statement (19), using the coefficient of static friction (μ_s).

$$\mathbf{F}_t \leq \mu_s \mathbf{F}_n \tag{19}$$

Moreover, rolling friction can also be implemented, which is typically used as a simple approach for adjusting the contact behaviour of spherical particles to represent more complex (non-spherical-like) behaviour. The Constant Directional Torque (CDT) model after Ai, et al. (2011) [3]), for example, is such a rolling friction model. Accordingly, a rolling resistance torque can be calculated by respecting the (normalised) relative angular velocity, a rolling friction coefficient, the respective radius and the normal force.

(Note regarding the formulations/descriptions in this Chapter: These correspond to a general Hertz-Mindlin (no slip) model, such as implemented in ThreeParticle/CAE and therefore in this form described in the according theory provided by Becker [14],

in which additional details can be found. Further, the described model is a typical default, such as also used in EDEM [51], hence in similar form described in the respective theory guide [50], in which also more details, models and literature references can be found; same applies to various other DEM codes.)

Further details of contact numerics can also be found in relevant literature, for example, by Kruggel-Emden, et al. (2009) [149], reviewing contact force models for spherical particles, or (especially regarding complex-shaped (non-spherical) particle contacts) in work by Matuttis and Chen (2014) [170] (and respetively in the related thesis by Chen (2012) [31]).

Particle forces

The resulting force (and torque) acting on each particle ($\mathbf{F}_{\text{particle}}$) gets calculated as given in Equation (20), as a sum considering the contact forces from the previous step ($\mathbf{F}_{\text{contact}}$) and also various additional forces (summarised as $\mathbf{F}_{\text{additional}}$), such as a gravitational force or forces induced from fields (e.g. defined in certain system areas, such as to represent streams as velocity fields, resulting in drag forces acting on particles).

$$\mathbf{F}_{\text{particle}} = \sum \mathbf{F}_{\text{contact}} + \sum \mathbf{F}_{\text{additional}} \tag{20}$$

(Torque/moment in equivalent form.)

Particle accelerations and time integration (velocities and positions)

Using Newton's second law (of motion), according to Equation (21), on each particle allows the determination of each particle's acceleration ($\ddot{\mathbf{x}}$) with the previously calculated particle force ($\mathbf{F}_{\text{particle}}$) and the particle's mass (m).

$$\mathrm{m}\,\ddot{\mathbf{x}} = \mathbf{F}_{\text{particle}} \tag{21}$$

(Angular acceleration in equivalent form.)

Subsequently, according to Equations (22) and (23), dual time integration leads to each particle's velocity ($\dot{\mathbf{x}}$) and displacement ($\mathbf{x}$). This integration results in the change of each particle's state within a time step.

$$\dot{\mathbf{x}} = \int \ddot{\mathbf{x}} \, dt \tag{22}$$

$$\mathbf{x} = \int \dot{\mathbf{x}} \, dt \tag{23}$$

(Angular velocity and rotation in equivalent form.)

Update of particle states and repeat loop

At the end of one cycle of this computation loop, an update is applied on each particle regarding each particle's individual state (i.e. position, spatial orientation, translational velocity, angular velocity). In general, also further system updates are typically required, such as regarding parts in motion, which are also changing their position/orientation during a time step.

If the calculation is to be continued after the update (not finished, neither aborted), the described computation loop is restarted – beginning again with the contact detection in the updated system, containing updated particle states.

2.1.3.3 Extending/advanced modules in an overview

In the previous chapter, the basic modules as the main steps of a general DEM computation loop were described, but modern DEM codes typically offer much more features, each for specific purposes. Listed in the following are several such extensions, as components of the computation loop, and as further extensions towards multi-physics, which consequently require the implementation of additional modules (based on Becker (2020) [15], thus regarding ThreeParticle/CAE [17]).

- General computation loop extending components
    - Further contact models; also as master/slave setup (e.g. Hertz-Mindlin master with additional liquid bridge slave model) (Chapter 2.1.2.3)
    - New particle creation (generation) (Chapter 2.1.2.4)

    - Bonding creation and handling (Chapter 2.1.2.6.1)
    - Fields (force, velocity) …
- Further extensions and methods towards multi-physical system simulation
    - Complex particle shapes (Chapter 2.1.2.1)
    - Part movements, six degrees of freedom (6DoF) (Chapter 2.1.2.6.2)
    - Multibody dynamics (MBD) (Chapter 2.1.2.6.2)
    - Heat transfer
    - Wear analysis
    - Fluid Dynamics (SPH)
    - Co-Simulation (coupling) …

2.2 Basics of belt conveyor systems

After the following overview regarding the development of belt conveyor systems from an evolutionary perspective, in which the use of DEM simulation in this context of belt conveyor system development is generally introduced, the overall setup and the main components of common conventional belt conveyor systems are described. Subsequently, the introduced use of DEM simulation for belt conveyor applications is dealt with in more detail, specifically focusing on the belt – and in this regard, particularly on dynamic belt behaviour to be considered in DEM simulations, which ultimately forms the general subject addressed by the methodology presented in this thesis.

2.2.1 Evolutionary overview of belt conveyor development

For relatively simple conventional types of belt conveyor systems, it is usually possible to estimate the belt behaviour and the resulting effects on the conveying process due to existing knowledge. The engineering work, especially designing and dimensioning, for such conventional systems is typically supported by available guidelines,

such as various standards, norms or design rules. According to these guidelines, the required system details, such as design aspects, material definitions, conveying parameters, etc. are adjusted in order to avoid errors for the operation of the conveyor system. CEMA [38] and DIN 22101 [53], as the two major standards, and corresponding specific guidelines, such as according to ContiTech [35], Dubbel [148], etc., offer various design guidelines and dimensioning methods for this purpose. (A setup overview of a conventional belt conveyor system, according to the guideline by ContiTech is given in the following Chapter 2.2.2.)

On complex belt conveyor systems, however, those conventional guidelines cannot be readily applied in a proper way, as they usually do not allow the consideration of highly complex effects that arise in unconventional and complex belt conveyor systems. This concerns systems for which design fundamentals are not yet available, as especially complex systems that are based on novel concepts or those involving novel adaptions. In such sophisticated systems, the behaviour of the belts and further effects are difficult to assess in an adequate approximation, so that the use of computer-aided engineering in the form of numerical simulation is advantageous and promising. In particular, DEM simulation and analysis is commonly used as a well-established supporting tool in the development of systems for handling and processing bulk materials, thus also specifically for belt conveyor systems.

For the use in belt conveyance, conventional DEM modelling techniques typically offer a limited possibility for the modelling of conveyor belts, where rigid surfaces are defined in order to represent the belts. Accordingly, this means that belt deformations cannot be simulated and that the modelling of dynamically deformable belts is not possible nor supported by default. However, in certain cases, particularly those of a complex nature, it is necessary to take such dynamic belt behaviour into account. Therefore, an appropriate modelling technique is required that allows a belt model to be considered as a dynamically deformable object that is capable of interacting accordingly with bulk materials as well as other system components, such as idlers or drums. Principles of the rigid belt modelling technique and moreover the aspects regarding the consideration of belts as deformable objects are explained in more detail in the chapters further below (Chapter 2.2.3 and following).

2.2.2 Basic setup of conventional belt conveyors

In Figure 2-13, the schematic structure and the functional principle of a simple belt conveyor system according to a design guideline provided by ContiTech [35] are shown. The main component of this conventional type of belt conveyor system is the endless conveyor belt (solid black; 1 and 2), which is in motion (as indicated with the white arrow), and on which the bulk material (dotted) is consequently transported from the feeding point (3) to the discharge point (4) of the conveyor. While the tail pulley (5) keeps the belt under tension, the head/drive pulley (6) drives the belt endlessly around. Along the conveyor line, which can range from a few meters to a few kilometres, the belt is supported and guided by arranged idlers (7 and 8). A surrounding steel frame usually forms the basic structure for supporting/mounting these components (not explicitly shown in the figure).

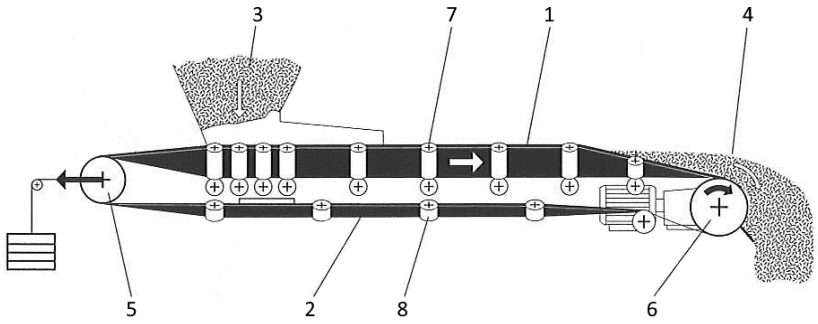

1 … conveyor belt – carry strand/side
2 … conveyor belt – return strand/side
3 … feeding point (loading of bulk material)
4 … discharge point (discharging of bulk material)
5 … tail pulley with tensioning system
6 … head/drive pulley
7 … idlers (at idler station on carry side)
8 … idlers (at idler station on return side)

Figure 2-13: Principle setup of a simple conventional belt conveyor system, adapted from [35]

Especially on the carry strand/side (or top run; the belt section on which the bulk material is transported; (1)), the belt is formed to a troughed u-shape, as shown in the cross-sectional view of the conveyor line in Figure 2-14, by inclined idlers (7). The figure shows an idler station (as a specific setup of idlers to be positioned along the conveyor line) containing such inclined idlers with distinctive inclination angle (on the left and right). This angle further corresponds to the belt's inclination angle and is therefore commonly referred to as troughing angle. Furthermore, a cross-sectional area of transported bulk material (A), as formed on top of the belt, is indicated in this view. Details in that regard are further depending on system properties, such as of

the actual bulk material in use (such as corresponding to frictional or cohesive effects). For calculation purposes or also for representation in 3D models, this area is commonly approximated/idealised/simplified as a symmetric shape, typically with two straight flanks, resulting in a simple triangular shape as the top part of the bulk material cross-section.

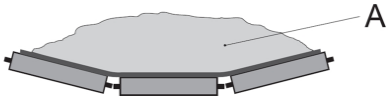

Figure 2-14: Cross-section of a troughed belt on inclined idlers, with bulk material cross-section area (A) on the belt [234]

On the return strand/side (or bottom run; the belt section for returning the belt from the discharge point back to the feeding point; (2)), where the belt is generally not loaded with bulk material (except for some rare special cases), the belt can simply be supported by idler stations containing only a single idler, resulting in a flat-shaped belt, or can also be slightly troughed, such as for centred belt guiding reasons (as also indicated in Figure 2-13, (8)).

Conveyor belts form the central components of belt conveyor systems – and are accordingly also the central system elements to be considered in respective DEM simulations (further discussed in the subsequent chapters (2.2.3 – 2.2.5); and also referring to the general topic of this thesis). Thus, relevant basics regarding conveyor belts are described in the following. Furthermore, the overall function of conveyor belts to carry conveyed material along a conveyor line is fundamentally enabled by idlers and pulleys (as illustrated in Figure 2-13), making them essential system components for supporting/driving conveyor belts. Consequently, idlers and pulleys are also addressed subsequently.

More details, such as additional component descriptions, related computation schemes, parameter specifications, reference values/recommendations, or various other general information, can further be found in pertinent literature, such as in guidelines (cf. ContiTech [35], CEMA [38], Dunlop [67] Goodyear [108], etc.), or in corresponding documents as by manufacturers or system developers.

2.2.2.1 Conveyor belts

Fundamentally, the functionality of a conveyor belt is ensured by the principal capability of the belt to allow high flexibility (in terms of bending) whilst also providing high tensile strength (further referring to low elongation under tension); i.e.: combining relatively low bending resistance with relatively high tensile resistance. Specific structural belt setups, as described in the following, enable this capability.

Generally, conventional conveyor belts show a flat shape, with a constant width and thickness in their cross-section, and are typically formed to an endless (ring-like) belt. Their structural composition commonly shows a multi-material setup, in which specific reinforcements, as traction elements (carcass), are embedded within a rubber-based volume (matrix). The basic type of this inner reinforcement further categorises belts into two major groups: textile (or fabric) belts – and steel cord belts. Based on this general categorisation, several standards define corresponding details, such as ISO 251 [125] (ref. textile belts) and ISO 15236-1 [124] (ref. steel cord belts).

In Figure 2-15 and Figure 2-16, the general inner structures of a textile belt and a steel cord belt are illustrated and described, furthermore highlighting the multi-material/multi-layer structure of conveyor belts.

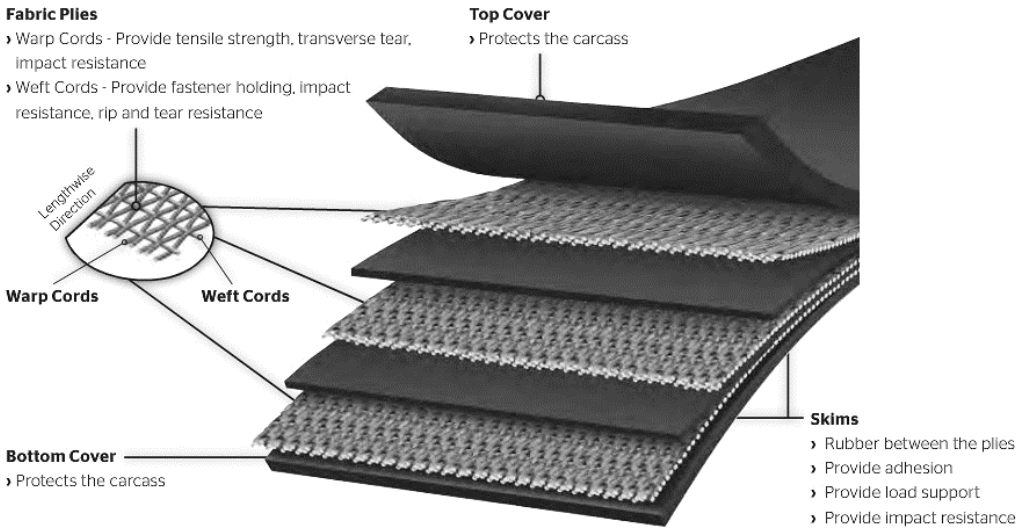

Figure 2-15: Principal composition of a textile conveyor belt [110] (ed.; adapted from [34])

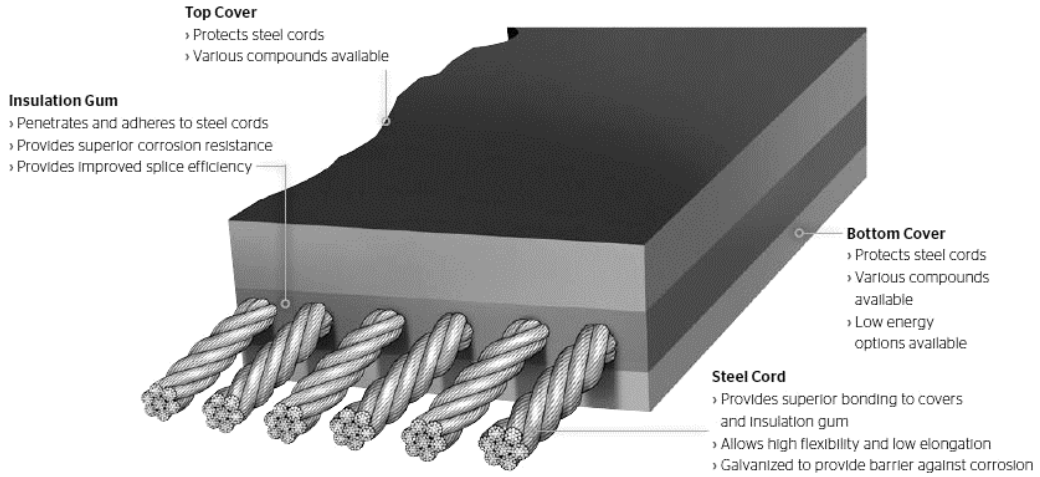

Figure 2-16: Principal composition of a steel cord conveyor belt [109] (ed.)

Based on these structural elements shown, numerous variants of belt types are available, for example relating to:

- the base materials used (top, bottom, inner (core) rubber);
- regarding textile belts: the fabric materials used (Nylon, Polyester, etc.), their woven structure, or the number of layers (plies);
- and regarding steel cord belts: the type and number/arrangement of steel cords, or if additional weft reinforcements (either in textile, but also in steel cord form) are applied.

(Note: Warp/weft relates to longitudinal/transverse orientation in relation to the lengthwise direction of the belt.)

Such specific belt types, with their detailed characteristics, typical parameter values, etc., can commonly be found in the previously referenced guidelines and in documents/datasheets as commonly provided by belt manufacturers/vendors, such as by Rema Tip Top [209], Continental (cf. [35]), Sempertrans (cf. [222]), etc.

In terms of overall differences between the two basic belt types, it can be concludingly noted that textile belts principally show benefits in terms of flexibility, whereas steel cord belts are generally able to withstand higher tensions. Furthermore, in terms of elongation characteristics, steel cord belts are typically significantly stiffer in tension, which in turn results in a lower relative operational elongation of such steel cord belts compared to textile belts in general.

2.2.2.2 Idlers and pulleys

Idlers and pulleys are important components of belt conveyor systems, which are (besides the conveyed materials) strongly interacting with the conveyor belt. In that regard, their individual purposes are mainly supporting and guiding – and respectively driving, tensioning and deflecting – a belt to allow a conveyor system to run as intended.

In general, idlers and pulleys are cylindrically shaped rigid steel mantle components, which are mounted rotatably around their centre axes. Apart from the tensioning pulley (and some specific applications), those parts are typically mounted stationary and are thus only capable of rotational movement.

Idlers (or also termed rollers) are typically installed in larger quantities, as they are arranged with the main purpose to support the belt along the conveyor line. Commonly, idlers are mounted/combined on idler stations, as exemplarily shown in Figure 2-17, comprising three idlers (in red) in a typical idler station as to be used for belt troughing (cf. Figure 2-14; e.g. with common troughing angles [°] of 20/30/35/40/45; acc. ContiTech [35])

Figure 2-17: A typical idler station setup comprising three idlers ([66]; adapted from [217])

Common idlers are typically available in several specified diameters and shell lengths (e.g. according to standards/guidelines as already referenced), and additionally, extended types are also available, e.g. with improved damping characteristics, such as to be used at the feeding point. Also, different types of idler station setups are further used for different purposes, such as basically allowing various troughing forms, but also regarding enhanced aspects, such as garland, or self-aligning idlers – or further even more-complex, application-specific types (such as for pipe conveyors, as later described in Chapter 2.2.5.2). (Further details in that regard can be found

in the previously referenced guidelines or also in further industry-related sources, e.g. Rulmeca [217], DYNA Engineering [68], etc.)

Pulleys (or also termed drums) are, in contrast to common idlers, typically individually positioned and generally larger in diameter (especially concerning head and tail pulleys). The operation of a belt conveyor system, specifically driving a belt and thus moving the conveyed material along the conveyor line, is fundamentally ensured by pulleys. In that context, and as already mentioned, pulleys pursue some specific purposes: tensioning, driving, and (if applied) also specifically deflecting a belt.

Tensioning (pre-tensioning) of the belt is induced by a tensioning system, often applied at the tail pulley (as in Figure 2-13), or alternatively in the return strand as an additional pulley system. Belt tensioning is essential to ensure a functioning power transmission for driving a belt by the driving (head) pulley. Besides this pre-tensioning, also the friction coefficient between the belt and the driving pulley, as well as the wrap angle of the belt around the driving pulley, are relevant in terms of successful power transmission. In that relation, advanced driving pulley surfaces can be used to enhance friction; or also, to increase the wrap angle above the default 180°, an additional deflection pulley can be added (see Figure 2-13, pulley to the left of the driving pulley). (See also basics in the referenced guidelines for more details.)

2.2.3 Rigid belt modelling – usage and limits

In conventional DEM simulation of belt conveyor systems, it is a typical approach to model a conveyor belt as a rigid body with an additional contact condition, which is capable of moving the bulk material on the belt and along the conveyor line as required when operating the belt conveyor. This specific contact condition is inducing relative movements, or further forces, in those bulk material particles that get in contact with the belt's non-deformable surface (Moving Plane model by/for EDEM [51], further described in the corresponding theory guide [50]). Overlying bulk material particles are consequently carried along by the lower, moving particles. This technique is also referred to as virtual movement, as, for example, according to Becker [13] (User Guide, corr. ThreeParticle/CAE [17]). In Figure 2-18 this approach is also simplified for illustrative purposes, whereby the arrows symbolise the

definition of the described virtual movement as a movement induction in those bulk material particles that hit the belt's surface.

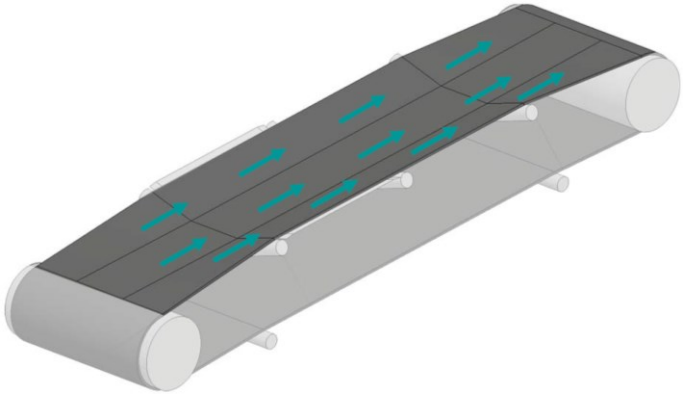

Figure 2-18: Rigid belt modelling with movement induction into the bulk material via a contact condition (symbolised as arrows), cf. [82]

According to this approach, the belts are considered as quasi-static objects. As such a rigid belt model is not affected by other system components, such as idlers and pulleys, those other components are consequently not required in such simulation setups. Accordingly, this technique requires relatively low modelling and simulation effort; and its application is sufficient under certain circumstances, as for the simulation of relatively simple belt conveyor systems where dynamic belt effects are a minor factor and where the focus of the analysis lies on non-belt related aspects. A representative example for this could be the material flow inspection at a transfer point between two belt conveyors, in which the actual belt behaviour does not significantly affect the material flow within the analysed section. Figure 2-19 shows such an exemplary DEM simulation, given by Jenike & Johanson [135], where the bulk material is guided by a chute system from one upper belt conveyor to a lower one. In cases such as this, the dynamic belt behaviour is not further relevant for the simulation as the focus of the analysis is set on other aspects, such as those relating to the chute, for example, its specific design etc.

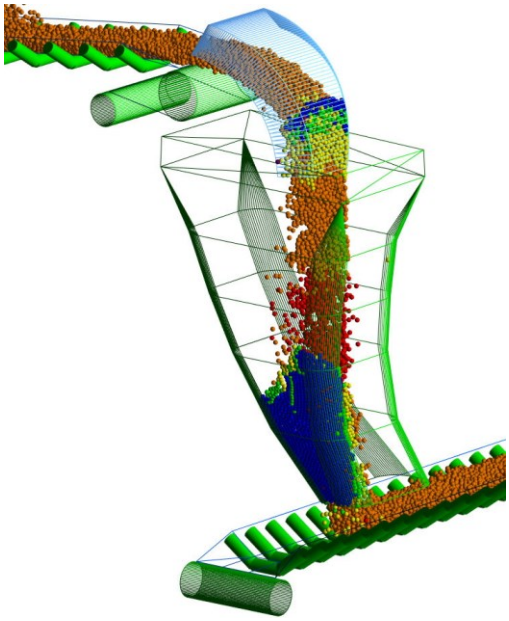

Figure 2-19: Bulk material flow analysis through a chute at a transfer point between two belt conveyors; DEM simulation with belts modelled as rigid surfaces [135]

Major disadvantages of using rigid belt models are that dynamic belt deformations, dynamic belt behaviour, and consequently, the resulting effects on the conveying process or system cannot be taken into account in the simulation. It is necessary to consider that such belt models are not able to deform, for example, under bulk material loads and due to a certain idler arrangement, nor react to any kind of influences on the belt, for example, bulk material impacts, etc. Hence, this rigid belt modelling technique is not suitable for all types of DEM simulation applications. Belts, which are modelled as rigid bodies, cannot be used for simulations of belt conveyor systems in which dynamic belt behaviour is significantly influencing the analysed processes or systems. The same applies to simulations in which the focus of the analysis requires dynamically deformable belts, such as for analyses of belt-related effects.

2.2.4 Aspects for the consideration of dynamic belt behaviour

When it comes to DEM simulation of belt conveyor systems, two general terms affect the modelling of the belts upfront, concerning whether simple rigid belt modelling is sufficient or an advanced belt modelling technique, that is able to consider dynamic belt behaviour, is necessary:

- Does the belt in its dynamic behaviour significantly influence the analysed process or system?
- Does the focus of the analysis require a belt with dynamic behaviour?

If both expressions can be negated for a considered case, rigid belt modelling is principally sufficient, as described in Chapter 2.2.3 and correspondingly explained in Figure 2-18.

In other cases, in which the consideration of belts with dynamic behaviour is necessary, an appropriate modelling technique is needed that allows an accordant behaviour of the digital belts in DEM simulations with adequate approximation. General approaches that allow this type of dynamic belt consideration are subsequently outlined in Chapter 3.1. One specific approach for the modelling of a belt with bonded particles (as a BP belt; according to the DEM-based approach as described in Chapter 3.1.2) is further building a basis for the developed methodology. Therefore, further details are given in the methodology's description, specifically in the structural belt setup description in Chapter 4.1.

Compared to the conventional approach, where belts are modelled as simple, non-deformable rigid bodies (as scc. Chapter 2.2.3), DEM simulations of belt conveyor systems with dynamically deformable belts are more demanding. In general, such dynamic belt simulations are more expensive to perform in terms of requirements and necessary efforts, in particular regarding the required software tools, the modelling and preparation efforts, and the computing power related to pre-simulation and actual simulation efforts. (See also approaches as described in Chapter 3.1.)

Using belt models with dynamic behaviour enable the consideration of dynamic belt interactions in DEM simulations. In particular, these interactions concern the effects between the belts and conveyed bulk materials, as well as between the belts and other system components, such as idlers or drums. The dynamic effects, especially local belt deformations, are thereby strongly depending on the relatively high deformational flexibility of typical belts.

In the following overview, various application examples of such systems, in which dynamic belt behaviour significantly characterises and further influences the analysed process or system, are listed. A concise description of some of these major

systems, with emphasis on the belts and their dynamic behaviour, is given in the next Chapter 2.2.5, especially in reference to the simulation examples given in Chapter 5.

- Sandwich conveyors
- Pipe conveyors
- Pouched belt conveyors
- Belt trippers
- Multibody dynamic systems with belts, such as
    - Round hay balers with belts
    - Dynamic belt centring/steering units for belt conveyors (e.g. self-guiding idler stations)
    - Dynamic curve-guiding systems for belt conveyors (e.g. bico-TEC by Kessler, et al. [143])

  and further similar applications.

Also, regarding analyses in which dynamic belt-related effects are relevant, include as listed in the following (with a short description given in Chapter 2.2.5.6).

- Effects regarding the belt – belt loads/deformations/stresses, e.g. belt sag
- Effects regarding further system components – e.g. loads on idlers/pulleys
- Effects on bulk materials – e.g. bulk material compression from belts
- Various other consequential/related effects – e.g. belt breakage

2.2.5 Overview of systems related to dynamic belt behaviour

In the following subchapters, descriptions of belt systems and also of analyses regarding certain effects, which are relevant to be considered in terms of dynamic belt behaviour, are given. Especially belt systems shown in exemplary simulations in Chapter 5 are explained further. In applications such as these, the proper consideration of belts as dynamically deformable objects, and further the interactions between belts and handled/processed bulk materials, as well as between belts and other system components, such as idlers or pulleys, are of crucial importance. Accordingly, the

digital belt models in simulations of such applications need to be appropriately modelled in order to represent such dynamic belt behaviour (leading on to the next Chapter 3, focusing on approaches for modelling and initialising such belt models).

2.2.5.1 Sandwich conveyors

Sandwich conveyors and similar systems, in which bulk material is handled between two belts (e.g. Snake Conveyors, as according to a design type by Dos Santos [58, 59]), are strongly depending on the deformational behaviour of those belts. In such unconventional belt conveyor systems, the pressures/forces on the bulk material that is clamped between the two belts, and the resulting frictional-related effects enable a steep inclined or even vertical bulk material conveyance. The setup and the working principle of an inclined sandwich conveyor are shown in Figure 2-20, whereby the conveyed bulk material clamped between the cover and the carrying belt is shown in the cross-sectional view.

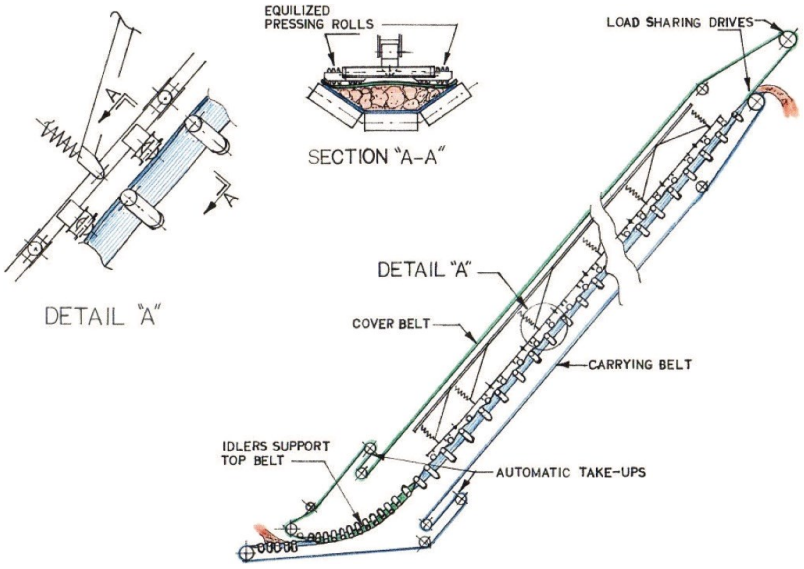

Figure 2-20: Sandwich conveyor system principle (by Dos Santos) [58]

In Figure 2-21, the two belts of a sandwich conveyor, a Snake Conveyor by Dos Santos International [60] (DSI), are shown at an inclined section of the conveyor line with bulk material between the belts. As can be seen, the covering belt is bulged by the bulk material that is clamped and thus conveyed between the two belts.

Figure 2-21: Belt deformations caused by the bulk material in a sandwich conveyor (Snake Conveyor by DSI) [60]

Further details and insights in various types of sandwich conveyors and similar systems are also given, for example, by VHV Anlagenbau GmbH (category: steep incline conveying) [245, 246] or by Doubrava GmbH (category: double belt conveyors) [61, 62].

In Chapter 5.4, an exemplary simulation of such an application of a vertically conveying sandwich conveyor using the developed methodology for the simulation of dynamically deformable conveyor belts is also described and analysed in detail.

2.2.5.2 Pipe conveyors

Pipe conveyors, or also termed tubular belt conveyors, are based on the principle that a conveyor belt is formed into the shape of a tube along the conveyor line by bringing the two edges of the belt together. The belt's cross-section is therefore not only troughed to a U-shape, as in conventional belt conveyors (see Figure 2-14), but formed to a circle using circularly arranged idlers. A small overlap of the belt edges prevents the closed tube from opening and from forming gaps. The conveyed bulk material gets transported inside of the tube, and for loading/unloading purpose, the tube is opened and closed again at the transfer points. A major advantage of a tube-formed belt is its enhanced curve-guiding flexibility, as both sides of the conveyor, the carrying and the return side, are formed to a tube. These described principles are shown in Figure 2-22 by Overland Conveyor Co., Inc. [193].

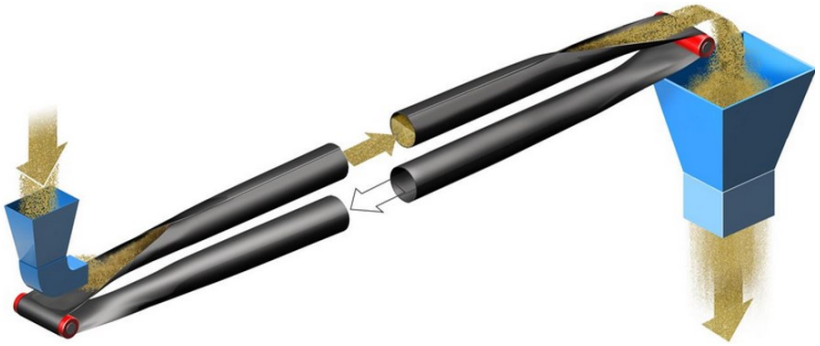

Figure 2-22: Pipe conveyor system principle [193]

At transfer points, especially for forming a flat belt to a tube and vice versa, but also for curve-guiding purposes, the deformational characteristics of the conveyor belt are of significant importance for the functionality of a pipe conveyor system. In Figure 2-23, the belt at a transfer point of a pipe conveyor system by Beumer Group GmbH & Co. KG [23] in operation is shown, whereby the guidance of the two belt edges and also their overlap at the tube-shaped belt section can be seen.

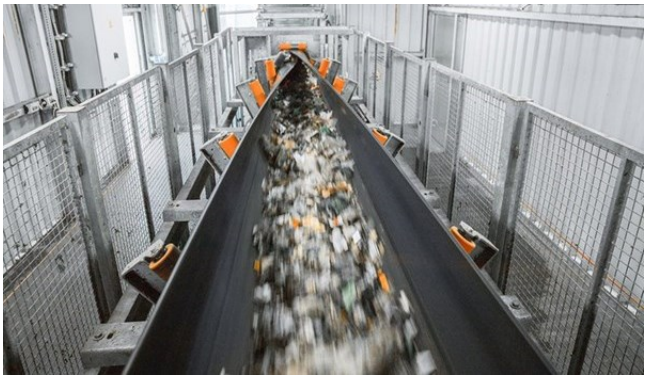

Figure 2-23: Belt forming at a transfer point of a pipe conveyor (by Beumer) [23]

More pipe conveyor systems and their applications are further given by Continental AG, described in a corresponding press release [33], or by Takraf GmbH (category tube conveyors) [231, 232]. Design aspects of pipe belt conveyors are given in the thesis by Zamiralova (2017) [261], and further research studies and analyses on pipe-formed belts are also given, for example, in various work by Hötte [119] or by Fedorko and Molnar [79].

An exemplary simulation of a representative pipe conveyor application, performed according to the developed methodology, is also described and analysed in detail in Chapter 5.5.

2.2.5.3 Pouched belt conveyors

Similar as in pipe conveyor systems, in pouched belt conveyor systems, the two belt edges of the conveyor belt are also brought together along the conveyor line. Therefore, there are principal similarities to pipe conveyors, such as regarding loading/discharging aspects at conveyor start/end points, and the closed belt cross-section along the conveyor line. But in contrast to pipe conveyors, the belt cross-section is formed to a pouched, bag-like shape instead of a circular, tube-like belt cross-section.

Such a pouched belt cross-section of a system termed SICON® by ContiTech [36, 37] is shown in Figure 2-24. This cross-sectional view also illustrates the guiding system for the pouched belt, by using adaptions to the belt edges in combination with special idlers. The resulting principle of hanging the belt on its two edges instead of supporting it on its underside (which is typical for conventional belt conveyor, as well as for pipe conveyor systems) is distinctive in the figure.

Figure 2-24: Cross-section of a pouched belt conveyor (SICON® by ContiTech), adapted from [36]

The overall functionality of such a system strongly relies on the belt's flexibility, especially regarding the behaviour of the pouched belt interacting with the transported bulk material. Also, the curve-guidance, as well as further adaptions, such as intermediate transfer points, are relying on the belt's deformable characteristics. Figure 2-25 (after ContiTech [37]) illustrates system-specific adaptions, such as a curve-

guidance through relatively low curve-radii using curve guiding stations with deflection pulleys (left), an intermediate feeding station (middle) and an intermediate discharge station (right).

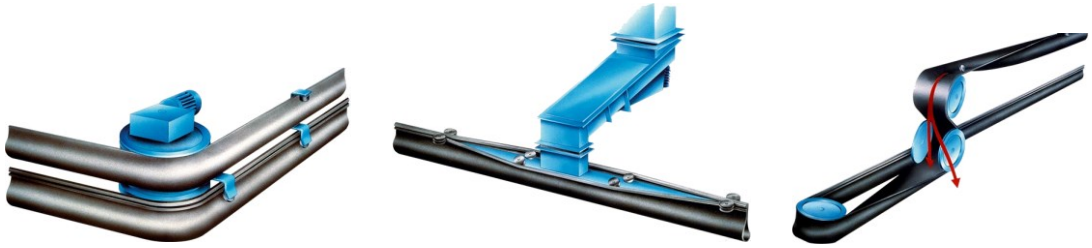

Figure 2-25: System-specific sections of a pouched belt conveyor (SICON® by ContiTech), adapted from [37]

Similar belt conveyor systems using a pouched belt are, for example, the Enerka Becker® System by Fenner Dunlop [81], the belt conveyor system by Innovative Conveying System (ICS) / Pietsch and Wheeler [201], or the SafeBelt System by Starclean [228, 229]. Further details of such systems using a pouched belt are also described, for example, in work by Hastie, et al. [116]. As a pioneering system in the field of rail-guided pouched belt conveyors, a patent by Mau (1952) [171] can be referenced.

2.2.5.4 Belt trippers

Belt trippers (or also tripper cars/trolleys) are systems to unload the conveyed bulk material from the belt of a conventional belt conveyor at a chosen point; therefore, as mobile versions, able to move along the conveyor line. This unloading is done by lifting the belt off the idlers and guiding it through the intermediate discharge station of the tripper. A mobile belt tripper lifting a conveyor belt in full operation from the idlers to convey the transported material into the chute of the discharge station is shown in Figure 2-26.

Figure 2-26: Lifting and unloading a conveyor belt with a belt tripper [236]

The belt's dynamic deformation is effecting the vertical curve of the belt during its lifting, depending on various operational related aspects, such as loading conditions, or performing start/stop processes etc. This aspect also generally applies to non-mobile vertical curves of belt conveyors, such as the unintentional lifting of a belt from the idlers in concave curves, for example, when the conveyor is not loaded or when the conveyor is started up.

Belt tripper systems are provided by various manufacturers, for example, by FEECO International [80] or Waconia Manufacturing Inc. [248]. Furthermore, specific details on concave belt curves, their design and their dimensioning are typically given by guidelines, such as by CEMA [38].

2.2.5.5 Round hay balers with belt systems

Belt systems of round hay balers, used to roll and compress hay to bales, are illustrative examples for complex applications of dynamic acting belts in multibody dynamics idler systems in combination with bulk material. In Figure 2-27, the patent sketch by Underhill and White (New Holland Belgium N.V.) [187] is describing the setup and the function of such a system. Accordingly, the hay at the bottom right section of the sketch is picked up by the moving baler from the floor. It is further transported into the baling system, where it is rolled to a circulating bale, as visualised in the centre of the sketch. A complex system of idlers (visualised in hatched pattern) is guiding the driven belt (direction symbolised with arrows next to the belt), whereby most of these idlers are translatory moveable, resulting in a highly-complex multibody dynamics system.

The dynamic belt behaviour and especially the dynamic interactions of the belt with the baled material as well as with the moveable idlers are essential requirements to enable the baling process. During this process, the increasing amount of baled hay affects the belt/idler system by deforming the belt and correspondingly moving the idlers.

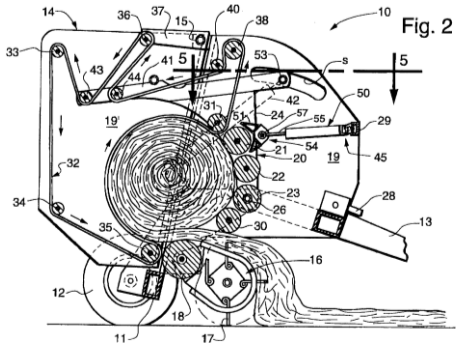

Figure 2-27: Patent sketch showing the general setup of a round hay baler, specifically containing a complex belt system [187]

At the end of the baling process, the picked-up hay is formed and compressed to a cylindrically shaped bale. To then release the finished bale out of the baler's belt system, the system is opened, typically by lifting the rear part of the baler, as shown on the round baler by New Holland N.V. in Figure 2-28 [40].

Figure 2-28: Round hay baler (by New Holland N.V.) [40]

Besides the roll-belt balers by New Holland N.V. [185, 186] as shown, similar variants of hay baling systems that also use flexible belts are used in applications such as in round balers by John Deere [137], by Massey Ferguson [169] or by Kuhn S.A.S. [151]. More insights in this technology in general, as well as further descriptions of round baler systems using belts, are also given, for example, in the thesis on hay balers by Renčín (2015) [210].

The simulation of an exemplary round hay baler's belt system is described and analysed in Chapter 5.6. In this example, a belt system similar to the one displayed in Figure 2-27 is modelled and simulated, applying the developed methodology for the simulation of belts with dynamically deformable behaviour. The presented simulation also shows the distinctive interactions of the belt model with the multibody dynamics system of the idlers.

2.2.5.6 Analyses of effects with relevance to dynamic belts

Some specific analyses cases that require the consideration of belts as interactive components are addressed in the following.

Belt-related effects

Effects regarding the belt itself (as an interactive component) generally relate to dynamic/local belt loads/deformations/stresses, such as typically expressed in belt sag. Details regarding belt sag can be found in pertinent literature; representatively referencing Wheeler (ref. [255]); with measurements for example shown in [120, 224] (anticipating Chapter 3.1.1, FEM-based belt modelling); (see also general guidelines, e.g. CEMA [38]). Furthermore, belt guidance aspects or belt stress analyses also relate to these effects.

Component-related effects

Component-related effects primarily concern loads from the belt on idlers and pulleys – and are of particular relevance to the functionality of a total system when such idlers/pulleys are furthermore able to change their position due to these loads. This concerns, for example, self-aligning idler stations or dynamic tensioning systems, in which the tensioning pulleys are translatory movable (e.g. as illustrated in Figure 2-13, with the system attached to the tail pulley on the left). Furthermore, transferred loads into steel frame parts can also be of use for structural analysis of various system components, such as for dimensioning purposes.

Handled/processed material-related effects

Effects in that regard generally concern reactions acting on handled/processed materials from the belt, such as pressure. As a typical example, this generally regards inner-bulk movements (e.g. milling effects), but in more complex belt conveyor systems, certain bulk-relating effects may even be more prominent, for example, in sandwich/pipe/pouched belt conveyors (as previously described in the Chapters 2.2.5.1/2.2.5.2/2.2.5.3). In systems as these, a dynamically deforming belt is typically strongly acting on the bulk material, as distinctive in Figure 2-21, where conveyed bulk material is compressed within two belts. Specific systems in which such effects in terms of bulk material compression are explicitly relevant are the belt systems in round hay balers, as explained in Chapter 2.2.5.5 (on Figure 2-27), in which the compressive loads on baled material – provided by the belt – consequently influences obtained bale structures.

Other consequential/related effects

Another effect, which is principally also based on such dynamic/interactive capabilities of belts, is belt breakage. Specific details in that regard can be found in pertinent literature; e.g. in the thesis by Markut (2020) [167] (as particularly related to this thesis, showing a belt breakage analyses with a belt model according to the methodology presented; cf. Chapter 5.7 for a similar example, illustrating the principally enabled breakage capability of a DEM-based belt model).

Chapter 3

General Approaches

The developed methodology for the simulation of dynamically deformable belts in DEM bulk material simulation includes two main methods. The first method regards the modelling technique of general belt-like structures to simulate dynamic belt behaviour in combination with the DEM. The second method refers to the assembling of digital belt models with specific geometries into certain given systems.

General principles of different approaches regarding these two main methods are discussed in the following. Per method, one specific approach is then pursued, thus forming the overall basis of the developed methodology. Further details, building on these specific approaches, are subsequently also described and determined within the methodology's description in the next Chapter 4.

3.1 Approaches for modelling deformable belts for use in DEM bulk material simulations

For the consideration of dynamically deformable belt behaviour in DEM simulations, an appropriate belt modelling technique is fundamentally necessary. In the following,

two general techniques for this type of belt modelling are discussed, accordingly allowing dynamic belt behaviour in principle either by using FEM-based or DEM-based approaches.

For each of these two general techniques, relevant basic modelling approaches focusing in particular on belt-related usage are described, with those descriptions furthermore complemented by respective examples.

In general, it must be taken into account that the relatively large belt deformations and the continuous movements of typically endless conveyor belts during the belt conveyor system's operation lead to an increase in the complexity of such simulations with dynamically deformable belt models. Therefore, all the following approaches for the modelling and simulation of such dynamically deformable belts are accordingly expensive to perform, especially compared to the relatively simple, non-deformable rigid belt modelling technique, as described in Chapter 2.2.3. However, for specific applications, this rigid belt modelling is not sufficient (respective aspects already described in Chapter 2.2.4). Thus, a proper technique for the modelling of belts that are able to depict such dynamic belt behaviour is needed. General approaches in that regard are described in the following chapters.

3.1.1 FEM-based belt modelling

In general, a FEM-based model can be used to allow the consideration of dynamic deformations in numerical simulation. Therefore, respective basics of the Finite Element Method (FEM), in particular for belt-related application, are further outlined as an excursus on uncoupled FEM belt modelling, as given in the next initial subchapter, Chapter 3.1.1.1. Although it does not contain DEM-based bulk material simulation per se, this related (uncoupled FEM) approach is of particular relevance for the subsequent approaches, which are using such FEM-based belt models in combination with DEM bulk material simulation.

The use of a FEM-based belt is the main principle that these subsequent approaches have in common. Besides this general commonality, those approaches are also closely related in regard to the basics for coupling FEM with DEM, specifically for the handling of interactions between a FEM belt surface with DEM bulk particles. Further subdividing aspects relate to software environments / numerical domains,

and specifically to their combinations for allowing particular ways to set up FEM-based belt models accordingly to be used in combination with DEM bulk material simulations.

3.1.1.1 Excursus: On (uncoupled) FEM simulation

The Finite Element Method (FEM), or also termed Finite Element Analysis (FEA), is a state-of-the-art and commonly used numerical simulation method for application continuum mechanics, especially for stress-strain analyses in engineering, with roots reaching back to the 1940s, as historically summarised by Tenek and Argyris (1998) [235]. As the FEM is applicable for the simulation of dynamically deformable bodies as continuous objects, the modelling of conveyor belts using the FEM is principally possible, as described in particular in the examples at the end of this chapter.

In the literature, a lot of work can be found regarding (uncoupled[6]) FEM conveyor belt analyses by a large variety of authors. An early application of FEM analyses regarding conveyor belts was published by Nordell and Ciozda (1984) [188], focused on transient belt stresses during starting and stopping. To simulate three-dimensional belt deflection, Wheeler (2003) [255] developed/applied a numerical method (based on the Finite Difference Method; FDM), which was further also a basis for Couch (2016) [39] in FEM-based conveyor belt analysis (with bulk materials considered as continuum media). Further insightful examples for FEM conveyor belt analyses, with regard to applications that are of interest in the context of this thesis, can also be referred to work by del Coz Díaz, et al. (2007) [49] or Schilling, et al. (2007) [221], both analysing tubular pipe conveyors (as described in Chapter 2.2.5.2). As described by del Coz Díaz, the bulk material loads on a FEM belt model are thereby defined using a load hypothesis according to which manually placed forces/pressures are acting locally on the FEM belt structure.

This uncoupled and thus relatively simple and effort-efficient approach is thoroughly sufficient for some (rather ordinary) applications, particularly when bulk material is not required to be specifically considered, such as when no bulk material is applied at all, or also, when no interactive effects between a belt and individual bulk material

[6] in contrast to coupled simulations (i.e. FEM-DEM), as covered in the next Chapter 3.1.1.2

particles are included (this concerns, e.g., using a manually defined load state to represent a bulk material on a belt, more specifically, the bulk material's weight effects on the belt).

An example herefore, with no bulk material involved, is the FEM simulation and analysis of belt turnover stations as shown in Figure 3-1, which shows the comparison of two different design types for belt turnovers (flat and troughed), presented by Zhang (2017) [264]. Initial work regarding such analyses was also published by Lemmon (2002 and 2009) [157, 158]. Such belt turnovers are used to turn conveyor belts 180 degrees as shown in the designs, and they are typically used at the return strand of a belt conveyor. The belt guidance through such a turning section can be arranged in different variants (e.g. as shown in the figure) to adjust and improve the overall performance of the turnover station. General design guidelines for belt turnovers are, for example, given by Dunlop [67], Goodyear [108], or CEMA [38]. Furthermore, there are several established design types that have been developed over the years, such as Mordstein turnovers (1961) [178, 179], or flat helix turnovers, as also discussed by Lemmon (2002; for Conveyor Dynamics Inc.) [157].

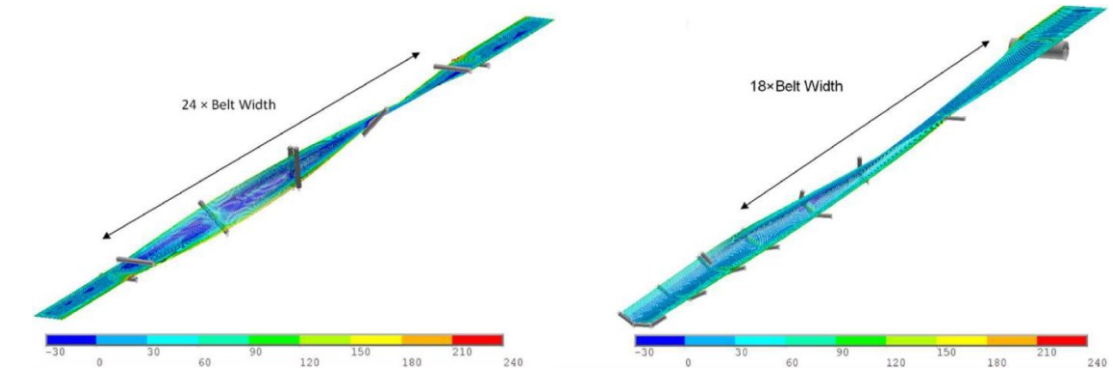

Figure 3-1: Comparison of two different types of belt turnover stations by stress analysis, using a FEM belt model/simulation, adapted from [263]

In Chapter 5.3, an exemplary simulation of such a troughed belt turnover station according to the developed methodology (Chapter 4), using a DEM bonded-particle belt model, as basically described in Chapter 3.1.2, is shown.

Further insights into the modelling of conveyor belts using the FEM is also given, for example, by Fedorko, et al. (2012) [77, 78], analysing force ratios and effects in the troughing (moulding) section and in the area of idler stations of a conventional belt conveyor, and also analysing the interactions of the belt of a pipe conveyor with

troughing (moulding) rolls that are located between the flat and the tubular belt section of this type of belt conveyor.

3.1.1.2 Coupled (FEM-DEM) simulation

According to this approach, a belt can be modelled in an additional simulation environment such as by using the Finite Element Method (FEM), as described in the previous Chapter 3.1.1.1. But to combine such a separate FEM belt simulation with a DEM bulk material simulation, an additional link between those both numerical simulation software environments is necessary. This link in the form of a software interface must provide ongoing data transfer from the DEM into the FEM environment and vice versa. It is accordingly termed two-way or bidirectional coupling. This type of coupling is needed to ensure proper handling of relevant information/data in both directions, from DEM to FEM and also from FEM to DEM.

Unidirectional coupling, in contrast, would allow data transfer in one direction only, which would not allow retroactive effects, as due to interactions between the belt and the bulk material, to be appropriately considered. This type of unidirectional coupling is therefore not suitable for simulations with dynamically deformable FEM belt models interacting with DEM bulk material particles. Nevertheless, a unidirectional coupling could be useful for other purposes, for example, using a one-way coupling from DEM to FEM to analyse loads on rigid FEM objects due to loads from bulk materials. In this context, Figure 3-2 shows a transfer chute simulation, in which Ansys Mechanical [7] is used in combination with Rocky [76] to analyse the DEM particle flow (left) through a FEM-modelled chute with the resulting stresses (middle and right) that are consequently occurring on system parts, such as the chute plates or the steel frame.

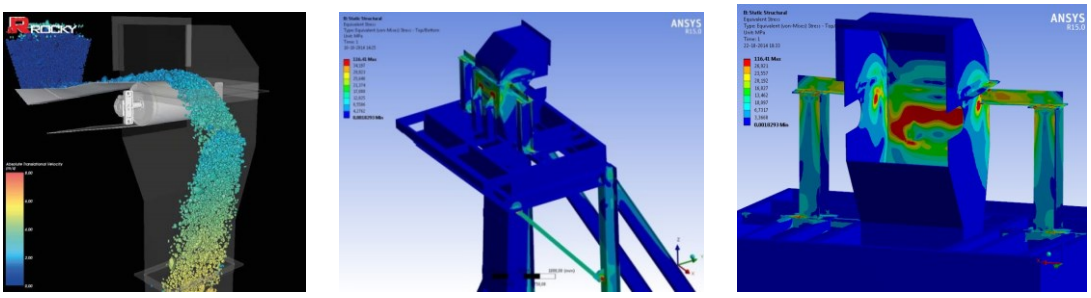

Figure 3-2: FEM-DEM coupling applied for a chute load/stress analysis [20, 216]

The required bidirectional FEM-DEM coupling approach is further divided into two forms, relating to whether a manually implemented software interface is defined or an already existing built-in coupling mechanism can be used. The general basics, which are described in the course of manual coupling, correspondingly apply to built-in coupling mechanisms.

Generally seen, this coupling approach describes a type of multi-physics simulation. Correspondingly, this circumstance is further discussed in Chapter 3.1.1.3, within the description of the approach of using multi-physics simulation software, which generally combines DEM with FEM within one software.

3.1.1.2.1 Manually coupled simulation

For the manual coupling of two separate, and more or less non-related DEM and FEM software environments, an additional coupling interface needs to be implemented, that is capable of handling/transforming relevant data between those both individual environments. This general process, in the form of a data handling cycle, is described and also shown further below, in Figure 3-3.

General methods for FEM-DEM coupling

For the coupling of discrete and continuum methods, as this coupling of DEM with FEM, many approaches for various purposes have been proposed in the literature. Belytschko and Xiao (2003) [18], for example, give insights in such general coupling methods. Particularly decisive for a specific coupling method are the respective details regarding the interactions between the DEM and the FEM, appearing in areas where discrete and continuum elements meet and interact with each other. In this regard, Itasca [131] categorises three forms of coupling types:

- Structural Element Coupling (1D)
- Interface Coupling (2D)
- Domain Bridging (3D)

Structural Element Coupling (1D) extends DEM particles with one-dimensional FEM structures, such as beams or cables. In this context, Interface Coupling (2D) does not refer to a software interface but relates to rigid DEM particles interacting

with FEM elements without overlapping in a DEM-FEM hybrid zone, such as according to Domain Bridging (3D). Also described as overlapping or bridging domain method (cf. [18]), Domain Bridging (3D) is used to consider zones as merged DEM-FEM areas in order to minimise spurious energy discontinuity in specific simulation applications [131].

In applications related to DEM bulk material conveyance with a FEM belt model, as in the context of this thesis, the DEM bulk material particles are impacting on the FEM belt structure as loose particles. Accordingly, Interface Coupling (2D) can be used to set up such a dynamically deformable conveyor belt in combination with a DEM bulk material simulation, which is also applied in a showcase by Itasca [131], described in Chapter 3.1.1.2.2 and shown explicitly in Figure 3-7. By now, Itasca offers a built-in coupling capability to connect their software solutions for DEM and for FEM to be used in one unified program [131], which is why this is described closer in the course of the next Chapter 3.1.1.2.2.

References for developments in FEM-DEM with surface interaction

For the consideration of solid DEM-FEM interactions, which is fundamentally necessary when DEM bulk material particles get in contact with a FEM belt model, various authors described general initial methods and techniques regarding an application in different fields of research. In that respect, Petrinic (1996) [199] published a study on shot peening process simulation using a combination of DEM and FEM, further detailed by Han, et al. (2000) [114, 115]. Owen, et al. (2001) [194, 195] proposed strategies and approaches for using a parallelised DEM FEM simulation in combination to analyse multi-fracture and multi-contact phenomena. The work of Oñate and Rojek (2004) [190] on dynamic analysis of geomechanics problems is further including exemplary applications in which DEM particles dynamically interact with FEM structures, such as DEM modelled rock materials interacting with FEM modelled tools, projectiles or pipes. Nakashima and Oida (2004) [184] combined the DEM and the FEM to solve basic terramechanics problems, specifically dynamic soil-tire contact, whereby the soil is modelled using the DEM and the interacting tire using the FEM. Further corresponding developments are also given by a large variety of authors, for example, regarding specific algorithms and approaches for mathemat-

ical handling of contacts between DEM particles and FEM structures, such as discussed by Lei and Zang (2010) [156] and Zang, et al. (2011) [262], Wellmann (2011) [254], or Khazaeli and Haj-zamani (2016) [144], etc.

FEM-DEM coupling for the purpose of conveyor belt simulation

Extensive research especially focused in the field of conveyor belt simulation based on the approach of manually coupling the FEM with the DEM was done by Dratt, Katterfeld and Wheeler, summarised and published in the thesis by Dratt (2016) [65]; with corresponding details also presented beforehand, such as concerning the prediction of belt deflection (2010) [140] (and further related work). For combining a typical DEM bulk material simulation with a FEM belt simulation, Dratt developed a coupling interface that is capable of bidirectional processing and accordingly exchanging necessary data between the two separate software environments of DEM and FEM. Therefore, Dratt's interface, which is although described in general terms, covers the specific coupling of two DEM software environments, PFC3D [132] and LIGGGHTS [46], each with the FEM software environment of Ansys [6]. For similar applicational setups, and also based on that FEM-DEM coupling approach, Shen, et al. (2018) [224] coupled Rocky [76] (DEM) with Strand7 [230] (FEM) , and also Shen, et al. (2019) [223] set up a coupling of open-source FEM (Code_Aster [72]) and DEM (LIGGGHTS) with a coupling interface programmed in Python [206], in particular for studies on dynamic belt deflection.

The fundamental coupling idea behind the approach (as by Dratt) is based on the correspondence between the smallest selective elements of both methods. For the DEM this refers to the single discrete elements, which are according to Dratt's approach modelled with spherical shape only (non-spherical particles may require appropriate reconsideration), and for the FEM this refers to the finite elements forming the belt model. The principle coupling strategy as a cyclic process with ongoing data exchange between DEM and FEM, according to Dratt (referring in this case to the coupling of LIGGGHTS with Ansys (Classic)), is shown in Figure 3-3.

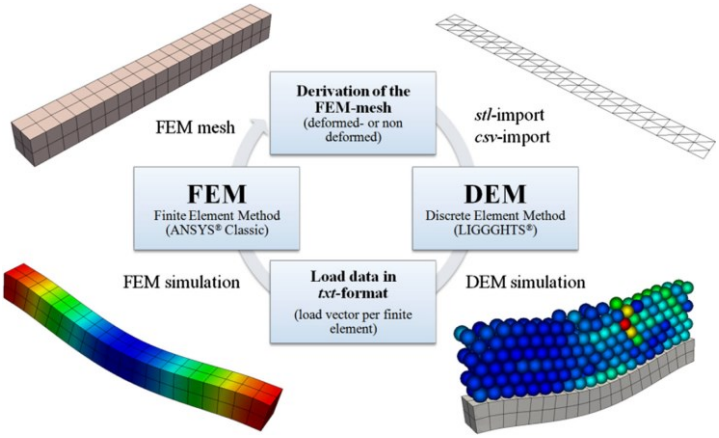

Figure 3-3: Ongoing data exchange loop representing the interface for bidirectional FEM-DEM coupling [63]

Dratt describes the details behind this principle scheme, such as regarding the aforementioned contacts between DEM particles with FEM structures, as illustrated in Figure 3-4. The figure shows DEM particles (top) acting on a FEM structure (bottom) via a derived STL-surface (middle). During the cycle, the geometry of the STL-surface gets accordingly updated, depending on the loads coming from the DEM particles.

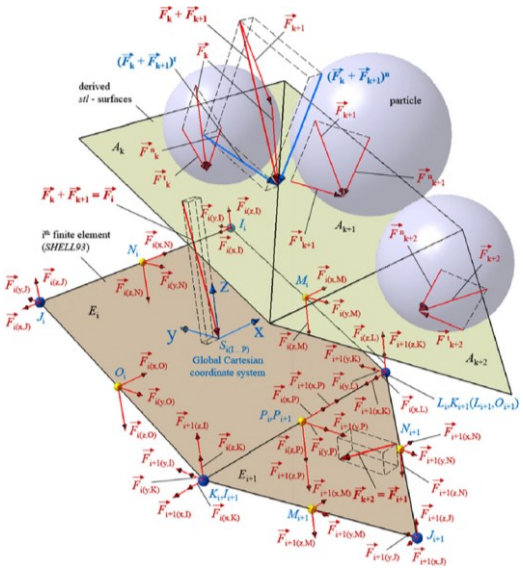

Figure 3-4: Particle-structure contact mechanisms in coupled FEM-DEM [63]

To illustrate the capabilities of the DEM-FEM coupling, especially using this mentioned coupling interface, Dratt simulated/analysed an exemplary section of a conventionally troughed conveyor belt, as shown in Figure 3-5.

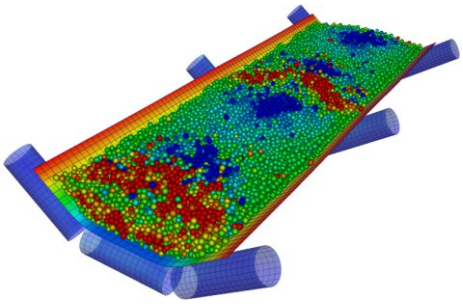

Figure 3-5: Bulk material on a troughed belt model with coupled DEM-FEM [65]

At this relatively simple section, Dratt discusses various aspects that could be of interest for using this simulation technique, such as for studies on belt deflection (belt deformation), bulk behaviour at idler stations, or flexure resistance due to the deformable belt. For example, Dratt highlights the vertical (and side) movements/accelerations of bulk material particles at idler stations due to occurring belt deformations, as visualised in Figure 3-6.

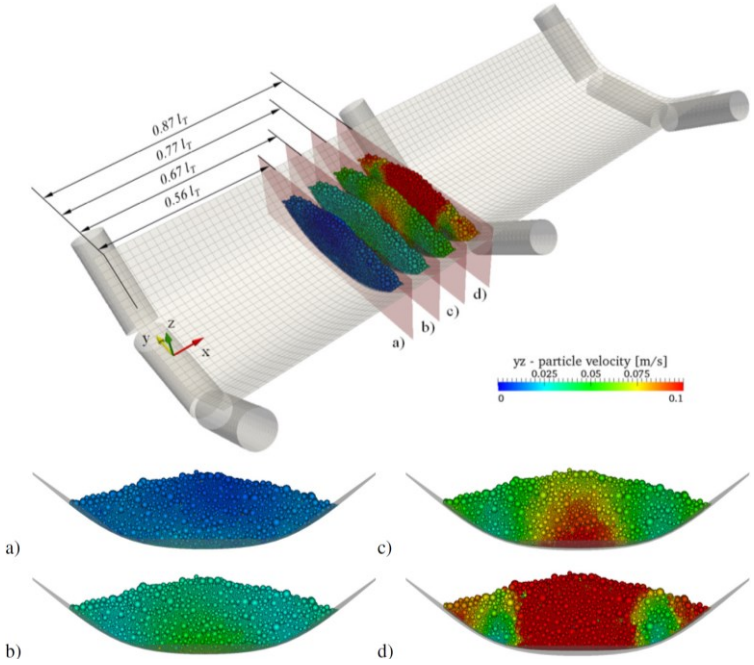

Figure 3-6: Analysation of relative bulk particle movements (yz velocities) in four sequential sections before the idler station of a troughed belt conveyor [64] ([65])

In this analysis, the belt is moving from left to right (in positive x-direction), and as can be seen, the bulk material is accelerated upwards (in positive z-direction; corresponding to negative gravity vector) right before the idler station. Actually, this operating condition is comparable to a quasi-static state but to obtain the deformed belt

geometry under specific load conditions (with certain bulk material loading, belt speed and belt tension), such a deformable belt modelling approach is necessary. The determination of this belt deformation without considering a bidirectional interaction between the belt and the bulk material would not be possible.

3.1.1.2.2 Built-in coupled simulation

The principles of this coupling technique are similar to those described in the previous Chapter 3.1.1.2.1, but instead of manually coupling two independent software packages, enhanced software with existing coupling mechanisms is used. Therefore, it is required that the two software programs are able to be coupled with each other, such as by using an additional superordinate software platform, for example, in the form of a data managing software workbench providing this coupling capability. Manual implementation of additional coupling interfaces, as according to the approach in Chapter 3.1.1.2.1, is thus obsolete.

Some software packages, often in the form of platforms or workbenches that comprise several subordinate software modules, offer pre-implemented coupling capabilities, which eliminate the need for manual implementation of additional interfaces. In this regard, Itasca [131], as already mentioned in the previous Chapter 3.1.1.2.1, allows three variants of FEM-DEM combination with a built-in coupling mechanism.

In Figure 3-7, a showcase by Itasca illustrates one of these variants, Interface Coupling (2D), to simulate a dynamically deformable FEM conveyor belt with DEM bulk material particles in one software program [131]. In this case, PFC3D [132] for DEM and FLAC3D [130] for FEM, both at version 6 by Itasca, are coupled using this coupling mechanism.

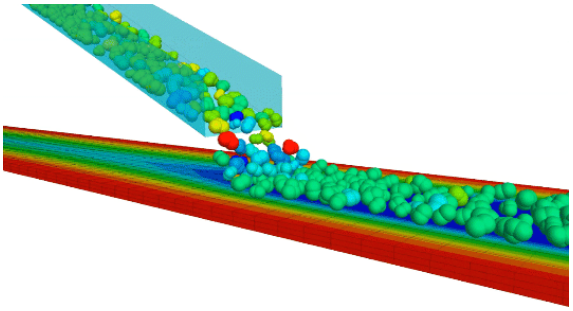

Figure 3-7: Built-in FEM-DEM coupling for loading bulk particles on a belt [131]

The application shows the dynamic interactions of a moving FEM belt model with continuously loaded DEM bulk material particles. The bulk material particles are deforming the belt, resulting in the belt sag as indicated with colour. Also, the bulk material particles are affected by the local belt deformations, but due to the relatively small belt deformations that are occurring, these retroactive effects on the bulk material particles are correspondingly small. In a dynamic analysation of this application, these effects are apparent from small relative particle movements along the conveyor belt, which are resulting from the belt's dynamically deformable behaviour. In contrast, with a rigid belt model (according to the technique described in Chapter 2.2.3), these effects would not be present.

Another example with an analogous reference is shown in Figure 3-8, in which the dynamically deformable FEM structure corresponds to a protection net in rockfall simulations. In this showcase by Itasca, the boulders (represented by complex-shaped particles) are moving down a hillside towards a barrier, which impedes the rockfall. The distinct deformations of the barrier, resulting from the impacting boulders, are shown and indicated in colour.

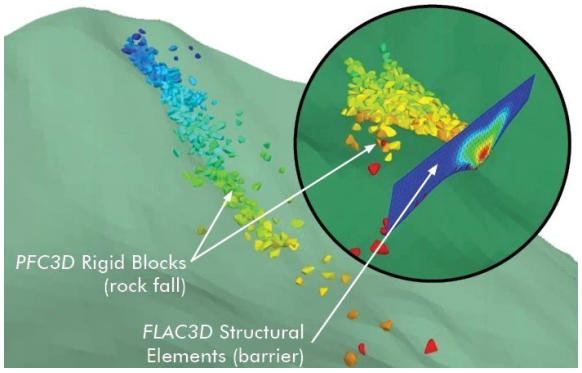

Figure 3-8: Built-in FEM-DEM coupling for the simulation of a rockfall protection net interacting with impacting boulders [131]

Besides Itasca, other software packages are also available, which in principle allow the ability to couple DEM and FEM by means of a built-in coupling mechanism. Such a coupling is available, for example, using the Ansys Workbench [6], in which the Ansys FEM module Ansys Mechanical [7] can be coupled with the DEM software Rocky [76]. In Figure 3-9, a coupling structure, set up in the Ansys Workbench, is exemplarily shown. In this case, the DEM and the FEM modules can be seen as

boxes with interconnecting lines that are representing the built-in coupling mechanism. The highlighted box in the centre is corresponding to the DEM module (Rocky) and the box to its right to the FEM module (Ansys Structural Analysis).

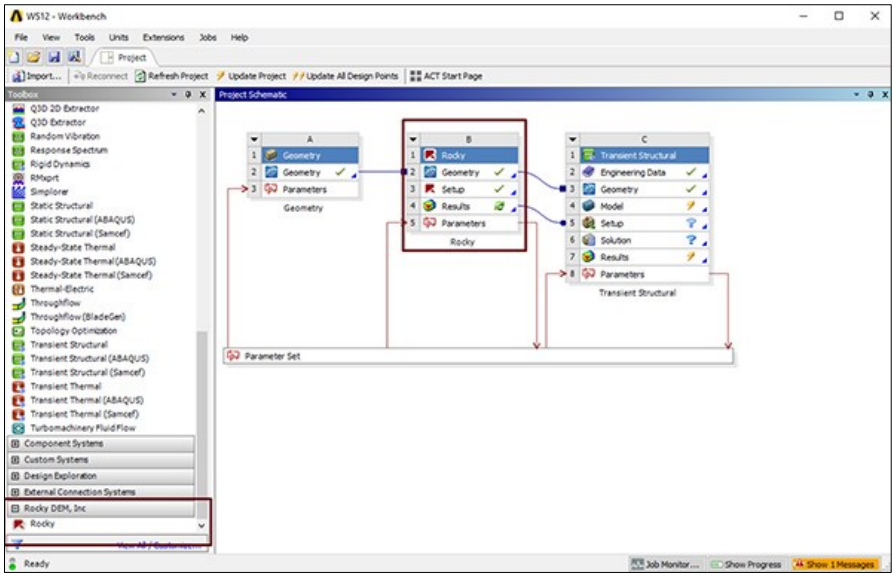

Figure 3-9: FEM-DEM coupling within the Ansys Workbench using the built-in mechanism to link Rocky (DEM) with Ansys Structural Analysis (FEM) [220]

A representative example for applying an existing coupling solution on a generally neutral base is using the software MpCCI [102] (by Fraunhofer SCAI), specifically in a DEM-FEM coupled simulation (co-simulation) with SimPARTIX [101] (for DEM) and Abaqus [44] (for FEM). Belt-relating showcases in this context are in particular presented by Bierwisch, et al. (2016) [25], for example, the elastic FEM-based panel interacting with DEM-particles shown in Figure 3-10.

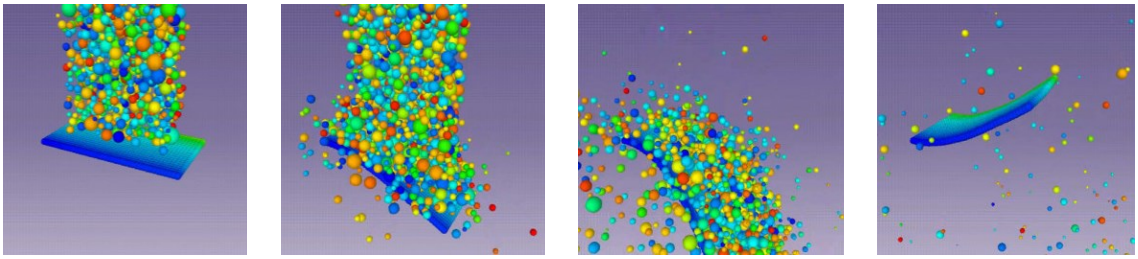

Figure 3-10: DEM-FEM co-simulation of particles falling on an elastic panel clamped on the left edge; adapted from [25]

Another different model setup of an elastic membrane, also with this DEM-FEM co-simulation scheme, is shown in Figure 3-11. In contrast to previous models, the surface of this membrane model is represented with multiple DEM-particles, which are linked to the mesh nodes of the base FEM model; those particles are responsible for the contact handling with additional particles. Also, this multi-particle structure is in its appearance generally comparable to later-described bonded-particle structures (affiliated to DEM-based modelling, Chapter 3.1.2), specifically regarding membrane-representing models as described in Chapter 3.1.2.3.1 and as shown in Figure 3-23, etc. (but with those DEM-based models accordingly not based on coupling).

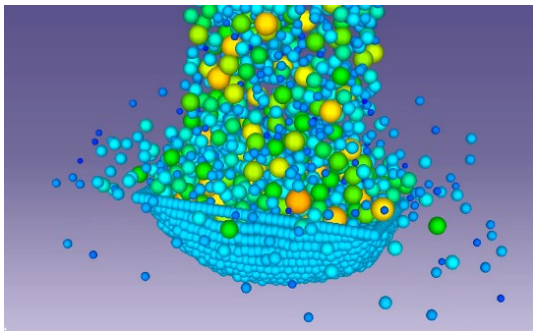

Figure 3-11: DEM-FEM co-simulation of particles falling on an elastic FEM-based membrane, modelled with particles linked to the nodes of the FEM mesh [103]

3.1.1.3 Multi-physics simulation

According to this approach, an enhanced software environment can be used, that is capable of a particular type of multi-physics simulation. In detail, this specific approach allows the modelling, simulation and analysis of a belt structure in parallel to DEM bulk material particles within a uniform software environment. This approach and its basics are generally related to the coupling approach as described in Chapter 3.1.1.2, but because of the already pre-implemented capability to combine the DEM with the FEM within one software environment, there is no further need for an additional coupling mechanism. As in the coupling approach, a FEM-based model is representing the belt structure. Such a belt model is thus not directly related to a DEM-structure (which would be the case for a DEM bonded-particle structure, as described in the next Chapter 3.1.2). As a basis for this approach, appropriate software is required, which is capable of handling both numerical domains, DEM and FEM, within

a uniform software environment. And as also similar to the coupling approach, especially the handling of the interactions between the DEM particles and a FEM-structured belt is fundamentally crucial.

As described in the following, this multi-physics approach can further be seen subdivided, according to whether the primary focus/purpose (and therefore the basis) of the considered software environment is either set on the FEM or the DEM. In this context, the approach of using FEM-based software with advanced capabilities regarding DEM is further termed DEM-in-FEM. Respectively, FEM-in-DEM relates to the approach of using DEM-based software with advanced capabilities regarding FEM.

Combining several physical phenomena, which are also assigned to different physical domains, in one numerical simulation generally describes the terminus multi-physics, such as according to Peters, et al. (2015) [198] (describing a specific discrete/continuous numerical approach to multi-physics, referred to as XDEM). Such phenomena can refer to, for example, aspects related to various areas of classical mechanics (as already mentioned in the context of the DEM and FEM) but also to further fields, such as thermodynamics, chemical processes, fluid dynamics, electrics, etc. From this point of view, the coupled approach as in Chapter 3.1.1.2 also corresponds, more precisely termed, to a coupled multi-physics approach. In contrast to that, the following DEM-in-FEM and FEM-in-DEM approaches require a uniform multi-physics simulation software instead of the coupling of two separate software environments, each specialised in a specific domain. As an excursus on such general multi-physics simulation software, a short illustrative overview on this topic, including some exemplary applications, is also given by Picciotto, et al. (2020) [200] using the software platform Simcenter STAR-CCM+ [225] (by Siemens PLM Software), which is also including DEM and FEM in principle. However, as the primary focus is set on Computational Fluid Dynamics (CFD), multi-physics in combination with fluid simulation methods are primarily intended in the case of this specific software, as also illustrated by Picciotto, et al.. In this context of combining methods (besides the already referenced XDEM and the subsequently outlined FDEM (Chapter 3.1.1.3)), also the Particle Finite Element Method (PFEM) (e.g. explained by Cremonesi, et al. (2020) [41]) can be mentioned, which combines FEM-based with particle methods, introduced initially to deal with free-surface fluid flows and fluid-structure interactions.

DEM-in-FEM

As described in Chapter 3.1.1.1, a belt model can be set up as a dynamically deformable structure in a FEM software environment. According to this DEM-in-FEM approach, an extending feature, such as an additional DEM software module, can be used to additionally model/simulate DEM particles within such a FEM-based software environment. This enhances the simulation to a specific type of multi-physics simulation, which fundamentally requires appropriate software, that is capable of handling specific discrete methods (according to the DEM) in parallel to continuum methods (according to the FEM). In principle, this allows the simulation of FEM belt models in combination with DEM bulk material particles within one environment.

Abaqus [44], for example, allows such a DEM-in-FEM simulation, as applied in the belt-related application published by Zheng, et al. (2017) [265], analysing effects of pipe conveyor belts loaded with granular bulk material. In Figure 3-12, the analysed cross-section of this application is showing the resulting transverse belt stresses (in Pa) of the simulated FEM belt model on the left, and the apparent normal forces on the DEM particles (in N) on the right. The simulation shown was performed with specific material data (regarding belt and bulk material parameters) at a given volume filling level of about 80%, as can be seen.

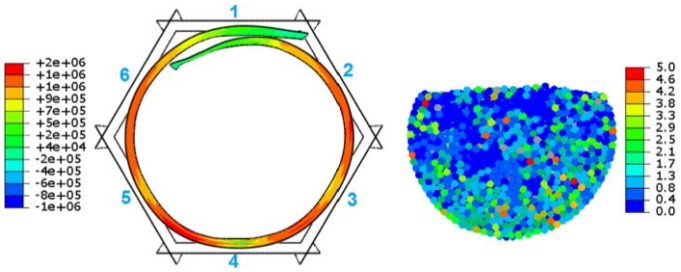

Figure 3-12: A (FEM) pipe conveyor belt filled with (DEM) bulk material particles, modelled and simulated using Abaqus (DEM-in-FEM multi-physics) [265]

FEM-in-DEM

The FEM-in-DEM approach describes the expansion of a DEM-based software towards the FEM. Therefore, this approach is similar to the above described DEM-in-FEM approach, as both their general basics relate to using one single multi-physics software environment, but for FEM-in-DEM, the focus of the base software is set on DEM simulation. Consequently, the fundamental software aspect, requiring specific

capabilities regarding the appropriate handling of FEM structures in combination with DEM particles, is also similar.

According to the FEM-in-DEM approach, specific FEM capabilities are enabled within a DEM-based software with extending features that allow an additional modelling/simulation of FEM-based objects in parallel to the DEM particles. Such objects can either be in the form of common FEM-based parts but also in the form of enhanced particles enabling certain FEM capabilities (FEM-based particles). If such a FEM-based object is further able to act deformable, it is principally conceivable to use this FEM part/particle to represent a dynamically deformable belt within the DEM-based multi-physics environment.

The implementation of FEM-based parts is principally allowed, for example, with ThreeParticle/CAE [17] (as a DEM-focused multi-physics software environment). This specific ability is meant to be used mainly for considering small and linear-elastic deformations of otherwise rigid walls, such as (relatively small) deformations of steel plates/frames due to certain bulk material loads (as in similar form also shown in Figure 3-2, using a coupling approach for that purpose).

The use of FEM-based particles (cf. models) in DEM simulations also relates to a method termed as combined Finite-Discrete Element Method (FDEM), as described by Munjiza, et al. (1995, 2004) [181, 183]. Also, as by Munjiza, a typical application for the FDEM is the simulation/analysis of masonry structures, in which FEM stone bricks are handled as DEM particles. An exemplary demonstration of the FDEM approach, which can be seen as relating to belts, is shown in Figure 3-13 recently published by Munjiza, et al. (2020) [182], showing a stability analysis of an FDEM shell-modelled cylinder under compression, resulting in buckling effects.

Figure 3-13: FDEM approach applied for the modelling of a cylindrical object (FEM-based/relating shell structure) [182]

In general terms, the FEM-in-DEM approach of modelling a FEM object for use in a DEM-based multi-physics simulation, particularly in the form of a deformable FEM particle, corresponds basically to aspects of this FDEM approach.

Although mentioned here (as it can be categorised relating to FEM aspects in general), this approach already shows affiliation with the following DEM-based modelling approach. (Using an enhanced flexible particle structure, for example, is further covered in Chapter 3.1.2.4.3.) Therefore, this concluding chapter of FEM-in-DEM connects to the next general chapter (3.1.2) describing DEM-based modelling; especially as the detailed mechanics within the following DEM-based structures to represent deformable DEM-based objects (with related methods, e.g. using bonded-particles) can also be seen as principally relating to FEM basics (as described in Chapter 2.1.2.6.1).

3.1.2 DEM-based belt modelling

Setting up dynamically deformable belt models entirely within a DEM environment, specifically by using complex-deformable DEM structures (as bonded particles), generally characterises this DEM-based belt modelling approach. Based on methods common for the DEM, such as using DEM particles and bonding elements (as described in the DEM basics in Chapter 2.1), this modelling technique represents a principal contrast to FEM-based belt modelling approaches (as covered in the previous Chapter 3.1.1). And as an uncoupled DEM approach, this DEM-based belt modelling consequently does not require additional extensions of the DEM to further specific FEM environments, neither via coupling interfaces/mechanisms nor by using some of the earlier outlined multi-physical approaches.

3.1.2.1 Belt model setup as a bonded particle (BP) belt

As also described closer in the following chapters, the main principles of this DEM-based belt modelling approach generally refer to using particle-based belt models. Furthermore, the modelling of such belts in this context is principally also based on using bonding elements (or at least bonding-related mechanisms). Those are essential, as they enable the fundamentally required capability of such a particle-based belt

model (thus resulting as a bonded-particle structure) to allow dynamically deformable behaviour. Therefore – as set up as a bonded-particle model (BPM), consisting of a multitude of specifically bonded particles – such a belt model can be referred to as a bonded-particle belt (BP belt).[7]

Relevant basics regarding this modelling approach are described by insights into the setup/usage/purpose of BPMs, introductory from a more general perspective, such as to be applied for deformable fibres, etc. (in Chapter 3.1.2.2); followed by applications specifically for belt-related purposes (in Chapter 3.1.2.3). Furthermore, aspects and techniques for resolving surface-related issues are introduced (in Chapter 3.1.2.4), specifically explaining general techniques for smoothing the surface of a BPM, which is otherwise typically resulting as macroscopically rough.

As an anticipatory note: This general approach of using BP belts, thus belt models consisting of a multitude of bonded particles, constitutes a central core element of the developed methodology as presented in this thesis. Therefore, more specific details on the structural setup of such belt models (according to the developed methodology) are further elaborated in Chapter 4.1.

Further initial aspects

As introduced, a BP belt is modelled by using a structure of multiple, specifically bonded particles. Such a BP belt is thus capable of representing dynamically deformable behaviour – but also further belt-related characteristics, such as belt-mass-related aspects, surface properties, stress-strain behaviour, or even breakage capabilities, are principally depictable by using this bonded-particle belt modelling technique.

As also already addressed, such BP belts consist of two main components, which are in combined form responsible for the resulting overall behaviour of the belt-representing model, such as to allow the characteristics mentioned above: (DEM) particles, in this context termed belt particles, and bonding elements (bondings), which are connecting those belt particles. Each with their specific details, the belt particles

[7] in previous publications also referred to as Discrete Element belt (DE belt; as particles correspond to discrete elements), cf. references in Chapter 1.5 (from a further perspective generally presenting a particle-based belt model)

and the bondings are defining a BP belt fundamentally. Thereby, the belt particles are generally responsible for geometry-related aspects, such as representing a belt's surface, whereas the bondings are generally responsible for the behaviour of the belt in terms of deformability, such as regarding stress-strain (load-deformation) behaviour.

Side note on the numerics of bondings: From a certain point of view, DEM bondings refer to a type of FEM-based submodel, which has been established as a common element to be used in the DEM. Therefore, this bonding technique for connecting DEM particles (as non-static particle-particle-linking) can be categorised accordingly as a method corresponding to the DEM. In general, however, this type of connection can also be referenced to a simple (one-dimensional) beam element as typical for FEM simulations. This circumstance can also be concluded from the descriptions given in the DEM basics for bondings in Chapter 2.1.2.6.1.

3.1.2.2 Bonded-particle models (BPMs) in general

For the modelling of a general bonded-particle model (BPM), multiple particles are positioned and further connected to each other in a specified way to result in an assembly of bonded particles as desired. The connections used for that purpose are defined by bonding elements, where every single bonding within the structure connects exactly two particles via a virtual beam element. (The essential basics behind bondings are respectively described in Chapter 2.1.2.6.1.).

Such BPM are thus able to represent advanced capabilities, such as deformation or breakage under certain conditions. In general, typical applications of such models refer to, on the one hand, the modelling of complex DEM particle-conglomerates to represent advanced material characteristics, and on the other hand, also to the modelling of specific system components. In the following, some representative examples herefore are addressed to provide insights into the use/purpose of such BPM in general. As the focus for using this modelling technique is specifically set in the context of DEM-based belt modelling, belt-related bonded-particle applications are covered explicitly in the subsequent Chapter 3.1.2.3. Thus, the following introductory applications for material setups and system components as BPM (asides from the mentioned belt-related applications) are outlined more briefly with the purpose to give a general overview regarding the intention/scope/usage of BPM.

3.1.2.2.1 BPMs for handled/processed materials

Using BPM in a handled/processed material-related context is typically applied with the purpose to add breakage and/or deformability (such as bending) capabilities to certain material setups. These material setups concern either forms of unified structures or also particle conglomerates in bulk materials.

Fracture

Allowing structures consisting of a multitude of bonded particles to break with specific characteristics is a basic intent of using bondings. This concerns, for example, typical fracture-related applications in the field of rock mechanics, such as presented by Potyondy and Cundall (2004) [203] describing a bonded-particle model for rock, and similar applications in related areas, such as in mining or process engineering. In this regard of modelling fracturable brittle materials, the application in Figure 3-14 by Gupta, et al. (2017) [112] illustrates breakage effects within a coal-representing sample. The sample is set up as a BPM showing a distinctive breakage behaviour under compressive load.

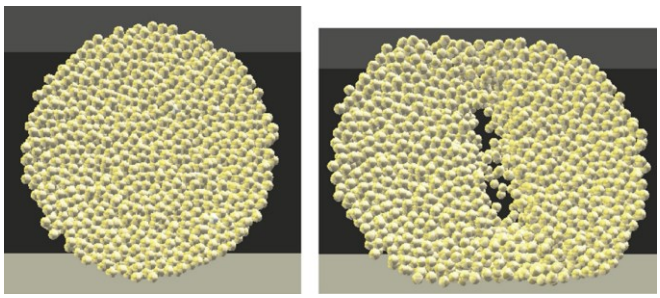

Figure 3-14: Fracture of a bonded-particle model under compressive load (known as Brazilian Test; intact (left) and broken (right) sample state) [112]

There are several advancements for this general purpose of modelling fracturable brittle material setups (such as rock masses and similar materials) principally applicable, as concerning, for example, further adapted bonding or complex particle models (see Chapter 2.1.2.6.1 for relating basics), as can also be found in pertinent literature (e.g. by Lisjak and Grasselli (2014) [159]).

In addition to the generally addressed rock-related usage, some more-specific use of a BPM for depicting a fracturable (brittle) material also relates to applications with

mechanically induced breakage, such as cutting and drilling processes (e.g. as shown by Yang, et al. (2020) [259], and by Ubach, et al. (2016) [243]), or applications with multi-material/multi-layer setups, such as damage effects in coatings (e.g. as shown by Ghasemi and Falahatgar (2020) [105]). Applications as those concern primarily setting up unified structures as BPM.

Furthermore, the modelling of complex bulk material setups consisting of individually breakable particles as particle conglomerates is further enabled by using many separated BPMs, each allowing breakage. In such complex bulk material setups, each conglomerate as a BPM holds the capability to break into smaller subfragments under certain load conditions (whereby the subfragment size is limited by the sub-particles forming the BPM). For the same coal-relating application shown above in Figure 3-14, Figure 3-15 shows several bonded-particle conglomerates, each representing one coal particle as a BPM that is thus capable of breaking individually.

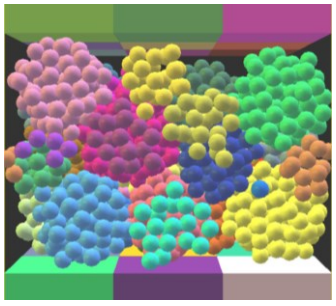

Figure 3-15: Bulk material consisting of breakable particles; modelled as several BPM, each allowing breakage [112]

Using bonded-particle modelling is thus an approach that allows particles within bulk materials to break individually – and specifically, such as depending on local conditions within a BPM. Another general approach for that purpose of particle breakage representation is using particle replacement, as described by de Bono and McDowell (2016) [47] in terms of particle breakage criteria (and in an early attempt applied for two-dimensional packing by Åström and Herrmann (1998) [8]). According to this approach, an individual particle is replaced with several smaller particles when a defined breakage criterion is met. Therefore, suitable definitions for replacing the particles and for breakage criteria are essential prerequisites. In comparison, this approach, on the one hand, reveals positive aspects in terms of computation efficiency, as fewer elements (particles/bondings) need to be computed in general. But on the

other hand, using BPMs for the modelling of breakable particles shows advancements in terms of allowing the depiction of certain (complex) effects, such as crack propagation or other specific breakage effects, such as local load-depending or even partial fracture.

Side note: To enhance the use of BPMs, some advancements may also be applied, such as disabling redundant contacts (contact detections), especially within BPMs. For example, as available in ThreeParticle/CAE [17] (by disabling self-contact for a BPM), this option has the effect that other forces than those from bondings are omitted (other forces as from particle overlaps within a BPM conglomerate, resulting from common contact models). Consequently, only bonding-related forces are computed for a respective BPM; inner particle contacts are ignored, leading to enhancements in computational terms. (This technique is further described in terms of the particle-related belt setup in Chapter 4.1.1.2.)

Typical applications in which bulk particles need to break into smaller fragments under certain load conditions are crushers and mills. Representative examples herefore with using BPMs as breakable particles in bulk materials are shown by Cheng, et al. (2020) [32], modelling a cone crusher for ore mineral processing, or also by Patwa, et al. (2016) [196], simulating the wheat milling process with wheat kernels modelled as BPMs.

In belt-related terms, such breakage mechanisms of a BPM apply to include breakage behaviour of an accordingly modelled belt structure, such as further shown in the belt breakage analysis application in Chapter 5.7.

Deformability/Flexibility

Besides such breakage reactions, bondings are furthermore able to react with deformations to certain load conditions. Basics in that regard are also introduced in Chapter 2.1.2.6.1, describing the setup of a single bonding element as a deformable beam. In the context of this thesis, these deformation characteristics of bondings are especially essential, as those fundamentally allow the representation of a belt as a flexible, and thus under load deformable, DEM-based structure (corresponding to a deformable BPM).

From a more general perspective, deformable BPMs are commonly applied to add forms of deformability to solid material setups. Regarding the modelling of handled/processed materials, such deformable BPMs are, for example, used to set up fibrous structures or to add certain deformation capabilities to complex BPMs, such as to combine initial deformability with subsequent breakage.

A relatively simple and thus common technique for modelling a flexible fibre as a BPM is to use single-line arranged bonded particles to represent such a flexible fibre, as illustrated by Guo, et al. (2013) [111] in Figure 3-16.

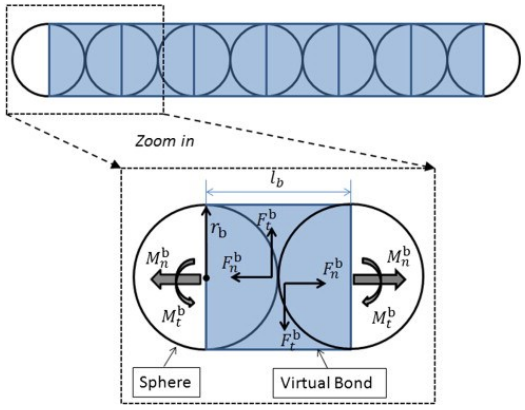

Figure 3-16: Setup of a flexible fibre model consisting of single-line arranged bonded particles [111]

Guo also performed validating tests for applying this modelling technique, specifically by comparing basic deformation tests (bending, stretching, twisting) with analytically determined results (acc. beam theory). Respectively, Figure 3-17 shows a fibre model in a bending test, in which one end of the fibre is fixed (left particle), and the following, via bondings connected particles sag due to the applied transverse load (F_t^0) on the other end of the fibre (right particle). The resulting deformation (y_0), as well as the fibre setup as a BPM consisting of single-line arranged spherical particles, are clearly distinctive.

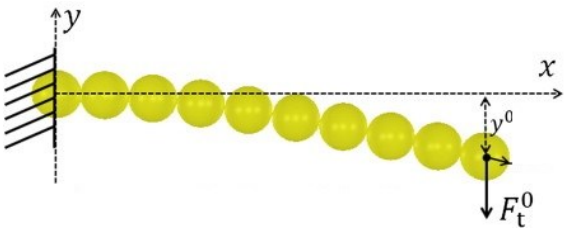

Figure 3-17: Deformed flexible fibre model in a bending test, adapted from [111]

Such BPMs for fibrous structures are further applied in numerous publications, for example, by Bergström (2018) [21]. From a field-related perspective, many applications in which the handled/processed materials consist of fibres can be associated with the agriculture industry; respectively referring to various stalk goods, such as hay/straw. Kemper, et al. (2014) [142], for example, uses a BPM for the purpose of simulating the mowing process with a rotary mower. The breakage of bondings that follows their initial deformation is thus essential in applications such as these. As a reference regarding the modelling of natural fibres using a BPM with a higher level of resolution, thus not in a single-line arrangement, Sadrmanesh and Chen (2018) [218] presented work on the tensile behaviour/failure of hemp fibres. More complex applications of using BPMs in the field of simulating agricultural goods are shown by Wang, et al. (2020) [251], modelling branched BPMs for simulating grain threshing, and further by Kovács, et al. (2017, 2018) [146, 147], modelling corn/maize stalks as complex and even inhomogeneous BPMs, including deformation and breakage capabilities. The distinct deformation of such a complex stalk-representing BPM before its breakage, thus representing the relatively tough cutting process of a flexible maize stalk, is illustrated in Figure 3-18. As a representative example, this application highlights the deformation capabilities of BPMs in general.

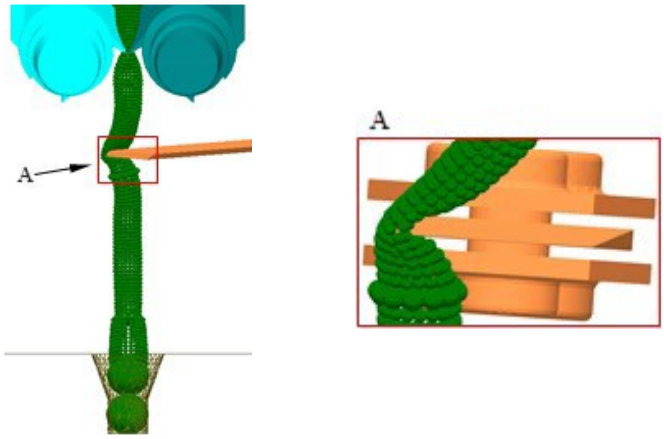

Figure 3-18: Deformation of a BPM representing a maize stalk, showing distinctive deformation before breakage (maize harvesting process simulation) [147]

More examples of selected potential use cases with deformable/breakable fibre models set up as BPMs are also given in an overview by Rocky (2020) [214], showing further exemplary media to be modelled, such as hair, barley, cotton, or even branched woods, as for simulating wood chipping processes.

These deformability/breakability characteristics – so far described in terms of modelling handled/processed materials, such as to allow particle conglomerates in bulk materials to deform/break under certain load conditions – already indicate the main principles for setting up DEM-based belt models (as BPMs). In general, the modelling of system components as BPMs (covered in the following chapter) is allowed by applying these principles on such typically larger-scaled components. This also comprises conveyor belts, which are thus capable of interacting/deforming dynamically. In that regard, and specifically referring to such a belt model as the central model concerning this thesis (see Chapter 4.1), the single-line fibre model, as shown in Figure 3-16, is explicitly emphasised, as the respective belt model can principally be referenced to an assembly of multiple fibres in a parallel arrangement. This aspect is also described in Chapter 4.1.2.3, specifically concerning the purpose to depict anisotropic belt behaviour.

3.1.2.2.2 BPMs to represent general system components

Before specific belt-related usage of BPMs is discussed (in the following Chapter 3.1.2.3), an initial overview of using BPMs for other, more general system components is given; belts furthermore represent a particular type of system component with specific behaviour/characteristics.

The basics for modelling various system components as BPMs generally follow the same principle and purpose as already explained in the previous section regarding handled/processed materials, specifically enhancing initially rigid models towards deformation and optionally breakage capabilities. In contrast, this applications concerns the modelling of system components, i.e. typically mechanical parts, which are not relating to handled/processed materials (such as rock structures or bulk materials). By applying this modelling technique on walls or similar boundary surfaces, such can principally be modelled as BPMs, consequently allowing respective characteristics as already stated (in contrast to common rigid DEM walls, described as parts in the DEM basics in Chapter 2.1.2.5, and as used according to the rigid belt modelling technique, described in Chapter 2.2.3). Since bonded-particle walls, especially with planar geometry, already refer to the modelling of belt-like objects, such are accordingly covered in the following chapter concerning belt-related BPM mod-

elling. Besides these later discussed belt-related components (e.g. including membranes and nets), further general system components, which are principally conceivable for the modelling as BPMs, may also include arms, beams, levers, etc. A common aspect of using BPMs to represent such system components is typically to enable deformation capabilities.

As an illustrative example for using BPMs for such general system components, Figure 3-19 shows a flexible cantilever beam as a BPM (by Obermayr (ed.), in [244], using Pasimodo [121]; based on Obermayr, et al. (2013) [189]). The structural setup of a model like this is principally also comparable to a parallel arrangement of several single-line fibre models (as described in the previous section; cf. Figure 3-16), where each fibre is also bonded to its adjacent fibres, resulting in a three-dimensional truss-structure-like bonding network.

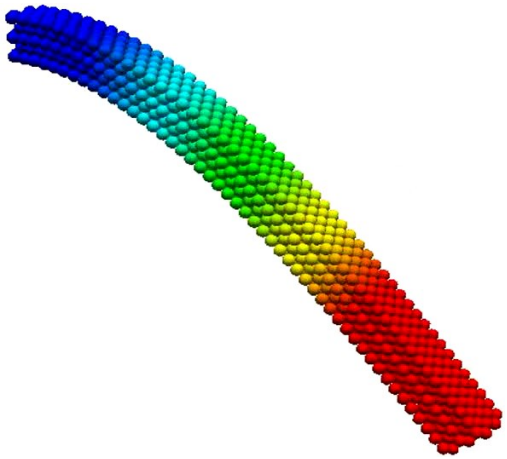

Figure 3-19: Cantilever beam as a BPM in bent state (deformation due to own weight, with the left end of the beam fixed) [244]

This specific beam model is made from regularly arranged close-packing particles. Amongst various others, similar beam applications were also published by Wang (2020) [249], analysing damping/oscillation effects of a similar beam model (ref. simple rectangular/cubic packing), or also by Wolff, et al. (2013) [256], applying a three-/four-point bending test on a beam model with particles in random packing.

Side note on proofing bonded-particle modelling: Evidence for the suitability of BPMs in terms of representable behaviour, specifically regarding dynamic deformability/flexibility, has been shown by several authors, particularly on such beam models, such as by proofing correlations of the DEM models (BPMs) to corresponding

FEM models or analytically determined results. Further details in that context can also be found in respective/referenced literature, exemplarily referring to Irazábal, et al. (2017) [123] (anticipating following contents of rock protection system modelling; showing such correlations using single-line BPMs, which are basically also relating to fibre models as shown previously, cf. Figure 3-16) or Guo, et al. (2013) [111] (as mentioned in the previous section, Figure 3-17; using analytically determined results for BPM validation purposes).

A more complex beam application with a heterogeneous BPM to represent a complex-structured reinforced concrete beam under four-point bending, including deformation as well as failure, is further shown by Karajan, et al. (2014) [139] (using LS-DYNA [160]). Figure 3-20 highlights the inner reinforcement structure inside this beam, modelled as an embedded BPM within the concrete-representing BPM; the figure also indicates the resulting local reinforcement conditions due to the applied load.

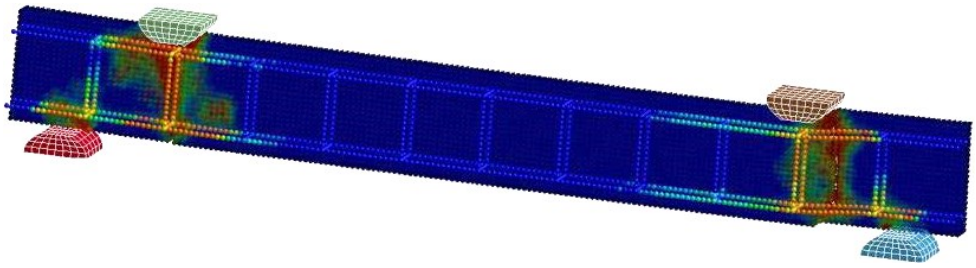

Figure 3-20: BPM of a reinforced beam under 4-point bending [139]

A different application representative for using several BPMs as multiple interacting system components resulting in an overall deformable setup was shown by Zhu, et al. (2019) [266], modelling a flexible ring net barrier for rockfall protection. In Figure 3-21, the basic model setup, made from several relatively simple single-line arranged BPMs, e.g. forming the interlocking rings, is shown (left), as well as the resulting deformations at the impact of a boulder, which is represented by a single relatively large spherical particle (right).

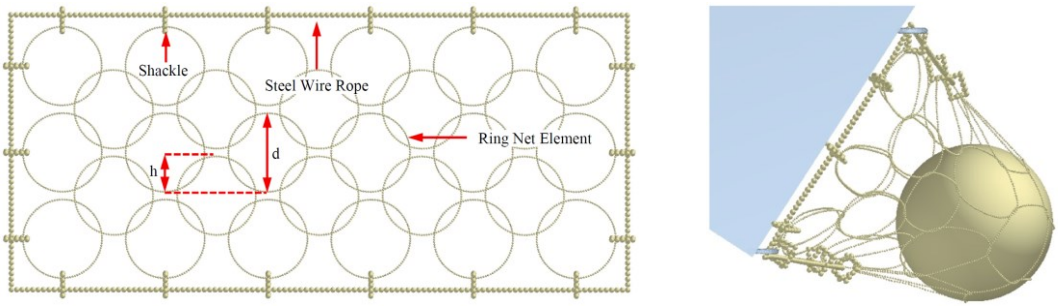

Figure 3-21: Ring net barrier, modelled with several BPMs (left; consisting of rings, shackles and a wire rope), and its deformation at boulder impact (right) [266]

Further potential applications for using BPMs as more complex types of system components are, for example, spring/damper components, such as vibration/shock absorbers, or various forms of brushes, where especially the bristles qualify for the modelling as flexible fibres (e.g. for cleaning processes with brushes including complex behaviours, such as regarding brush-bulk material interactions).

3.1.2.3 Bonding-based modelling approaches for belt-related applications

Commonly, belts as specific types of system components typically are flat geometries, which are, in contrast to various other system components, typically capable of reacting relatively flexible, especially in terms of bending. Therefore, belts and similar components (as relating to these mentioned characteristics; e.g. membranes, nets) are potential objects for using a bonded-particle-based modelling technique, specifically when belt-typical flexible/deformable behaviour is required to be represented by a DEM-based model.

As a notable introduction specifically into dynamic conveyor belt modelling, Yan and He in 2010 [258] used a multitude of connected segments (c.f. bonded particles) with the purpose of depicting the dynamics of a conveyor belt. The relatively simple system setup is shown in Figure 3-22, showing the deformable belt consisting of several single-line arranged and connected segments. The model is set up in the multibody dynamics simulation environment of MSC Adams [180] (thus not including DEM-related aspects per se, such as additional particles to interact with the belt). For the analysis, the pre-tensioned belt model is driven (more specifically accelerated) by one pulley due to frictional interactions between the pulley and the belt.

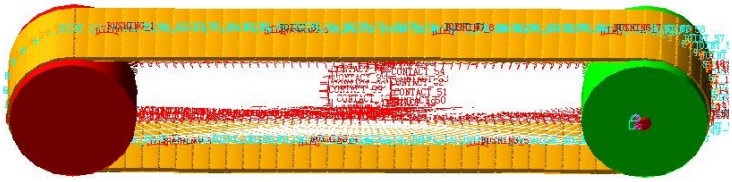

Figure 3-22: Endless conveyor belt model consisting of multiple connected segments [258]

3.1.2.3.1 BPMs to represent closed-surface structures (ref. membranes)

In more general terms, regarding not directly conveyor belt modelling as introductory shown, but relating to principles relevant to belt modelling, an early approach was presented by Kuhn in 1995 [150] for the modelling of flexible boundary structures to be used in three-dimensional DEM simulations. The presented particle network forms a flexible flat geometry (cf. membrane); thus basically relating to belt modelling. Although not explicitly stated as a BPM, the model shows fundamental similarities, such as regarding the contact handling (of wall particles with bulk particles via common DEM contact mechanisms) as well as the particle connection characteristics within the wall structure, which is enabling flexibility (cf. bondings).

Continuing this flexible structure modelling, an approach of DEM-based modelling concerning belt-like objects was, for a representative example, applied by Lorentz (2007) [162], setting up a deformable flat (initially plane) object as a single layer of connected particles. This respective model, a flat rectangular object formed by spherical particles arranged/bonded in a rectangular pattern, is shown in Figure 3-23. The figure further shows a specific load applied to the model causing it to bend characteristically.

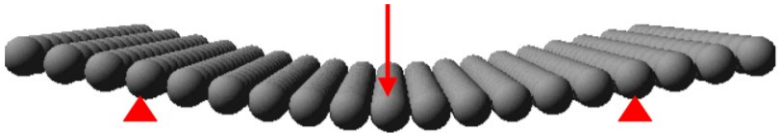

Figure 3-23: Initially plane, rectangular BPM deforming under load; particles arranged in a single layer in rectangular pattern [162]

In Figure 3-24, the specific application of this model within a more complex system setup is shown. Dynamic interactions with additional particles (above and beyond the deformable model itself) are causing the in-between placed model to deform as a

flexible object. From a belt-related perspective, this situation can already be transferred to interactions as required for conveyor belt models capable of dynamic behaviour: with idlers on the lower side and with bulk materials on the upper side of such a belt.

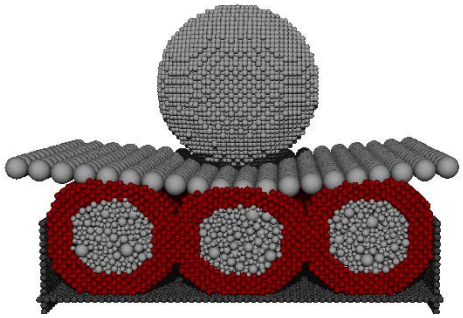

Figure 3-24: The rectangular BPM deforming dynamically in a given use case, resulting from contacts with further DEM-modelled objects above and below [162]

Another representative reference application for the modelling of a surface-like object as a single-layer BPM was also published by de Bono, et al. (2012) [48], modelling a flexible cylindrical membrane with the purpose of containing bulk material particles. In this work, particles are positioned as shown in Figure 3-25 (left), forming a cylinder instead of a planar object (as previously shown in Figure 3-23). Furthermore, on a more detailed level, shown in Figure 3-25 on the right, the particles are thereby triangularly arranged/bonded, thus corresponding to a tight two-dimensional pattern (which contrasts to the previously shown rectangular pattern).

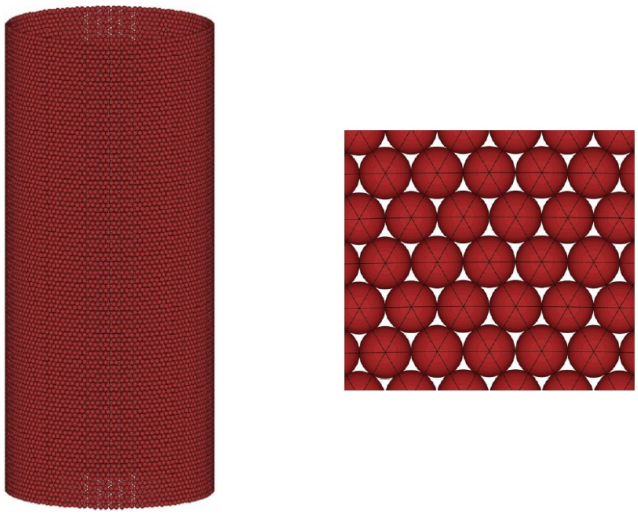

Figure 3-25: Cylindrical membrane BPM (left), in detail modelled with triangularly arranged bonded particles (right), adapted from [48]

Aspects regarding these two types of basic particle arrangement patterns (rectangular/triangular) are also discussed in more detail within Chapter 4.1.1.1 regarding the basic pattern to be used for belt modelling in the context of this thesis (rectangular). Also, the cylindrical model as shown can already be referenced to a simple, relatively short version of an endless belt model.

Further applications of BPMs for flexible structures are also shown in the showroom of the DEM software Pasimodo [121], applied at the University of Stuttgart [244]. Besides examples of two-dimensional flexibles (ref. fibres), also surface-representing BPMs are demonstrated, such as the flat membrane shown in Figure 3-26 (by Fleißner (ed.), in [244]). Formed with triangularly arranged spherical particles, this membrane model is structurally similar to the one in Figure 3-25. The colour coding represents the tensile forces in the bondings resulting from an impacting torus.

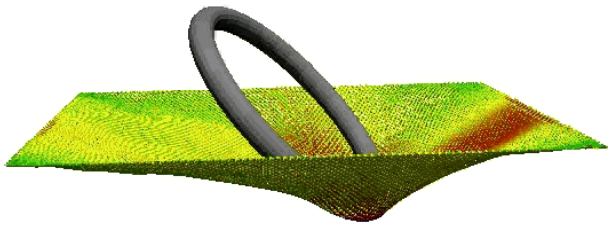

Figure 3-26: Torus impacting and deforming a flat membrane BPM [244]

3.1.2.3.2 BPMs to represent open-surface structures (ref. nets)

In addition to the modelling with the purpose to represent closed surfaces, as shown so far and as also regarding common belt modelling, the modelling of open-surface structures based on bonded-particle techniques is generally also relevant in belt-related terms. Such objects with open surfaces generally correspond to nets/grids/wire-meshes, etc., in various forms, as outlined subsequently in selected references. The connecting link from modelling such open-surface structures to belt modelling is due to similarities in dynamic model characteristics, such as enabling certain deformations/flexible behaviour.

A common field for applying bonding-based net structure modelling is the numerical simulation of rockfall protection nets and fences. For such applications, the net-representing models fundamentally require dynamic deformation capabilities allowing

relatively large deformations and including damping characteristics to depict the effects resulting from impacting rocks/boulders.

A commonly used technique to model large-scale nets for such applications using the DEM is visualised in Figure 3-27, after Bertrand, et al. (2008) [22], showing the detail of a hexagonal wire mesh setup. The principle shown is to place particles at intersecting points of the net (a) and bondings to connect them, thus representing the wires (b). Representatively for a bonding-like connection, especially in this context of relatively distant bonded particles, the term remote interaction is also found in the literature (e.g. Bertrand), indicating a contrast to conventional contacting particle interaction at overlapping particles.

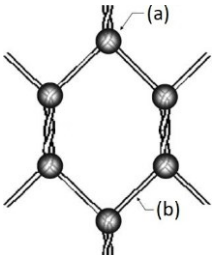

Figure 3-27: Detail of a BPM forming a hexagonal net structure; particles (a) connected via wire-representing bondings (b), adapted from [22]

Illustrative applications for rock protection net simulations based on this technique are shown in the following (published by Thoeni, et al. (2011, 2014) [238, 239]; further applications can also be found in pertinent literature, e.g. by Previtali, et al. (2020) [205]).

A rectangular net model centrally loaded by a mass block, resulting in a net deformation as to be expected, is shown in Figure 3-28.

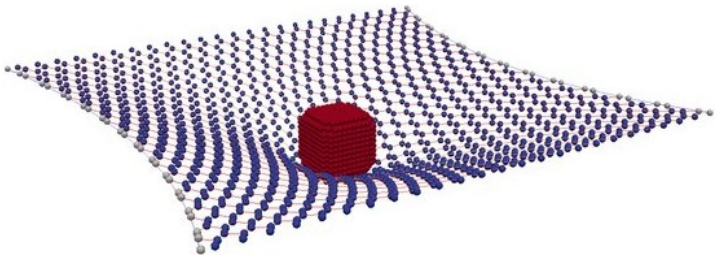

Figure 3-28: Hexagonal wire net as a BPM, deformed by a mass block, adapted from [239]

Furthermore, a larger net model applied for the analysis of dynamic effects from impacting boulders in a specific application is shown in Figure 3-29. The relatively strong deformation of the net model resulting from the impacting boulder is clearly distinctive (right).

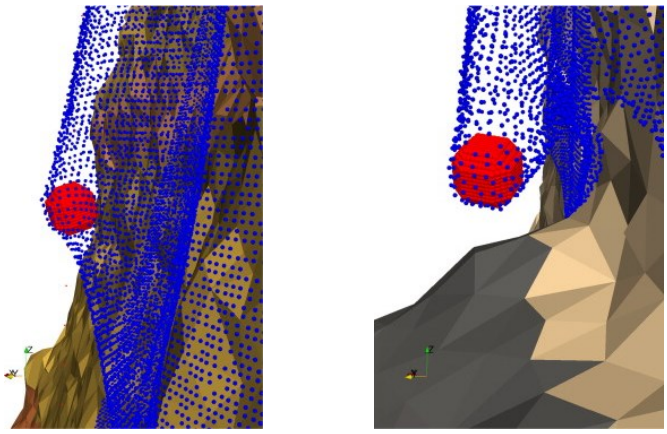

Figure 3-29: Practice-oriented, large-scale application of a wire net as a BPM, with an impacting boulder resulting in relatively large model deformations (right) [238]

From the perspective of belt modelling, these applications/models underline the capabilities in terms of deformability and flexibility, as well as regarding large-scale applicability, which is principally made possible by using this technique of bonded particles.

3.1.2.4 Surface-related issues & associated techniques

A detailed look at the BPMs shown so far reveal a characteristic, which is attributable to the applied arrangement of multiple spherical particles: a macroscopically rough surface representation (further referred to as rough surface). Usually, it is intended that the surface of a BPM represents a flat/smooth surface, but as further explained in the following subsection, a rough surface – generally comparable to a nubby surface – is typically resulting.

After the following overview chapter on rough surface aspects, basic approaches are outlined that are principally conceivable/suitable to address the issues of rough surface representation. These are basically techniques to obtain a kind of continuous/gap-free surface to cover a bonding-based structure, i.e. creating a BPM with a merged/seamless surface.

As important to the belt modelling technique presented in this thesis, these surface-related aspects are also dealt with in more detail in the methodology's description, specifically in Chapter 4.1.1, explaining the particle structure proposed for DEM-based belt modelling – hence particularly regarding a smooth surface representation as required for common conveyor belts. Anticipating, these specifications regard the use of overlapping cuboidal particles to obtain a smoothened belt surface, thus relating to the approach introduced in Chapter 3.1.2.4.2; the subsequent and as evident more complex approach of using flexible (particle) surfaces is additionally presented in the form of an introductory/basic overview into this alternative technique, with further aspects in that context also addressed in the evaluation/selection of the approaches to belt modelling that follows in Chapter 3.1.4.

3.1.2.4.1 Rough surface – origin & resulting effects

The microscopically rough surface as addressed is evident from the previously shown BPM setups, such as clearly distinctive in the fibre model setup in Figure 3-17. Instead of representing the fibre with a smooth surface, the model structure resembles a chain of spherical particles. These surface characteristics also affect belt-related flat BPMs, as previously shown in Figure 3-23 of a BPM forming a flat membrane with a rough surface resulting from rectangularly arranged spherical particles. Even with a higher resolution, thus with more (and consequently smaller) particles representing the surface of a BPM, this effect is still apparent (e.g. Figure 3-19; BPM of a cantilever beam).

Specifically considering a smooth surface representation, as usually intended, corresponding surface-related issues are the major consequences from this type of rough surface representation, mainly manifesting in unintended contact effects. These effects typically affect surface-related characteristics, such as friction or rebound behaviour (of additional BPM-contacting particles). Therefore, the macroscopical roughness must be taken into account when determining characteristics, such as the frictional behaviour of particles moving/sliding over such a surface (which affects as a superimposition to the already applied contact model, see Chapter 2.1.2.3).

To conclude those surface-related issues: The larger the contacting particles, compared to the surface-forming particles of the BPM, the more attenuated these surface-related issues take effect.

Side note derived from this statement: Especially when relatively large contacting particles are in use – such as regarding rock protection net applications in which the impacting boulders are typically large in comparison to the net-forming particles (cf. Figure 3-28/Figure 3-29) – such simplified surface modelling/representation (cf. Figure 3-27) is basically sufficient. Thus, in cases as these, the mentioned issues are of a rather subordinate level. For general applications, however, in which the contacting particles are not of such large sizes – such as regarding common belt conveyor systems for bulk materials – those surface aspects need to be adequately considered.

3.1.2.4.2 Using overlapping & non-spherical particles

A basic and relatively simple approach to smoothen the surface of a BPM is to use overlapping particles, thus more closely arranging particles further resulting in reducing the roughness. Obviously, contacting of overlapping particles must be disabled, as already mentioned within the general BPM descriptions, in Chapter 3.1.2.2.1 (side note on self-contact). Also, the resulting setup basically refers to multisphere particle geometries, as shown in the course of the DEM basics in Chapter 2.1.2.1, but as characteristical for BPMs, individual spherical particles are accordingly connected with bondings to allow enhanced behaviour.

With advance reference to the later shown figures in the methodology's description (e.g. Figure 4-2), an example of a flat BPM with overlapping particles is shown in Figure 3-30 in advance. The overlaps are set to close the gaps between the particles, leading to a smoothened surface, especially compared to the previously shown membrane in Figure 3-23. Nevertheless, a remaining roughness is still apparent. The figure further includes an exemplary contacting particle, pointing to influences from the roughness on characteristics mentioned previously (e.g. friction-related).

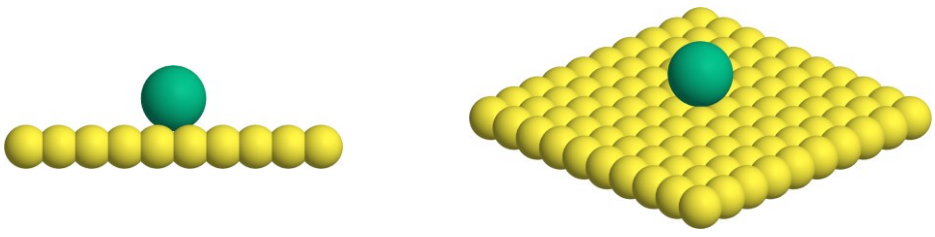

Figure 3-30: Overlapping particles forming a flat BPM; with an additional contacting particle (side/isometric view; left/right)

It can be inferred that in order to smoothen the surface increasingly, an increasing number of particles and bondings is required. Therefore, smoothing the surface with this approach is generally opposed to higher computational efforts due to the higher amount of numerical elements to be computed (particles and bondings).

An enhancement in that regard is using non-spherical particle geometries, which allow arranging the particles with larger distances while still forming a smooth (and in the case of overlapping particles, an even closed) surface. Exemplarily, fibre modelling using overlapping capsule-like particles in a single-line arrangement can be mentioned; referencing Langston, et al. (2015) [155] (furthermore connecting those particles at their spheres to form a flexible fibre model with a smoothened surface). More details regarding this approach of using non-spherical particle geometries, specifically in belt-modelling terms, are additionally covered in work by Fimbinger (2018) [82].

Especially later shown BP belts modelled according to the methodology presented in this thesis, such as shown in the exemplary applications in Chapter 5, can be referred to visualise this approach. Representatively, a section of such a model is shown in advance in Figure 3-31, illustrating the use of cuboidal-shaped particles in order to smoothen the surface of a BPM.

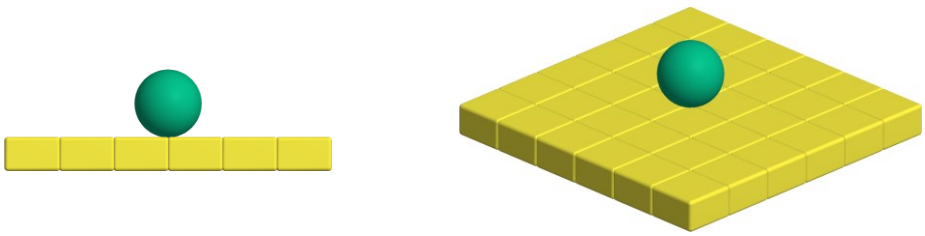

Figure 3-31: Cuboidal-shaped particles forming a flat BPM; with an additional contacting particle (side/isometric view; left/right)

Even complex-shaped particles demand a certain increased computational effort, compared to simple spherical particles, modelling a smoothened BPM with fewer particles and bondings is made possible, affecting the computational efficiency positively (especially in comparison to using dense overlapping particles).

As relevant to belt modelling according to the methodology presented in this thesis, these outlined techniques (overlapping/non-spherical particles) are in more detail described within Chapter 4.1.1, as parts of the particle-related structural belt setup.

3.1.2.4.3 Using flexible (particle) surfaces (ref. PFacets)

In advance: Due to its generally relatively complex nature, especially in contrast to the previously introduced method of using overlapping cuboidal particles, which already indicated a suitable method for belt-related purposes, this approach of using flexible particle surfaces is in terms of this presented methodology not further followed. (Further details in this regard are also described in the conclusive assessment and decisions in Chapter 3.1.4.) Nevertheless, and especially for the purpose of completeness, this alternative method is also addressed.

Applying methods that allow a flexible surface to cover a bonding-based particle structure principally describes this approach introduced in the following. Furthermore, this approach basically describes a complex surface-smoothening extension to be applied on particle structures, specifically by enhancing the structures so far explained (as made from individually rigid, tough complex-shaped particles) towards flexible surface-forming multi-particle structures.

The approach of adding a covering surface onto a ground structure, which is basically comparable to a BPM, is fundamentally attributable to Effeindzourou (using Yade [226]), summarising relevant details in this context in the corresponding PhD thesis (2016) [71] (comprising several papers; as further referenced in the figures). In this course, Effeindzourou established the term PFacet, presenting a deformable triangular element, which can specifically be applied for the purpose of creating a surface as described above.

Figure 3-32 illustrates the basics of a PFacet; on the left, the resulting closed surface covering the model is shown, and on the right, explaining insights into this structure are given. The model is basically defined by three nodes as the ground structure, correspondingly giving three spheres (in blue) to represent the corners of the model. Two triangulated surfaces are formed from these three spheres, one on the upper and one on the lower side, as visualised in the figure (right). The spheres further span three cylindrical surfaces, forming the rounded edges of the model as smooth cylinders, resulting in the total model as shown.

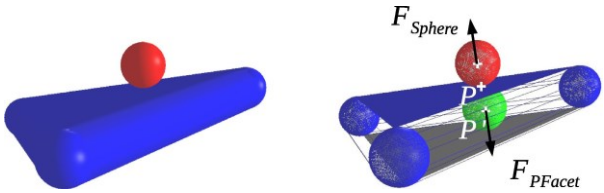

Figure 3-32: PFacet model and contact handling concept with virtual particle [70]

The contact handling concept, when an additional particle (sphere in red) is contacting this PFacet (in blue), is illustrated with the virtual particle (sphere in green). This virtual particle represents the contact partner and is consequently only apparent during the contact; effects are distributed accordingly into the nodes, thus into the ground structure (which can basically relate to the bonding structure within a BPM). (Cf. also Bourrier, et al. (2013) [27].) Side note: By omitting the triangular surfaces, the modelling of smooth grid structures, such as for net representation, is made possible (cf. Thoeni, et al. (2016) [237]).

By using several concatenated PFacets, it is furthermore possible to assemble larger models consisting of more than three nodes. Such a setup of two connected PFacets is shown in Figure 3-33 (thus comprising four nodes). Thereby, two nodes correspond to both PFacets, resulting in two shared spheres and one shared cylinder. The figure further indicates aspects in terms of multi-contact, which is required to be handled appropriately.

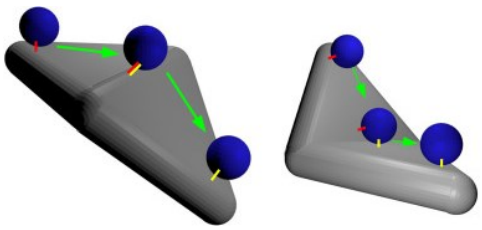

Figure 3-33: Two PFacets in convex (left) and concave (right) configuration; also indicating multi-contact (each middle particle affecting both PFacets) [69]

A larger application of this technique is further shown in Figure 3-34, in which the pull-out of a flat membrane out of a particle-filled box is shown (left); with the membrane consisting of multiple PFacets as also shown (triangulated surface; right).

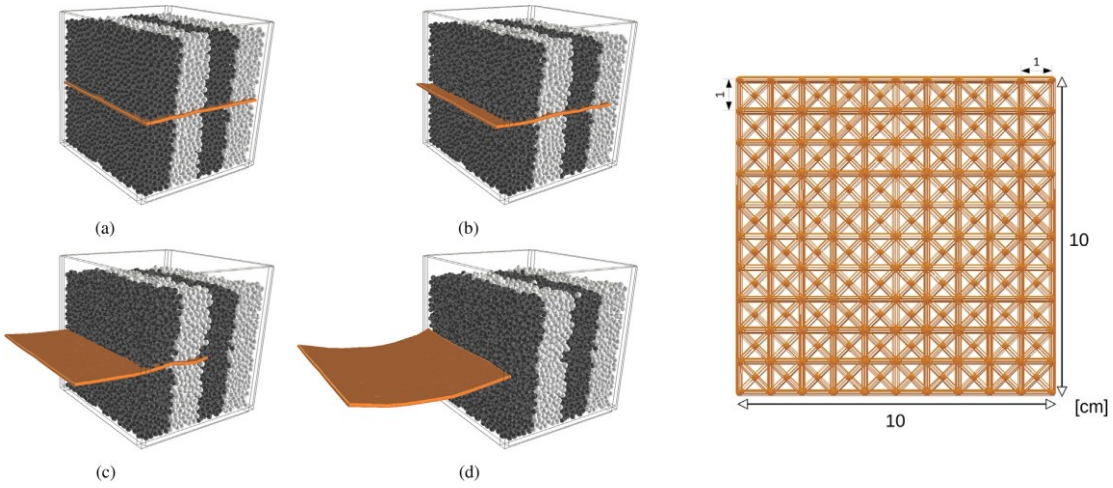

Figure 3-34: Membrane pull-out of a particle-filled box (a-d); PFacet structure of the membrane (right) [69]

A similar technique with using such flexible surfaces on a particle-based model, specifically in belt-related terms, is further presented in a recently performed case study from 2020 by Rocky [215], shown in Figure 3-35. This exemplary application shows a principal approach to simulate the dynamically interacting belt system of a round hay baler with the flexible elements available in Rocky [76] (since version 4.1 (2018), cf. [211]; further details in the Rocky blog [213]). The operating principle of this mechanical system was introductory explained in Chapter 2.2.5.5.

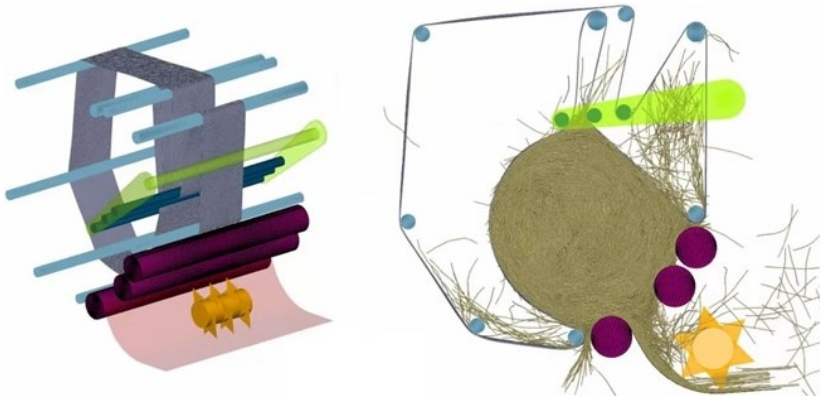

Figure 3-35: Round hay baler system modelled using flexible elements, adapted from [215]

Such a belt system of a round hay baler is also modelled/simulated using the methodology as presented in this thesis, shown in Chapter 5.6, and initially published by Fimbinger (2020) [90].

3.1.3 Excursus: On block diagram belt modelling

Besides these techniques, which are based on the modelling of belts as objects in a three-dimensional manner (as typical for DEM simulations), it is also possible to perform dynamic belt simulations by using (graphical) block diagramming software. Thereby, a belt conveyor is modelled as a dynamic system consisting of multiple connected blocks, which each represent physical subsystems, such as specific belt sections, driving units, belt tensioning units, etc. Each of these blocks is furthermore defined with individual details, such as to represent a specific inclination at a particular belt section, or to define resistance-related parameters, etc.

A specific software that offers such a module to model/simulate/analyse the behaviour of dynamical belt conveyor systems is, for example, SimulationX by ESI [74]. An example of a belt conveyor, set up by using visual modelling in the form of a block diagram in the graphical programming interface of SimulationX, is shown in Figure 3-36, in which also various block libraries (on the left) and some analysation possibilities (on the bottom) are indicated.

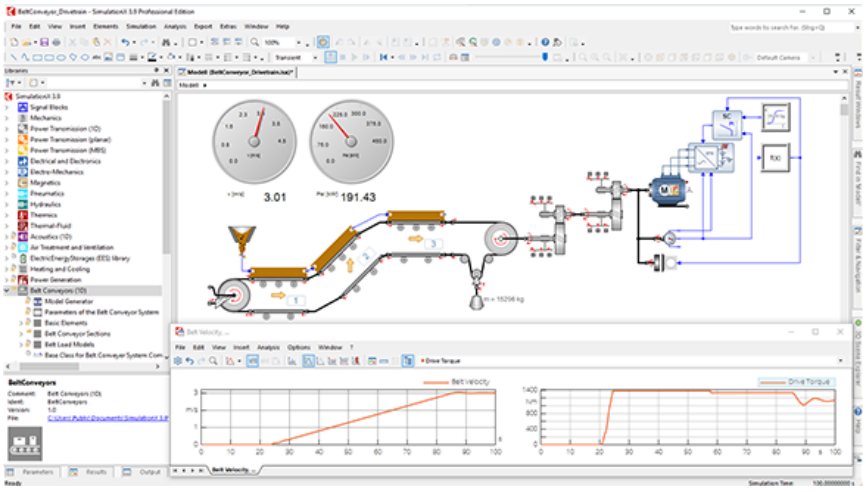

Figure 3-36: A belt conveyor block diagram model (centre), consisting of block elements (e.g. indicating an inclined conveyor section, a driving unit, etc.) [75]

Since the modelling of belts as three-dimensional (dynamically deformable) objects is not intended when using such block diagram simulations, this technique is only mentioned for completeness. It is thus not further covered within the course of this thesis.

3.1.4 Conclusive assessment and decisions for belt modelling

In conclusion to the previously assessed approaches: DEM-based belt modelling is further set as the general approach to be pursued in the context of this thesis.

In the following, several aspects in this regard are discussed, which were in their principles already addressed in prior publications by Fimbinger (as listed in Chapter 1.5). Generally, the assessment is also made with reference to the objectives stated in Chapter 1.2.

Aspects regarding the decision towards DEM-based belt modelling

As described in Chapter 3.1.1, FEM-based approaches are principally conceivable for belt modelling purposes, and as shown, have in some specific forms also been established for the simulation of certain cases/studies regarding conveyor belts, such as for depicting conveyor belt sections to analyse specific belt-related effects. Successful work in this field has already been demonstrated, especially with bidirectional coupling approaches, such as in detail by using a manually implemented coupling interface to connect two individual numerical environments (solvers), resulting in a FEM-DEM coupled simulation (see Chapter 3.1.1.2). Furthermore, in their mechanics principally similar to FEM-DEM coupling, FEM/DEM multi-physics approaches, as basically FEM-DEM combined within one user environment (cf. Chapter 3.1.1.3), are theoretically possible but would require specific solutions, particularly regarding the intended belt simulation purposes, which are generally limited in the extent required and desired. In this context with regard to limitations and availability, FEM-DEM coupling may be favourable, as it principally allows the combination of two specific (thus individually suitable) solutions, each for DEM and FEM separately.

In terms of required efforts and usability, this type of FEM-DEM coupled belt simulation can be considered as relatively complex and costly to be applied in general, as asides from the DEM software as a basis, additional FEM software and also an additional coupling interface are required – further also with compatibility as a crucial prerequisite. Furthermore, the interface may also require a customised solution, which typically requires additional efforts, such as in programming/implementation,

to successfully enable coupling as desired. Furthermore, the use of such a data processing coupling interface leads to a potential performance bottleneck because of the ongoing data transfer and data conversion between the two separate environments.

Regarding engineering-related usability, relatively skilled users (appropriately trained regarding the specific techniques for setting up this kind of simulation setup, as further regarding using particular DEM, FEM and coupling interfaces in combination) are a fundamental prerequisite for successfully applying this approach in practice. Another aspect, which also relates to usability, is that a combined visualisation (such as for combined analyses) of FEM belts together with DEM bulk material particles is typically not possible with this approach per se. Further additional features are needed to enable such capabilities.

From these points of view, this approach reveals a rather complex nature, further appearing relatively demanding for general use in common engineering practice. Nevertheless, particular bidirectional FEM-DEM coupling approaches (as established for certain conveyor belt simulations, thus representatively for FEM-based belt modelling) generally enabled dynamic conveyor belt simulation and have in the past also been proven to be useful for specific purposes, such as regarding cases in which the above-associated aspects are not that decisive.

As a promising alternative to this FEM-based approach, DEM-based belt modelling further reveals general potentials in dynamic belt modelling terms – especially with regard to the aspects mentioned above. As explained in Chapter 3.1.2, DEM-based approaches are principally suitable for belt modelling, whereby the main modelling scheme is to form a belt consisting of multiple particles connected to a bonded-particle model (BPM), which is due to this setup capable of representing complex/dynamic belt behaviour. Although not explicitly applied for (conveyor) belt applications so far, various belt-related applications (e.g. membranes, nets) already indicated promising prospects for using these DEM-based techniques for such purposes.

Several advantages are further associated with this approach, such as particularly regarding the aspects mentioned above:

Since only DEM features are used (to model belts besides bulk materials), it becomes possible to set up, perform, and also analyse such a simulation completely within the

DEM environment only; thus, without extra efforts in terms of additional software/coupling and related issues. Also, in that regard of extra efforts, the contact handling mechanisms between the belt and bulk material are relatively simple to be considered: common DEM contact handling is applicable due to the fact that a DEM-based belt is represented as a particle structure.

Furthermore, as shown in Chapter 3.1.2.3, related simulations with relevance to this topic, such as BPMs applied for fibres, membranes, and also net-like structures, showed promising aspects. Several applications, such as especially the shown net structures for rockfall protections, highlighted this approach as potentially advantageous for belt simulation purposes, such as in terms of large-scale application and further deformation capabilities.

Moreover, advantages of this bonded-particle belt modelling technique in terms of computational efficiency aspects were already notable in the early development stages of the methodology presented in this thesis. Correspondingly performed simulations, also with relatively large belt models as BPMs, already revealed beneficial aspects in terms of computational efforts required (cf. as referenced in Chapter 1.5); thus basically indicating this DEM-based approach as beneficial in this regard.

The chosen approach of DEM-based belt modelling

To summarise, this DEM-based approach offers the opportunity to use features established in the DEM to set up and conduct simulations of belt conveyor systems with consideration of dynamic belt behaviour (in general also concerning relatively large applications). It reveals promising aspects to be suitable for engineering-related purposes, such as design studies of complex and even relatively large belt conveyor systems or also for various belt-related analyses (cf. Chapter 2.2.5 for such applications/analysis purposes).

As highlighted, this approach is thus worth to be pursued, and therefore set to form an essential basis of the presented methodology.

To illustrate the basic setup of such a DEM-based belt model as proposed, a conceptual illustration of a short endless belt, modelled correspondingly as a BPM, is shown in Figure 3-37. The spheres and the lines between indicate the belt particles and their

connecting bondings. Generally, this principle belt-representing setup as outlined also refers to modelling approaches shown in Chapter 3.1.2.3.

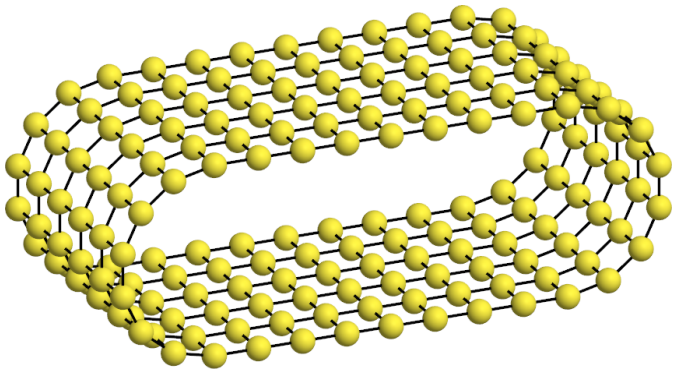

Figure 3-37: Schematic of a simple endless belt model as a BPM (BP belt)

Further specifications defining this DEM-based / BP belt modelling technique in detail are presented subsequently in Chapter 4.1, thus forming a fundamental part of the presented methodology. In general, those specifications relate to, on the one hand: the particles forming the belt, and on the other hand: the bondings connecting those particles to a BPM.

Sub-approach regarding surface-related issues (surface representation)

A general sub-approach, which is relevant to this type of DEM-based belt modelling regards the representation of BPM's surfaces, as described in Chapter 3.1.2.4. A concise consideration in this context is given in the following; anticipating that the developed methodology presents the representation of belts by means of complex-shaped (cuboidal) particles with a certain overlap to smoothen the belt model's surface, which is further also correspondingly explained in Chapter 4.1.1.

Initially, spherical particles were used for belt modelling, thus resulting in relatively rough belt-representing surfaces; even when closer-packed, overlapping particle arrangements were applied (see basically Chapter 3.1.2.4.1, and also initial publications by Fimbinger as referenced in Chapter 1.5).

As an improvement, complex-shaped particles were then used instead to represent the belt, as shown in works that followed, resulting in a smoothened belt surface (according to principles described in Chapter 4.1.1).

As presented, specifically the use of relatively flat cuboidal particles with rounded edges (see Chapter 4.1.1.3) revealed positive effects, not only regarding directly surface-related effects (as by smoothening the surface), but also in terms of efforts, as the number of elements to be computed significantly decreased (fewer particles and fewer bondings; even though the particles are complex-shaped).

Regarding a different approach, the implementation of techniques to dynamically reconstruct a DEM-based models' surface, such as corresponding to PFacets (Chapter 3.1.2.4.3), would principally allow even further smoothing of a belt's surface. However, the additional effort typically to be expected with this approach contrasts with the surface-related improvements to be expected (which are rather to be classified as minor, since previous results with cuboidal-shaped particles already showed effectively smoothened surface effects). Furthermore, in that regard, a belt model is required to be triangulated when using, for example, such a PFacet technique (as shown in Figure 3-34 on the right), which, in contrast to using rectangularly arranged cuboidal particles, not only increases the number of elements but further affects the base structure, which is intended to be rectangular to provide advantages in terms of parameter definition as well as analysation (as closer described in Chapter 4.1.1.1).

Due to its purposeful characteristics, the sub-approach of using complex-shaped particles with additional overlapping is pursued in terms of surface-smoothening; thus, applied in the context of this thesis and therefore further described/specified in Chapter 4.1.

3.2 Approaches for initialising and assembling belt models for use in specific systems

Some of the contents of this chapter are generally based on Fimbinger (2019) [88], reproduced in respective form and furthermore adapted/supplemented with enhancing content; with the kind permission of NAFEMS. (Additionally, see also prior publications as listed in Chapter 1.5).

Besides the general belt modelling technique as discussed in the previous chapter, a practical and purposeful approach is fundamentally required to get a specific digital belt model, such as accordingly modelled in the form of a BP belt, in its correct assembled position – thus to be placed as intended within a given (belt conveyor) system setup.

When placed in such a common assembled position, different belt conditions occur along the belt, typically resulting from local belt loads and expressing as local belt deformations, and further corresponding as local belt stresses. These local conditions must be strictly considered to perform a correct belt simulation – independent from the actual belt modelling approach, thus, principally regarding FEM- and DEM-based modelling. However, since DEM-based (BP belt) modelling was set as the basis regarding this thesis, the following aspects for belt initialisation are furthermore also discussed in terms of assembling such BP belts.

There are two major approaches to digitally assemble a belt model into a specific system, considering these mentioned conditions:

On the one hand: using commonly simple-shaped belt initialisation of a belt at rest (initialisation in minimum-energy state), whereby a subsequent assembling process is then required to form the belt from this simple undeformed state (thus without complex conditions apparent) into its final assembled state.

And on the other hand: using more-complex belt initialisation of a belt in a state close to the final assembled state (initialisation in almost-final state), which is principally based on using CAD belt models, as commonly available. Additional (typically rather complex) assembling processes are omitted, but enhanced initialisation techniques are fundamentally required, basically to consider the previously outlined belt conditions when an already deformed belt is to be initialised.

Both approaches are explained in the following, and a conclusive assessment is subsequently made, where one of these approaches is proposed to be pursued further. This specific approach (anticipating: almost-final state initialisation) is then developed to be used as a central part of the methodology presented in this thesis, thus in more detail covered in the respective section regarding belt initialisation within the methodology's description (Chapter 4.2).

3.2.1 Belt initialisation in state-of-rest

Initialising a belt at rest corresponds to generating a specific belt model in a state of equilibrium (thus in minimum energy), which is typically trivial and therefore commonly known: For a finite belt, this minimum-energy state would be a completely flat and undistorted surface without any elongations or stresses (zero-energy state), and an endless belt would form a perfectly circular cylindrical ring. A closer look at this circular ring state of an endless belt would further show that every bonding is actually preloaded with the same bending stress, originating from the intention that the belt would get into the zero-energy state if cut open by further unbending into a flat form (which is prevented due to the endless joint of the belt).

The initialisation of a belt in such a described state-of-rest is relatively simple to perform. In either of the two described ways (flats/rings), a belt can be initialised with the exact same state-of-rest conditions (zero energy or minimal bending state) all over the belt model in a very simple geometric form – as a flat or as a cylindrical surface. The challenging problem of this method, however, is the assembling of such a flat or cylindrical belt model into a given (conveyor) system after its initialisation. At the end of an initialisation-following assembling process, the belt is formed into its final assembled position and is commonly held by idlers, drums, or also due to gravity.

This additionally required simulation, prior to the actual simulation of interest – thus termed as pre-simulation, is basically required when using this approach of initialising a belt in state-of-rest. Depending on the actual system to be simulated, the pre-simulation effort required when using this approach can span from relatively low (such as addressed in illustrating examples in the subsequent Chapter 3.2.1.2) to disproportionately high (e.g. when looking at complex conveyor systems, such as described in Chapter 2.2.5; e.g. sandwich/pipe conveyors, to be set up in total).

These aspects of required pre-simulation efforts are also assessed later as critical criteria regarding the usage of this approach, specifically on relatively complex applications; especially as the alternative approach of initialisation in almost-final state promises advantages in that regard (see assessment in Chapter 3.2.3).

3.2.1.1 The two ways of assembling state-of-rest initialised belts

To perform an assembling process, thus, to form a belt from its initialised state at rest (flat-/circular-shaped) into a commonly more-complex assembled state, the belt can either be pulled (flat belts) or stretched (circular belts) to be formed into an assembled state within a conveyor system.

(Note: The belt conveyor system to illustrate the assembling processes in the following relates to the system as initially presented in Figure 2-18, regarding conventional belt modelling with using a rigid belt model; it is furthermore also the base system relating to Figure 3-41, and also for the exemplary application of the conventional belt conveyor system covered in Chapter 5.2, with using belt initialisation in almost-final state.)

3.2.1.1.1 Pulling a flat belt

Pulling can be performed with finite (rectangular flat) belts by dragging one end of the belt along the conveying line – through the stationary conveyor – and finally connecting this end to the other end of the belt to gain an endless belt model. This process is schematically shown in Figure 3-38 at the top; with the final assembled BP belt shown at the bottom.

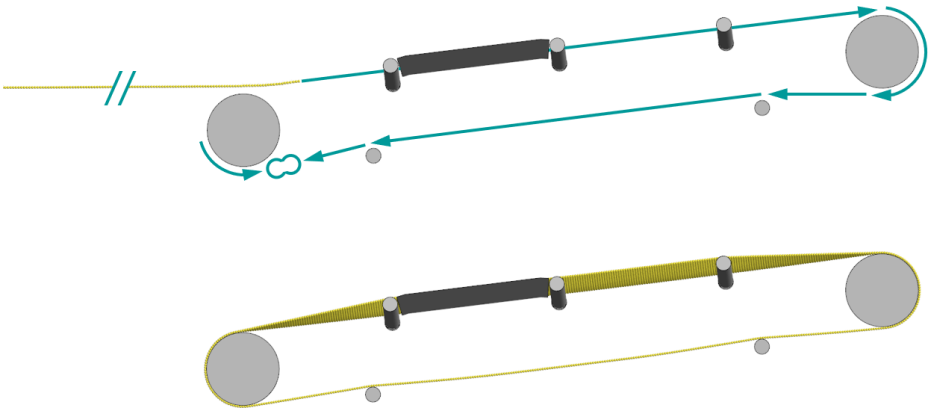

Figure 3-38: Pulling method: assembling a belt initialised in flat shape by pulling through the conveyor system

The endless connection to be made is illustrated at the bottom left, representing the completion of the BP belt model by bonding-creation between the two opposite belt ends.

(Note: This process is principally comparable to the installation of physical conveyor belts into typical (rather large) conveyor systems.)

3.2.1.1.2 Stretching a circular belt

Stretching can be performed with endless (circular) belts by initialising such a type of undeformed belt model among a disassembled conveyor system – and further moving the components of this disassembled system (idlers and pulleys) so that the belt gets deformed and finally placed inside the completely assembled conveyor. Figure 3 shows this stretching method to assemble a simple endless belt model into its final assembled position (top to bottom; concerning the same setup as shown previously for pulling a flat belt in Figure 3-39).

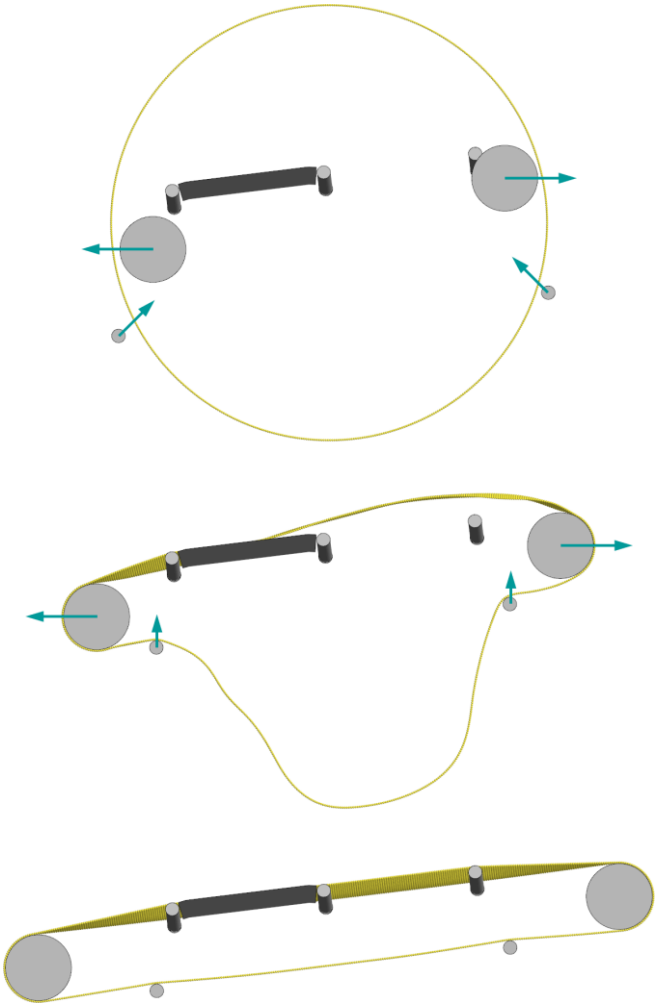

Figure 3-39: Stretching method: assembling a belt initialised in cylindrical shape by moving several system components (idlers/pulleys) to assemble the system

(Note: This process is principally comparable to the installation of physical belts into certain rather small belt systems when endless belts are installed, e.g. referring to the installation of belts into common flat belt drives; or principally also regarding the belt system of the round hay baler, Chapter 2.2.5.5.)

3.2.1.2 Illustrating usage in belt simulation applications

In the belt-related applications as shown in the context of approaches for deformable belt modelling (FEM-/DEM-based; Chapter 3.1), the applied belt models were typically initialised in such a state-of-rest as described, as commonly in a flat finite form. This is basically due to the fact that in those applications/analyses, the belts were able to be assembled with feasible pre-simulation efforts, as the levels of complexity in terms of systems and consequently in terms of belt assembling were typically within reasonable limits to allow this kind of initialisation.

Several of the referenced belt simulations in relevant sections within Chapter 3.1 (belt modelling approaches) relate principally to this initialisation approach. For illustration purposes, Figure 3-40 by Shen, et al. (2018) [224] (actually corresponding to a FEM-based approach), representatively shows a belt section of a common belt conveyor indicating the undeformed flat belt model (on top), which is further shown as placed on two idler stations (bottom; specifically highlighting belt deflection).

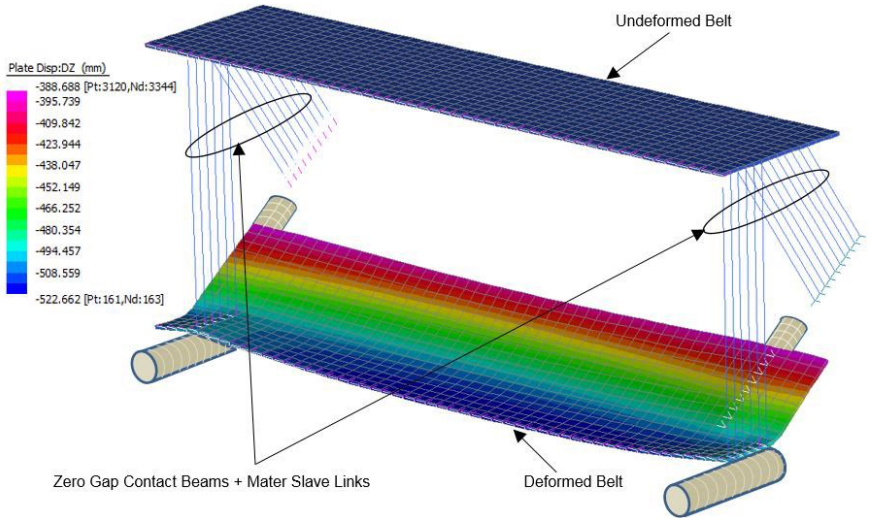

Figure 3-40: Conveyor belt model on idlers, also with undeformed state [224]

3.2.2 Belt initialisation in almost-final state

Initialising a belt in a form close to its final (fully) assembled state generally describes this approach of belt initialisation in almost-final state.

In the digital design of belt conveyor systems, the belts are usually modelled as digital CAD models with an idealised geometry; estimated to represent the digital belt model in a close-to assembled form. Such a CAD belt model principally offers the potential to be used as a basis for the initialisation of a BP belt model and further to allow an according belt simulation. This basic CAD-to-DEM principle, as a form of belt conversion, describes the general method which is fundamentally required to apply this approach.

The principles of this CAD-to-DEM, representatively for initialisation in almost-final state, are shown in Figure 3-41, where a CAD belt model within a simple belt conveyor system (left) is used as the basis to be transferred (converted) into a BP belt to be used in a DEM simulation (right; again concerning the same application as already shown/addressed exemplarily in Chapter 3.2.1.1).

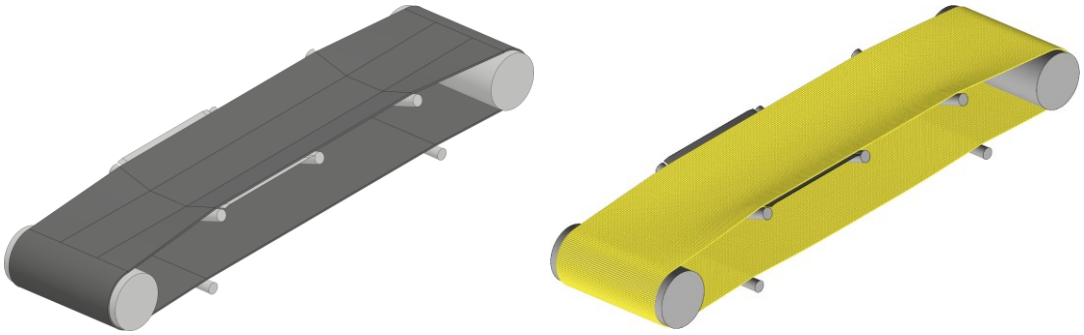

Figure 3-41: CAD model of a simple belt conveyor (left) and corresponding DEM simulation setup (right); illustrating CAD-to-DEM with belt conversion

Benefits and challenges

Basically, initialising a belt in an almost-final state eliminates the pre-simulation efforts to assemble a belt into the conveyor by an additional (prior) assembling process, as described previously in terms of state-of-rest initialised belts (Chapter 3.2.1). Additional efforts in assembling the belt, such as pulling the belt along the conveyor line or stretching the belt by moving components, is entirely obsolete.

When initialised in an almost-final state, only a relatively small final forming is required, where the belt, as initially present in this almost-final state, is formed into the final (fully-assembled) state. This final forming process depends on how accurately the CAD belt model is designed in relation to the final state. Final forming effects are expected at the beginning of a simulation due to the deviations between an idealised CAD belt (thus resulting in the initialised belt model) and the final assembled belt state, which is resulting at the end of this forming; these forming effects are expected as transient oscillations, furthermore representing a marginal pre-simulation as prior to the final belt state ready for actual simulation purposes. Deviations between the idealised CAD model and the final belt state are typically present, such as in troughed areas, in transitions between flat and troughed sections, or due to belt sag, etc.

In order to ensure a correct simulation with belt behaviour as intended, the occurring local belt conditions of a belt initialised in almost-final state must be defined properly. Applying these conditions is relatively challenging (especially in contrast to the simple condition definition as for state-of-rest initialised belts; cf. Chapter 3.2.1), as the belt must be initialised with different conditions at every point of the belt, depending on the local deformation state. For the computation of such a belt model, a complex analysis of the deformed belt geometry must be performed, local belt conditions must be considered, and the relevant results must be adapted and applied to the belt model at initialisation – so that the resulting belt model gets initialised with correct belt conditions as to be appearing in this almost-final state.

Anticipatory note: To enable this described CAD-to-DEM conversion process, a computer algorithm has been developed by Fimbinger to compute and set the belt conditions based on a given geometry from a CAD model to result in a corresponding DEM belt model as a BP belt; developments in that context are respectively described/presented in Chapter 4.2.

To concludingly give general insights into the subject of belt condition consideration at initialisation, a closer look at the BP belt from the relatively simple example shown in Figure 3-41 (on the right[8]) is given in Figure 3-42. In this figure, the following characteristics can be seen: on the left: the particle structure of the belt (BP belt with

[8] detailed view of the BP belt at the idler station in the carry strand on the right (next to the pulley)

simple spherical particles); and on the right: the bonding network connecting those particles, showing a rectangular bonding network (with bondings in longitudinal and in transverse belt direction).

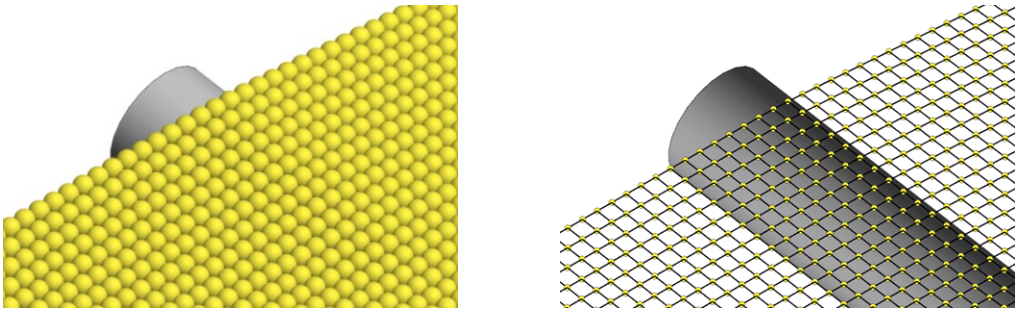

Figure 3-42: Detailed view on a converted (BP) belt, thus initialised in almost-final state; showing its particle structure (left) and inner bonding network (right)

Additionally, a promising sub-approach regards the consideration of belt velocity by adding proper velocity information to each belt particle along the belt model. This not only allows a belt to be initialised in almost-final, but further also in operating state (with an already running belt). (More details regarding this approach, as implemented into developed conversion algorithm, are further covered in Chapter 4.2, and more specifically in Chapter 4.2.4.3).

3.2.3 Conclusive assessment and decisions for belt initialisation

In conclusion to the previously assessed approaches: belt initialisation in almost-final state using CAD-to-DEM conversion is further set as the general approach to be pursued in the context of this thesis.

Generally, the minimisation of simulation effort is a necessity in every area of numerical simulation. More powerful hardware or changes in software algorithms are used to increase the performance of simulations, but in many cases, the simulation efforts can be effectively reduced by omitting superfluous computations, such as principally avoidable pre-simulations. This aspect especially highlights the conclusive decision to pursue the approach of almost-final state initialisation.

In the following, a concise discussion regarding belt initialisation approaches is further given, which were in their principles already addressed in prior publications by Fimbinger (as listed in Chapter 1.5). Generally, the assessment is also made with reference to the objectives stated in Chapter 1.2.

State-of-rest initialisation

In short, this initialisation approach principally allows simple application but requires additional assembling efforts to form the initialised belt into its assembled state. This additional assembling effort is essentially a negative aspect in more complex applications, as the larger and the more complex a belt system gets, the more inefficient the method of initialising a belt in state-of-rest results.

For relatively small and simple belt applications, where the geometrical deviations between the initialised and the assembled form are likewise small and rather simple, this approach is principally feasible as assembling is then typically kept within reasonable limits. But for long/complex belt (conveyor) systems, complex movements of either the belt (pulling) or of the components (stretching) over correspondingly long and complex distances are required, which typically results in a disproportionate high pre-simulation effort. This required pre-simulation effort for assembling processes as in context with belt initialisation in state-of-rest must be taken into account, since, especially for large/complex applications as outlined in Chapter 2.2.5, it is quite possible that pre-simulation efforts exceed reasonable limits (e.g. as exceeding the effort for the actual simulation of interest, which is following to the pre-simulation).

The following approach of belt initialisation in almost-final state is expedient in that terms, as reducing required pre-simulation efforts drastically, near to a minimum.

Almost-final state initialisation

Summarised, this approach is based on converting a CAD belt model into a DEM based model, thus allowing initialisation of the belt in a form that is already close to the final assembled state (CAD typically provides idealised forms, as without belt sag etc.) And as already outlined, this CAD-to-FEM approach thus is highly effective in terms of reducing pre-simulation efforts but requires the belt to be initialised in

this form accordingly. To allow this conversion properly and furthermore user-friendly, an algorithm was developed and implemented into an easy-to use software tool (BeltConverter by Fimbinger [94]; further details see also Chapter 4.2, and specifically Chapter 4.2.5).

Another positive aspect of this CAD-to-DEM conversion approach, in terms of usability, is that it allows a digital CAD model of a belt to be converted nearly directly (almost like drag-and-drop) into a dynamic BP belt model – ready to be initialised into a DEM simulation system setup, typically comprising further components (idlers/drums) – with consideration of local belt conditions as required.

From a broader perspective, this specific approach of almost-final state initialisation, with computation of conditions by analytically analysing the present state (instead of calculating these conditions in demanding pre-simulations) is generally also suitable for other problem areas, where costly pre-simulations are commonly performed.

As an exceptionally effective and high-performant method for initialising digital models, the approach of initialisation in almost-final state is thus a fundamental base of the methodology developed. Further details on this method are correspondingly given in Chapter 4.2.

Chapter 4

The Methodology

The core of the methodology for the simulation of dynamically deformable belts in DEM bulk material simulation is formed by two major parts: the structural belt setup and the belt initialisation. General principles/approaches regarding these two topics were discussed in the previous Chapter 3, including the underlying approaches.

The first method defines a general modelling technique of belt-like structures as bonded-particle models (BPM), thus forming a bonded-particle belt (BP belt) to allow dynamic belt modelling based on the DEM. (Chapter 4.1.)

As the second method, the technique to get such BP belts with specific geometries into certain given systems, based on belt initialisation in almost-final state, is defined. (Chapter 4.2.) Subsequently to that, visualisations and verification principles regarding BP belt initialisation according to these two methods are given. (Chapter 4.3.)

Besides these two major core methods, further extensions are also related to this developed methodology in total; in particular, the extending method for modelling numerically smooth-surfaced cylinders, which is specifically relevant to belt conveyor applications as regarding the modelling of idlers/pulleys (thus, used in the exemplary applications in Chapter 5), is therefore correspondingly covered (in Chapter 4.4).

The developments presented/elaborated in the following are explicitly introduced using the DEM software ThreeParticle/CAE [17], on the basis of which the associated illustrative figures of DEM simulation setups and further related content are created accordingly. Details and motives underlining the use of this software were already

indicated in previous sections (such as particularly in terms of DEM simulation basics described in Chapter 2.1.2) and furthermore reveal within following chapters, especially by highlighting features that were exclusively implemented in ThreeParticle/CAE as a result of the methodology presented in this thesis (e.g. referring to the adapted bonding model specifically relevant for BP belt modelling, in detail introduced in Chapter 4.1.2.2, or the keyword file (INP) format supporting quaternion data, described in Chapter 4.2.3.2).

4.1 Structural belt setup

Some of the contents of this chapter are generally based on Fimbinger (2019) [88], reproduced in respective form and furthermore adapted/supplemented with enhancing content; with the kind permission of NAFEMS. (Additionally, see also prior publications as listed in Chapter 1.5).

The developed methodology defines a specific setup for the structure of belt models as BP belts. This specific setup relates to details regarding the particles and their connection via bondings to represent a belt-like structure. In this context of belt modelling, the term “particle” generally refers to “belt particle”, which are the particles that are arranged and connected to form such a BP belt as a corresponding BPM. (Bondings, as explained in the DEM basics, Chapter 2.1.2.6.1, describe virtual beam elements connecting each two particles together in a defined way.)

Note: With respect to the focus of this thesis, the modelling techniques given in the following are developed to allow a virtual belt model to represents belt-typical behaviour in general. If a specifically given physical type of conveyor belt is required to be represented, the corresponding parameters of the virtual belt model need to be appropriately tuned. For such specific purposes, adjustments of these parameters are typically required, as by determination using appropriate tests. In that regard, some common simple tests include, for example, tensile tests or bending tests, may further be complemented by extending scenarios, such as tests on running endless belts, etc.

In the following, the details regarding the structural belt setup of BP belt models are grouped as regarding particles, on the one hand, and bondings, on the other hand;

generally referring to the principal setup of BP belts as consisting of those two major elements (particles/bondings).

4.1.1 Particle-related

The particles forming a belt are specifically relevant in terms of surface and mass characteristics; further to represent a belt in total. Especially regarding the surface, contacts with further (non-belt) particles, as commonly forming bulk materials, are correspondingly handled over those belt particles.

4.1.1.1 Single-layered structure of rectangularly arranged particles

For the modelling of a belt (in terms of overall behaviour within a system; thus not requiring detailed insights into the belt's inner composition), the use of only one single layer of particles is advantageous. The required simulation effort is related disproportionally to the number of particles and the number of bondings, which is why a single layer is advisable for computational efficiency reasons. Due to modelling and analysing aspects, such a simple belt structure with only one single layer is recommended.

For a simple systematic arrangement of particles in a single layer, two principal ways are conceivable: arrangement in a rectangular or in a triangular pattern. These two different types of particle arrangement are shown in Figure 4-1, where also every two adjacent particles are already indicated as bonded, thus illustrating a small section of a BP belt with the respective (single-layered) particle pattern (which were generally addressed/referenced in Chapter 3.1.2.3.1 regarding the approaches for belt-related bonded-particle modelling.)

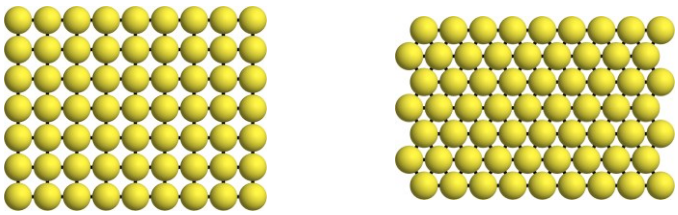

Figure 4-1: Principal forms of particle arrangement: rectangular (left) and triangular (right); shown in a representative flat belt section

Although a triangular pattern represents a close-packed form, this arrangement is evaluated as not beneficial for belt simulations, as a rectangular arrangement reveals significant advantages in terms of the definition of belt parameters and further also in terms of the evaluation of simulation results. This is basically due to the fact that a rectangular arrangement allows definition/analysis in this rectangular form, thus enabling the representation of longitudinal and transverse belt directions.

Furthermore, under the condition of modelling with the same particle-particle-distances, a higher computational effort is also required with triangular patterns, because in comparison, this arrangement requires more bondings and also more particles per area (general effect of triangular close-packed patterns; cf. Figure 4-1).

4.1.1.2 Contactless particle overlapping and self-contact abilities

A technique as an adaption to the belt's internal contact-handling model is used to allow the particles within the belt to penetrate each other without any effects of contact. The particles that overlap in this way neither repel nor rub against each other.

Generally, using this particle overlapping results in positive effects due to disabled belt particle contacting. This refers, on the one hand, to computational aspects, as no inner-belt contacts need to be computed, and on the other hand, to beneficial aspects in terms of model behaviour in general, as interactions between overlapping belt particles only depend from the bondings; thus, distorting contact effects from belt particle contacts with each other are omitted (and only the bondings are responsible for the interactional behaviour of the particles within a BP belt as intended).

With this method of overlapping particles, the particles within a belt model are principally able to be arranged more densely, as already discussed in principle regarding the surface-related issues of BPMs in Chapter 3.1.2.4.2. Figure 4-2 visualises the difference between an arrangement with spacing between particles (left) and a dense arrangement with overlapping particles (right).

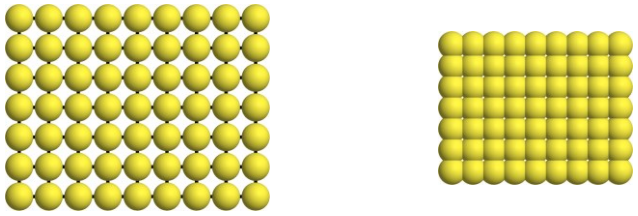

Figure 4-2: Particles with spacing (left) and overlapping particles (right)

As a consequence (and as already addressed), a dense arrangement of belt particles is smoothening the modelled surface, such as to improve surface-related issues, but also results in a larger number of required particles per area – in particular with spherical particles, such as shown. Therefore, the use of complex-shaped particles to address this issue is described subsequently in Chapter 4.1.1.3.

The following described method of using contact groups to disable inner-belt contact generally allows this contactless overlapping to be applied to a belt model. In addition to that (as basically derived from this contact group approach), a convenient way to disable contacts within a bonded-particle model was also implemented to be available in the software platform of ThreeParticle/CAE (as an additional option to turn on/off self-contact in a BPM, for which particles within a BPM are further assigned a bonding ID, which is basically similar to contact group definition as described in the following.)

Contact groups definition & enabling self-contact for certain applications

As resulting from globally defined belt particle overlapping, all contacts of particles that belong to a belt are deactivated, which corresponds to a completely deactivated belt contact condition. But in certain cases, specific/partial belt contact is required to be activated, for example, between two separate belts that get in contact with each other, such as in sandwich conveyors (see Chapter 2.2.5.1), or further, when a belt is required to contact itself, such as at the belt edges of a pipe conveyor (see Chapter 2.2.5.2).

To implement such enhanced contact-related properties, a basic approach of using contact groups is applied. Accordingly, particles within BP belts are assigned to contact groups in order to specifically activate or deactivate contact conditions.

As a simple illustration of this approach, the two belts of a sandwich conveyor can be defined each with a different contact group. By generally deactivating the contacts within each group (thus within each belt), and further activating contact between the two groups (thus between the belts), inner-belt contacts are not considered whilst both belts are able to allow respectively defined contact when brought together.

A more complex case concerns self-contact within a belt model, as when two surfaces of the belt of a pipe conveyor are brought together; because when contact within an entire belt is deactivated, the belt model would accordingly interpenetrate itself instead of reacting with contact. For ordinary circumstances and most types of belt conveyor systems, a belt usually does not get in contact with itself, and therefore, the entire deactivation of contact within a belt is practicable for general applications. However, in special applications or under certain conditions, this type of belt self-contact can't be ignored and is thus to be considered in belt simulations accordingly. As already addressed, this exemplarily concerns pipe conveyors, as shown in Figure 4-3, where the two edges of the belt are in contact to form the tubular shape (green/blue), thus resulting in belt self-contact as to be considered.

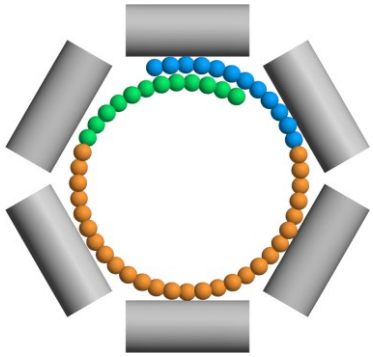

Figure 4-3: BP belt for a pipe conveyor system with three different contact groups defined (indicated in colour) to allow self-contact at the belt edges (green with blue; cross-sectional view)

On this pipe conveyor, the use of an enhancement to the previously described technique by using contact group definitions within the belt is further explained. Therefore, the belt is basically seen in a fibred structure (such as generally used/described in terms of applying anisotropic belt behaviour in Chapter 4.1.2.3). In this context, fibres refer to the parallel arranged single lines of particles in longitudinal belt direction, thus principally sectioning the belt. By fibre-based contact group assignment, and furthermore, defining pairs of contact groups to act with/without contact, self-

contact between certain belt areas is made possible. (Areas in that context correspond to groups of (typically several adjacent) fibres within the same contact group.). This principle is illustrated in Figure 4-3 in the cross-sectional view of the tube-formed BP belt, in which every particle refers to a parallel arranged fibre, further used for assigning into three different contact groups as indicated in colour. To allow self-contact as required, the contact groups at the two belt edges (green and blue), are required to act with contact; thus contact is activated between those two contact groups. All the other contact group pairings are defined with disabled contact, including definitions within each group (green-green, blue-blue, orange-oreange), as well as between adjacent groups (green-orange, orange-blue). The additional contact group (orange) between the two belt edges is defined to separate the two outer contact groups that are defined with contact activated. (If only two contact groups would be defined with contact activated, contact would consequently result within the belt model, at adjacent particles belonging to the different contact groups.)

A theoretically possible approach that would allow a general form of global self contact within a belt, further with including the advantages of overlapping between adjacent particles would be to deactivate only those contacts between neighbouring particles, whilst activating contact between every other particles. This means, that for every single particle the contact to its directly surrounding eight particles is deactivated, but contact to every other particle is activated, which is illustrated in Figure 4-4, with a representative particle in the middle, which is deactivated regarding contact to its directly surrounding particles (ring around this centre particle).

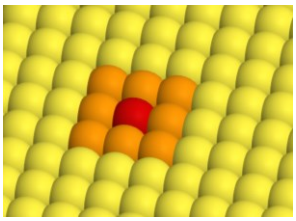

Figure 4-4: The eight surrounding particles around a particle of focus (red)

(A further enhancement would, for example, be to also include the next surrounding particles further contacting to these first surrounding particles, to also be set as deactivated regarding contact with the centre particle; etc.)

Applications for such general self-contact relating to conveyor belt applications, as the basic field of interest for this methodology, are rather uncommon and thus not

followed in more detail. For an implementation of this general self-contact approach a specific definition, for example, based on the particle ID, would be required. If the particle IDs within a BP belt follow a systematic pattern (such as according to the developed CAD-to-DEM algorithm for belt initialisation as presented in Chapter 4.2), this pattern could principially be used for such purposes.

Concluding this matter regarding contact activation/deactivation as described, and further referring back to the computational benefits which are related to omitting contacts within belts, aspects in this computational respect need to be taken into account: The more contacts (and more specifically their detections, which fundamentally influence the computational effort; cf. Chapter 2.1.3.2) can be omitted, the lower the computational effort. Therefore, deactivated contacts are generally to be aimed for; and if required, as due to certain circumstances (such as regarding the addressed specific applications), contacts should be defined at an effective level, i.e. with as few particles activated for contact as possible.

4.1.1.3 Cuboidal particle geometry

To be applied for BP belt modelling, several different particle geometries were evaluated (cf. Fimbinger (2018) [82]), whereby cuboidal particles with rounded edges proved to be convenient to be applied and also advantageous in several aspects, as outlined subsequently. In addition, and to begin with, aspects regarding the default spherical particles, which are principally feasible for belt modelling, as also shown in the previous chapters, are addressed – furthermore with comparison to cuboidal particles.

Spherical particles

Generally, spherical particles are advantageous in terms of computational efficiency per particle due to their simplest geometrical form. And, unlike all other volume geometries, spheres show no geometric differences in terms of spatial orientation, so that it is not necessarily required to specifically align the orientations of the individual particles within a belt model when using such spherical particles.

For the modelling of a BP belt, it is reasonable to set the sphere diameter of belt particles (approximately) equal to the belt thickness, as a single particle layer is to be used (as described previously).

Note on belt thickness upscaling: If a relatively thin belt is to be represented, and thus a disproportionally large number of particles would be required to model the BP belt, upscaling of the particles by increasing their size within reasonable limits generally results beneficial, as in terms of lowering the computational efforts in two respects: due to the fewer particles (and thus bondings) required, but also due to larger particles in general, as affecting the time step positively (cf. Chapter 2.1.2.1 and 2.1.3.1). In accordance with the adapted belt thickness, certain effects on the total belt system need to be appropriately considered when applying such upscaling. (Cf. Chapter 2.1.2.1 on particle upscaling techniques in general DEM modelling terms.)

A disadvantage of using particles with spherical geometry, in particular compared to flatter geometries, is that more particles need to be arranged to form a gap-free and smoothened belt surface, especially when the particles overlap (see Figure 3-30; cf. Chapter 3.1.2.4.2, surface-related issues). As a consequence, a higher computational effort is generally required due to the increased amount of particles (and further their connecting bondings).

An initial adjustment in that regard is to distort the spheres to ellipsoids by enlarging the radii in longitudinal and transverse belt direction, which leads to reducing the number of particles required. But this adjustment would further require proper aligning of particles in their spatial orientation along the belt, especially when general belt geometries (non-flat) are to be initialised.

Another disadvantage of using spherical (or also ellipsoidal) particles is that belt surface parameters, in particular regarding friction, are difficult to be defined properly due to the macroscopically rough surface resulting (cf. Chapter 3.1.2.4.1). Moreover, this macroscopical roughness is also depending on the distances between adjacent particles, which is furthermore not set as constant, as the belt is modelled to be flexible also in terms of lengthening. I.e. this means the roughness is influenced dynamically by the belt's flexibility, as when belt particle distances change, which is not intended.

Nevertheless, modelling with spherical particles is principally possible for some applications, as already shown in related examples as referenced in Chapter 3.1.2.3, regarding BPMs for belt-related applications, in which spherical particles were typically used.

Cuboidal particles

By setting up a BP belt model with cuboidal particles, the belt's surface can be depicted in a suitable approximation, as already outlined in the general approaches regarding surface-related issues in Chapter 3.1.2.4.2.

Indispensable to the arrangement of belt particles is the correct spatial orientation of each particle within a belt model to be represented properly. In accordance with the developed methodology, the coordinate axes (x, y, z) of arranged particles are assigned to the belt directions (longitudinal, transverse and thickness direction). Therefore, the length axis (x) of a cuboidal particle is in each position aligned to the local longitudinal direction of the belt, etc.

Regarding the dimensioning, it is reasonable to set the cuboids thickness to represent the belt thickness; the length and the width essentially depend on the expected deformations of the belt. (In terms of belt thickness upscaling, see also the note in the previous section regarding spherical particles; correspondingly applicable to cuboidal particles as well.)

Generally, a compromise between computational aspects and the level of approximation is relating to this length/width dimension. Larger dimensions result in fewer particles and, therefore, a lower resolution of the mesh-like belt model, which is advantageous regarding the computational effort, but may lead to defects whilst deforming the belt. Distorting or even falsifying effects may occur with particles set as too large (which is strongly dependent on the actual applicational case). Commonly reasonable length and width dimensions of about two times the thickness were proven successfully on simple test systems (such as further also on the exemplary applications as shown in Chapter 5), thus to be used for several common conveyor belt models. Also larger ratios of typically up to three or four times the thickness are

definitely possible but require individual evaluation. Generally, the fewer the expected deformations in a belt system, the larger the length/width may be set – to increase computational efficiency whilst sufficiently depicting the belt.

A disadvantage of basic cuboidal particles are sharp edges, as usually affecting the stability and thus further the computational efficiency in a negative way. Therefore, the cuboids are adapted with rounded edges. These rounded edges are also advantageous due to better smoothening the belt surface whilst deforming (as no sharp cuboid edges protrude from the belt surface).

In Figure 4-5, a particle with cuboidal geometry and rounded edges is shown (right), as equivalent to four spherical particles (left). The dimension ratio of the cuboid is exemplarily set to two, as previously discussed, thus with the length/width of the cuboid twice the sphere diameter (cuboid thickness). This contrasting example demonstrates the effective reduction of particles (and therefore also bondings) to enhance the efficiency in total by using cuboidal particle geometries. As can be deduced from the figure, in this specific example the number of particles (and further the number of bondings) is reduced to one quarter. This advantageous effect of cuboids in contrast to spheres increases strongly when overlapping of particles is enabled, as described in the previous Chapter 4.1.1.1.

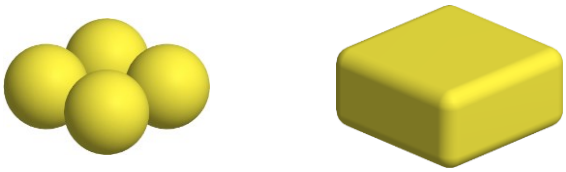

Figure 4-5: Four spherical particles (left) and an equivalent cuboidal particle (right)

Contactless overlapping is further also applied for cuboidal particles, with principally the same techniques and advantages as previously described in Chapter 4.1.1.1. With overlapping allowed, thus belt particle contact deactivated, gapping between two adjacent particles can be omitted, as during belt elongation. (This basically requires proper considerations, specifically of the size of elongations to be expected).

But moreover, overlapping allows smoothening of the belt surface whilst applying relatively strongly rounded edges, as illustrated in Figure 4-6, showing three adjacent cuboidal belt particles (isometric view on top, side view with overlaps indicated on bottom). Those particles show strongly rounded edges with deactivated contact at

overlap as distinctive – with forming a smooth belt surface. The upper limit of edge rounding is trivial: rounding radius equals half the cuboids thickness; which is principally beneficial towards the aspects mentioned above (in context with edge rounding), but generally requires larger overlaps to smoothen a belt, thus affecting the particle size in length and width (or the number of particles used), and furthermore results in correspondingly strongly rounded edges at the belt model edges. Therefore, a compromise of rounding radii, set to about one-quarter of the thickness, proved effective in several applications.

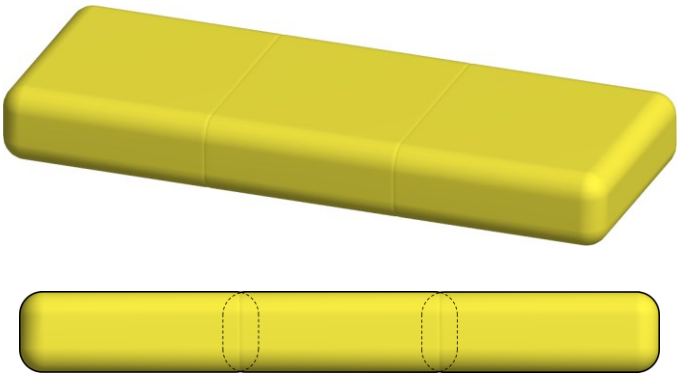

Figure 4-6: Three overlapping cuboidal particles with rounded edges forming a smoothened surface (isometric/side view, top/bottom)

(Note in that regard, proposing a specifically adapted cuboid for belt modelling: A cuboid as a primitive particle geometry consists of several elements that regard computing in terms of contact interactions: six planes, and if adapted with rounded edges, also twelve quarter-cylindrical edges as well as eight eighth-spherical corners (cf. Figure 4-5, right). However, only two planes (representing the two sides of a belt) and the rounding elements attached to these two planes are required to handle common belt surface contact. Consequently, the other elements, which are thus not relevant to contact, are basically possible to be removed/ignored from contact, which forms a proposed theoretical particle model adaption. Further aspects regarding particle geometries as such were also addressed/introduced by Fimbinger (2018) [82].)

Additionally, regarding cuboids, those are also beneficial in terms of belt visualisation; even if a belt is modelled as non-cuboidal (e.g. spherical), a solely visualising overlay of a cuboidal geometry can be applied as adapted to belt particles so that a smoothed belt surface is visualised.

In conclusion, cuboids are certainly eligible for the use as particle geometry for the modelling of BP belts in many applications. Specifically cuboids with rounded edges in a single-layer rectangular arrangement and with contactless overlapping allowed are thus proposed to be used for belt modelling purposes (regarding particle aspects). Specifications regarding further the connection of such particles with bondings are given in the following Chapter 4.1.1.4.

4.1.1.4 Particle-related parameters

Parameters that are basically relevant to the BP belt model's behaviour are, on the one hand, belt surface related, and on the other, belt mass related.

Several other properties of belt particles were also described in the previous sections, such as regarding particle dimension-ratios or contact groups (or even particle IDs).

Belt surface related

Surface-related aspects concern specifically contact effects as frictional interactions. Those regard two fundamental interaction pairs: belt-bulk and belt-components (idlers/drums); and as a third specific interaction pair, relevant for certain applications as previously already addressed: belt self-contact, either between two separate belt models (e.g. sandwich conveyor) or even within a single belt model (e.g. pipe conveyor).

With the cuboidal particle setup as proposed, macroscopic surface influences can be effectively avoided, which basically allows a relatively convenient determination of relevant parameters in this context of contact handling. Typical models/parameters as commonly used for such contacts, for example, between the belt and the conveyed bulk material, can principally be applied and further determined using established methods for that purpose (e.g. Hertz-Mindlin; cf. Chapter 2.1.2.3).

Belt mass related

The general mass property of the belt particles is trivial to set, as the sum of the individual belt particle masses is required to correspond to the mass of the total belt, which is typically known (such as determined using the mass-per-meter property of

a given belt). Also, as particle masses are commonly resulting from a defined density parameter, particle mass divided by its volume further gives this required belt particle density to be set (which is due to the contactless particle overlapping typically slightly below the actual physical belt density to be represented).

4.1.2 Bonding-related

Bondings are the essential elements to fundamentally enable the dynamically deformable behaviour of a BP belt model.

Generally, the particles to form a BP belt model are arranged according to the principles as previously defined in particle-related terms (in Chapter 4.1.1). Within such a particle setup, each bonding specifically connects two adjacent particles, resulting in the BP belt, as composed of particles and bondings. The applied bondings further allow certain behaviour, such as specifically in terms of deformability/flexibility. (Several basics in that regard are further addressed in terms of DEM basics in Chapter 2.1.2.6.1 and in the DEM-based belt modelling approaches in Chapter 3.1.2).

In the following, further specifications relating to the bonding structure of BP belts, specifically to represent belt-typical behaviour (such as basically including flexibility and anisotropic behaviour), are given.

4.1.2.1 Rectangular bonding grid structure

As presented in the previous Chapter 4.1.1.1, a belt is structured in a rectangular pattern, as shown in Figure 4-1 on the right. This rectangular particle arrangement is further forming a correspondingly rectangular bonding grid underlying the (cuboidal) belt particles, which is specifically beneficial as the bondings are consequently corresponding to the longitudinal and the transverse belt directions. (And furthermore, no diagonal bondings are distortingly influencing this orthogonal bonding grid.) This rectangular grid-form as proposed for BP belt bonding structures is illustrated in Figure 4-7, where the links between the cross points represent the virtual bondings, thus connecting each particle to one another as shown, respectively in the longitudinal and in the transverse belt directions.

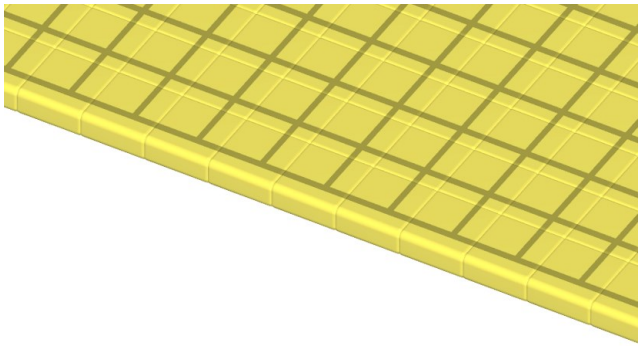

Figure 4-7: Rectangular bonding grid within a BP belt made of cuboidal particles

Especially as corresponding to the main directions of a belt (longitudinal/transverse), this type of grid structure with length/width oriented continuously arranged bonding chains is generally evaluated as beneficial in terms of representation/approximation of belts as intended with this methodology for dynamic belt simulation. This structure is furthermore suitable, especially in terms of defining and analysing such BP belts, such as further regarding the methods/techniques and also parameter-related aspects that follow.

Generally, such a rectangular bonding structure as illustrated results in the main cross-sectional areas of belts being represented with multiple, parallel arranged bondings (again, regarding the main belt directions: longitudinal/transverse). Furthermore, as already described in bonding-related basics, the general cross-sectional area of bondings is simply circular. Consequently, the cross-sections of belts are virtually represented with multiple parallel-arranged circular bonding areas, which is illustratively shown in Figure 4-8.

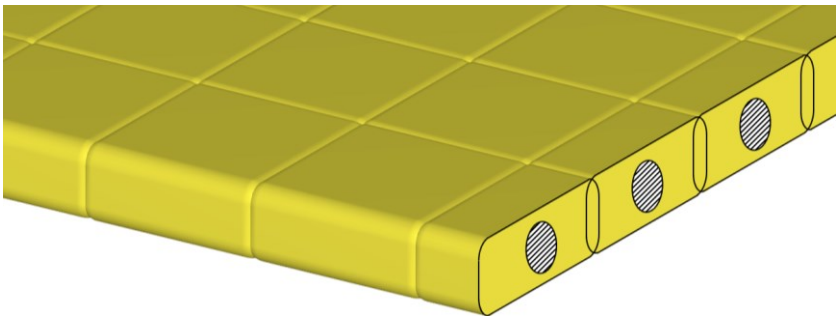

Figure 4-8: Parallel bondings in a BP belt with their virtual circular cross sections visualised (hatched areas; cross-sectional view of a BP belt)

This aspect is further also dealt with in terms of bonding-related properties in Chapter 4.1.2.4; such as proposing to set areas as equal (the sum of the circular bonding cross-sections as equal to the belt cross-section to be represented (which is physically rectangular)) in order to allow a convenient definition of tensile properties (basically regards the bonding's Young's modulus). In general, however, it is in any case necessary to take aspects relating to this form of bonding structure as described into account when modelling BP belts.

4.1.2.2 Enabling belt-typical flexibility behaviour

An essential method of this belt simulation methodology to allow a digital BP belt model as described to depict belt-typical flexibility behaviour is introduced as follows.

Principally, as conveyor belts consist of multiple materials (as described in Chapter 2.2.2.1: typically consisting of different layers of base (rubber) material with embedded textile plies or steel cords), the belt-representing bondings must fundamentally be able to depict certain effects attributable to inhomogeneous material behaviour. Due to the material mix (and some further related geometrical influences, e.g. resulting from the lay patterns of embedded steel cords), a typical conveyor belt is stiff in its tensile behaviour and flexible in its bending behaviour. Therefore, the bonding model applied in the BP belt is customised in order to allow this kind of bending/tension behaviour. For this purpose, a bonding reduction factor ($f_{b,red}$) as an additional bonding property to define a belt's ratio of bending resistance in relation to tensile resistance is introduced. This factor thus generally indicates the bending flexibility of a belt in reference to its tensile stiffness.

The following Equations (24)-(27) show the relevant numerics regarding the implementation of the adapted bonding model, including the bonding reduction factor ($f_{b,red}$) to adjust a bonding's flexibility. As elaborated in cooperation (Becker and Fimbinger [16]) in 2017 in the course of this methodology's development, it was further implemented in ThreeParticle/CAE initially in 2017 (as an available bonding model since version R1.1). (The underlying bonding numerics are generally based on common bonding numerics, such as by Obermayr, et al. [189], further relatively simple but effectively extended with $f_{b,red}$.)

$$F_b = \begin{bmatrix} Y_b A_b & & \\ & \alpha_s G_b A_b & \\ & & \alpha_s G_b A_b \end{bmatrix} \zeta_b \tag{24}$$

$$F_{b,d} = f_{b,d} \begin{bmatrix} \sqrt{\frac{Y_b A_b}{L_{b,0}} m_r} & & \\ & \sqrt{\frac{\alpha_s G_b A_b}{L_{b,0}} m_r} & \\ & & \sqrt{\frac{\alpha_s G_b A_b}{L_{b,0}} m_r} \end{bmatrix} v_{rel} \tag{25}$$

$$T_b = \begin{bmatrix} 2G_b I_b & & \\ & Y_b I_b & \\ & & Y_b I_b \end{bmatrix} \kappa \; f_{b,red} \tag{26}$$

$$T_{b,d} = f_{b,d} \begin{bmatrix} \sqrt{\frac{2G_b I_b}{L_{b,0}} I_r} & & \\ & \sqrt{\frac{Y_b I_b}{L_{b,0}} I_r} & \\ & & \sqrt{\frac{Y_b I_b}{L_{b,0}} I_r} \end{bmatrix} \Omega_{rel} \; f_{b,red} \tag{27}$$

(Regarding a bonding element, and correspondingly the two connected particles (indicated with (p)), with:

F_b	… Force (rlt. tension/compression, shear)	Y_b	… Young's modulus
$F_{b,d}$	… Damping force (rlt. tension/compression, shear)	G_b	… Shear modulus
T_b	… Torque (rlt. bending, torsion)	A_b	… Cross-sectional area
$T_{b,d}$	… Damping torque (rlt. bending, torsion)	I_b	… Geometrical moment of inertia
ζ_b	… Strain	($Y_b I_b$	… Bending stiffness)
v_{rel}	… Relative translatory velocity (p)	($2G_b I_b$	… Torsional stiffness)
κ	… Relative angular displacement (p)	α_s	… Timoshenko shear coefficient
Ω_{rel}	… Relative angular velocity (p)	$L_{b,0}$	… Initial length
$f_{b,d}$	… Damping factor	m_r	… Reduced mass (p)
$f_{b,red}$	… Reduction factor	I_r	… Reduced mass moment of inertia (p)

respectively translated, after Becker and Fimbinger (2017) [16].)

This bonding model principally allows defining a form of inhomogeneous bonding behaviour; more specifically, it enables the capability to represent deviating behaviour between tension/compression and bending, as it is required for the flexible behaviour of typical belts.

The effects on the bending/tension behaviour of a bonding model by adjusting the introduced reduction factor are further illustrated in Figure 4-9. Thereby, an initial bonding model is shown on the left ($f_{b,red} = 1$), and an adjusted model with a decreased reduction factor resulting in an increased bending flexibility is illustrated on the right ($f_{b,red} = 0.1$). Both models have their ends fixed on the left end and are applied the same tensile load (top) and bending load (bottom). The colouring indicates the particle displacements representing the elongation (top) and the sag (bottom) of the models under load.

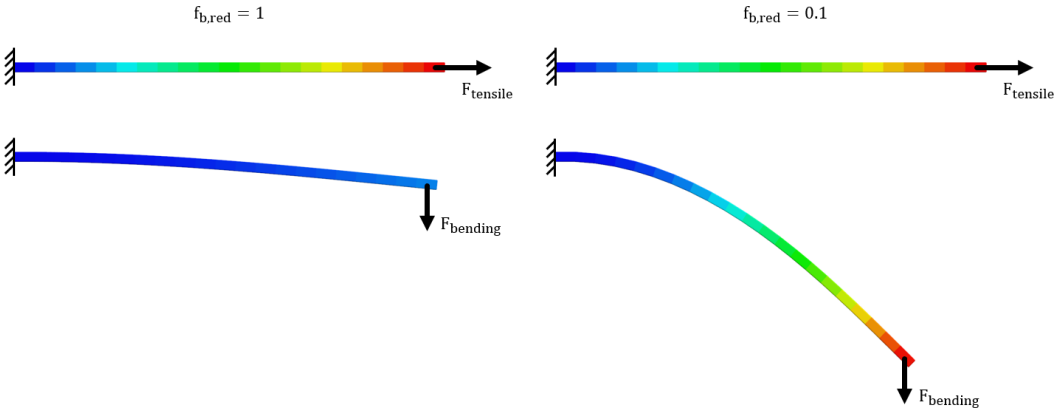

Figure 4-9: Bonded particles under tensile (top) and bending load (bottom), with a reduction factor of 1 (left) and 0.1 (right)

As distinctive, the reduced factor ($f_{b,red}$ from 1 to 0.1) is decreasing the bending resistance of the bondings (as resulting when comparing the bending characteristics at the bottom), but essentially: without influencing their tensile resistance (shown at the top). To summarise the influence in that regard: The divergent reduction factor leads to a behaviour that is equal in tension but differs in bending, which is fundamentally required for common belt representation. (Typically with $f_{b,red} < 1$.)

In the subsequent Chapter 4.1.2.4, several aspects regarding bonding-related parameters, as also including this discussed technique that enables the enhanced belt-typical behaviour (characterised with flexible bending and stiff tensional behaviour), are further addressed.

4.1.2.3 Fibred belt setup to enable anisotropic behaviour

Depending on their internal structure, certain types of belts further show different behaviour in longitudinal and in transverse belt direction, which is here generally referred to as anisotropic belt behaviour. As an illustrative example, conveyor belts with longitudinal embedded steel cords but only minor transverse reinforcement consequently react stiffer in longitudinal than in transverse belt direction (e.g. see Figure 2-16, and generally Chapter 2.2.2.1 for such conveyor belt setups). When such anisotropic belt behaviour is required to be considered in belt simulations, such as to adequately depict this certain type of belt as mentioned, these characteristics need to be depicted by the representing belt model correspondingly.

For enhancing the capabilities of BP belts as presented, a convenient modelling technique is introduced that enables different belt characteristics in longitudinal and transverse belt directions, further allowing this anisotropic belt behaviour to be depictable. Therefore, this technique is based on using different bonding definitions in the longitudinal and the transverse belt directions. To allow such definitions to be set individually, the grid that forms a BP belt is further structured into fibres. In this context, fibres refer to the rows of bonded particles in the longitudinal direction of a BP belt. With this fibred structuring, the following is obtained: The bondings within each fibre correspond to the longitudinal direction, whereas the bondings between every two adjacent fibres correspond to the transverse direction. In Figure 4-10, this structuring is illustrated in a bonding grid underlying a BP belt (fibres and different bonding definitions indicated in different colours).

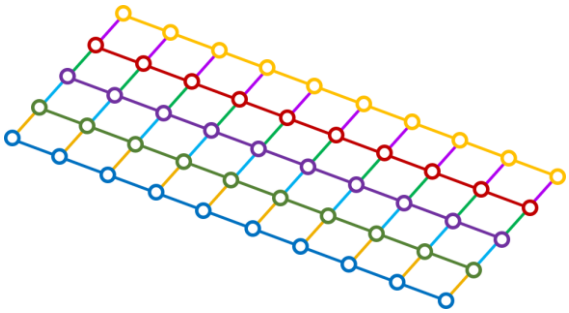

Figure 4-10: Five parallel fibres in the bonding grid of a BP belt; different bonding definitions indicated in colour

To generally allow this form of individual bonding definition, each fibre is required to be made from a particle type different to the ones in its adjacent fibres. This is also indicated in Figure 4-10 with the coloured particles (indicated as spheres) forming each fibre as a chain of the same type of particle. With this modelling technique, the bondings between two particles of the same type represent inner-fibre bonding (thus, in longitudinal direction), and accordingly, bondings between two particles of different type represent trans-fibre bonding (thus, in transverse direction).

Various forms of heterogenous belt structuring

A relatively simple method, which is sufficient for the definition of general BP belts with deviating behaviour in longitudinal and transverse belt direction, is using two alternating fibre types (correspondingly two different particle types). To illustrate this method: With the particle types A and B each forming a fibre type, and those fibres further alternatingly arranged side-by-side to form the BP belt, the different bonding definitions are set as follows: for longitudinal bondings: A to A and B to B (inner-fibre); and for transverse bondings: A to B (trans-fibre). This kind of BP belt structuring with two alternating fibre types is also implemented in the developed software tool for belt initialisation (BeltConverter; cf. Chapter 4.2.5); and is, for example, clearly recognisable in the shown application of the belt turning station in Chapter 5.3.

For several other, typically advanced purposes relating to this BP belt structuring, such simple alternating fibre types are probably not sufficient, and other forms of structuring are required (e.g. using all induvial fibre types), as outlined in the next sections.

As a further enhancement, to allow even further variations of bonding definitions within a BP belt, all individual fibre types principally allow specific bonding definitions in respect to individual fibres. Each series of bondings along the longitudinal direction can be defined individually with this type of all individual fibre structuring. This structuring can find application, for example, to model fibres individually in terms of varying reinforced characteristics (e.g. regarding embedded steel cords).

Besides the purpose of modelling different bonding behaviour, fibres can further be used in terms of self-contact definition, as already addressed in Chapter 4.1.1.2.

Therefore, the fibres are meant to be grouped into certain contact groups, to be further defined as to act with/without contact with each other (e.g. to allow the two belt edges of a pipe conveyor belt to get in contact; see Chapter 4.1.1.2). This grouping requires a corresponding fibre setup, basically relating to the contact groups. (E.g., the pipe conveyor belt in Figure 4-3 requires fibres in correspondence with the contact groups (three types); and, if anisotropic behaviour is to be included as well, alternating fibres within each contact group are further required. (Resulting in at least six types in total; but using all individual fibres is principally also feasible for such cases, which is furthermore convenient in terms of modelling.)

Other advantages of using this fibre technique are furthermore related to the analysation of the belt. In this regard, fibred BP belts principally allow fibre-based analysations, such as in respect to a specific bonding direction (inter-fibre/trans-fibre analyses; thus to analyse various results in longitudinal/transverse belt directions separately), but further also to isolate single fibres for detailed analysation (e.g. to isolate belt edges; as demonstrated in Figure 4-11, indicating deviations in elongation (bonding strain) along the belt edges of a pipe conveyor belt at the feeding point, thus during pipe-unforming/forming; full system, see Chapter 5.5.) For such individual isolation of single fibres, BP belt structuring with all induvial fibre types is required.

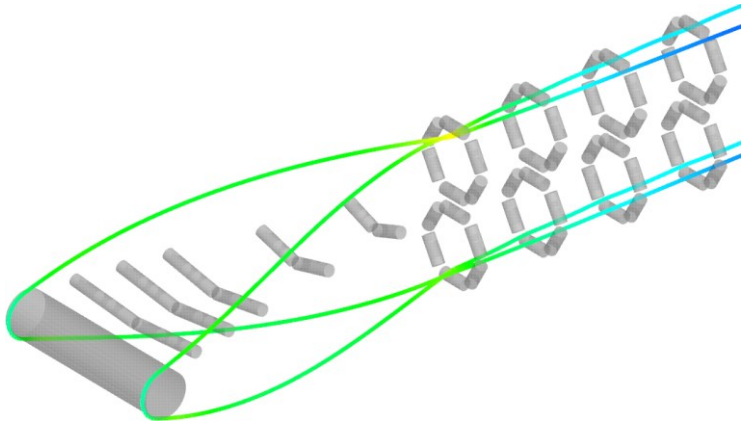

Figure 4-11: Isolated fibre analyses of the two belt edges of a BP belt at the feeding point of a pipe conveyor (bonding strain deviations indicated in colour) [88]

BP belt structuring with all individual (different) fibres is also implemented in the developed software tool for belt initialisation (BeltConverter; cf. Chapter 4.2.5). The shown analyses in Figure 4-11, regarding the pipe conveyor presented in Chapter 5.5, is an illustrative example for using this kind of structuring.

Additionally to this longitudinally-oriented fibred structuring of a BP belt, other structuring schemes, also based on the same principles of using different bonding definitions within a BP belt, are also feasible. By specifically defining certain local bondings within a BP belt, more complex belt modelling is principally allowed, such as by defining certain types of bondings at belt joints (representing the physical connection of two belt ends to form endless belts) or also to implement specific local belt defects. This kind of local BP belt structuring requires that the particles at these certain sections are set accordingly in terms of their particle type in order to enable very specific local bonding definitions to be applied. For example, the belt breakage study shown in Chapter 5.7 illustrates this manual form of BP belt structuring.

4.1.2.4 Bonding-related parameters

The numerics as given in Equations (24)-(27) already indicate the influences from various parameters for defining a certain bonding behaviour. In the scope of BP belt modelling as presented, several major parameters in that bonding-related context are discussed subsequently, also including general aspects in terms of their determination as to depict specific belt-typical characteristics, such as regarding the deviating bending/tension behaviour (by means of the introduced reduction factor).

Generally, some bonding-structure-relevant properties also derive from the particle-related parameters (Chapter 4.1.1). In particular, this relates to the general particle arrangement, which correspondingly gives the geometry of the bonding grid, more specifically the longitudinal/transverse-oriented bonding lengths and the number of parallel bondings representing a belt cross-section (as described in Chapter 4.1.2.1). This resulting bonding grid is the base structure, in which the comprising bondings are required to be adjusted to represent belt-like characteristics (as mentioned several times: general flexible characteristics, deviating bending/tension behaviour, or also anisotropic (length/width-deviating) behaviour). Furthermore, load-related effects (interactional as well as from the belt mass) are also attributable to particles, as bondings are virtual (surface- and mass-less) beam elements. Several effects in these regards (contact with bulk or system components, or belt weight effects) act via the belt particles, which are further linked to the bonding grid for transferring corresponding loads into the bonding structure as presented.

The descriptions given below are explicitly explained on a set of parallel-arranged bondings, as illustrated in Figure 4-12, representing a main direction of a BP belt. Respectively, especially with regard to anisotropic belt modelling as described in Chapter 4.1.2.3, to be considered for longitudinally and transversely oriented bondings separately (or furthermore, if applied, on a more specific level regarding local bonding definitions, e.g. to represent individual reinforcement areas or belt joints).

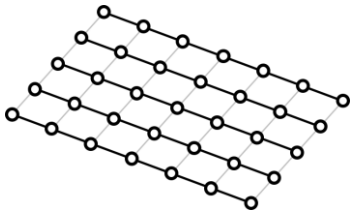

Figure 4-12: Bonding grid of a BP belt with parallel bondings representing a main belt direction highlighted

The properties of these bondings require certain parameter definitions in order to represent belt-like behaviour. The major influencing parameters in this regard are the bonding's: (cf. Eq. (24)-(27))

- Area (A_b, commonly defined with the bonding radius r_b)
- Young's modulus (Y_b; and respectively the shear modulus (G_b), commonly defined via Poisson's ratio (ν_b))
- Reduction factor ($f_{b,red}$)
- Damping factor ($f_{b,d}$)
- (Breakage criteria, if applied)

(Furthermore: the initial bonding length ($L_{b,0}$) and the number of parallel bondings in the respective cross-section (n_b) as derived from the particle-based structure, as explained before.)

These parameters as listed are principally capable of representing specific belt behaviour, for which a certain set of parameters has to be determined, typically, by adjusting relevant parameters until a desired belt behaviour is digitally reproducible. Thereby, mutual influences of parameters need to be considered, for example, between the area and the Young's modulus in terms of belt elongation under load. One convenient and straightforward approach regarding the definitions of such a bonding parameter set is presented in the following.

Area and Young's modulus

In this context, a start condition is proposed to set the bonding area in relation to the belt cross-section area intended to be depicted (A_{belt}). Therefore, as already announced in Chapter 4.1.2.1, the cross-section of the parallel bondings ($A_b\ n_b$) is set as equal to this belt cross-section area, which is typically rectangular with the belt's cross-sectional width and thickness ($A_{belt} = w_{belt}\ t_{belt}$); resulting in Equation (28) (and with the bonding radius r_b trivially following from the circular bonding area: $A_b = {r_b}^2\ \pi/4$).

$$A_b = \frac{w_{belt}\ t_{belt}}{n_b} \tag{28}$$

With this condition, the bonding's Young's modulus (Y_b) is allowed to be set equal with the one to be depicted, regarding the tensile behaviour, as determined from the stress-strain relationship, typically from tensile tests on belts (with respect to the condition at which the belt is intended to be used; e.g. worn-in belt). Reference values herefore are also provided by manufacturers/vendors, commonly also in width-related form as the belt modulus ($Y'_{belt} = Y_{belt}/w_{belt}$). (See Chapter 2.2.2.1 regarding references.) From a belt modulus, the bonding's Young's modulus follows as:

$$Y_b = Y_{belt} = Y'_{belt}\ w_{belt} \tag{29}$$

With the area (A_b) and the Young's modulus (Y_b) set (as values relating to physical values), two major parameters (as unitless factors) define a BP belt's flexibility characteristics: the bonding reduction factor ($f_{b,red}$) and also the bonding damping factor ($f_{b,d}$).

Bonding reduction factor and damping factor

Regarding the determination of these two factors, it is proposed to perform parameter-finding simulations. Thereby, these factors are adjusted to obtain certain flexibility characteristics of the BP belt as it is intended. As relatively simple and easy-to-apply, two possible principles are proposed as useful for this purpose:

- with one-end-fixed (cantilever beam)
- with two ends supported (transverse flexibility test, three/four-point bending)

Both principles are relatively common. For example, especially cantilever beams are already shown/referenced in several applications for bonded particle modelling in Chapter 3.1.2, e.g. in Figure 3-17 or also Figure 3-19. According to this one-end-fixed principle, a section of a BP belt is held at one end and dynamically deformed from either only its own weight (as typical), or, if required, also with an additional load applied, such as by a weight attached to the other belt end. Due to its common nature, this principle is further described in the following. (Generally, the described determination process is applicable in a similar form on various other principles, as subsequently outlined.)

(Side note: Initial work on this one-end-fixed principle was covered in a related study by Bialowas (2017) [24] (further supervised/supported by Fimbinger) confirmed general feasibility in these terms – with the work including comparative observations of physically tested belts and FEM simulations, further with DEM-based belt models (as specifically provided by Fimbinger; with an applied DEM model relating to a simple form of spherically-shaped linear bonded-particles (cf. fibres, etc. in Chapter 3.1.2.2.1); furthermore covering initial testing of such DEM-based/bonded-particle approaches in general, as explained in the basics in Chapter 3.1.2).)

According to the descriptions before, the simulation of a one-side-fixed BP belt section, already deformed under its own weight, is illustrated in Figure 4-13.

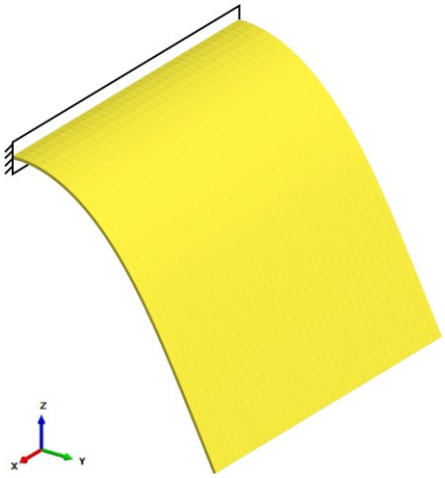

Figure 4-13: One-side-fixed BP belt section deforming under its own weight

As can be derived, the characteristics of interest in this application are invariant to the number of parallel arranged fibres, as those react/deform equally (under the typical condition that each fibre has the same homogeneous bonding definitions; in this regard, see also Chapter 4.1.2.3). Thus, the evaluation of such a single fibre is generally sufficient in this context (cf. also Figure 3-17 in Chapter 3.1.2.2.1).

To determine the two factors ($f_{b,red}$ and $f_{b,d}$) the deformation behaviour of the belt (specifically the belt sag) is analysed – in terms of final deformed position, indicating the reduction factor ($f_{b,red}$), and in terms of dynamic oscillation, indicating the damping factor ($f_{b,d}$).

An overview of varying results from varying reduction factors ($f_{b,red}$) is given in Table 4-1 (with $f_{b,d}$ fixed). The resulting belt deformation (at rest, after oscillating in this final deformed state) is shown in the side view, as well as indicating the lowering (or also the displacement) of BP belt particles in colour.

$f_{b,red}$ →		
0.1	0.3	0.5
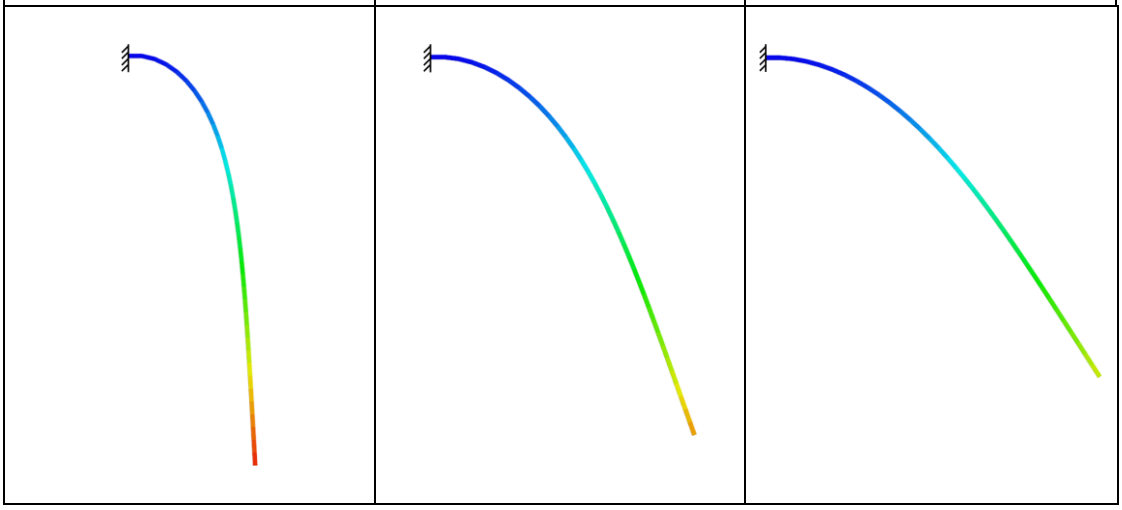		

Table 4-1: Influence of the reduction factor on the one-side-fixed BP belt

The influence of the damping factor ($f_{b,d}$) is illustrated in Table 4-2 (with $f_{b,red}$ fixed), showing the velocity of the particle at the unfixed end, plotted in graphs over time.[9]

[9] in equally scaled graphs; applies also to the next table

$f_{b,d} \rightarrow$		
0.05	0.15	0.25
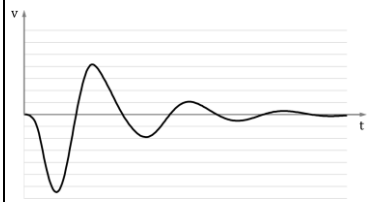		

Table 4-2: Influence of the damping factor on the one-side-fixed BP belt (velocity at the unfixed end over time)

Table 4-3 shows a combined version, where both aspects, reduction and damping ($f_{b,red}$ and $f_{b,d}$) are brought together as graphs of the displacement of the particle at the unfixed end, plotted over time.

		$f_{b,red} \rightarrow$		
		0.1	0.3	0.5
$\leftarrow f_{b,d}$	0.05	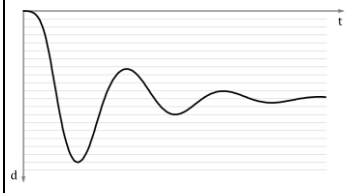	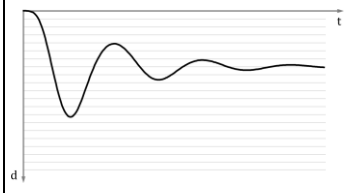	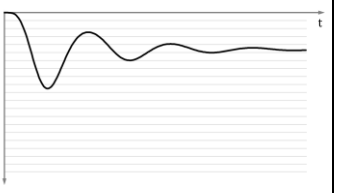
	0.15	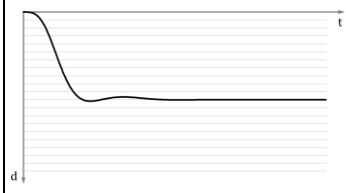	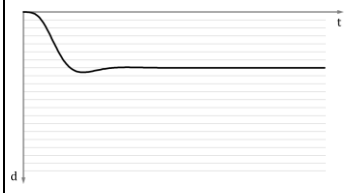	
	0.25	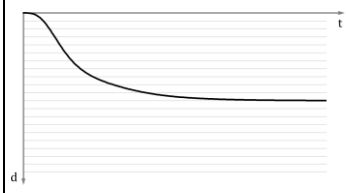	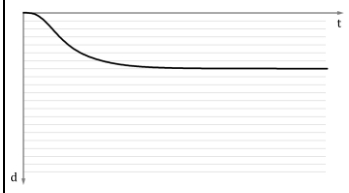	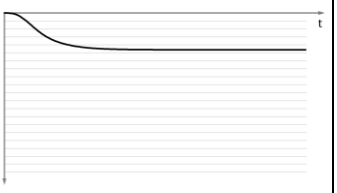

Table 4-3: Influences of reduction factor and damping factor on the one-side-fixed BP belt combined (displacement of the unfixed end over time)

Considering these results (either in individual or combined form), the factors $f_{b,red}$ and $f_{b,d}$ can be set accordingly to represent the shown flexibility behaviour.

Other determination approaches, such as based on principles with two ends of the BP belt supported, require analyses in a similar form: regarding the final deformation ($f_{b,red}$) and time-depending (dynamic) effects ($f_{b,d}$). Such approaches concern, for example, setups as the transverse flexibility test (cf. ISO 703 [126]) or three/four-point bending setups (e.g. see references in Chapter 3.1.2.2.2). (Especially three/four-point bending would further allow pre-tensioning of the belt during the determination, which can be beneficial in terms of respecting this pre-tensioned condition, if of interest.)

Breakage capabilities

As an advancement, BP belt breakage is generally possible to be considered, as such capabilities are principally feasible to be implemented in BP belts by using bonding breakage criteria (e.g. typically based on Mises ([247]) stresses; other specific criteria in customised form see also basics in Chapter 2.1.2.6.1). In that regard, several BPMs specifically for this purpose of depicting breakage are generally also presented in Chapter 3.1.2.2.

In the example of a belt breakage study in Chapter 5.7, this advancement towards bonding breakage is applied. In this specific case, an area of interest is locally modelled according to the manual BP belt structuring proposed in Chapter 4.1.2.3. The longitudinal bondings in this area are further set to allow breakage via using the bonding model of ThreeParticle/CAE, which further also allows random deviations of breakage limits across several bondings to create a form of inhomogeneity within BPMs regarding its breakage behaviour (cf. ThreeParticle/CAE User Guide [13]).

4.2 Belt initialisation

Besides the general modelling of BP belts, as described in the preceding Chapter 4.1, the developed methodology further comprises a method regarding the initialisation of such BP belts, specifically BP belt initialisation in almost-final state (in the following generally also referred to as (belt) initialisation).

In the corresponding approaches in Chapter 3.2, relevant basics in that regard were already discussed, explicitly outlining the differences/benefits/challenges of this approach of almost-final state initialisation, specifically in contrast to state-of-rest initialisation.

In the first following subchapter (Chapter 4.2.1), aspects regarding the application of this form of belt initialisation (in almost-final state) are further addressed, in particular concerning the effects that occur during belt forming from almost-final (initialised) state into final (assembled) state, which is typically expressed in the form of transient oscillation.

As a major part of this developed methodology, the belt initialisation (in almost-final state) is based on initialising (DEM) BP belt models based on CAD belt models containing the desired (typically deformed) belt shapes. The presented conversion procedure in this context, further referred to as CAD-to-DEM, forms the basis for this belt initialisation technique in general. Various considerations/descriptions, specifications, and developments relating explicitly to this CAD-to-DEM process as forming a major part of the methodology presented in this thesis are further covered in the subsequent chapters. Especially the developed conversion algorithm as described (in Chapter 4.2.4) is forming the core of this technique (CAD-to-DEM); as furthermore implemented in the software tool BeltConverter (introduced in Chapter 4.2.5) to allow convenient conversions of CAD belt models into respective DEM belt models.

4.2.1 Almost-final state initialisation and transient response

As described, the initialisation of a BP belt is fundamentally based on using a corresponding CAD belt model that contains the desired form of the belt to be initialised.

Such belt-representing geometries in CAD data format are typically available from the design data of belt systems, in which those belts are embedded, thus modelled, commonly in idealised form – specifically approximated/estimated to be relatively close to the final assembled form of such a belt. (With the final assembled form including belt sag, corresponding troughing, etc.; see also exemplary applications in Chapter 5.) Such design-related CAD models are generally not directly applicable to the CAD-to-DEM procedure, specifically regarding the BeltConverter, as certain preparations to the CAD model are required; as closer described in the respective section regarding CAD (input) data in Chapter 4.2.3.1. Generally, these preparations concern the transformation of a (usually voluminous) belt model into a surface-mesh structure that represents the bonding grid of the final BP belt.

For further demonstration purposes, Figure 4-14 shows the section of a belt system intended to be applied for a dynamic belt simulation according to the developed methodology. (This belt section corresponds specifically to the feeding point of the pipe conveyor presented in Chapter 5.5). The preparation of the original belt model (left) resulting in the prepared surface model in quadrilateral-meshed form of the belt (right) is illustrated. The detailed views give further insights, showing the original voluminous belt model (left), and the meshed surface of the prepared belt model (right).

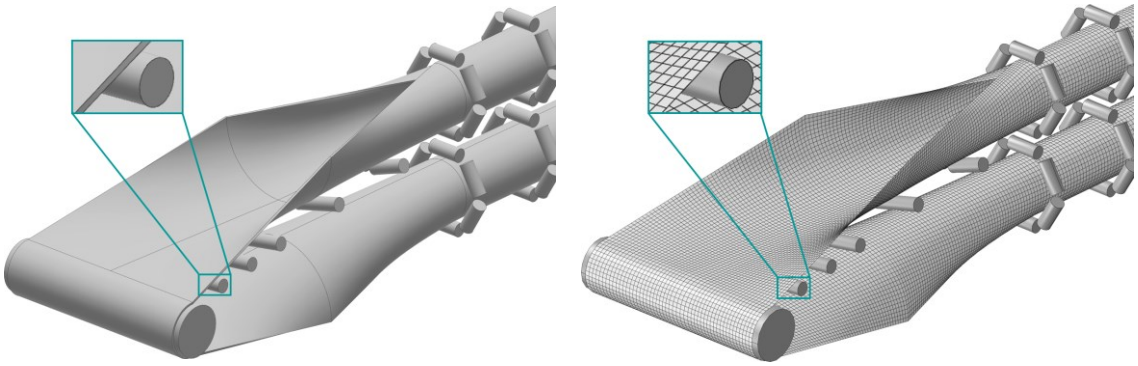

Figure 4-14: CAD model of the belt system with a voluminous belt model (left), further prepared as a quadrilateral-meshed belt model for conversion (right)

Note: The flat-to-troughed section is intentionally formed showing a rather non-ideal geometry (as shown), in order to highlight transient oscillation effects, described in the following. Generally: the closer the CAD belt geometry is approximated/estimated to the (final) form of the assembled belt, the lower the efforts required for such

a pre-simulation result (which is, e.g., the case for the exemplary application of the conventional belt conveyor as shown in Chapter 5.2).

After the preparation (see also Chapter 4.2.3.1.2), the CAD belt model is converted into a BP belt with the developed conversion tool BeltConverter (see also following chapters).

The resulting BP belt initialised within relevant system components (idlers/pulleys) is shown in Figure 4-15, on the left. When this simulation with the setup as shown is started, the BP belt forms from the almost-final state as initialised into the final (assembled/operating) steady-state, as shown on the right. This simulation basically refers to a pre-simulation, as it compensates for these addressed differences further to reach the starting condition of the actual simulation of interest that follows this pre-simulation.

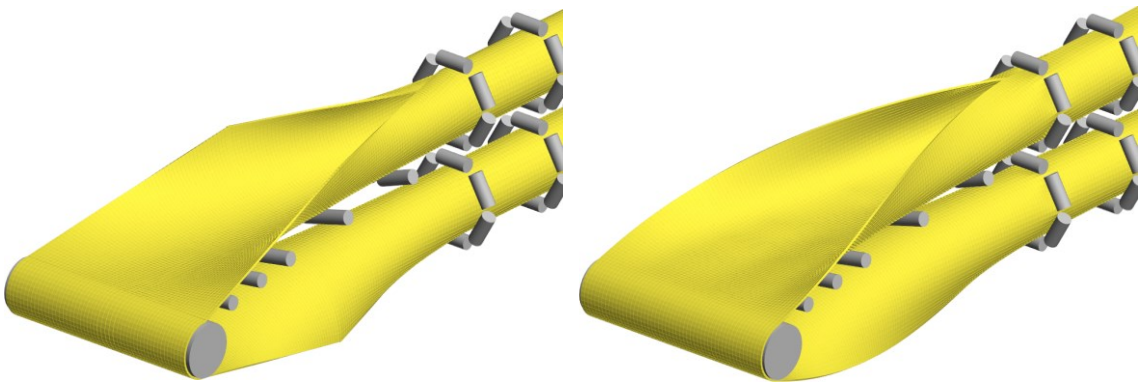

Figure 4-15: Initialised BP belt (left) in almost-final state, and this BP belt after pre-simulation (transient oscillation), thus formed into its final steady-state (right)

As an extension to the initialisation in almost-final state, the CAD-to-DEM conversion further allows the definition of a belt velocity to be included at initialisation (see also Chapter 4.2.4.3). This way, an already running belt, thus in operating state, can be initialised, as illustrated in Figure 4-16, where the velocity of each belt particle within the BP belt is shown in vector visualisation.

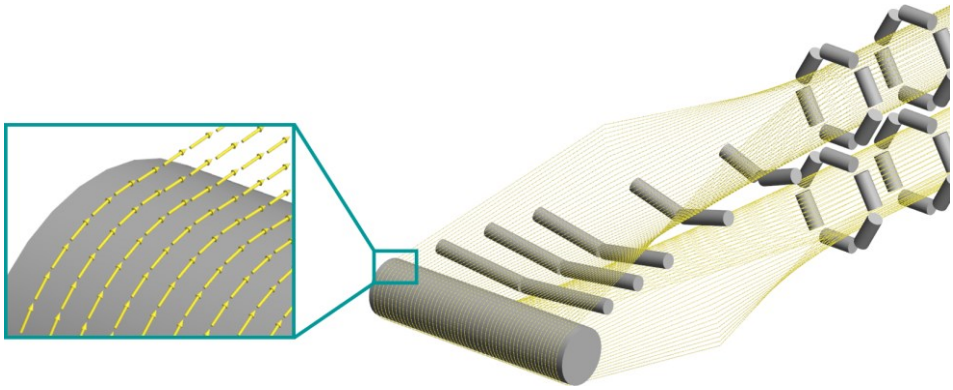

Figure 4-16: Initialised belt velocity

During the relatively short pre-simulation as previously introduced, a BP belt settles into a final steady-state, typically by expressing a transient response, which happens relatively quickly, typically within fractions (hundredths/tenths) of simulated seconds. In terms of such a transient oscillation of a BP belt, several aspects are to be considered. Generally, the entire system – comprising not only the BP belt, but furthermore possible already initialised bulk material particles, and also idlers and pulleys, as in this context in more detail also covered in Chapter 4.4, regarding the use of smooth-surfaced cylinders for such parts – forms into an equilibrium state by balancing unstable model states that are initialised.

A major effect, especially at the very beginning of this oscillation of the BP belt, is the occurrence of relatively high belt particle velocities – in translational and also rotational form. This effect is shown in Figure 4-17, illustrating several time steps during the transient oscillation process (of the belt system shown before) with the particle velocities[10] of the BP belt visualised in colour.

[10] translational velocity magnitudes (and in similar form also regarding rotational velocities, as generally showing a very similar picture)

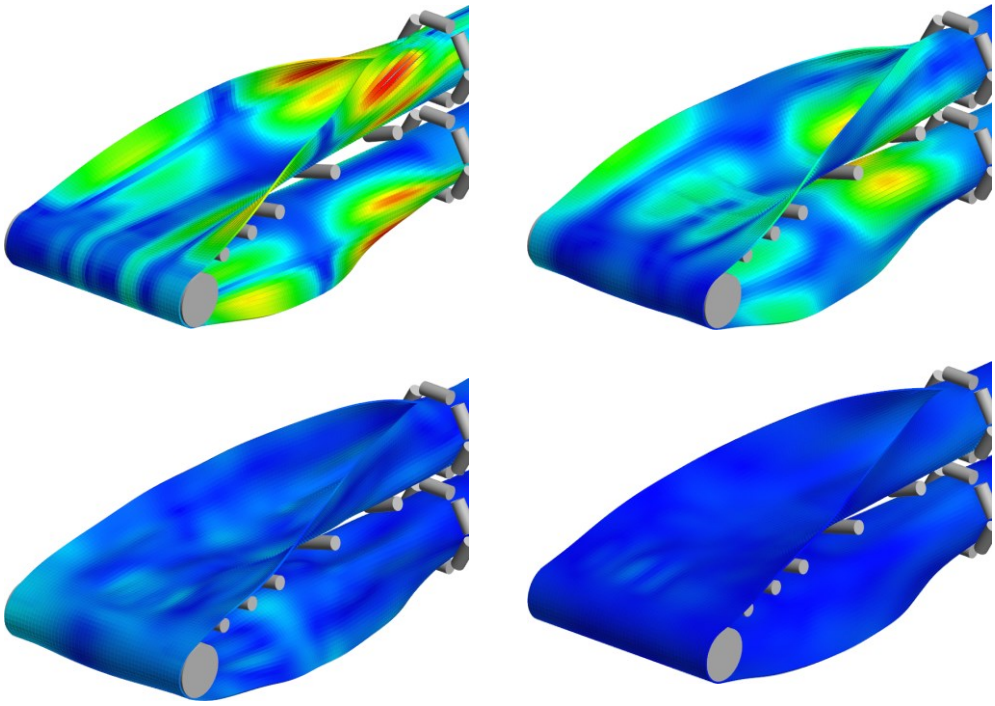

Figure 4-17: Transient oscillation of the BP belt (from top left to bottom right) (local particle velocities indicated in colour)

Note: As revealed in the figures, this specific example demonstrates the belt formation process and the related effects more clearly – explicitly due to the rather less closely/non-ideal approximated belt geometry introduced/described before (regarding/below Figure 4-14). This base geometry leads to more pronounced effects occurring during the transient oscillation process. Also, more time steps[11] are consequently required to reach steady-state, compared to cases where belt geometries are approximated in a more favourable form, as it is generally intended (see also other exemplary applications in Chapter 5). However, the oscillation shown (Figure 4 18) corresponds to only approx. 0.04 simulated seconds, which furthermore emphasises the high potential of this presented initialisation method (almost-final state) in terms of reducing pre-simulation efforts to a marginal minimum.

As evident from the figure, a BP belt can react with relative strong oscillation effects, resulting in (also irregularly) high particle velocities occurring during the deformation of the BP belt into its steady-state, especially at the beginning of the pre-simulation process (top right). Such high particle velocities further require relatively

[11].

small time steps to be set in order to obtain a stable simulation (cf. also Chapter 2.1.3.1). However, since these initially high particle velocities decrease with progressing of the transient oscillation, the time step can principally be increased accordingly. This can either be done conventionally by pausing at certain save intervals and changing the time step manually – or alternatively in a convenient way by using the "keyword timing" feature available in ThreeParticle/CAE (by defining that the time step is changed to an increased value when a certain simulation time is reached/exceeded, which does not require a tight save interval as for the method using manual change at pause; see also Keywords Guide [12] for more information in that regard).

In addition, setting certain particle velocity limits (for translational as well as rotational velocities of the belt particles) can also be used in this context to influence the described transient oscillation process advantageously. This specifically relates to stabilising the simulation due to keeping velocities within limits, and above all to reaching the desired (almost-final/steady) state with fewer time steps, as those can accordingly be set to already increased values, and thus, affects to require even lower computational effort/time.

With reaching the final (steady) state, the transient oscillation, thus the pre-simulation, is finished – and the DEM simulation setup, including the BP belt in the desired assembled/operational state, is ready to be used for the following simulation as intended.

Generally, the addressed transient oscillation process forming the pre-simulation requires only a minor effort, compared to the actual simulation of interest that follows, and above all, especially compared to the pre-simulation efforts required for trivial/conventional assembling methods of belt models, as by forming them into their assembled state with starting from a state-of-rest (see Chapter 3.2.1).

In conclusion, by decreasing the required efforts in these terms of pre-simulation to almost a minimum, this technique of belt initialisation in almost-final state proves enormous benefits.

In the following chapters, details of the essential CAD-to-DEM procedure, as addressed in the previous sections in terms of using the developed conversion tool BeltConverter, are given.

4.2.2 The CAD-to-DEM process in general

As introduced, the presented belt initialisation method is based on using a process, further referred to as CAD-to-DEM, that principally describes initialising a DEM belt model (a BP belt) based on a given CAD belt model.

The central core of this CAD-to-DEM process is the developed algorithm for performing the computation from CAD to DEM data, thus presenting a conversion algorithm. The main tasks of this algorithm are the determination of the particles and bondings to form the BP belt (accordingly to represent the given (CAD) geometry) – but further the consideration of local belt conditions due to this typically deformed belt geometry. The developed algorithm is furthermore programmed/implemented to be used via a software tool that allows convenient belt conversion via an added graphical user interface (GUI). Details in these regards are specifically given in the chapters after; comprising input/output data specifications (CAD/DEM; Chapter 4.2.3), essential modules of the conversion algorithm (Chapter 4.2.4), and finally, the description of the software tool to be used for belt conversion (BeltConverter; see Chapter 4.2.5). Prior to these detailed elaborations, several aspects, considerations and definitions are given in the following subchapters, which are fundamentally relevant to the developments made and described.

4.2.2.1 General requirements on belt models intended for conversion

In general, one CAD-to-DEM process handles the conversion of one belt model from CAD to DEM – with the provided CAD data fulfilling specific requirements as defined in detail in Chapter 4.2.3.1, and the computed DEM data resulting as described in Chapter 4.2.3.2 and Chapter 4.2.4.4 (further to be used specifically in ThreeParticle/CAE).

According to the almost-final state approach, it is intended that the belt model to be converted represents a belt in a particular (close-to assembled) geometry such as to fit into a belt (conveyor) system. Therefore, such a belt model typically contains a correspondingly deformed/distorted geometry. Also, as a general prerequisite, the belt model is required to respect belt-typical geometrical characteristics (as a flat

belt-like object with almost constant belt width, without sharp edges within the belt's surface, and without self-penetration).

Furthermore, the model is allowed to either represent a finite or an endless belt, which refers to belts, which in their state-of-rest show either a rectangular (finite) or a ring-shaped cylindrical (endless) form. Both those types with their state-of-rest are shown in the following chapter, in Figure 4-18 and Figure 4-19, further indicating their geometrical characteristics.

4.2.2.2 Principles for the consideration of deformation states

As common, the undeformed state of belts is considered flat and undistorted/untensioned. This fundamental consideration is crucial to further account for belt deformations as the differences between this undeformed state and a given deformed state.

Furthermore, with reference to the previous Chapter 4.1 regarding BP belt modelling, a grid is applied as the underlying structure to form a BP belt, which shows a perfectly plane, rectangular form in its undeformed state. In any deformed state, on the other hand, this grid is correspondingly distorted. The basic principle for considering the deformation state of a given belt model is based on the juxtaposition of these two grid forms, since both states are to be provided: The deformed grid results when applied to the given belt model (principally comparable to meshing techniques; cf. Chapter 4.2.3.1.2), and the definition of its undeformed version is trivial (e.g. by the grid-cell dimensions in the undeformed state; see Chapter 4.2.4.2.1). Thus, the local grid differences that correspond to local deformation conditions, which are to be considered at the initialisation of the (deformed) BP belt, are principally determinable.

A further illustration of this principle is also given on the finite belt model in grid visualisation in Figure 4-18. Thereby, the deformed grid, as resulting from the given geometry in which the BP belt is to be initialised, is shown on the left and its corresponding undeformed state on the right.

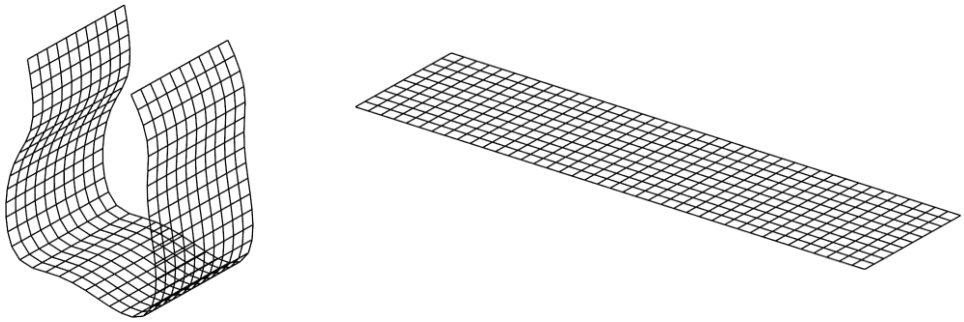

Figure 4-18: A finite grid in a deformed / in its undeformed state (left/right)

In other words, this described consideration of grid differences further follows the principle that the derived conditions (from these grid differences) added to the deformed BP belt at its initialisation result that the BP belt tends to deform into its state-of-rest – as it is fundamentally intended. Regarding finite belts, the state-of-rest is equal to the undeformed state, as illustrated in Figure 4-18. For endless belts, on the other hand, the state-of-rest forms a perfectly circular cylindrical ring, such as illustrated in Figure 4-19; again, with the grid-visualised belt in a deformed geometry on the left and its corresponding state-of-rest on the right.

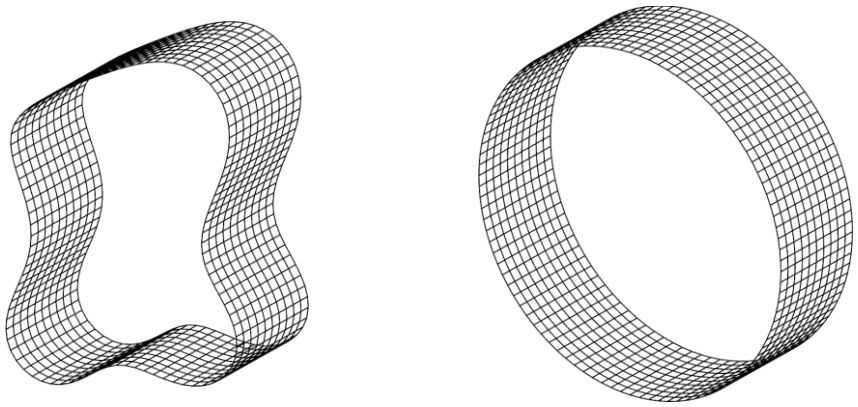

Figure 4-19: An endless grid in a deformed / in its undeformed state (left/right)

Note regarding endless belt models: As defined, a plane-rectangular grid forms the undeformed state of a belt; thus, the state-of-rest of an endless belt has still a (bending) deformation remaining in the grid (due to the endless-joint geometry). If cut open, the resulting grid would correspond to that of a finite belt and would thus further deform as such; ref. Figure 4-18.

(For further illustrations of these addressed effects on actual initialised BP belts, see also Chapter 4.3.)

4.2.2.3 An overview of the conversion algorithm

The essential process steps of the developed algorithm to convert a given geometry, including the considerations as laid out previously, are described below. More detailed descriptions of these modules are further given in Chapter 4.2.4, also including relevant mathematical/numerical details.

As already mentioned, the initial prerequisite for the algorithm concerns the given CAD data, containing the belt model, which is to be prepared as a grid (see previous Chapter 4.2.2.2; e.g. Figure 4-18). Outlining this preparation: the initially given belt model, commonly as a volume model, is required to be transferred into a middle surface model and further meshed with a rectangular grid. Details in that regard are closer described in Chapter 4.2.3.1.2.

CAD data import

The first step of the conversion algorithm is the import of the given CAD model data (as outlined above: in grid-form). Thereby, this grid data is further prepared for computational use, such as by considering grid-points as corresponding to particles and grid-lines as corresponding to bondings, further by adding an identification (numbering) scheme in order to perform the subsequent computations. In Chapter 4.2.4.1, this data import and the essential data preparation is explained in more detail.

Particle and bonding computation

The data import follows the main computation to form a BP belt based on the loaded grid data, comprising the computation of particles and bondings. The particles are computed in terms of their positions (which is trivial, as equal to the grid-points) and their spatial orientations (which is more complex, as depending on the local grid distortions). Bondings are computed as the connections between particles, based on the grid and further including corresponding deformation information, which is added via the (local) grid differences from the given deformed state to the ideal undeformed (plane-rectangular) state of the grid (see previous Chapter 4.2.2.2). Details on the computation of the particles and the bondings to form the BP belt are further described in Chapter 4.2.4.2.

Applying initial velocity

An enhancing module allows the adding of initial belt velocity to the computed BP belt, further to allow an already moving belt to be initialised. Therefore, the velocity is added to each particle as a vector in the respective (local) longitudinal direction of the belt. This module is further described in Chapter 4.2.4.3.

DEM data export

In the final step of the conversion algorithm, the computed data is exported as DEM data, and therefore written into an output file. In order to conform to a specific DEM data format (as defined in Chapter 4.2.3.2), the computed raw data, resulting from the computation steps prior to this module, is accordingly prepared and formatted. As the final result of the conversion algorithm, the exported data contains the computed particles and bondings to form the BP belt – representing the initially given CAD belt geometry and also including the deformation conditions as described in the chapter before – which can be initialised by loading this created BP belt file into the corresponding DEM simulation setup (cf. Chapter 4.2.1). In Chapter 4.2.4.4, this DEM data export is dealt with in more detail.

4.2.2.4 Relevant background information

The considerations and specifications, given in the following two subchapters, address elementary details further related to the contents covered in the following chapters, specifically in terms of computation (particularly with using quaternions), and further details regarding the implementation as a program code into a corresponding software program.

4.2.2.4.1 Using quaternions to handle spatial orientations/rotations

In terms of three-dimensional computations, 3D vectors are customary to represent/handle 3D spatial positions/distances, thus, correspondingly used in the following computations (further, with vectors in this context generally referring to 3D vectors, accordingly.) Regarding the representation/handling of spatial orientations/rotations in such three-dimensional computations, on the other hand, three basic forms/notations are principally conceivable:

- Euler angles,
- Rotation matrices,
- Quaternions.

As they reveal the most favourable characteristics, quaternions are explicitly used for the following computations; which can be concluded from the considerations as follows:

Euler angles are relatively simple as representing an orientation with three angles, but their use is in this context not sufficient – especially with regard to the bonding state computation covered in Chapter 4.2.4.2.3, whereby the handling of the introduced special cases[12] would not be possible with Euler angles. As it is further described/shown in this referenced Chapter, using quaternions resolves this issue instantly. Also, in terms of numerical operations required, quaternions are preferred over Euler angles. In contrast to rotation matrices, which deal with 3D spatial orientations by representing them in 3x3 matrices (thus comprising nine scalars), quaternions, which do so by containing a (3D) vector and an additional (rotation-angle-representing) scalar value (thus comprising only four scalars in total), are consequently more compact and efficient, and overall more stable. (cf. [19])

In general, the advantages associated with the use of quaternions can also be seen from the computations concerned (as referring to respective equations).

(More details in these regards of spatial orientation/rotation handling, furthermore specifically regarding quaternions, can further be found in pertinent literature, such as by Ben-Ari (2017) [19].)

4.2.2.4.2 Software-specific information regarding the implementation into a software program/application

The developed conversion algorithm forms a major part of the presented thesis for belt simulation. It is in this course specifically implemented into a software program based on the .NET Framework (VB) by Microsoft [172].

[12] concerning rotations representing more than 180° (cf. somersaulting difference quaternions)

Besides several common libraries of the .NET Framework, especially the library System.Numerics is essentially used for the implementation of the algorithm into a program code, as in particular concerning the handling of 3D vectors and quaternions (cf. [173]). Vectors and quaternions are relevant in terms of dealing with positions and orientations in three-dimensional space, thus, specifically for computing particles/bondings of a BP belt. In this context, and specifically relating to the computations in Chapter 4.2.4, relevant data types ("Vector3" and "Quaternion") and their related methods, operators, etc. (e.g. regarding vector cross product via "Vector3.Cross(…)", quaternion initialisation with "Quaternion.CreateFromAxisAngle(…)", and further) are provided; see also corresponding documentation [173], and specifically the applied operations in Chapter 4.2.4. Generally, the application of vectors and quaternions is established in mathematics, especially regarding applications/computations in three-dimensional space (as relating to this given applicational case of implementing the developed conversion algorithm); further details regarding the basics of vectors/quaternions can be found in a wide range of related literature.

In order to allow convenient use via a graphical user interface (GUI), such as to adjust several parameters for the conversion process, the programmed code is furthermore compiled into a Windows Forms Application (WFA; .NET Framework) as an executable .exe-file. This added GUI is introduced in the subsequent Chapter 4.2.5, presenting the developed conversion algorithm as implemented into a software application/tool.

The software tool's compiled executable (.exe-file) is also distributed via the digital platform GitHub [107].

4.2.3 Specified CAD/DEM data requirements

For enabling a proper conversion from CAD to DEM, as introduced in the preceding Chapter, several general requirements concern the input and the output data. Especially from the perspective of the developed conversion algorithm as embedded in the software tool BeltConverter (see Chapter 4.2.5), those input/output data specifications are explicitly defined as described below.

4.2.3.1 Input data (CAD)

Specifically prepared CAD data is most fundamentally required to allow further data processing. In general, these preparations are concerning the definition of a belt as a middle surface model in quadrilateral-meshed form. Such a meshed belt-representing surface already indicates the grid that corresponds to the bonded-particle structure of the resulting BP belt, into which the initial CAD belt model is intended to be converted. An introduction highlighting the initial purpose of this grid-representation of given CAD belt models was already shown in Chapter 4.2.2.2.

Besides these specifications relating to the belt model per se, a supported input file format is also specified to enable importing of data files containing these CAD belt models for further conversion.

In summary, the input data contains/provides specifically prepared CAD belt models in a file format, which enables further processing/computation. Details in those regards are correspondingly given in the following subchapters.

4.2.3.1.1 Supported belt shapes

As already described in Chapter 4.2.2.1, a CAD belt geometry provided for conversion is fundamentally required to show belt-typical characteristics, such as forming a relatively flat object with almost constant belt width and no sharp edges within the surface of the belt.

Furthermore, the model is required to either correspond to a finite or an endless belt, as already illustrated previously in Chapter 4.2.2.2. The general characterising aspects for those two supported belt model types are as follows:

The finite belt model type shows one continuous outer belt edge with four corners, which are typically approximately rectangular, resulting in four distinctive belt edges. Furthermore, every two opposite belt edges correspond to each other and are thus about the same length. Also, the belt model is required to respect the above mentioned belt-typical characteristics, specifically concerning the distances between opposite belt edges, e.g. as representing belt width. An exemplary finite belt structure is illustrated in the previous Figure 4-18.

The endless belt model type corresponds to an endless-joint finite belt, further characterised by two continuous outer belt edges (and no corners along these edges). As with finite belt models, the distances between those two opposite belt edges represent the belt width (again, with respect to the belt-width criteria regarding belt-typical characteristics). In the previous Figure 4-19, an exemplary endless belt structure is illustrated.

Note regarding Möbius belts: A Möbius belt model type is not supported to be converted as such, but an easy-to-use process is proposed to allow this special type of belt geometry to be initialised as well. Basically, a Möbius belt is also an endless belt geometry, but with only one continuous outer belt edge (see, e.g. [165]). Its geometry can be described as resulting from endless-connecting a finite belt model, but in a turned form by bringing together opposite edges (diagonal corners) to form one single continuous belt edge, as indicated in Figure 4-20. This form of connecting a finite belt model is also proposed as the basis to model such a Möbius belt: By removing a single row of grid lines (ref. bondings) through the width of a meshed Möbius belt, a finite belt model is resulting that allows being used for conversion. After the conversion, the removed area can be manually closed to result in the intended endless Möbius belt geometry. In this context, it is advisable to select a location at which directly adjacent elements can be transferred to close the belt geometry (respecting the 180° orientation difference of the opposite particles). This principle is schematically illustrated in Figure 4-20, with the first removed and then manually set endless-connection indicated.

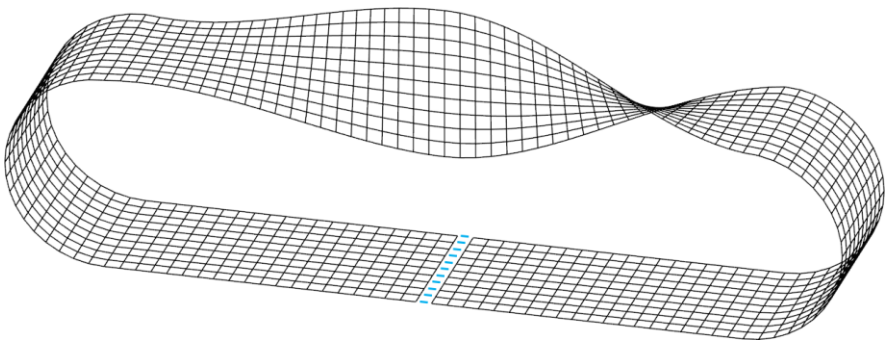

Figure 4-20: Möbius belt modelling approach (converted as a finite belt, with the endless joint indicated in the middle of the bottom strand)

4.2.3.1.2 CAD model preparation

As introduced in Chapter 4.2.2.2, a CAD belt model intended for conversion is required to provide a grid structure that represents the (typically deformed) belt geometry. The preparation of a common CAD belt model into such a grid structure is described in this chapter.

Middle surface model

As an essential requirement, a belt model for import is defined only by its middle surface. This middle surface representation of a belt is further explained with Figure 4-21, where a section of a voluminous belt model with a distinctive belt thickness (t_B) is shown from the side (thus looking at a belt edge). The required (middle surface) belt model is indicated as an offset surface in the middle between the two outer surfaces of the voluminous belt model (hence with an offset distance of half the belt thickness, as also illustrated).

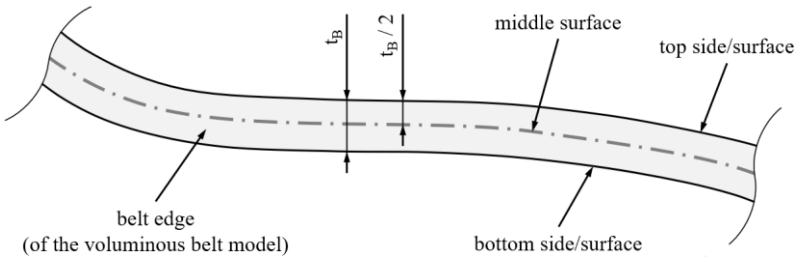

Figure 4-21: Side view on the edge of a voluminous belt model (with a belt thickness t_B) illustrating its middle surface between top and bottom side

Further, one input data file is supposed to contain one single belt-representing object in the form of such a described surface model only. Therefore, other model data than this required middle surface belt model, such as the voluminous belt model, must not be included in the input data file.

Meshed model

For the conversion process, a belt model must contain specific grid information. This grid is required as an essential basis, as it allows the converter to detect the intended bonded-particle structure. For that purpose, grid lines are referring to bondings, and

grid cross points are referring to positions of particles (that are consequently bonded according to the given grid structure).

To extend a prepared (middle surface) belt model into such a grid model, it is proposed to discretize the original surface model by using meshing techniques. Such meshing allows applying a specific mesh (in this case, the required grid) onto the surface model; as by using mesh generator software, such as Gmsh [104] (free software), which allows user-friendly and relatively fast meshing. Also, various software with other main purposes, such as Abaqus [44], allow effectively and, in some cases, more specific meshing. Also, various CAD software may be used to create a meshed belt model. (Note in that regard: As the developed algorithm allows specific rounding of input data values (specifically regarding grid positions), even a multi-surface model with small gaps to form the grid structure can be used. In such a model, multiple quadrilateral surfaces (already referring to quads; see next paragraph) are arranged to form the final belt surface – with small gaps between them, which are closed when imported for conversion due to the rounding of input values as mentioned.)

As described in Chapter 4.1, a BP belt in its undeformed state – as it is generally addressed in this chapter – shows a plane and perfectly rectangular (single-layered) bonded-particle structure. Therefore, the meshing of the deformed belt model must be done by using quadrilateral elements (as commonly termed quad elements or simply quads) only. Those quads are then correspondingly representing the deformed rectangles in the deformed state of the belt as given by the provided CAD geometry. Furthermore, it is vital to define the meshing settings/rules with respect to the general structural belt setup (Chapter 4.1) to create a proper mesh, as intended for the conversion into a specific BP belt. Such mesh-generation specific settings concern especially the quad dimension/arrangement controls and related definitions, which influences the size characteristics of the mesh/grid.

In this regard, and as already indicated in Chapter 4.1.2.1 (for example, in Figure 4-7), the characteristics of a BP belt describe the underlying grid structure to start with an offset to the outer belt edges, as furthermore visualised in Figure 4-22.

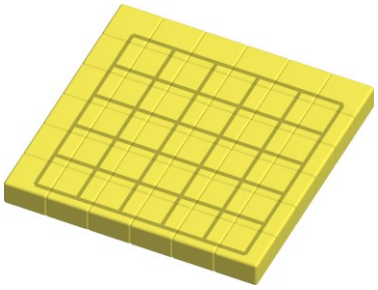

Figure 4-22: Grid underlying a BP belt model, illustrating the offset between the belt edges and the grid

The offset from a belt edge to its corresponding grid edge is equal to half the defined particle dimension in the respective direction, as evident from Figure 4-23, which shows a representative cross-section of a belt model to explain this aspect (as relating to the transverse direction (by representing the offset at both longitudinally oriented edges) for finite and endless belts; and for finite belts additionally also to the longitudinal direction (representing the offset at both transverse oriented belt ends/edges) accordingly).

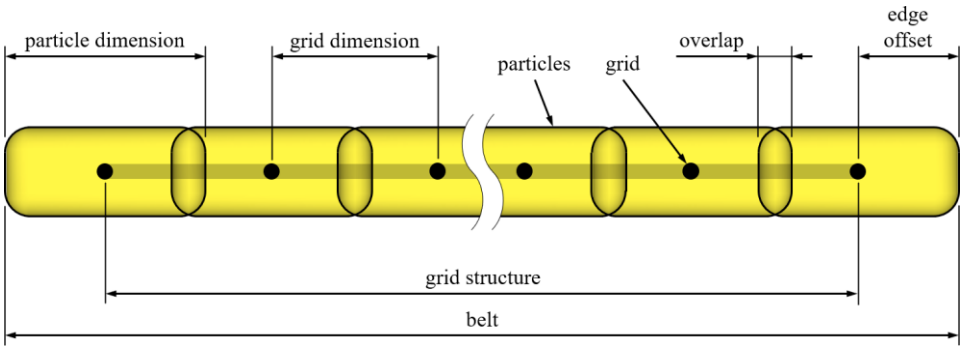

Figure 4-23: Cross-sectional view of a BP belt with its grid indicated, showing the edge offset and further relevant dimensions

As further already indicated in this figure, the grid dimensions are typically smaller than the particle dimensions (due to the introduced overlapping, see Chapter 4.1.1.2); thus, grid sizes are not representing the offsets directly. The geometric relationships in this context are further addressed on this representative cross-sectional view of a BP belt with its underlying grid structure.

This described edge offset is to be included when preparing the model (e.g. in the course of the middle surface creation by use of suitable methods as conveniently available in CAD).

An illustrative example conforming to the descriptions given above is further shown in Figure 4-24, in which detailed views on the edge of the belt indicate the details addressed before. The figure shows a voluminous belt model, further prepared into a middle surface model, which is quadrilateral meshed, and finally converted into a BP belt (top to bottom). This specific belt model is created/prepared by using Autodesk Inventor [9] and is meshed by using Abaqus [44]. It furthermore corresponds to the exemplary application of a conventional belt conveyor shown in Chapter 5.2.

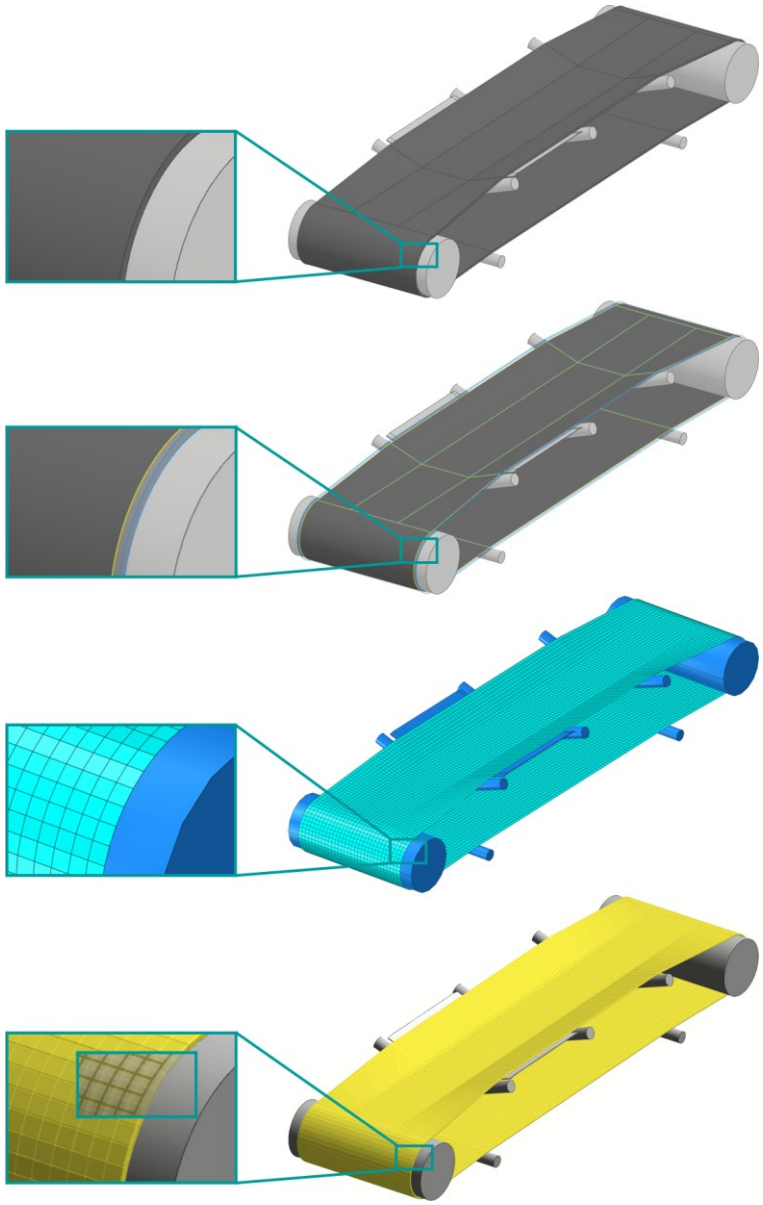

Figure 4-24: Belt model to BP belt, with a detailed view on a belt edge; voluminous belt model, middle surface model, quadrilateral meshed model, BP belt (from top)

The following list summarises major aspects/considerations to be taken into account when creating a grid (meshed) belt model:

- The resulting model contains one single continuous grid only, either:
  - in finite form, or
  - in endless form.
- The grid is made of quadrilateral elements (quads) only, which are arranged on the belt's middle surface in a (deformed) rectangular pattern.
  - Therefore, the arrangement shows parallel rows of quads containing the same number of quads (applies for the longitudinal and the transverse direction).[13]
- The quads should be within the same size range (about the same length/width)
- The grid represents a bonded-particle structure, typically in an already deformed state, therefore containing local deformations given by the grid.
- Those deformations result in grid distortions and further deviations between the quads, which in general should be kept low; concerning:
  - Overall length deviations, and
  - Local angle deviations.
- The quads ideally show an almost rectangular form, as relatively low distorted rectangles (with only minor deviations from rectangular vertex angles).

Those mentioned characteristics can already be seen in the preceding Figure 4-24, and also in Figure 4-14, illustrating belt initialisation in almost-final state. Further, such grid-structured belt models are the basis for conversion and initialisation of BP belts, such as used in all the exemplary applications in Chapter 5.

4.2.3.1.3 File format

As a suitable file format to allow the import of prepared CAD belt model data for conversion, STL[14] file format in ASCII[15] encoded form is set as input format.

[13] As with quads, this applies accordingly also to links and points forming the grid.

[14] Standard Triangle/Tessellation Language; originally documented by 3D Systems, Inc. [1, 2].

[15] American Standard Code for Information Interchange; cf. ISO/IEC 646 [127].

The use of STL fulfils essential prerequisites: Most basically, this file format is able to contain grid-like belt models (as STL files contain triangulated 3D model data; and the required quadrilaterals can be formed with two triangles each; cf. Figure 4-26). Furthermore, STL is a commonly supported and widespread export format. Almost all 3D data software (CAD, but also meshing/simulation software) allow STL export. In that regard, STL is also established as a kind of generally supported default format for (triangulated) 3D model data, such as to import part models into DEM applications (typically in rigid form; see also Chapter 2.1.2.5).

An ASCII encoded STL file contains human-readable text data, as shown in Figure 4-25. For the developed conversion software tool BeltConverter, ASCII encoded STL is preferred to be used as input format so far. This is based on two main aspects: The human-readable format allows visual data checks as well as manual modifications to the input file, which is especially beneficial during software development. Furthermore, even if a specific 3D software does not support an ASCII encoded STL export per se, subsequent format translation/conversion is generally possible such as with the help of various additional software.

Figure 4-25 explains the main structure/syntax of a general ASCII encoded STL file. The keywords and separating characters (line breaks, spaces/tabulators) are mandatory. Each numerical value ($n_{i...}$, $v_{i...}$) allows signed (positive/negative) values in floating-point number, or also exponent format (with e-sign; e.g. 1.234564e-002). (Note: Dimensional unit information (metre/millimetre/inch etc.) is not explicitly given within STL data, but numerical values are consistent within a file.)

As shown in Figure 4-25, a united object (solid) is defined (optionally with a name, indicated with s) containing any number of facets as planar surfaces (further defined as polygons, more specifically triangles). One facet subelement (indicated with index i) is representatively shown within the solid (s). Facets are explicitly defined as triangles, each with three respective vertex points and a side-defining surface normal vector. In this regard, the vertex values ($v_{i...}$) set the three-dimensional positions of each of the three vertices, and the facet normal values ($n_{i...}$) the (normalised) facet normal vector (as direction information), pointing orthogonally on one side of the corresponding triangle's surface. (As indicated, each n and v contains x,y,z values, thus corresponding to 3D vectors.)

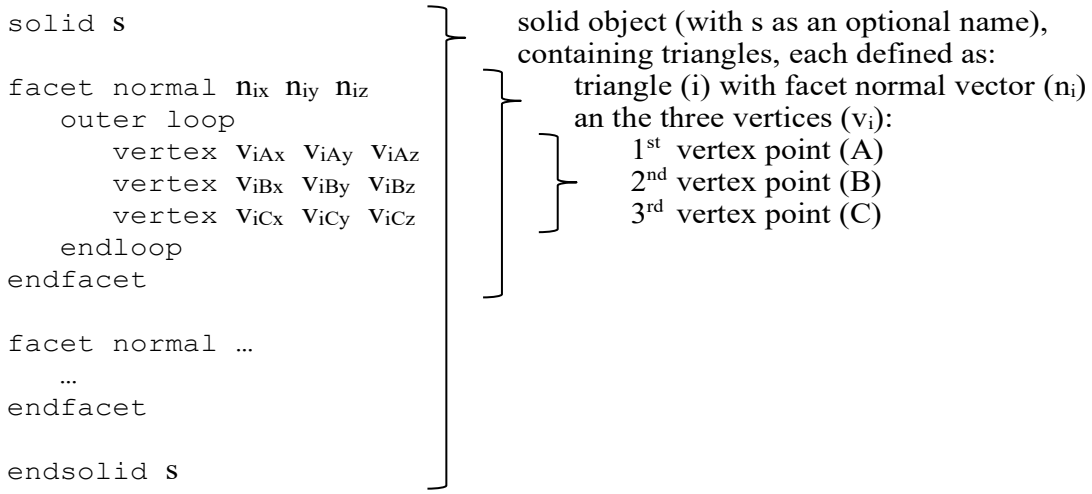

Figure 4-25: Structure/syntax of a STL file (ASCII encoded)

As previously described in Chapter 4.2.3.1.2, a belt model for conversion is consisting of multiple quads forming the grid. In triangulated form, as required for STL data, each of those quads is represented by two triangles, as exemplarily illustrated in Figure 4-26.

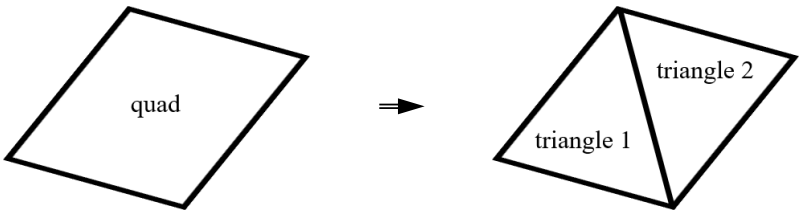

Figure 4-26: Representation of a quad in triangulated form, as for STL, consisting of two plane-parallel triangles (1 and 2)

This triangulation of quads, and thus of a quad-structured grid, is further to be respected in the conversion algorithm, as each quad within the grid of a belt model is represented by two associated triangles. (Further descriptions in that regard are given in Chapter 4.2.4.1.2, specifically as part of the pairing of associated triangles in the preparation step after the import of an STL file for conversion).

Additional comments – regarding binary STL, point clouds, and mesh-data

Besides the described STL in ASCII encoded form, also binary encoded STL exists, which basically contains the same information of triangulated 3D model data, but in 32-bit floating-point number format (which is indecipherable to a human; but results

in smaller file sizes at the same amount of information). Enabling import of binary STL would be principally feasible for future implementation but is (due to the aspects previously described) of minor importance; hence this is not yet supported.

In principle, it would also be an alternative approach to use point-only data that simply contains three-dimensional point definitions of multiple points, such as (x,y,z) point cloud data. But as such point-only data does not clearly define a grid structure, i.e. defining which points are linked, deeper analysations in that regard would be necessary at the import/preparation step (ref. Chapter 4.2.4.1) when such data is prepared to be used for the conversion algorithm (still bearing the risk of misinterpretation of links).

Another quite promising alternative would be the use of data formats capable of containing mesh information (specifically quad-meshed structures), such as the Abaqus [44] input file format. Using such a format would principally be a suitable approach, especially for lowering the preparation effort required when using the proposed STL format to consider a quad grid in a triangulated STL model (which, however, is within reasonable limits; see Chapter 4.2.4.1.2, pairing of associated triangles). Nevertheless, as such mesh-relating formats are more or less application-specific (e.g. Abaqus input format for FEM purposes), and as STL is generally more common, highly supported for export, and overall widespread in 3D engineering, STL is still preferred as the basic import data format. (Expanding the supported input data towards such formats, especially the Abaqus input format, would principally be a possible future implementation but is not prioritised due to its minor importance.)

4.2.3.2 Output data (DEM)

The final result of the conversion algorithm is the computed BP belt written into an output file which enables further use, specifically: the initialisation of the converted BP belt in a DEM simulation application.

The file format specified for this purpose is the keyword file (INP) format of ThreeParticle/CAE (.inp-file), which allows convenient usage by loading (importing) and thus initialising a computed BP belt. (In this context, and as covered in the preceding Chapter 4.1, the presented belt modelling technique generally relates to

ThreeParticle/CAE, which has been proven suitable, and for which specific implementations are made correspondingly (e.g. regarding the enhanced bonding model to allow belt-typical behaviour; cf. Chapter 4.1.2.2); thus, generally allowing a BP belt to be initialised as intended.)

Also, the INP format reveals to be beneficial in general, as it fundamentally allows containing all the required data for defining a BP belt computed by the conversion algorithm (also including pre-deformation states of bondings), and furthermore shows a human-readable format. Due to these aspects, it is principally also possible to further translate the output data into related formats, readable by other modern DEM software environments that support this type of BP belt initialisation accordingly. Especially, the human-readable format is advantageous, as it allows manual adaption of the converted BP belt data, such as to change certain properties of the computed model (e.g. for local belt structuring, cf. Chapter 4.1.2.3, as applied to define the area of belt breakage in the example in Chapter 5.7).

Relevant aspects in terms of INP file usage, specifically for BP belt initialisation, are closer described in the following. In the respective Keywords Guide by Becker (2019) [12], full descriptions can further be found.

INP – keyword file syntax

Basically, an INP file can be loaded – at any time (time step) – to append or change the current simulation setup. Therefore, such an INP file contains command lines based on keyword syntax.

In terms of BP belt modelling, those command lines and the respective keywords specifically concern the initialisation of the two elements that form a BP belt: particles and bondings. In this context, the content of an exemplary INP file is shown in Figure 4-27 (shown in Notepad++ [118] using a User Defined Language, enabling the colouring style as shown: indicating major keywords in green (as defining the general subject of each keyword line, starting with "*"), followed by parameter-defining keywords in blue, string (name) definitions in red, and comment lines (starting

with "//") in light grey); with the general syntax[16] as evident (further details, see Keywords Guide [12]).

```
// add particles that are intended to be bonded subsequently:
*manualBondingGeneration, particle='b', ID(1), position(0.2;0;0), quaternion(1;0;0;0), transVelocity(1;0;0)
*manualBondingGeneration, particle='b', ID(2), position(0.3;0;0), quaternion(1;0;0;0), transVelocity(1;0;0)
*manualBondingGeneration, particle='b', ID(3), position(0.4;0;0), quaternion(1;0;0;0), transVelocity(1;0;0)

// add bondings connecting the above defined particles:
*addBonding, IDA(1), IDB(2), positionA0(0.2;0;0), positionB0(0.28;0;0), quaternionA0(1;0;0;0), quaternionB0(1;0;0;0)
*addBonding, IDA(2), IDB(3), positionA0(0.3;0;0), positionB0(0.38;0;0), quaternionA0(1;0;0;0), quaternionB0(1;0;0;0)
```

Figure 4-27: INP keyword file syntax for bonded-particle initialisation

As shown, the relevant keywords concern, on the one hand, the initialisation of particles that are intended for bonding ("*manualBondingGeneration"), and on the other hand, the initialisation of the bondings connecting those particles ("*addBonding"). Furthermore, several parameter definitions are shown, each for particles and bondings, for specifying their details.

As an essential parameter, the particle "ID" defines each particle with a unique number. Those IDs are then also used to define the initialisation of a bonding, which connects two specific particles (by referring to them via their IDs, with "IDA" and "IDB"). As can be seen, the bondings in the exemplary INP file are initialised to connect the three (prior to the bondings initialised) particles in an ascending row, connecting ID 1 with ID 2 and ID 2 with ID 3 (forming the bonded particle line of 1-2-3).

Regarding the initialisation of a particle:

- "particle" defines the particle type (e.g. as a certain cuboidal particle (cf. Chapter 4.1.1.3), optionally corresponding to a specific contact group (cf. Chapter 4.1.2.3), with a defined material, etc.),
- "ID defines a unique identifier
- "position" defines the three-dimensional position and
- "quaternion" defines its spatial orientation;
- "transVelocity" optionally defines translational velocity[17].

[16] such as the separation of sequential keywords with a comma, the separation of multiple values set to a parameter by using brackets divided by a semicolon, and the decimal delimiter as a dot

[17] In similar form, "rotVelocity" optionally defines rotational velocity.

And regarding the initialisation of a bonding: the parameters “positionA0”, “positionB0”, “quaternionA0”, “quaternionB0” define the initial bonding condition as the virtual relative arrangement of particle A (IDA) and particle B (IDB) at which the bonding between them is in its undeformed (zero) state. This concept is also schematised in Figure 4-28.

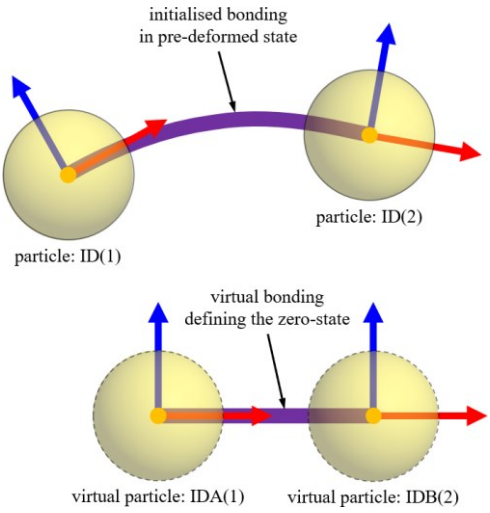

Figure 4-28: Schematic to define an initialised bonding in a pre-deformed state, based on virtual particles forming a virtual bonding that defines the bonding’s zero-state (each particle defined as common, with position and orientation)

As illustrated in this figure, by setting these zero-state parameters, it is possible to initialise the bonding between two particles in an already (pre-)deformed state. This deformed bonding state results from the relative difference between the state at which the two particles are initialised (acc. particle initialisation) and their (virtual) zero-state definition (acc. bonding initialisation). Deformed bonding initialisation, such as enabled with this principle of zero-state definition, is indispensable for BP belt initialisation, as introduced in Chapter 4.2.2.2 before.

(According to the INP format, values regarding units refer to metre, as the length unit, and respectively, metres per second, as the translational velocity unit.)

Looking at the example given in Figure 4-27, the particles are initialised in a line along the x-axis at a distance of 0.1 m (which results from the difference between the particle positions; from the values 0.2, 0.3, and 0.4). The initial bonding conditions further define a virtual arrangement of each two bonded particles in a shorter distance, specifically at 0.08 m, resulting from the differences between each positionA0

and positionB0 (from the values 0.2 and 0.28, and 0.3 and 0.38). Therefore, as the initialised particle distances (0.1 m) are larger than those defined zero-state distances (0.8 m), the bondings are initialised with this corresponding elongated condition, specifically lengthened by 0.02 m (from 0.08 m lengthened to 0.1 m; which corresponds to 125% relative elongation). Furthermore, as there are obviously no differences in terms of quaternions between initialised and zero-state, the initial bonding condition in this shown case does not include rotational deformations. Basically, the definition of rotational deformation for an initial bonding condition is similar to those for elongation, as resulting from the differences in the quaternions between the initialised state and the zero-state (cf. relative orientations in Figure 4-28).

(Side note: As mentioned before, several approaches that emerged during the development of the presented methodology were applied for implementation as supported features to be available in ThreeParticle/CAE[18], as also this principle for bonding initialisation including a deformed condition, or generally also the definition of spatial orientations with using quaternions (as an alternative to using default Euler angles); as particularly relating the BP belt initialisation as presented. Overall, such enhancing features provide general added value in the sense of extending and improving the scope of applicability in the field of advanced/complex DEM simulation.)

Furthermore, also regarding the parameter definitions, some of the particle/bonding parameters are principally optional; such as the particle velocity, which is set to zero if not explicitly defined. In that regard, initial bonding conditions are also optional: If an initial bonding condition is not explicitly defined, the bonding is initialised at zero-state with the particle arrangements as it is initialised (according to the definitions from the particle initialisation; as no virtual zero-state is given); i.e., positionA0/quaternionA0 equals the position/quaternion of particle A as initialised; the same applies for particle B.

More details regarding keywords/parameters according to the INP format can also be found in the respective guides ([12, 13]) associated with ThreeParticle/CAE.

[18] e.g. see Chapter 4.1.2.2, the adapted bonding model implemented in ThreeParticle/CAE.

In Chapter 4.2.4.4, as the final step of the conversion algorithm, relevant details for writing computed data of a BP belt into an output file conform to this specified INP format are furthermore given.

4.2.4 Essential modules of the conversion algorithm

In the following, the main modules of the developed conversion algorithm are described in detail – which were further implemented (in accordingly programmed form) as the core modules in the software tool BeltConverter, presented in Chapter 4.2.5. These main modules concern the central computation mechanisms for belt conversion from 3D-CAD- into DEM-data, as generally introduced in the preceding chapters, and as specifically already outlined in the algorithm overview in Chapter 4.2.2.3.

In addition to these main modules as described in the following, several additional modules/methods/functions are also implemented in the developed software tool, as to allow the resulting conversion software to run properly. Such further modules are generally of common nature and are thus not addressed in more detail. They concern, for example, typical data handling operations or the GUI that is added to allow intuitive operability (for using the conversion algorithm as embedded in an executable software tool; see Chapter 4.2.5).

4.2.4.1 CAD data import and preparation

Initially, an imported CAD file (containing the belt geometry intended for conversion) is translated into processable data. This translated data is furthermore prepared to conform to a specific scheme, fundamentally enabling the subsequent computations to be made. In addition, several data checks allow early evaluation in terms of data suitability as part of these initial steps.

The result from this import/preparation procedure is a specific data set that contains numerical information representing the grid-like structure of the imported belt geometry, which is furthermore conforming to enable the computation of particles and bondings that follow as described in the next Chapter 4.2.4.2. Especially the addressed preparation steps are in this regard of crucial importance.

4.2.4.1.1 Translation

As specified in Chapter 4.2.3.1.3, a CAD input file intended for conversion contains the geometry in ASCII encoded STL format. To enable further processing, the contents provided by such a CAD input file, containing text data in multi-line string format (cf. Figure 4-25), need to be translated into computable data. Therefore, several trivial string operations/functions are applied for raw text data parsing and translation into computable data. With general reference to Figure 4-25, this mainly concerns the splitting of loaded text (initially given as non-computable string data) into fragments which are further converted into numerical data type format suitable for computation. Accordingly, every triangle-defining block within the STL file (indicated as facet in the aforementioned figure) is processed to result as computable data, correspondingly as one facet normal vector (n_i) and three vertices (v_{iA}, v_{iB}, v_{iC}) per triangle.

As a result, the translated data contains a list of (typically many) triangles, each defined by its three vertices as points in 3D vector format and additionally its facet normal also in 3D vector format. (3D vectors with x,y,z decimal values.)

4.2.4.1.2 Preparation

In preparatory steps, the imported triangles, which are intended to form the 3D geometry of a belt model (according to the specifications as described in Chapter 4.2.3.1.2, as a middle surface model in meshed form), are further processed to result in a data set that forms the basis for the subsequently performed computation of particles and bondings. In essence, these preparatory steps generally comprise the following listed issues, which are further discussed below; and which are generally also evident when comparing Figure 4-29 and Figure 4-30, showing a section of a belt-representing structure before and after preparation:

- Pairing of associated triangles (combining every two triangles to a quad)
- Forming a point and link structure (corresponding to a grid of linked points)
    - Systematically numbering/sorting the points that form this grid
    - Systematically assigning link references at each point

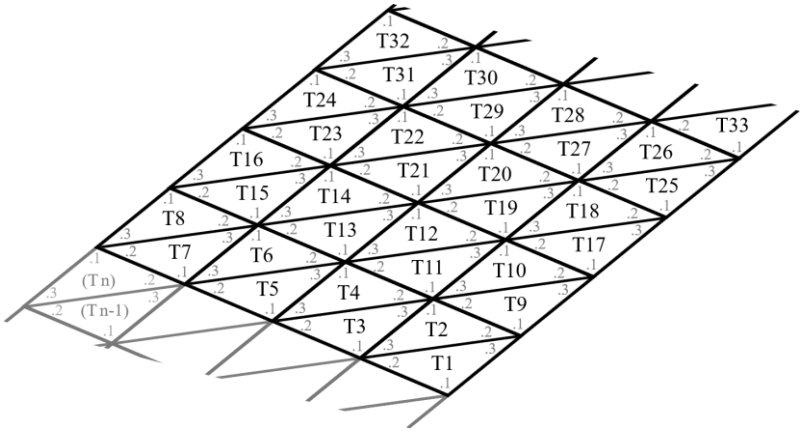

Figure 4-29: Imported grid – consisting of triangles (T), each with three vertices (.1-.3) (the left side ((Tn) and (Tn-1)) only applies for endless belts)

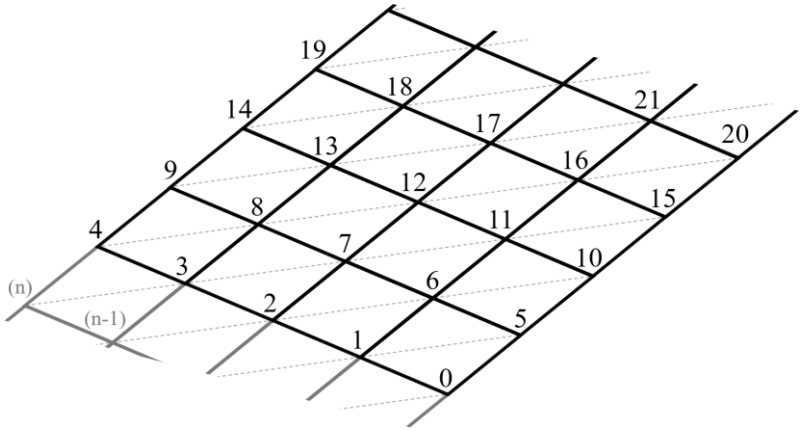

Figure 4-30: Prepared grid – consisting of quads, further showing a systematic point numbering scheme (the left side ((n) and (n-1)) only applies for endless belts)

These issues are not to be considered in a full-sequential order (such as listed) but in a cross-related form, as several aspects are fundamentally relating to each other, which is also evident from the descriptions given in the following subsections. These descriptions basically relate to the list given above, beginning with an explanation of the basic point/link data structure (including point numbering), providing insights into the pairing of associated triangles, and finally, explaining the link assignment systematics applied to each point.

After an outline on checking this prepared data in terms of general data suitability (in Chapter 4.2.4.1.3), an overview of the data as resulting from these preparation steps is furthermore given in the conclusive Chapter 4.2.4.1.4 – also summarising the terminology as evolved through the following sections in a summarising overview in

Figure 4-51 (see this figure for further illustrative clarification of various terms, e.g. points, links, longitudinal/transverse directions, fibres/rows, etc.).

Point and link data structure

The previously shown Figure 4-29 shows a representative section of a belt model formed by the imported triangles, with each triangle (t) containing the position data of its three vertices (A, B, C). Obviously, multiple redundant entries for point positions are resulting due to the shared vertices of adjacent triangles. By transferring the triangle data into point and link data (with the omission of redundant entries), as illustrated in Figure 4-30, the amount of data that represents the grid-like belt structure is significantly reduced. In this context, the prepared data essentially corresponds to a point list and a link list, both of which are in relation to each other; further with points in the point list giving information of their positions in 3D vector format, and with the links in the link list giving information of the point-point connections that ultimately form the grid (i.e. which pairs of points are linked with each other).

Fundamentally, the created point list is sorted in order to apply a numbering scheme to the grid structure, as shown in Figure 4-30. The point sorting/numbering scheme is set as follows: (With the numbering starting at zero, as is customary in numerics[19].)

- Starting from a corner (finite belt) or from an edge point (endless belt)
- Ascending in the transverse belt direction in first-order
- Ascending in longitudinal belt direction in second-order
- Until every particle is considered (numbered/sorted)

Note regarding belt directions: For endless belts, the longitudinal direction is defined by the orientation of the (two opposite) belt edges; but for finite belt models, the orientation (longitudinal/transverse) is not unambiguously evident, as both pairs of opposite belt edges are principally possible to correspond to either the longitudinal or the transverse direction. Thus, the option to switch directions is added in the algorithm at this preparatory stage, specifically regarding finite belt models.

[19] general software-related details regarding the implementation of the presented algorithm into a software program, see Chapter 4.2.2.4.2 (cf. also .NET [172])

Also, the endless joint in an endless belt obviously concerns the linking of the last (transverse) row of points with the first (transverse) row of points (see also Chapter 4.2.4.1.4, specifically Figure 4-50).

Furthermore, it would actually be possible to sort the link list in a similar ascending order, but this is not necessary because the links are referenced from the point list anyway and can thus be retrieved as sorted via this sorted point list (cf. following paragraph).

The point list and the link list are fundamentally interconnected via cross-references. Therefore, every point comprises the information which links are connected to it – as a reference to the corresponding links (in the link list). Also, the reference gives the information in which direction a link is oriented in relation to this specific point (positive/negative longitudinal/transverse direction), which is specified as described in the section after next (regarding systematic link assignment). Every link, on the other hand, contains the information which two points are linked by it – given in similar form via reference to the corresponding points (in the point list). This interconnection between the two lists is later illustrated in Figure 4-48, in Chapter 4.2.4.1.4, showing the prepared data structure (also including the specific link assignment as discussed in the section after next).

Pairing of associated triangles

The above-mentioned preparations are basically parallelised with the following process, which is furthermore performed to respect every pair of associated triangles[20] that represent each quad-element (corresponding to the quad-based mesh as originally applied to the belt model, according to Chapter 4.2.3.1.2; cf. also Figure 4-29/Figure 4-30). This (back-)transformation into a quad-based grid is required for the subsequent computation of the bonded-particle network and basically corresponds to a combination of every two associated triangles. It is performed by analysing the grid and further by removing the diagonal link that triangulates each quad (as indicated with the dashed lines in the previous Figure 4-30). The remaining link structure shows a quadrilateral network as the originally applied quad-based mesh.

[20] As described in the paragraph corresponding to Figure 4-26, a belt model provided in STL format is given in triangulated form, thus with two associated triangles for each quad.

Finding the pairs of associated triangles for removing the diagonal links is principally straightforward, as shortly outlined in the following.

At first, the analysis is started by focusing on the belt edges (in longitudinal direction) because when one pair of associated triangles is found on such an edge, the next neighbouring pairs of triangles (on this edge) are resulting trivially, as illustrated in Figure 4-31. Therefore, the triangles connected to points at such an edge are considered for combination – as closer addressed subsequently.

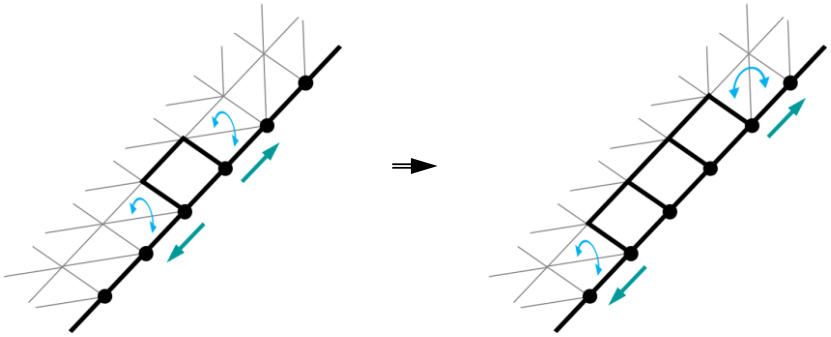

Figure 4-31: Pairing of associated triangles to quads along the edge

Also, this process is consequently progressive along the longitudinal direction, as combining triangles until the edge is finished (either by reaching the corner(s) (finite belt) or when the two progressing fronts converge (endless belt)). After finishing this first row of points, the next row, as adjacent to this completed one, is performed the same way; and the process is correspondingly repeated until the opposite end of the belt (the opposite edge) is reached. This process is schematically illustrated in Figure 4-32.

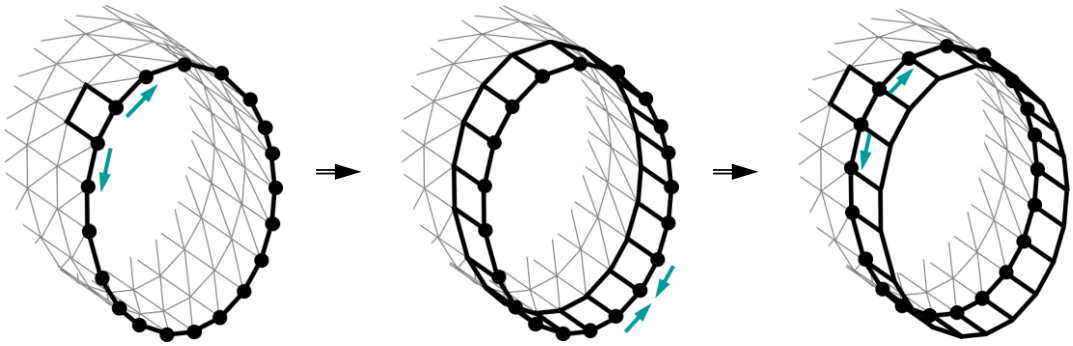

Figure 4-32: Pairing of triangles along the edge; when the row is finished (middle), starting with the next row following (right) (and so on)

Principally, this described procedure of sequentially pairing triangles, thus proceeding progressively through the grid, allows being used for sorting purposes (as explained in the previous section) in parallel to this pairing.

The following paragraphs regard the finding of initial triangles to start the pairing:

As stated before, it is required to find an initial pair of two associated triangles, specifically at an edge, to start a sequential pairing process. Basically, there are some specific triangle arrangements that allow clearly determinable allocations, such as when exactly one or four triangles are connected to an edge point (corresponding to two or five links connected to this point), as illustrated in Figure 4-33 and Figure 4-34.

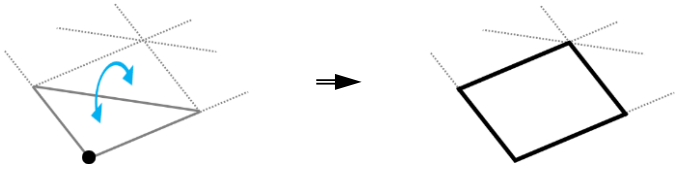

Figure 4-33: Point at one triangle (two links) – pairing is explicit (represents a corner point)

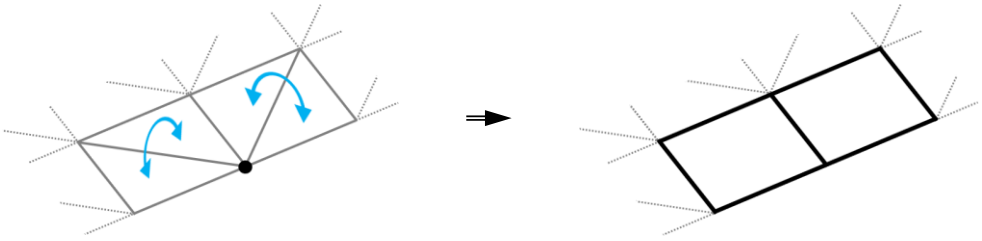

Figure 4-34: Point at four triangles (five links) – pairing is explicit

In case no edge point with such a clearly determinable allocation exists, further considerations are required. Obviously, those further cases concern arrangements when two or three triangles are connected to an edge point (corresponding to three or four links connected to this point), at which a clear triangle assignment is not readily possible, as illustrated in Figure 4-35 and Figure 4-36. In these cases, only looking at the number of elements (triangles/links) that are connected to a point does not give the final information about which triangles are associated to form the intended quad-structure.

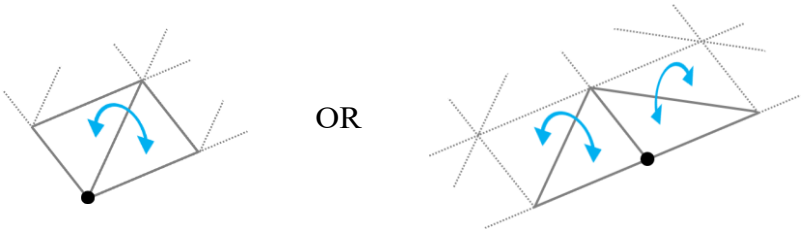

Figure 4-35: Point at two triangles (three links) – pairing is not explicit

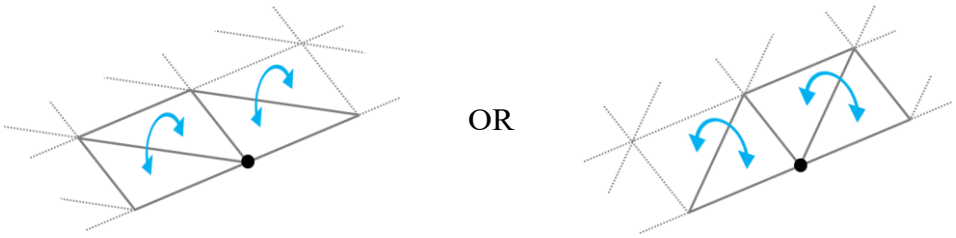

Figure 4-36: Point at three triangles (four links) – pairing is not explicit

In the case of two triangles (Figure 4-35), those two can either be associated to each other (forming a corner, as shown on the left), but also not (forming two separate quads, as when arranged along an edge, as shown on the right). And in the case of three triangles (Figure 4-36), the middle triangle can either be connected with one or the other additional triangle (with the left one, as shown on the left; or with the right one, as shown on the right).

Two further approaches are feasible to determine the associated triangles in such cases: on the one hand, considering the angles between links, and further, using facet normals.

The angle consideration is generally feasible, as the quads are principally envisaged to correspond to rather slightly distorted rectangles. Accordingly, triangles can be associated in order to form such rather small distorted rectangles with link angles closer to rectangular, which is outlined in Figure 4-37. This figure illustrates the case from the previous Figure 4-36 on the left, with the two principally possible options for associating the triangles in focus: either resulting in slightly distorted rectangles (as shown on the top), as intended accordingly with angles closer to 90°, in comparison to the alternative option which is resulting in strongly distorted rectangles (as shown on the bottom, with angles strongly different to 90°).

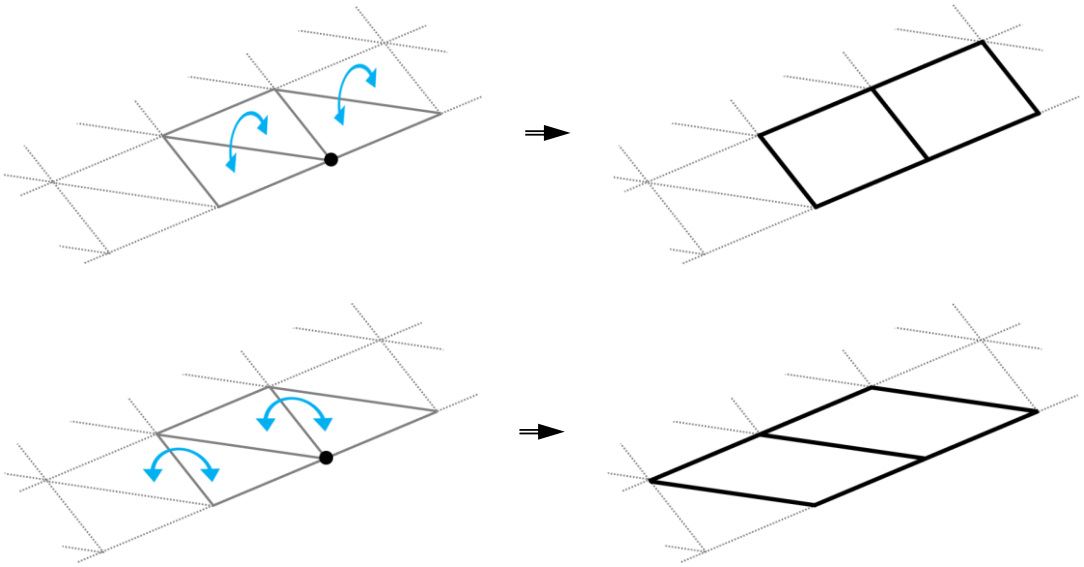

Figure 4-37: The two principally possible pairing forms for a point at three triangles – the first returns quads with smaller deviations from a rectangle (the second one returns a stronger distorted quad structure, which is not intended)

Also, the consideration of facet normals (n) is principally feasible because their directions are required to be parallel for two associated triangles. This condition can be useful in general – as to check the correspondence of two as-associated-found triangles (e.g. with the principles as described before) – but moreover, it can also be of use for identification purposes in the context of triangle association. Therefore, differences between two adjacent facet normals indicate that those two adjacent triangles are not associated (but the alternative two triangles consequently are, which are furthermore required to show parallel facet normals). This circumstance occurs specifically in bent belt geometries, as facet normal differences basically indicate a bend-line in the transverse belt direction. In Figure 4-38, the determination principle in such a case (as basically corresponding to Figure 4-37) is illustrated, with the highlighted triangles in focus and their found association as resulting when considering differences of facet normals as described. (The alternative option, similar to Figure 4-37 on the bottom, is not set due to the differences in their facet normals; hence the other option is resultingly found and set for triangle association, as indicated; and as comparable to Figure 4-37 on the top.)

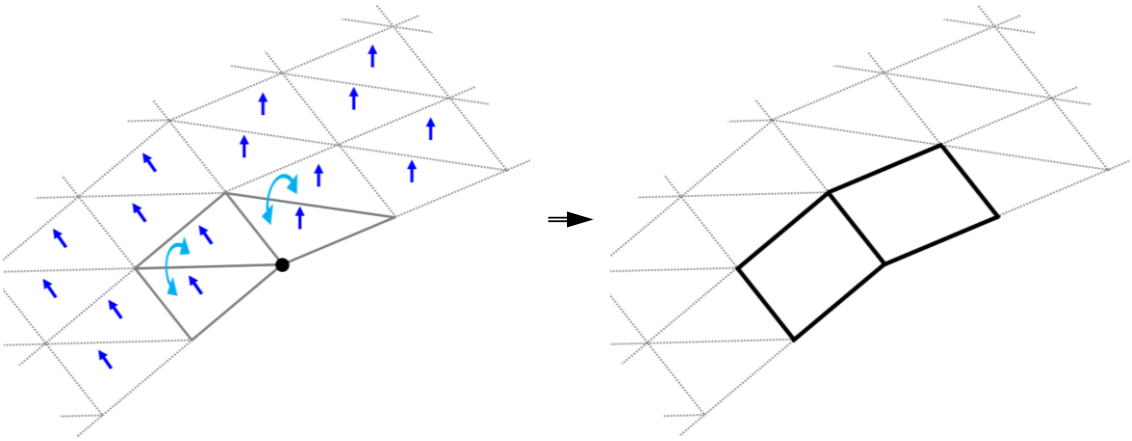

Figure 4-38: Pairing using facet normal directions for a point at three triangles at a bent area – where two facet normals are parallel (which are thus paired) and the third is not (facet normal directions indicated with arrows)

At the end of the described preparation step, the initially imported belt data (which is comprising a multitude of triangles) is prepared as a grid of linked points in quadrilateral form. The result at the end of this step is a list of the points (and corresponding of the links between them) that define the grid structure, furthermore sorted in ascending order as described (first in transverse, then in longitudinal direction), and with only those links remaining to form a quadrilateral grid as required. (Further details see the section following after, summarising the result of the CAD data import, which is further passed on to the subsequent computation of particles and bondings.)

Systematic link assignment

Each point within the grid must be attached to either two, three, or four links – with these three cases indicating specific locations in the grid, as further illustrated in Figure 4-39, with:

- Two links as a corner point
- Three links as an edge point
- Four links as a (common) surface point

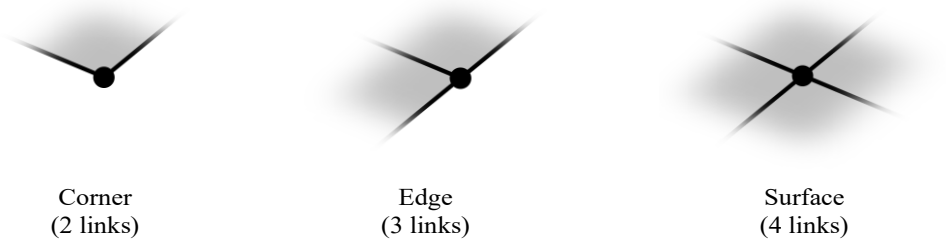

Figure 4-39: Number of links connected to a point indicating its location in the grid

According to the maximum number of links attached to a point, each point has four reference slots available that allow link references to be assigned (to refer to entries in the link list); further with the option to leave unused slots blank, thus allowing to set only two or three references as well.

This basic setup with four reference slots per point is additionally extended with a scheme that allows respecting the direction of assigned link references. Therefore, each of the four slots represents a specific direction: (Again, starting the numbering at zero, as is customary in numerics.)

Slot 0 – Positive longitudinal
Slot 1 – Positive transverse
Slot 2 – Negative longitudinal
Slot 3 – Negative transverse

With longitudinal/transverse direction in relation to the grid (as stated before); and with positive/negative direction in relation to the respective point (to which those links are correspondingly assigned to). This scheme is also illustrated in Figure 4-40 on a common grid point with four links attached.

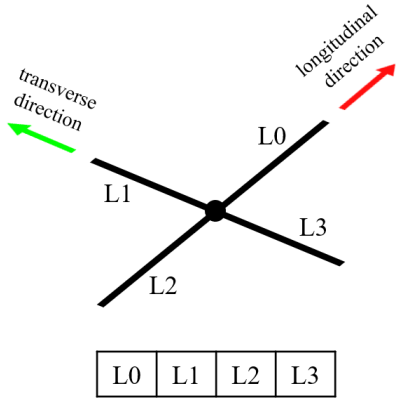

Figure 4-40: Link (L0-L3) assignment in slots (table) respecting grid directions

If fewer than these four links are attached, the slots that do not apply are correspondingly left out (and are thus not assigned with a link reference). With this scheme, common surface points (with four links), edges (with three links), and corners (with two links) are possible to be depicted, further including information of different link orientations, which is of importance for subsequent computations (given in Chapter 4.2.4.2). Besides the common case shown in Figure 4-40, in which all slots are filled with references, further different cases of edges and corners are shown in Figure 4-41 and Figure 4-42, also indicating which slots are not assigned with a link reference.

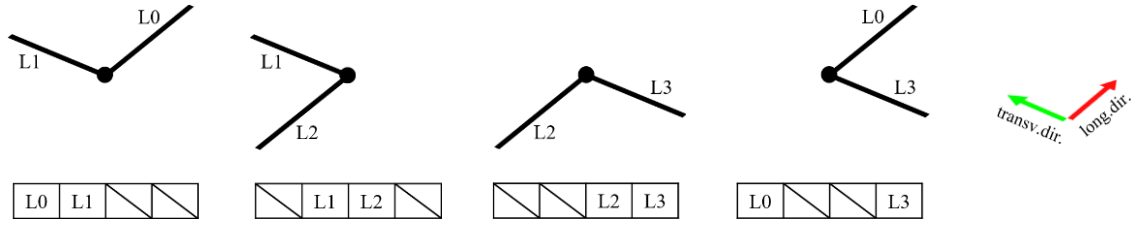

Figure 4-41: Link assignment for corner points

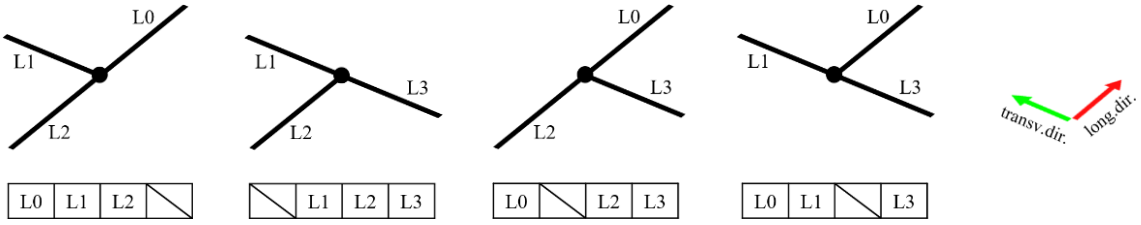

Figure 4-42: Link assignment for edge points

To determine the slot assignment as introduced, the numbering scheme already applied to the point list is useful (with points ascending at first in transverse and then in longitudinal direction). Thereby, this systematic assignment basically corresponds to reconsidering the points within the point list one after another, specifically in terms of the links that are attached to each point, as this information is already given from the grid structure (in correspondence with the link list), but the specific link references are at this stage not assigned to envisaged slots as introduced above. To perform this assignment, each point with its attached links is considered individually, as a point of focus, further analysed as below.

The systematic link assignment is based on considering the differences between point numbers (in the following also referred to as (point) IDs) of two linked points: accordingly, the point ID differences (ΔP_{ID}) are determined, which are each relating to

one of the (up to four) links connected to the specific point of focus. These point ID differences are trivially resulting from the IDs of two linked points:

$$\Delta P_{ID} = P_{ID} - P_{ID\,focus} \tag{30}$$

with $P_{ID\,focus}$ as the ID of the point of focus, and P_{ID} as the ID of a point connected to this point of focus via a link; performed respectively for every link attached to the point of focus, giving either two, three, or four ΔP_{ID}s, each corresponding to a respective link. Thus, by analysing these ΔP_{ID}s, the assignment of the corresponding links into the slots is made possible, as described in the following paragraphs.

In the transverse direction, the point IDs follow a one-step order; thus, if an ID difference magnitude is exactly one, an orientation in that direction is determined, specifically according to the following conditions:

If $\Delta P_{ID} = +1$	the cor. link is in positive transverse direction	(slot 1)
If $\Delta P_{ID} = -1$	the cor. link is in negative transverse direction	(slot 3)

Condition set (31)

This aspect is obvious, as when looking at the initial example clarifying the numbering scheme in Figure 4-30, and is furthermore also evident in various next figures regarding longitudinal determination. Additionally, Figure 4-43 shows this determination principle on a common section within the grid.

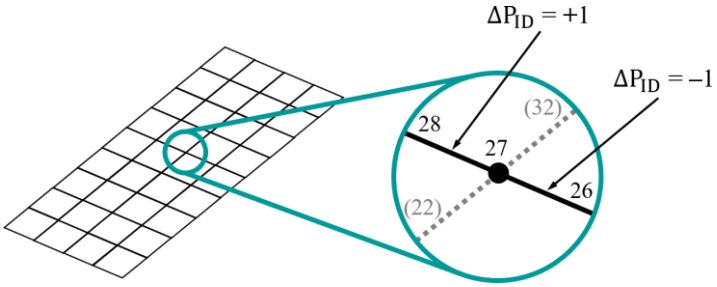

Figure 4-43: Link determination in transverse direction (cf. Condition set (31); grid ref. Figure 4-49)

Consequently, in contrast to the transverse direction, which is resulting from an ID difference magnitude equal to one, an ID difference magnitudes unequal to one cor-

respondingly indicates a longitudinal orientation. But these cases require further considerations, specifically to respect effects from endless belt types (as further described in the section after next).

With only one ID difference magnitude unequal to one, the determination is according to the following conditions:

If exactly one link conforms to the condition $|\Delta P_{ID}| > 1$ then:

If $\Delta P_{ID} > 1$ the cor. link is in positive longitudinal direction (slot 0)

Else $(\Delta P_{ID} < 1)$ the cor. link is in negative longitudinal direction (slot 2)

Condition set (32)

This condition furthermore corresponds to points along the ends of a finite grid (the first and the last row of points, which only contain one longitudinal link), as exemplarily shown in Figure 4-44.

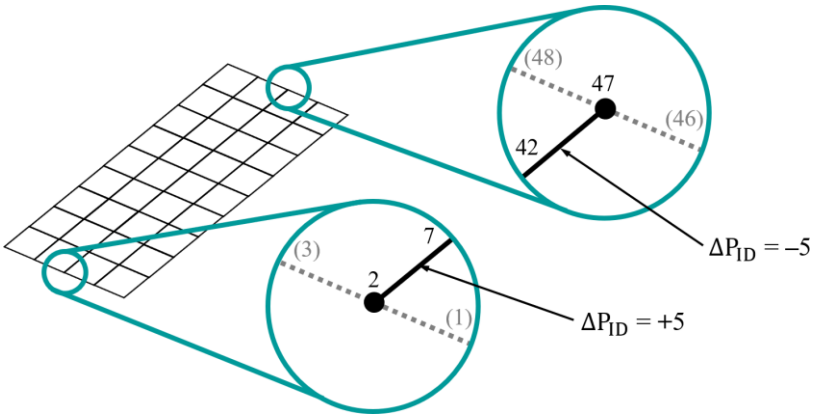

Figure 4-44: Link determination in longitudinal direction at the ends of a finite grid (cf. Condition set (32); grid ref. Figure 4-49)

With the common case of two ID differences conform to this condition of magnitudes unequal to one, the determination must respect a specific case that occurs in endless-joint grids, in which the endless-joining links are interrupting the common ascending point order at these points (as in these area the first and last row are correspondingly linked; cf. the numbering scheme in the bottom left in Figure 4-30). This is respected as follows:

If exactly two links conform to the condition as previous ($|\Delta P_{ID}| > 1$) with two ΔP_{ID}s (ΔP_{ID1}, ΔP_{ID2}) brought into the order to fulfil $\Delta P_{ID1} > \Delta P_{ID2}$ conform to the conditions as before $|\Delta P_{ID1}| > 1$ and $|\Delta P_{ID2}| > 1$ then:

If $sign(\Delta P_{ID1}) \neq sign(\Delta P_{ID2})$ (common case)
the link cor. to ΔP_{ID1} is in positive longitudinal direction (slot 0)
the link cor. to ΔP_{ID2} is in negative longitudinal direction (slot 2)

Else $(sign(\Delta P_{ID1}) = sign(\Delta P_{ID2}))$ (case at endless joint)
the link cor. to ΔP_{ID1} is in negative longitudinal direction (slot 2)
the link cor. to ΔP_{ID2} is in positive longitudinal direction (slot 0)

Condition set (33)

These cases are illustrated in Figure 4-45 at different points, one in a common section (top; conforming to the common case) and at both rows at the endless-joint (first/last row as linked together), which further give the result as indicated (middle and bottom).

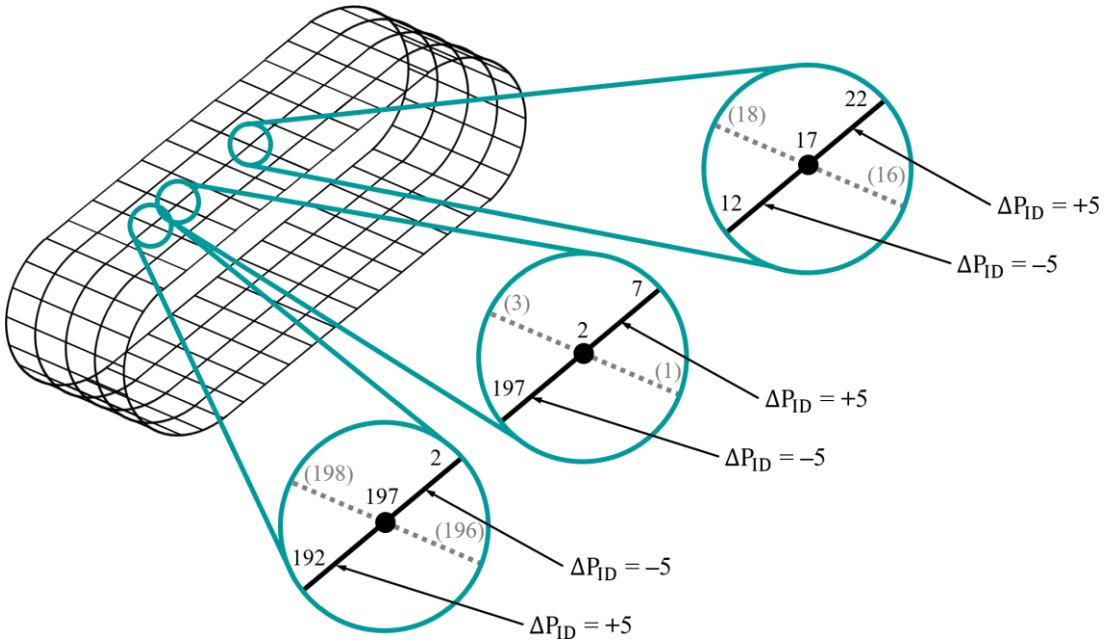

Figure 4-45: Link determination in longitudinal direction at a common surface point (top) and at the endless joint of an endless grid (middle/bottom) (cf. Condition set (33); grid ref. Figure 4-50)

According to this determination scheme, each link reference is assigned to one of the four slots, thus representing a specific direction of each link in reference to the point

of focus – which is, as giving essential orientation information, important for the following computations (see Chapter 4.2.4.2).

In parallel to this link assignment at points as described, also the links are reconsidered in a similar form in order to contain point references in a certain order. For that purpose of point assignment, the two referenced points at each link are assigned to point in positive grid direction (either in positive longitudinal or positive transverse direction) when following from the first to the second referenced point. This assignment is trivial, as a simple switch of the order of the two referenced points is required when the order is determined as not conform. This principle is schematically also illustrated in Figure 4-46, showing a transverse link (top), a common longitudinal link (middle), and a longitudinal link at an endless joint (bottom).

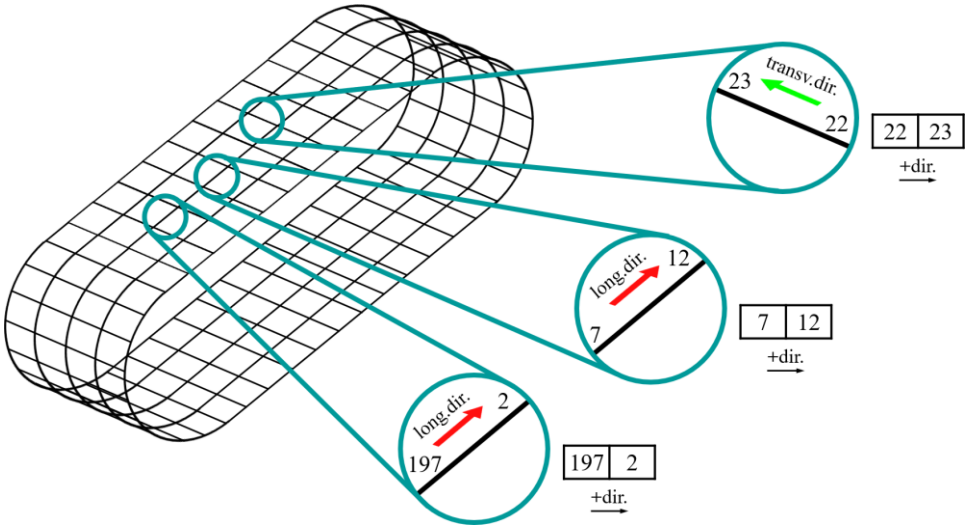

Figure 4-46: Sorting scheme for the referenced points in the link list (sorted following the positive direction; as indicated in the tables) (grid ref. Figure 4-50)

(Note: This point assignment is principally not necessarily required for computational reasons, but adds further systematics through the uniformly structured result, which is generally favourable, e.g. with regard to correspondingly structured data (ref. computing/writing of bondings cf. Chapter 4.2.4.2.3/Chapter 4.2.4.4.)

4.2.4.1.3 Data check

In the course of the precedingly described data translation and data preparation, several validity/comprehensibility checks can be performed:

- The loaded data must contain only one solid – as only one single and continuous belt-representing object is allowed.
- The number of triangles must be even – as two triangles form each quad, and the grid is required purely quadrilateral; thus, no single triangle is allowed.
- Relative length deviations of all the links are not exceeding certain limits, respectively in longitudinal/transverse direction (as links refer to DEM bondings, which are supposed to be within a manageable length range. I.e., deviations in terms of link (bonding) length differences are intended to be rel. low.)
- Angle deviations between links at each point are not exceeding certain limits:
    - two adjacent links: angle to be about 90° (+/- permissible deviation)
    - two opposite links: angle to be about 180° (+/- permissible deviation)

  (I.e., distortions in terms of local angle deviations are intended to be rel. low. See also Figure 4-47.)

(Note: These described checks fundamentally refer to the CAD belt model characteristics specified in Chapter 4.2.3.1.2, specifically to the section (and the conclusive list) regarding meshing to apply a quadrilateral grid on a middle surface model.)

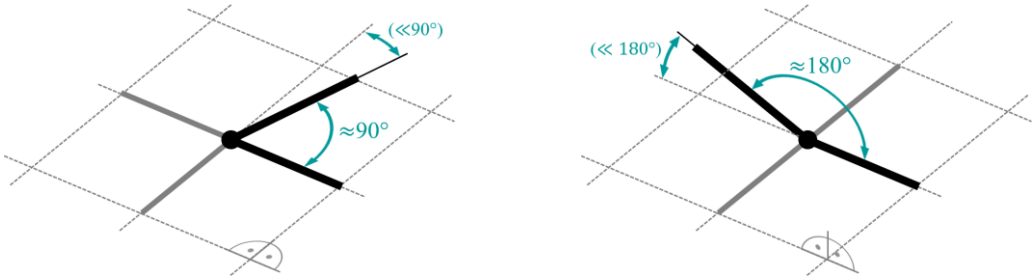

Figure 4-47: Angular ranges between adjacent (left) and opposite (right) links, shown as linked at a common grid point; generally indicating relatively low local angular distortions from a rectangular grid

4.2.4.1.4 Resulting data

The resulting data, which forms the basis for the computation of particles and bondings following in the next Chapter 4.2.4.2, basically represents a grid structure consisting of linked points. Therefore, this data is provided by a sorted list of points and a list of links, both of which are related to each other. The list of points is sorted in systematically ascending order, as previously described and as again indicated in the later shown figures; first in transverse, and then in longitudinal direction. The link

assignment made to each point furthermore gives the directions in which attached links are oriented in relation to each specific point. An illustrative example of the structure, also showing the point-link relation, is given in Figure 4-48 on a section of the exemplary grid from Figure 4-49 – with the corresponding lists of points and links further indicating their relations as cross-references between points and links.

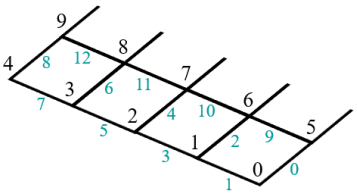

Point Nr.	Position (x,y,z)	Link slots			
		0	1	2	3
0	…	0	1		
1	…	2	3		1
2	…	4	5		3
3	…	6	7		5
4	…	8			7
5	…	…	9	0	
6	…	…	10	2	9
7	…	…	11	4	10
8	…	…	12	6	11
9	…	…		8	12
…					

Link Nr.	Linked points	
0	0	5
1	1	3
2	1	6
3	1	2
4	2	7
5	2	3
6	3	8
7	3	4
8	4	9
9	5	6
10	6	7
11	7	8
12	8	9
…		

Figure 4-48: Structure of the two lists, point list (middle) and link list (right), for the first section of a finite grid; cross-references indicated (with links in colour)

(Note: As already implied, each list begins at zero, as common in numerics.)

Furthermore, resulting data corresponds to one of the two basic belt types, either representing a grid of a finite or of an endless belt model, as shown exemplarily in the following figures – with Figure 4-49 showing a finite grid consisting of 5x10 points and Figure 4-50 showing an endless grid consisting of 5x40 points, each with their grid-forming links.

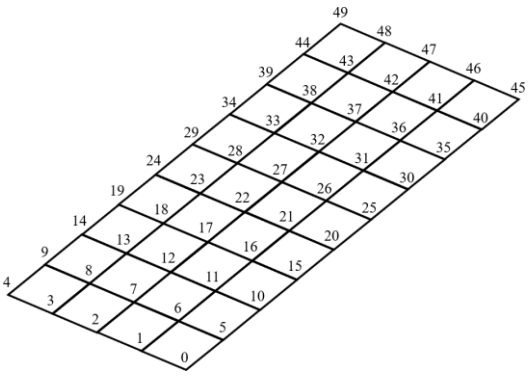

Figure 4-49: Representative example of a finite grid

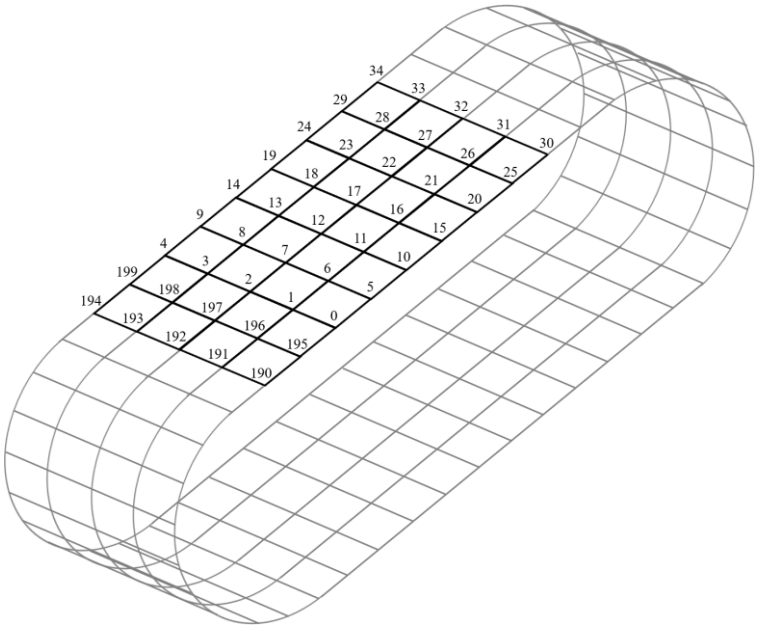

Figure 4-50: Representative example of an endless grid

In these figures, typical characteristics of resulting point/link data forming such grid structures are shown; with the major difference between these two types evident, as an endless belt shows additional links between the first and the last row of particles, thus resulting in only two instead of four belt edges.

Ultimately, the resulting data (as a point list and a link list) indicates a BP belt structure – with the points corresponding to particles and the links corresponding to their bondings. This data is further transferred to compute the particles and bondings, accordingly including local conditions to form the BP belt in the given (pre-deformed) state. This computation is covered in the following module, as described in the next chapter.

In concluding addition, Figure 4-51 gives an overview of the essential terminology used in context with the (prepared) grid structure, whereby reference is generally made to terms already mentioned previously (points, links, etc.) but furthermore indicates the major variable names (particle/bonding) used in the following computations.

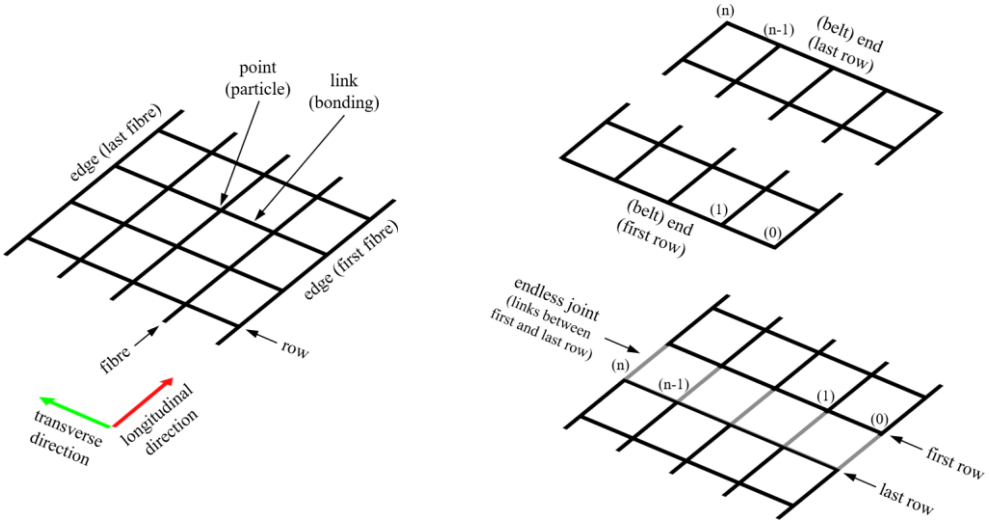

Figure 4-51: Grid structure terminology – general section (left) / ends of a finite grid (top right) / endless joint of an endless grid (bottom right)

4.2.4.2 Particle and bonding computation

The core data for the final output, as computed by this presented conversion algorithm, contains the definitions to allow the initialisation of a BP belt to represent a specifically deformed belt model as intended (see also Chapter 4.2.1 in that regard). For this purpose, the computed data comprises the following major information[21], with their detailed computation as described in the chapters after next:

- Particle states: Placement of each particle (position & spatial orientation)
- Bonding states: Condition of each bonding, defined by:
  - Particle A, zero-state (position & spatial orientation)
  - Particle B, zero-state (position & spatial orientation)

Whereby, in computational terms, each particle's position & spatial orientation is represented as a 3D vector & a quaternion (with the corresponding data types and their specific properties, operators, methods, etc., acc. System.Numerics [173].)

Generally, the imported and prepared data (in the form of the proceeding described point and link list) is used to compute BP belt data, comprising a particle and a bonding list as explained in the chapters after next.

[21] at least; which refers to further include additional data, e.g. initial belt velocity, see Chapter 4.2.4.3.

4.2.4.2.1 Deformed-to-undeformed grid state considerations

For the computation of the core data, it is fundamentally necessary to analyse the deformed grid information and consider local differences to its undeformed state, as in principle already introduced in Chapter 4.2.2.2. As obvious, the deformed grid is corresponding to the distorted grid structure provided by the imported and prepared CAD data (acc. previous Chapter 4.2.4.1). The undeformed grid, on the other hand, is corresponding to a (virtually considered) undeformed state of a BP belt grid; in this context, additionally defining a BP belt at zero-state.

Zero-state grid and belt-tensioning definitions

The zero-state of a grid is specified to show a perfectly flat rectangular form (see general belt modelling technique in Chapter 4.1). The grid dimensions (i.e. the link lengths) of this zero-state affect the elongation state at which a given and thus deformed grid is initialised. (As the links further correspond to the bondings of the BP belt.)

Resulting from this context, belt pre-tensioning is allowed to be included at BP belt initialisation, particularly by defining a zero-state link (bonding) length with a certain amount shorter than the imported/given and thus to-be-initialised link (bonding) length. This circumstance is furthermore illustrated on a representative example: With a zero-state length defined with 40 mm and a length in the imported grid of 44 mm, the resulting bonding gets correspondingly initialised in lengthened form (lengthened as from 40 mm to 44 mm, thus corresponding to a 110% strained state; cf. paragraph after next). Furthermore, zero-state link lengths are generally required to be defined for both belt directions separately; commonly to initialise a certain belt pre-tensioned state in the longitudinal direction, but no such pre-tensioning in the transverse belt direction. These addressed aspects are schematically illustrated in Figure 4-52, with a grid indicating a (virtual) zero-state (which is defined with the two zero-state lengths as shown) on the left, and a deformed grid as imported (thus as to be initialised) on the right (with the lengths also as shown, as resulting from the imported data).

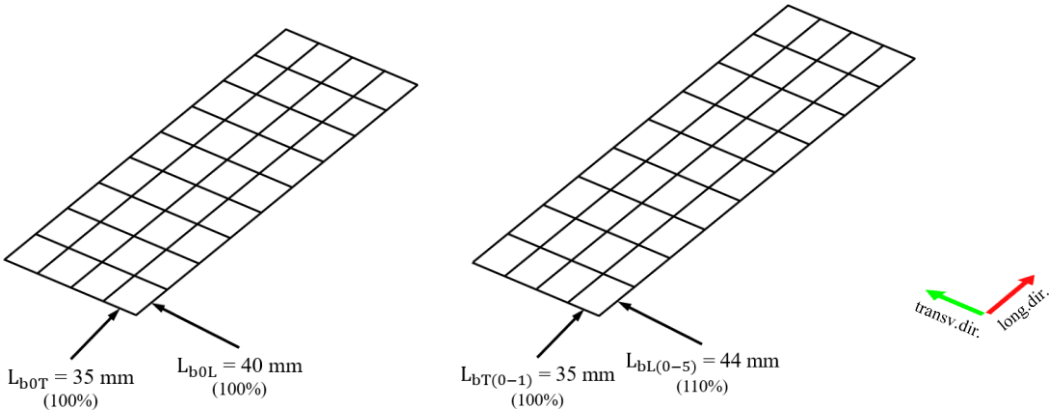

Figure 4-52: A grid with its defined zero-state (left) and its given/imported state (right), pre-deformed in long. dir. ($L_{...L}$; 44 mm/40 mm), not pre-deformed in transv. dir. ($L_{...T}$; 35 mm/35 mm) (indices in brackets indicate linked points)

In this illustrative example, the imported grid, and therefore the correspondingly initialised BP belt, is meant to contain pre-tensioned bondings in the longitudinal grid direction. This reveals from the link/bonding lengths differences between the zero-state and the initialised state, as differences are apparent in longitudinal (40 mm/44 mm) but not in transverse (35 mm/35 mm) direction.

Accordingly, to define the zero-state of a grid, both zero-state lengths ($L_{b0L}$and L_{b0T}; correspondingly regarding the longitudinal and the transverse belt direction) are required to be defined by the user. This definition is either possible by providing these two values directly, as typical (with absolute values, i.e. in units of length) – but is alternatively also possible by providing relative values. In this context, relative values are meant to define the elongation state with which the BP belt is to be initialised, specifically as each a factor that defines the strained state in longitudinal $(1 + \varepsilon_{bL})$ and in transverse $(1 + \varepsilon_{bT})$ direction. According to common strain relation (strain equals to change in length divided by original length), the zero-state lengths follow (for both directions) with

$$L_{b0L} = \frac{L_{bmL}}{1 + \varepsilon_{bL}} \tag{34}$$

$$L_{b0T} = \frac{L_{bmT}}{1 + \varepsilon_{bT}} \tag{35}$$

with L_{bmL} and L_{bmT} as mean lengths resulting from the given grid (trivially as the sum of the lengths divided by the amount of these summed lengths; respectively for each direction). Furthermore, with Figure 4-52 in mind, relative value definition is further illustrated: the imported grid is meant to be initialised with longitudinal elongation (from 40 mm to 44 mm), but with no elongation in transverse direction (with 35 mm remaining 35 mm). To define this state with relative instead of these absolute values, equivalent strained states are required to be set accordingly, specifically with 110% in longitudinal ($1 + \varepsilon_{bL}$) and 100% in transverse direction ($1 + \varepsilon_{bT}$).

Further relating aspects in regards to considering link/bonding lengths are covered in the next chapters, as particularly relevant to the computation of the initialisation states of particles and bondings (further, with specific zero-state lengths specifically relating to determining zero-states of bondings, which correspondingly includes the consideration of zero-bonding-lengths as described above).

4.2.4.2.2 Particle state computation

As already mentioned, each particle's state – as its position and its spatial orientation – is required to be computed accordingly to form the resulting BP belt as intended.

Whereas position determination is rather trivial (as addressed in the following subsection), especially spatial orientation computation requires closer consideration, as in detail described in the subsections after next.

Transferring the positions, IDs, and link references (and extending the point list into a particle list)

The positions of particles are trivially resulting as equal to the positions of points as provided in the prepared point list (cf. previous Chapter 4.2.4.1.4).

Due to this fundamental correlation, the prepared point list is directly transferred (extended) to form the base data of the particle list, which contains each particle forming the resulting BP belt. In this context, each particle in the particle list is defined with:

- its position (**p**) as a 3D vector,
- its ID (as the list number; acc. grid numbering scheme; cf. Chapter 4.2.4.1.2),

- and furthermore contains the references to its attached links (as later transferred into bondings, accordingly described in the next Chapter 4.2.4.2.3), thus giving the information which particles are linked to this particle;

but further data are additionally required to be computed, as each particle is fundamentally also defined with:

- its spatial orientation ($\mathbf{q}$) as a quaternion, which is covered in the following section (and generally results from the linked points),
- and optionally its velocity ($\mathbf{v}_\mathrm{p}$; see Chapter 4.2.4.3).

(Note: Point data is extended to particle data specifically by adding these last two properties, which are consequently required to be computed per point/particle. Also, this set of data for defining a particle is generally also evident when looking at the particle initialising keyword line in Figure 4-27, in Chapter 4.2.3.2, regarding the DEM output data format. In this regard, the particle type[22] is principally also relevant to particle data but not explicitly included at this point, as it is considered as related to the particle ID, which is further explained in Chapter 4.2.4.4 (cf. also fibred structuring in Chapter 4.1.2.3).)

Spatial orientation determination (as a rotated coordinate system)

For the following computation processes, the preparation of the imported data as given in Chapter 4.2.4.1.2 is fundamentally relevant; specifically regarding the numbering scheme and the systematic link assignment applied to the point (thus particle) data.

Spatial orientation computation is performed systematically for each particle in the particle list, further by considering each particle's local grid condition (by including its attached links). Thereby, a particle of focus (with its position $\mathbf{p}_\mathrm{focus}$) is considered with its linked particles (and their positions $\mathbf{p}_0 \ldots \mathbf{p}_3$), as illustrated in Figure 4-53. The order of these linked particles further follows the link assignment systematics specified in Chapter 4.2.4.1.2 (see reference slots), and are thus also indicating grid directions (positive/negative longitudinal/transverse) as shown.

[22] see the corresponding bullet point following Figure 4-27 in Chapter 4.2.3.2

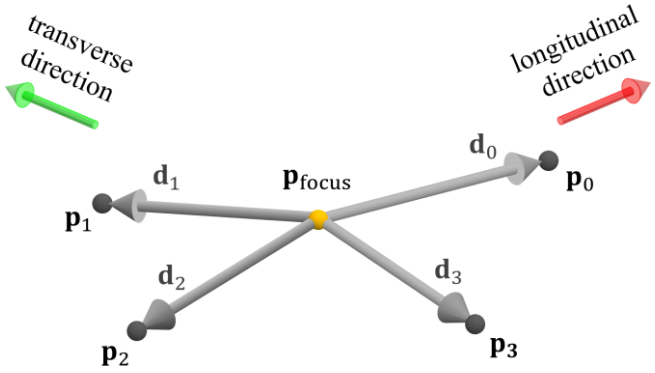

Figure 4-53: A common point/particle in focus ($\mathbf{p}_{focus}$) with its four linked points ($\mathbf{p}_0 \ldots \mathbf{p}_3$); illustrating the distance vectors ($\mathbf{d}_0 \ldots \mathbf{d}_3$) (cf. Eq. (36))

The distance vectors ($\mathbf{d}_0 \ldots \mathbf{d}_3$), pointing from the point of focus to the linked points, are determined accordingly with:

$$\mathbf{d}_i = \begin{cases} \mathbf{p}_i - \mathbf{p}_{focus} & \text{if } \mathbf{p}_i \text{ exists} \\ \mathbf{0} & \text{otherwise} \end{cases} \tag{36}$$

with $\mathbf{p}_i$ resulting from a reference slot i; thus, with no $\mathbf{p}_i$ resulting/existing when a slot i is blank (cf. systematic link assignment in Chapter 4.2.4.1.2; Note in that regard: different schemes with blank slots indicate different cases of edges (one blank slot) or corners (two blank slots), accordingly shown in Figure 4-41 and Figure 4-42).

(Also, $i \in \{0, 1, 2, 3\}$; which applies in general also to related contents as below).

The distance vectors are furthermore set in relation to the respective zero-state lengths ($L_{b0L}$and L_{b0T}), giving length-related[23] distance vectors $\mathbf{d}'_i$ as:

$$\mathbf{d}'_i = \begin{cases} \mathbf{d}_i / L_{b0L} & \text{if } i \in \{0, 2\} \\ \mathbf{d}_i / L_{b0T} & \text{otherwise } (i \in \{1, 3\}) \end{cases} \tag{37}$$

(with the first condition regarding links in longitudinal direction ($i = 0$ and/or $i = 2$), and the second condition regarding links in transverse direction ($i = 1$ and/or $i = 3$)).

In order to determine the spatial orientation of the particle of focus, a local particle coordinate system is used. This coordinate system is specified on the zero-state of the grid, which shows as a perfectly flat-rectangular setup without elongation (thus representing the undeformed grid state, as also described/shown in the previous

[23] indicated with " ′ " (e.g. $\mathbf{d}'_0$); as length-related correspondingly representing a dimensionless quantity

Chapter 4.2.4.2.1). In this zero-state, the particle coordinate system is specified to be oriented in line with the grid, as illustrated in Figure 4-54 (with the local particle coordinate system at zero-state formed with u_0,v_0,w_0).

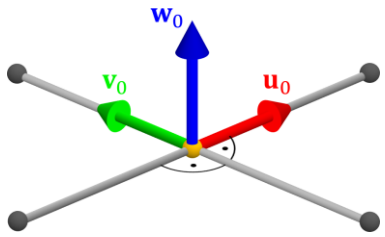

Figure 4-54: Local zero-state particle coordinate system (u_0,v_0,w_0) in the undeformed grid (u_0 in longitudinal, v_0 in transverse direction) (vectors not scaled)

In a general state, on the other hand, the particle coordinate system (u,v,w) is oriented accordingly, depending on the grid distortions in contrast to the zero-state. I.e., if a grid is brought from zero-state into such a general (and typically deformed) state, the orientation of the particle's coordinate system of focus is changed as a result of the re-arrangement of the other particles linked to it. And, vice versa, when reversing this procedure back to zero-state, the initial zero-state orientation is reached again.

Figure 4-55 illustrates a generally oriented particle coordinate system in a typically deformed grid state, as given via (length-related) distance vectors.

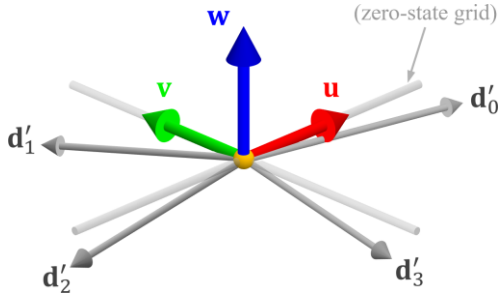

Figure 4-55: Local particle coordinate system (u,v,w) in the deformed grid (with the local zero-state grid shown for reference) (u,v,w not scaled)

As indicated, the particle coordinates are referring to the major (particle-local) belt directions:

- u – longitudinal,
- v – transverse,
- w – thickness (surface-normal).

For illustration purposes, this distortion-depending orientation change can be observed on an equivalent mechanical system, in which the links (thus bondings) are represented as spring-like elements attached to a central particle. In the zero-state, all the elements are meant to be at rest (not tensioned) and oriented in flat-rectangular form, as in Figure 4-56 and Figure 4-57 on the left. If the attachment points are moved to distort the system, the particle's orientation is changed correspondingly, such as illustrated each on the right. The resulting orientation is thereby dependent on the change of each element, comprising its change of angle and its change of length. In this context, Figure 4-56 illustrates an example seen from the top (i.e. looking at the grid's surface, orthogonal to the longitudinal and transverse direction), and Figure 4-57 another example seen from the side (i.e. looking in transverse direction; thus parallel to the grid's surface), both to highlight the resulting orientation of the particle coordinate system. (Note: The computation principle in the following can also be seen as basically relating to this outlined system.)

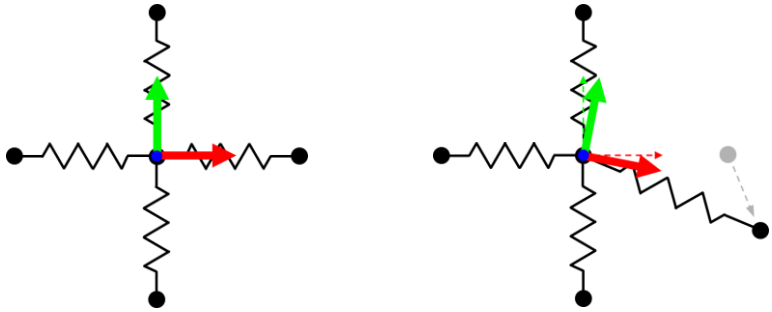

Figure 4-56: A distortion example of a rectangular cross-network (mid-point rotatable) – initial/distorted state (left/right) (cf. grid in top view; negative w-dir.)

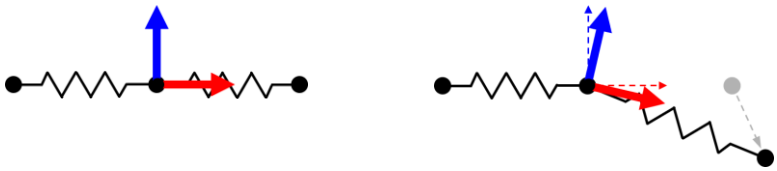

Figure 4-57: A distortion example of a linear network (mid-point rotatable) – initial/distorted state (left/right) (cf. grid in side view; positive y-dir.)

In regard to computing the particle orientation as a (u,v,w) coordinate system, the following procedure is proposed:

(Anticipatory note on normalised/non-normalised vectors: The in the following addressed direction-pointing vectors are determined in a general, and thus non-normalised form (e.g. represented as $\mathbf{w}$) – not directly normalised for numerical reasons (as referring to the aspect that each computational process may affect accuracy). (See, e.g., Eq. (40), in which normalised forms of the direction(-pointing) vectors are not necessarily required.) The normalised form of a vector (as a unit vector) is explicitly indicated with " ̂ " (e.g., $\widehat{\mathbf{w}}$, as shown in Eq. (39); and further also relating to vectors resulting from operations, e.g. as applied to the cross-product shown in Eq. (42)), accordingly referring to common vector normalisation (as with, e.g., $\widehat{\mathbf{w}} = \mathbf{w}/|\mathbf{w}|$). (Further note: This indication further regards the actual direction vectors as corresponding to non-normalised direction-pointing vectors; see also paragraph following Eq. (41).))

By Equation (38), the direction-pointing vector $\mathbf{w}$ is determined as the sum of the cross products of each pair of adjacent links, specifically by using the respective (length-related) distance vectors as shown in the equation. Accordingly, each cross product gives a normal vector to each link-pair, further including a weighting from the length and angle between the links, which is contributing respectively to the total w-direction.

$$\mathbf{w} = (\mathbf{d}'_0 \times \mathbf{d}'_1) + (\mathbf{d}'_1 \times \mathbf{d}'_2) + (\mathbf{d}'_2 \times \mathbf{d}'_3) + (\mathbf{d}'_3 \times \mathbf{d}'_0) \qquad (38)$$

(As cross products with $\mathbf{0}$ result in $\mathbf{0}$, specific cases with fewer than four attached links/points, such as representing edges or corners, are considered accordingly, as correspondingly non-existing links/points are not influencing the w-direction.)

Fundamentally, as the order of the attached links/points is explicitly defined (acc. systematic link assignment, Chapter 4.2.4.1.2), the w-direction is oriented as conforming to this scheme. (It is thus pointing to the same side of the grid as a fictitious cross product of the local longitudinal and transverse direction at this point of focus; see Figure 4-58. And due to the systematic link assignment, this w-orientation is also consistent for each particle in the grid; i.e., pointing on the same side of the grid/belt; see also the last section in this chapter, giving an overview of the resulting orientation scheme, specifically Figure 4-66 and Figure 4-67.) Due to this context, the w-direction is basically representing the positive (local) thickness direction of the BP belt.

Figure 4-58visualises and explains this first step of the proposed procedure, illustrating the three different cases (common surface, edge, corner) with **w** resulting from the sum of the cross products (acc. Eq. (38)).

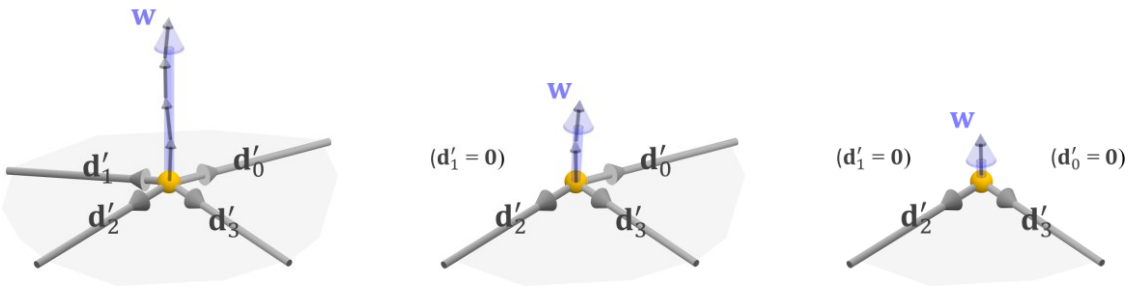

Figure 4-58: Determination of **w** via the sum of the cross products (visualised as forming/underlying **w)** according to Eq. (38)

In the next steps, a second direction is determined to define the rotational alignment of the particle coordinate system around this already determined w-axis.

Therefore, an auxiliary vector $\mathbf{u}^*$ is computed according to Equation (39). This vector lies in the plane formed by **w** and **u** (with $\mathbf{u}^*$ generally not congruent to **u**; however, pointing on the same side, as also indicated in Figure 4-59).

$$\mathbf{u}^* = \sum_{i=0}^{3} \left(\mathbf{v}\mathrm{Transform}\left(\mathbf{d}'_i \,,\, \mathbf{q}\mathrm{CreateFromAxisAngle}\left(\hat{\mathbf{w}} \,,\, -\,\mathrm{i}\,\frac{\pi}{2} \right) \right) \right) \quad (39)$$

Where $\mathbf{v}\mathrm{Transform}(\,)$ represents a function returning a vector by transforming (specifically rotating) a vector (parameter 1) to a new spatial orientation using a quaternion (parameter 2). And where $\mathbf{q}\mathrm{CreateFromAxisAngle}(\,)$ represents a function returning a quaternion created from an axis given by a vector (parameter 1) with the rotation given as a scalar value (parameter 2; in radiant). (Those functions are commonly available within numerical libraries capable of handling vectors/quaternions; in this context specifically relating to the library System.Numerics [173].)

This computation step gives the sum of the (length-related) distance vectors, each individually rotated by a multiple of 90° ($\pi/2$) around w to each point towards the positive longitudinal direction. (The principle underlying this rotation is the fact that in zero-state each link is 90° offset to its next adjacent link; cf. Figure 4-54. Furthermore, a conventional vector sum (without the individual rotation of each distance

vector) is not possible to be used, as for arrangements with $\mathbf{d}'_0 = -\mathbf{d}'_2$ and $\mathbf{d}'_1 = -\mathbf{d}'_3$, this would result in $\mathbf{0}$ (which is not suitable for further computation, as regarding the following cross product). (In this regard, results close to $\mathbf{0}$ are also problematic, particularly in a numerical context.) The computation principle proposed resolves this issue with the principle that each distance vector adds to the orientation of $\mathbf{u}$, with correspondingly respecting each offset of $i \cdot 90°$ around $\mathbf{w}$ (specifically in negative rotation direction).) Figure 4-59 further visualises and further explains this step of determining $\mathbf{u}^*$.

(Similar to the preceding computation step (ref. the sum of cross products; Eq. (38)), specific cases with fewer than four attached links/points are again considered accordingly, as non-existing links/points are not adding to the sum (as by adding $\mathbf{0}$).)

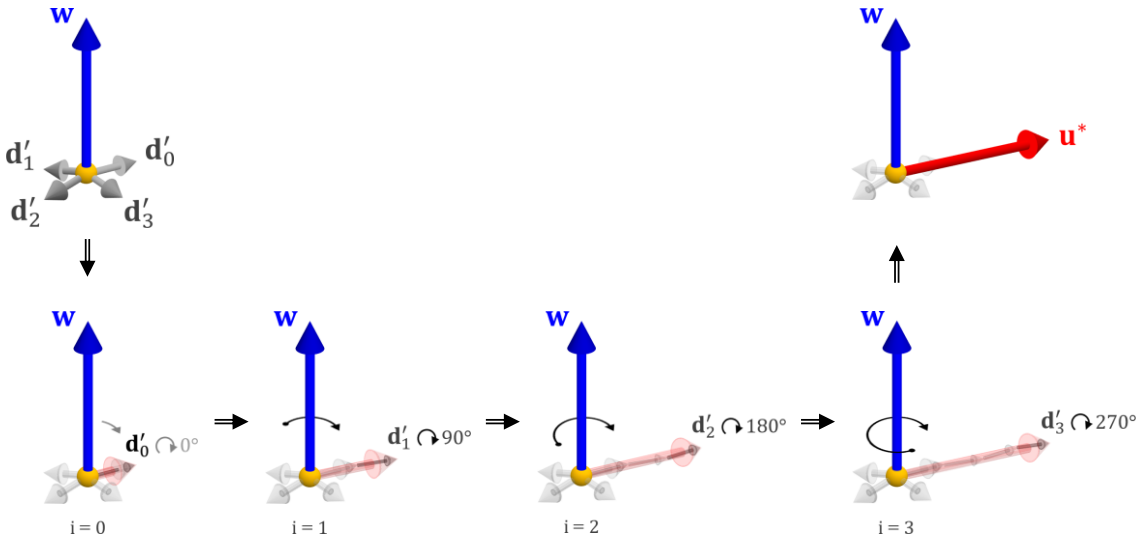

Figure 4-59: Determination of $\mathbf{u}^*$ via the sum of the (individually) rotated length-related distance vectors (around $\mathbf{w}$; sequence at the bottom) according to Eq. (39)

By using this auxiliary vector $\mathbf{u}^*$, the direction-pointing vector $\mathbf{v}$ results according to Equation (40) (as the cross product, which returns the normal vector on the plane formed by $\mathbf{w}$ and $\mathbf{u}^*$; which is further also illustrated in Figure 4-60, also indicating the relation of the u-direction, as accordingly addressed after).

$$\mathbf{v} = \mathbf{w} \times \mathbf{u}^* \tag{40}$$

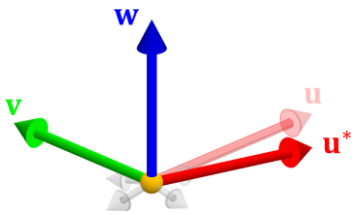

Figure 4-60: Determination of **v** via the cross product according to Eq. (40); also with **u** indicated as following from Eq. (41)

After successfully determining **w** and **v**, the orientation of the particle coordinate system is principally fully defined.

The last direction-pointing vector **u** is trivially resulting with:

$$\mathbf{u} = \mathbf{v} \times \mathbf{w} \tag{41}$$

These three direction-pointing vectors **u**, **v**, **w**, typically provided in normalised form as the actual direction vectors ($\hat{\mathbf{u}}$, $\hat{\mathbf{v}}$, $\hat{\mathbf{w}}$), give the spatial orientation of the particle of focus in this form as a rotated coordinate system, as initially illustrated in Figure 4-55.

Translation of spatial orientation (into quaternion data)

As stated in the overview in the superordinate chapter and as introduced in Chapter 4.2.3.2 regarding the output data format, the spatial orientation of a particle is required as a quaternion. Correspondingly, a translation of the spatial orientation format – from the previously determined form as a rotated coordinate system with its corresponding vectors (**u**, **v**, **w**) into a quaternion (**q**) – is required.

This translation regards a function that returns a quaternion containing the orientation of a given coordinate system, more precisely with respect to an initial (unrotated) coordinate system (that forms the base reference to which the rotated coordinate system is oriented to). For the particular case regarding particle orientation in terms of the BP belt computation, the initial coordinate system of the particle is trivially set as equal with the global coordinate system (x,y,z), as later shown in Figure 4-65.

Before this particular case is discussed, the general principle that forms the underlying basis of the addressed function is outlined, as regarding the determination of the quaternion between two coordinate systems both with general orientation (and thus,

with the initial coordinate system not necessarily equal to the global coordinate system, cf. Figure 4-61). This general principle is subsequently concretised to the relevant case where the initial coordinate system equals the global coordinate system.

As illustratively explained in Figure 4-61, the addressed quaternion basically describes a relationship in terms of spatial orientations between an original and a rotated coordinate system. The figure indicates this relationship, as the rotated orientation state (represented by the coordinate system $\mathbf{u}_{rot}$, $\mathbf{v}_{rot}$, $\mathbf{w}_{rot}$) is resulting from applying the quaternion $\mathbf{q}_{ini.rot}$ onto the initial orientation state (represented by the coordinate system ($\mathbf{u}_{ini}$, $\mathbf{v}_{ini}$, $\mathbf{w}_{ini}$)).

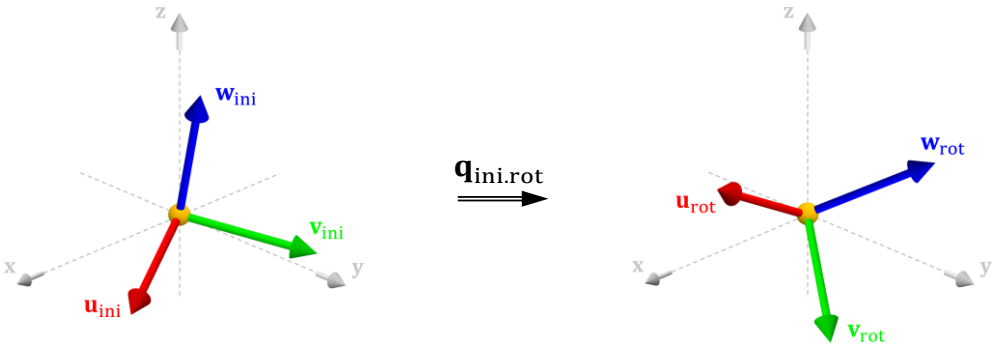

Figure 4-61: A rotated orientation state ($\mathbf{u}_{rot}$, $\mathbf{v}_{rot}$, $\mathbf{w}_{rot}$) resulting from applying a quaternion $\mathbf{q}_{ini.rot}$ to an initial orientation state ($\mathbf{u}_{ini}$, $\mathbf{v}_{ini}$, $\mathbf{w}_{ini}$)

In order to determine this quaternion $\mathbf{q}_{ini.rot}$ a computation scheme based on using two successive angular rotations is explained in the following. (Side note: In principle, also other schemes are conceivable for this purpose, with general reference to some common mathematical principles, e.g. Euler angles or rotation matrix determination/transformation; cf. also System.Numerics [173] in these regards.)

At first, a quaternion $\mathbf{q}_{I}$ is determined that corresponds to the (first) rotation, by which the initial coordinate system is rotated so that one initial coordinate coincides with its corresponding rotated coordinate. In the shown case in Figure 4-62, this regards the coordinate u (by rotating the initial coordinate system so that $\mathbf{u}_{ini}$ coincides with $\mathbf{u}_{rot}$); which is further described in Equation (42) (with the statements as shown, as the axis of rotation is required to be orthogonal to both involved coordinates and is thus resulting as their cross product; and the angle of rotation follows as the angle between two vectors commonly with the arccosine of their dot product).

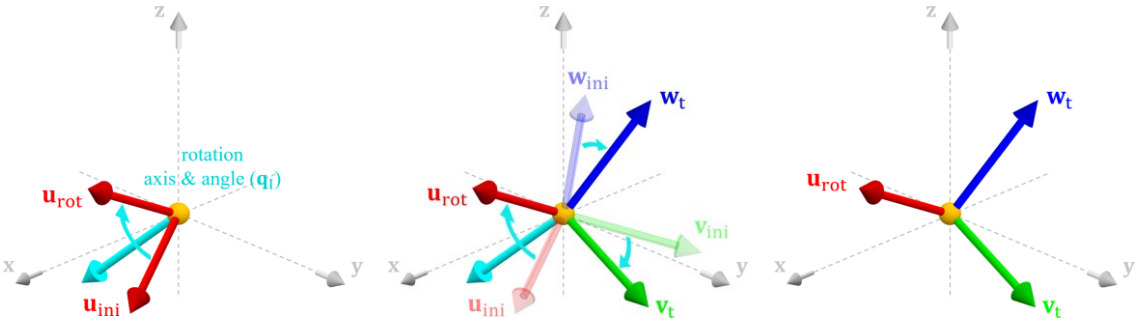

Figure 4-62: First rot. step – coinciding $\mathbf{u}_{ini}$ with $\mathbf{u}_{rot}$; axis/angle determination, applying the rotation on $\mathbf{u}_{ini}$,$\mathbf{v}_{ini}$,$\mathbf{w}_{ini}$, and the result $\mathbf{u}_{rot}$,$\mathbf{v}_{t}$,$\mathbf{w}_{t}$ (from left to right)

$$\mathbf{q}_I = \mathbf{q}\text{CreateFromAxisAngle}\left(\left(\mathbf{u}_{ini} \widehat{\times} \mathbf{u}_{rot}\right),\ \cos^{-1}\left(\hat{\mathbf{u}}_{ini} \cdot \hat{\mathbf{u}}_{rot}\right)\right) \qquad (42)$$

This further gives a transitional orientation state, accordingly with the transitional coordinate system ($\mathbf{u}_t$, $\mathbf{v}_t$, $\mathbf{w}_t$), from this described rotation of the initial coordinate system ($\mathbf{u}_{ini}$, $\mathbf{v}_{ini}$, $\mathbf{w}_{ini}$) by the determined quaternion $\mathbf{q}_I$:

$$\begin{aligned} \left(\mathbf{u}_t = \mathbf{v}\text{Transform}\left(\mathbf{u}_{ini}, \mathbf{q}_I\right) = \mathbf{u}_{rot}\right) \\ \mathbf{v}_t = \mathbf{v}\text{Transform}\left(\mathbf{v}_{ini}, \mathbf{q}_I\right) \\ \mathbf{w}_t = \mathbf{v}\text{Transform}\left(\mathbf{w}_{ini}, \mathbf{q}_I\right) \end{aligned} \qquad (43)$$

Following this first rotational step, a second quaternion $\mathbf{q}_{II}$ is determined, which corresponds to a further rotation of this transitional coordinate system to coincide the remaining two coordinates respectively. This can be done with one of the remaining coordinates, as the other correspondingly follows (cf. Figure 4-63). The principle behind this second rotational step is the same as for the first step; whereby $\mathbf{v}_t$ is rotated to coincide with $\mathbf{v}_{rot}$, as illustrated in the example in Figure 4-63 (following the previously shown case from Figure 4-62) and as further described in Equation (44).

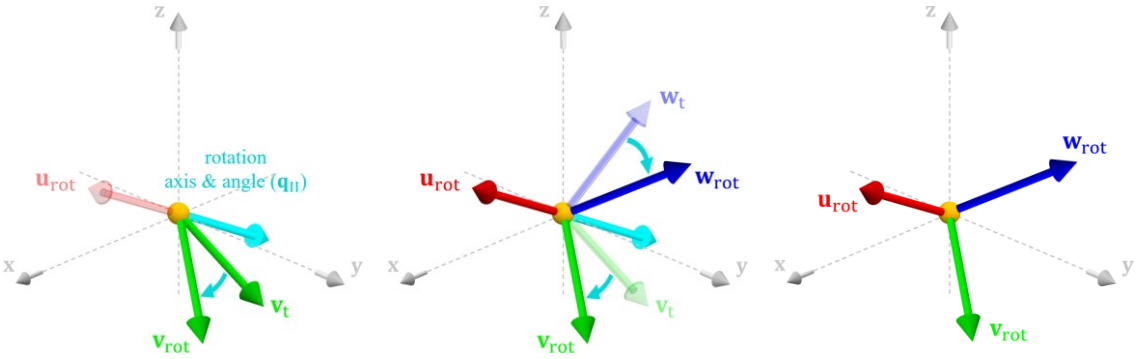

Figure 4-63: Second rot. step – coinciding $\mathbf{v}_t$ with $\mathbf{v}_{rot}$; axis/angle determination, applying the rotation on ($\mathbf{u}_{ini}$),$\mathbf{v}_{ini}$,$\mathbf{w}_{ini}$, and the result $\mathbf{u}_{rot}$,$\mathbf{v}_{rot}$,$\mathbf{w}_{rot}$ (from left to right)

$$\mathbf{q}_{II} = \mathbf{q}\text{CreateFromAxisAngle}\left((\widehat{\mathbf{v}_t \times \mathbf{v}_{rot}}),\ \cos^{-1}(\hat{\mathbf{v}}_t \cdot \hat{\mathbf{v}}_{rot})\right) \qquad (44)$$

Also, the vector that defines the rotational axis is either resulting in the positive or the negative direction of the coordinate that was coincided in the first rotational step (further defining the direction of rotation). (E.g., in the specific case as shown in Figure 4-63, the rotational vector as the respective cross product is corresponding to negative $\mathbf{u}_{rot}$).

The condition – that by applying the second rotational step (represented by $\mathbf{q}_{II}$) on the transitional coordinate system ($\mathbf{u}_t$, $\mathbf{v}_t$, $\mathbf{w}_t$) the rotated coordinate system ($\mathbf{u}_{rot}$, $\mathbf{v}_{rot}$, $\mathbf{w}_{rot}$) is resulting – is to be fulfilled; which is furthermore described with:

$$\begin{aligned} (\ \mathbf{v}\text{Transform}(\mathbf{v}_t\ ,\ \mathbf{q}_{II}) &= \mathbf{v}_{rot}\ ) \\ (\ \mathbf{v}\text{Transform}(\mathbf{w}_t\ ,\ \mathbf{q}_{II}) &= \mathbf{w}_{rot}\ ) \end{aligned} \qquad (45)$$

($\mathbf{u}_t$ is correspondingly not influenced by $\mathbf{q}_{II}$, since it coincides with the rotational axis and is already equal to $\mathbf{u}_{rot}$; cf. paragraph before and especially Eq. (43).)

As shown with (43) and (44), the sequence of applying both determined quaternions ($\mathbf{q}_I$ and $\mathbf{q}_{II}$) on the initial coordinate system ($\mathbf{u}_{ini}$, $\mathbf{v}_{ini}$, $\mathbf{w}_{ini}$) gives the rotated coordinate system ($\mathbf{u}_{rot}$, $\mathbf{v}_{rot}$, $\mathbf{w}_{rot}$) – which is basically intended as introduced above (cf. Figure 4-61; where the sequence of $\mathbf{q}_I$ and $\mathbf{q}_{II}$ basically forms $\mathbf{q}_{ini.rot}$). By combining this quaternion sequence as a corresponding concatenation of $\mathbf{q}_I$ and $\mathbf{q}_{II}$, the final quaternion $\mathbf{q}_{ini.rot}$, which is in this course also normalised (to a unit quaternion), is resulting:

$$\mathbf{q}_{\mathrm{ini}\rightarrow\mathrm{rot}} = \mathbf{q}\mathrm{Normalize}\left(\mathbf{q}\mathrm{Concatenate}\left(\mathbf{q}_{\mathrm{I}}\,,\,\mathbf{q}_{\mathrm{II}}\right)\right) \tag{46}$$

(with $\mathbf{q}\mathrm{Concatenate}()$ returning the concatenated quaternion of two given quaternions as the parameters (with respecting their sequence), and $\mathbf{q}\mathrm{Normalize}()$ returning a normalised (thus unit) quaternion from any quaternion given as the parameter; cf. System.Numerics [173].)

Additional relevant notes:

I. As already indicated, also other sequences of coinciding coordinates than the one shown are principally possible (with u followed by v as shown; e.g. w followed by u, etc.).
II. In addition, special cases need to be identified and considered individually, particularly when the two vectors for coinciding are already parallel, as this would give a zero vector from their cross product (which is not allowed to be used as a rotation axis vector). These cases represent 0° or 180°, with the quaternion trivially following from the rotation axis set to either one of the two other coordinates and a rotation angle of 0° (0) or 180° (π) respectively. (E.g., referring to (and more specifically replacing) Eq. (42): if $\mathbf{u}_{\mathrm{ini}} = -\mathbf{u}_{\mathrm{rot}}$ then $\mathbf{q}_{\mathrm{I}} = \mathbf{q}\mathrm{CreateFromAxisAngle}(\hat{\mathbf{v}}_{\mathrm{rot}}\,,\,\pi)$.)
III. Also, nearly parallel vectors are problematic, specifically in numerical terms, and are thus addressed as special cases to overcome numerical inaccuracies occurring from vector operations with almost parallel vectors. In this regard, prior to the quaternion determination, a pre-rotation is applied to the rotated coordinate system, specifically with 90° ($\pi/2$) around a different coordinate vector than of focus for coinciding. Resultingly, a quaternion determination as according to the proposed rotational steps for common cases, as stated previously, is made possible under favourable circumstances (as the angle between the two vectors for coinciding is accordingly around 90°); and to determine the originally apparent quaternion (of the almost parallel coordinate setup), the pre-rotation has to be considered accordingly, by concatenating the pre-rotation in reverse form. This procedure is schematically also described in Figure 4-64.

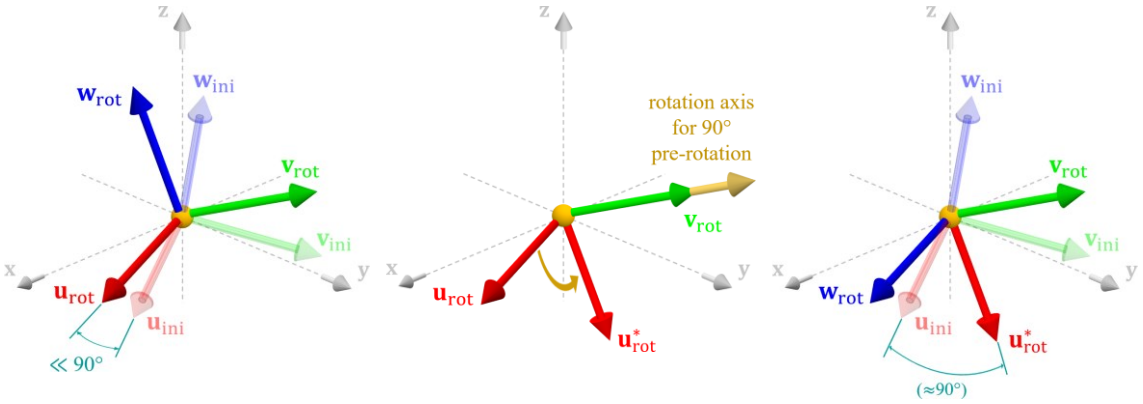

Figure 4-64: Addressing the computation issue with nearly parallel vectors ($\mathbf{u}_{rot}$ and $\mathbf{u}_{ini}$; left) – 90° pre-rotation of $\mathbf{u}_{rot}$ around $\mathbf{v}_{rot}$ to form $\mathbf{u}^*_{rot}$ (middle) – resulting with an angle between $\mathbf{u}^*_{rot}$ and $\mathbf{u}_{ini}$ of about 90° (right)

For this illustrated case in which $\hat{\mathbf{u}}_{ini} \approx \hat{\mathbf{u}}_{rot}$, the computation of $\mathbf{q}_I$ is correspondingly extended as follows: (based on the descriptions given before)

$$\begin{aligned}
\mathbf{u}^*_{rot} &= \mathbf{v}\text{Transform}\left(\mathbf{u}_{rot}\,,\ \mathbf{q}\text{CreateFromAxisAngle}\left(\hat{\mathbf{v}}_{rot}\,,\ \frac{\pi}{2}\right)\right) \\
\mathbf{q}^*_I &= \mathbf{q}\text{CreateFromAxisAngle}\left(\left(\mathbf{u}_t \times \mathbf{u}^*_{rot}\right)\,,\ \cos^{-1}\left(\hat{\mathbf{u}}_t \cdot \hat{\mathbf{u}}^*_{rot}\right)\right) \\
\mathbf{q}_I &= \mathbf{q}\text{Concatenate}\left(\mathbf{q}^*_I\,,\ \mathbf{q}\text{CreateFromAxisAngle}\left(\hat{\mathbf{v}}_{rot}\,,\ -\frac{\pi}{2}\right)\right)
\end{aligned} \qquad (47)$$

(Applies accordingly also if $\hat{\mathbf{u}}_{ini} \approx -\hat{\mathbf{u}}_{rot}$.)

As introductory already mentioned, this computation principle generally described in the previous steps (comprising the two rotational steps and the special cases handling) is further concretised to the particular case related to particle orientations where the initial coordinate system is set as equal to the global coordinate system, thus with $\mathbf{u}_{ini} = \mathbf{x}$, $\mathbf{v}_{ini} = \mathbf{y}$, $\mathbf{w}_{ini} = \mathbf{z}$. In this regard, Figure 4-65 shows a particle with its initial coordinates as in accordance with the global coordinate system (x,y,z), on which a determined quaternion ($\mathbf{q}$) is applied to bring this particle into orientation as intended – as coinciding with the oriented coordinate system (u,v,w), which was determined in the previous section of spatial particle determination.

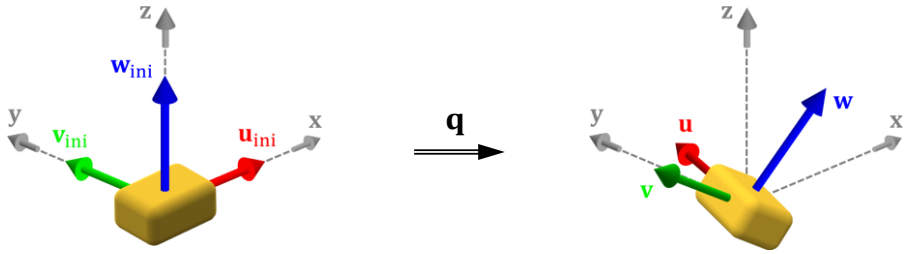

Figure 4-65: A quaternion $\mathbf{q}$ applied on the default particle orientation ($\mathbf{u}_{ini}$,$\mathbf{v}_{ini}$,$\mathbf{w}_{ini}$ = $\mathbf{x}$,$\mathbf{y}$,$\mathbf{z}$) resulting a computed particle orientation ($\mathbf{u}$,$\mathbf{v}$,$\mathbf{w}$)

Furthermore, as already stated at the end of this previous section, a coordinate system is fully defined by two vectors giving two defined coordinate directions (as the third correspondingly follows; see also Eq. (41)). This condition is also evident from the just described rotational steps to coincide coordinates sequentially, where actually only two coordinates per coordinate system are required. With considering these aspects, a function $\mathbf{q}\mathrm{GetQuaternionFromXYtoUV}()$ is specifically implemented that returns the quaternion $\mathbf{q}$ from two vectors defining the rotated coordinate system as $\mathbf{u}$ and $\mathbf{v}$ (given as the two parameters), which further correspond to the initial coordinates of x and y:

$$\mathbf{q} = \mathbf{q}\mathrm{GetQuaternionFromXYtoUV}(\mathbf{u}, \mathbf{v}) \tag{48}$$

This implemented function accordingly comprises the previously described computational steps, further respecting the conditions mentioned above (whereby $\mathbf{u}_{rot} = \mathbf{u}$ and $\mathbf{v}_{rot} = \mathbf{v}$).

Overview of the resulting orientation scheme

The determination principles described constitute the particle orientations following the systematic scheme defined in Chapter 4.2.4.1.2 – specifically relating to the ascending numbering scheme of points, and thus particles, and further relating to the systematic link assignment indicating major belt directions. Consequently, all the particles that form a BP belt are oriented according to these systematics, with the intended result to show a consistent orientation scheme when looking at the total BP belt structure. This consistent scheme is illustrated in Figure 4-66 on a simple representative endless belt model seen in isometric view (top) and from the side (bottom),

with the individual particle orientations indicating the major directions as it is intended.

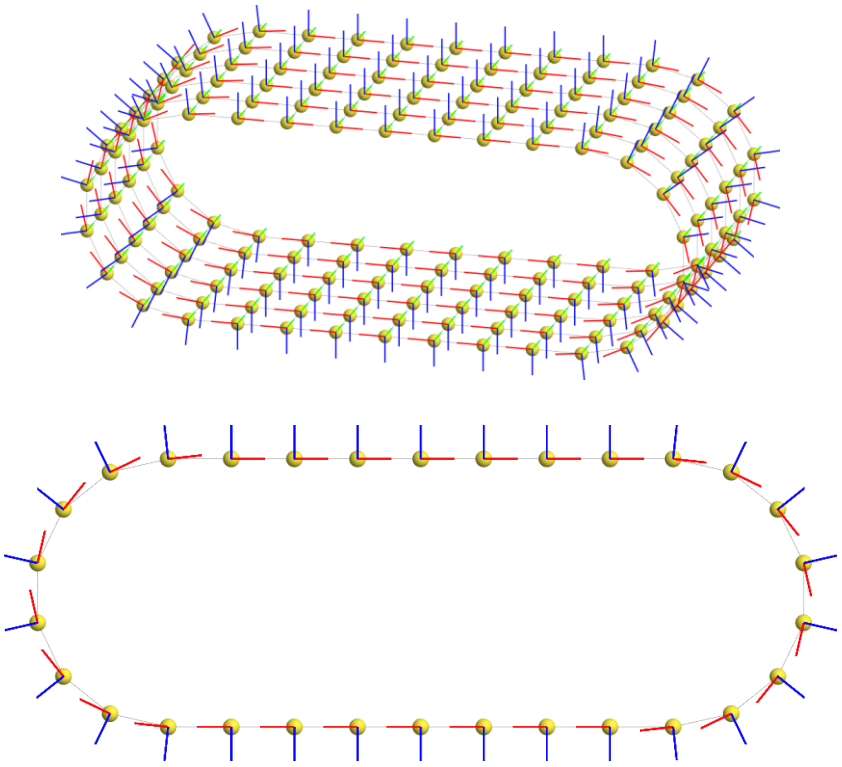

Figure 4-66: Particle orientation scheme illustrated on a simple (endless) BP belt

Additionally, the orientation differences between every two linked particles are also intended to be relatively small, which is basically resulting as the local angular deviations in a given grid are to be kept relatively low (as specified in Chapter 4.2.4.1.3 and respectively Chapter 4.2.3.1.2). Such minor orientation deviations are also visible in Figure 4-66, at the left and at the right where the belt is bent to go around pulleys (correspondingly resulting in local angular deviations in the grid), with particle orientations varying rather slightly from one particle to the next (e.g. by looking at w-axes, showing relatively small angular deviations ($\ll 90°$)).

(Note regarding an additional check: As an additional extension based on these conditions described, a simple feasibility check of the determined particle orientations is possible to be added – by considering the relative orientation differences between every two linked particles that form the BP belt in total; which are intended to fulfil the above-introduced conditions.)

A specific example of a computed particle setup is further shown in Figure 4-67, at a section of a converted BP belt in its initialised state – with the presented/resulting orientation scheme clearly evident from the particle's orientations, as additionally visualised with local particle coordinate systems.

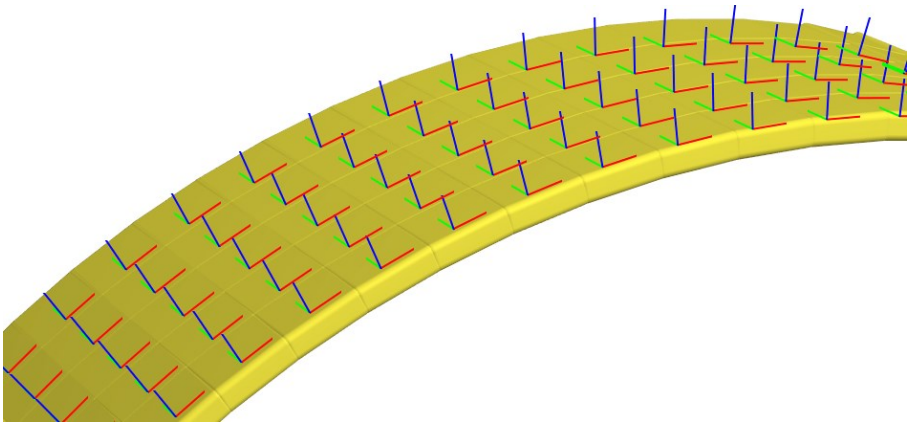

Figure 4-67: Particle orientations in a deformed section of a converted BP belt

4.2.4.2.3 Bonding state computation

Within a computed BP belt, the bondings are required to give information about the local deformation states, which specifically refers to deformation information that results from considering the deformed grid state in relation to the undeformed grid state (as described in Chapter 4.2.2.2). For this purpose, each bonding is capable of containing this type of information, specifically as the zero-states of the two bonded particles, accordingly described in Chapter 4.2.4.2.1. The determination of these zero-states (individually per bonding) is thus required to define each bonding's state and further the total BP belt as intended.

Transferring the particle IDs that represent pairs of bonded particles (and extending the link list into a bonding list)

Similar to the point list being transferred into the particle list (cf. first section in the previous Chapter 4.2.4.2.2), the link list is also transferred into the bonding list by extending link data to represent bondings. Thereby, each bonding in the bonding list is resulting with:

- the ID of the first particle to be bonded (particle A), and

- the ID of the second particle to be bonded (particle B)

(with referencing the IDs of the particles in the particle list); and with additional data (required to be computed) defining the zero-states of the two bonded particles with:

- the zero-state position of the first particle ($\mathbf{p}_{A0}$), and
- the zero-state orientation of the first particle ($\mathbf{q}_{A0}$),
- the zero-state position of the second particle ($\mathbf{p}_{B0}$), and
- the zero-state orientation of the second particle ($\mathbf{q}_{B0}$).

(Note: Link data is extended to bonding data specifically by adding these last four properties, which are consequently required to be computed per link/bonding. Also, this set of data for defining a bonding is generally also evident when looking at the bonding initialising keyword line in Figure 4-27, in Chapter 4.2.3.2, regarding the DEM output data format.)

In the following, each bonding is principally considered individually, with the indices A and B indicating the two bonded particles (as referencing to the particle list), each with their determined properties. (I.e., comprising each position ($\mathbf{p}_A$/$\mathbf{p}_B$) and orientation (quaternion $\mathbf{q}_A$/$\mathbf{q}_B$ / particle coordinate systems $\mathbf{u}_A$,$\mathbf{v}_A$,$\mathbf{w}_A$/$\mathbf{u}_B$,$\mathbf{v}_B$,$\mathbf{w}_B$) as resulting from the previous computations, given in Chapter 4.2.4.2.2).

Note: According to the systematic assignment described in Chapter 4.2.4.1.2 (in the paragraph corresponding to Figure 4-46), the sequence from first to second bonded particle (A-to-B) is assigned to correspond to a positive grid direction (either in positive longitudinal or positive transverse direction).

Bonding orientation determination (longitudinal/transverse bondings)

Basically, each bonding represents a local section of the grid, oriented either in the longitudinal or in the transverse direction, which follows from the IDs of the two bonded particles (see the following Condition set (50), which is further based on the numbering scheme specified in Chapter 4.2.4.1.2). Thereby, the particle ID difference of a bonding results from the IDs of the two linked/bonded points/particles (P_{IDA} and P_{IDB}; as generally similar to Eq. (30)):

$$\Delta P_{ID} = P_{IDA} - P_{IDB} \tag{49}$$

This difference is further relevant for the determination of the direction in which the bonding is oriented (longitudinal/transverse). The condition in this context derives relatively simple, according to the point/particle numbering scheme (cf. Chapter 4.2.4.1.2/Figure 4-30), in which the transverse direction corresponds to a single-step ascending order; thus, this transverse direction shows an ID difference of exactly one; hence, the following condition set applies:

If $|\Delta P_{ID}| > 1$ the cor. bonding is in longitudinal direction (L_{b0L} applies)

Else ($|\Delta P_{ID}| = 1$) the cor. Bonding is in transverse direction (L_{b0T} applies)

Condition set (50)

With these conditions, the consideration of each bonding – as oriented in longitudinal or in transverse direction – is allowed, which is correspondingly further applied in the following (e.g. in Equation (51)).

Generally, it is required as a fundamental prerequisite that the distance between the two zero-state particle positions is equal to the zero-state length of the bonding, respectively for longitudinal/transverse cases, as further described by the condition:

$$\|\mathbf{p}_{B0} - \mathbf{p}_{A0}\| = \begin{cases} L_{b0L} & \text{if } |\Delta P_{ID}| > 1 \text{ (longitudinal)} \\ L_{b0T} & \text{otherwise } (|\Delta P_{ID}| = 1; \text{transverse}) \end{cases} \tag{51}$$

Accordingly, the zero-state length of a currently focused bonding is corresponding to either the longitudinal zero-state length or the transverse zero-state length (L_{b0L} or L_{b0T}; as introduced in Chapter 4.2.4.2.1).

The considered zero-state setup / determining initial zero-state values

The zero-state coordinate systems of two bonded particles are fundamentally required to be equally oriented. Furthermore, their positions are also required to be set with coinciding coordinate directions, either regarding the longitudinal- or the transverse-oriented coordinates (which generally refers to coinciding u/v coordinates). This derives basically from the undeformed grid (cf. Figure 4-52, Figure 4-54, etc.) and is further illustrated in Figure 4-68, in which two longitudinally-bonded particles

are shown in coordinate system representation (as introduced in the preceding Chapter 4.2.4.2.2: as u,v,w coordinate systems), further comprising the general conditions to set the zero-states accordingly (as it is furthermore summarised in the list following below, as corresponding to Eq. (54)). Besides the zero-states of both particles (as indicated with index 0), which is of focus in this chapter's context, the figure also shows a general lengthened and also bent bonding state (indicated in transparent visualisation), correspondingly referring to the particle states as already determined (in Chapter 4.2.4.2.2).

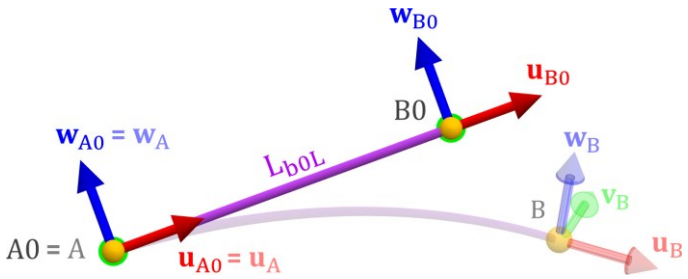

Figure 4-68: Zero-state definition of bonding between two points A0/B0; and the pre-deformed initialised bonding between the two points A/B indicated additionally

This shown figure specifically concerns a longitudinal bonding case, thus regarding the coinciding alignment of the u coordinates as shown; accordingly, similar applies for the case of a transverse bonding, in which the v coordinates are coincidingly aligned instead.

According to this presented setup, the first particle (A) is considered fixed; thus, the second particle (B) is the particle relevant in terms of defining the bonding state. By using this relatively simple approach, the zero-state of the first particle results directly with its position:

$$\mathbf{p}_{A0} = \mathbf{p}_A \tag{52}$$

and its orientation in quaternion form:

$$\mathbf{q}_{A0} = \mathbf{q}_A \tag{53}$$

Furthermore, the zero-state position of the second particle (B) follows – with respecting the orientation of the bonding (cf. Eq. (51)) – with:

$$\mathbf{p}_{B0} = \mathbf{p}_A + \begin{cases} L_{b0L}\,\hat{\mathbf{u}}_A & \text{if } |\Delta P_{ID}| > 1 \text{ (longitudinal)} \\ L_{b0T}\,\hat{\mathbf{v}}_A & \text{otherwise } (|\Delta P_{ID}| = 1; \text{transverse}) \end{cases} \quad (54)$$

as can be derived from Figure 4-68 (specifically regarding longitudinal cases, and respectively transferred for transverse cases by applying direction v instead of u) – and as generally derived from the following considerations (as fundamentally also referring to the setup presented):

- $\mathbf{p}_A$ equals $\mathbf{p}_{A0}$ as the fixed start point,
- condition (51) to be fulfilled, regarding either L_{b0L} or L_{b0T}, whichever applies
- considering the aspect that A-to-B follows a positive direction, thus also from A0 to B0, and more specifically with a coinciding arrangement of:
    - $\mathbf{u}_{A0}$ and $\mathbf{u}_{B0}$ (thus: $\hat{\mathbf{u}}_A$) in the case of a longitudinal bonding, and
    - $\mathbf{v}_{A0}$ and $\mathbf{v}_{B0}$ (thus: $\hat{\mathbf{v}}_A$) in the case of a transverse bonding.

The last data to be computed is the orientation of the second particle (B) in quaternion form ($\mathbf{q}_{B0}$), which in most cases follows as equal to the quaternion of the first particle ($\mathbf{q}_{A0}$). However, certain special cases require a closer consideration in this context, as described in the next section.

Special cases with somersaulting difference quaternions / determining the remaining zero-state values

As just outlined, in general cases, the zero-state quaternion of the second particle results as equal to the first particle's zero-state quaternion – but for certain special cases, more specific consideration/computation is required. In particular, such special cases concern particle arrangements that give a somersaulting difference quaternion between the two bonded particles. The occurrence, the resulting effects, and further the handling of such special cases with somersaulting difference quaternions is schematically explained in the following figures; starting with Figure 4-69, showing the side view of a relatively simple bonded particle arrangement representing an endless BP belt in which such a special case occurs as highlighted.

For reasons of comprehensible illustration, the following figures show particle arrangements in an orthogonal (2D-based) perspective, hence with particles aligned

orthogonally to the view plane. Such a perspective consequently allows the illustration of quaternion rotations in a comprehensible angular format. Thereby, as also indicated, these angles relate to the respective rotation axis vector (around which the angles are shown) as according to the quaternions (these vectors are due to the perspective orthogonal (positive/negative) to the view plane).

The case given in Figure 4-69 specifically shows a view plane equivalent to the global x-z-plane, correspondingly with the particles aligned in this plane, and further with the rotation axis vectors of the quaternions parallel (positive/negative) to the global y-coordinate.

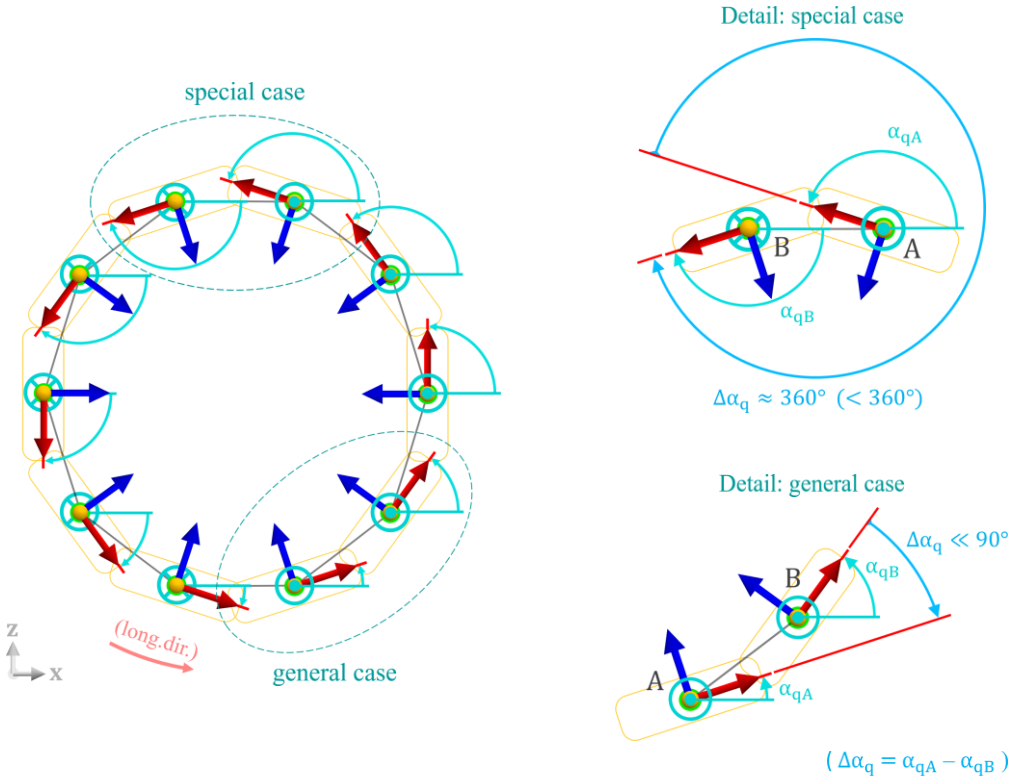

Figure 4-69: A special case with a somersaulting difference quaternion (indicated with $\Delta\alpha_q \approx 360°$), in contrast to a general case (showing $\Delta\alpha_q \ll 90°$)

As can be seen in the figure, in most of the shown cases, the difference quaternion between two bonded particles returns a relatively small rotational difference ($\ll 90°$); but in one special case shown, which is highlighted in the upper area, the difference quaternion returns almost one full rotation ($\approx 360°$ but $<360°$). (Correspondingly, such a special case is referred to as giving a somersaulting difference quaternion.)

As with quaternions capable of containing more complex 3D orientation data, the principles visualised correspondingly apply to general 3D particle arrangements as well (cf. also subsequent descriptions and computations). Correspondingly, such an almost full rotation is possible to occur in a general spatial arrangement, as further schematically illustrated with Figure 4-70 (in this case regarding the transverse direction), in which another particle arrangement is shown (in the same orthogonal perspective as introduced before, but in this case in a more general view plane, not necessarily equivalent to planes formed by main-axis). In this shown setup, the addressed special case occurs in the lower area, as highlighted, where the difference quaternion again returns almost one full rotation (≈360° but <360°); furthermore, following the same scheme as before, which is evident when looking at the rotational axis of the quaternions of focus in such special cases.

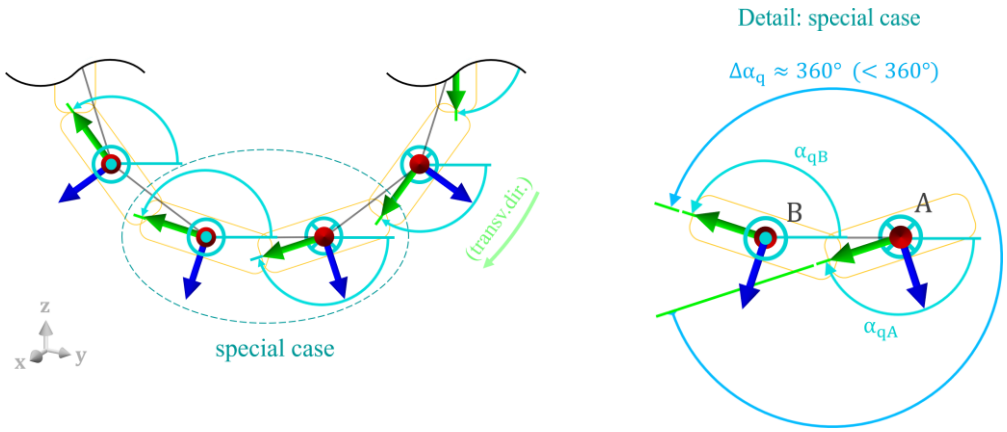

Figure 4-70: Another special case with a somersaulting difference quaternion ($\Delta\alpha_q \approx 360°$) occurring in a general spatial arrangement (in transverse direction)

As evident from these figures, special cases with such somersaulting difference quaternions occur in bondings where the quaternions of the two bonded particles are defined with rotations in opposite directions, thus returning a difference quaternion which is one full rotation deviating from the actual rotational difference as intended. This circumstance basically results from the computation of the particle orientation as given in the previous Chapter 4.2.4.2.2, according to which each particle orientation is determined in relation to the global coordinate system, further with returning the simplest (thus shortest) form of orientation (as also indicated in the two previous figures, Figure 4-69 and Figure 4-70, by showing angles not exceeding a magnitude of 180°).

Consequently, related aspects must be considered when determining the zero-state of a bonding that corresponds to such a special case, as described subsequently. For every other (general) case, the zero-state quaternion of the second particle is relatively simple determined as equal to the first particle's zero-state quaternion, which has already been shown/introduced (cf. Figure 4-68).

If a special case is not explicitly considered further (thus, only considered as a general case, consequently with both zero-state quaternions set as equal), the bonding state that gets initialised contains a high rotational deformation state, as it is added one full rotation to the rotational deformation that is actually intended to be initialised. (This circumstance again refers to the term somersaulting as corresponding to a rotational deformation state which is relatively close to one full rotation; cf. initialised bonding state in the following figures.) This effect that would result without further consideration of special cases is schematically illustrated in Figure 4-71, relating specifically to the special case highlighted in Figure 4-69 (which, however, applies to special cases in general – for example, as to the special case from Figure 4-70). At the bottom of Figure 4-71, the highly rotationally deformed bonding that would result at initialisation, as resulting from the relatively large somersaulting difference quaternion occurring between the zero-state and the initialised state of the particle's orientation, is indicated schematically (with $\Delta\alpha_q \approx 360°$).

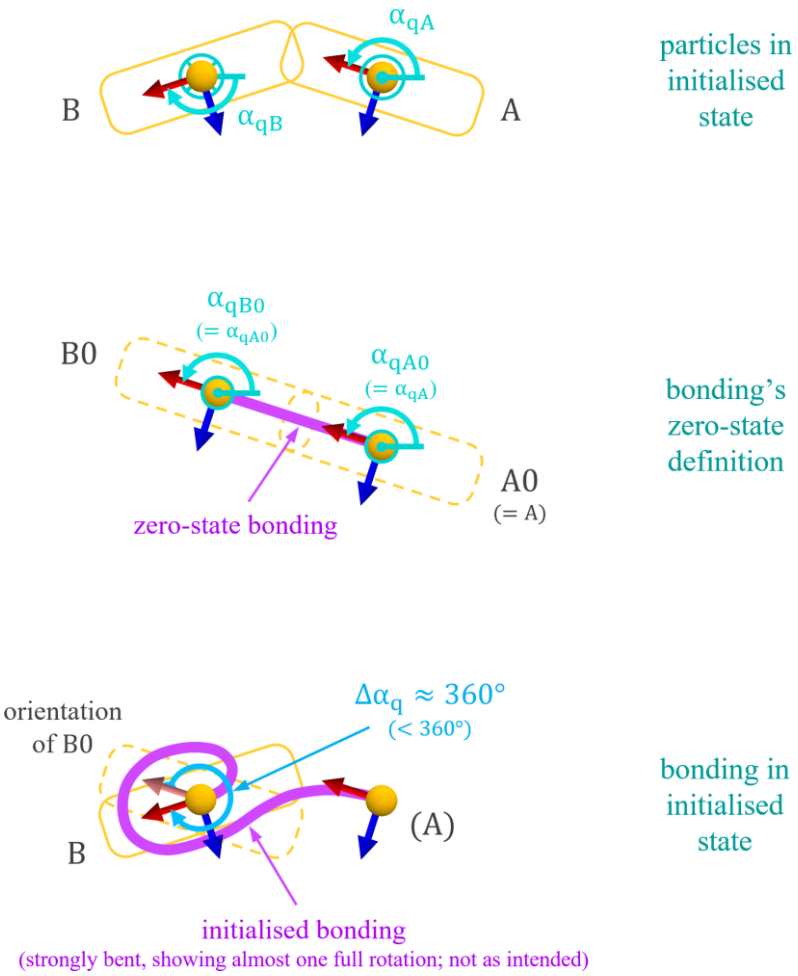

Figure 4-71: Bonding initialisation without considering the somersaulting difference quaternion – resulting in a strongly pre-deformed (bent) state of the initialised bonding (schematically shown, as indicating almost one full rotation)

Obviously, when such a somersaulting quaternion is detected, the zero-state quaternion of the second particle cannot be set simply as equal to the quaternion of the first particle – but further requires a full rotation to be superimposed. Figure 4-72 illustrates this resolving inclusion of such a full-rotation-quaternion (again, specifically regarding the case as dealt with above).

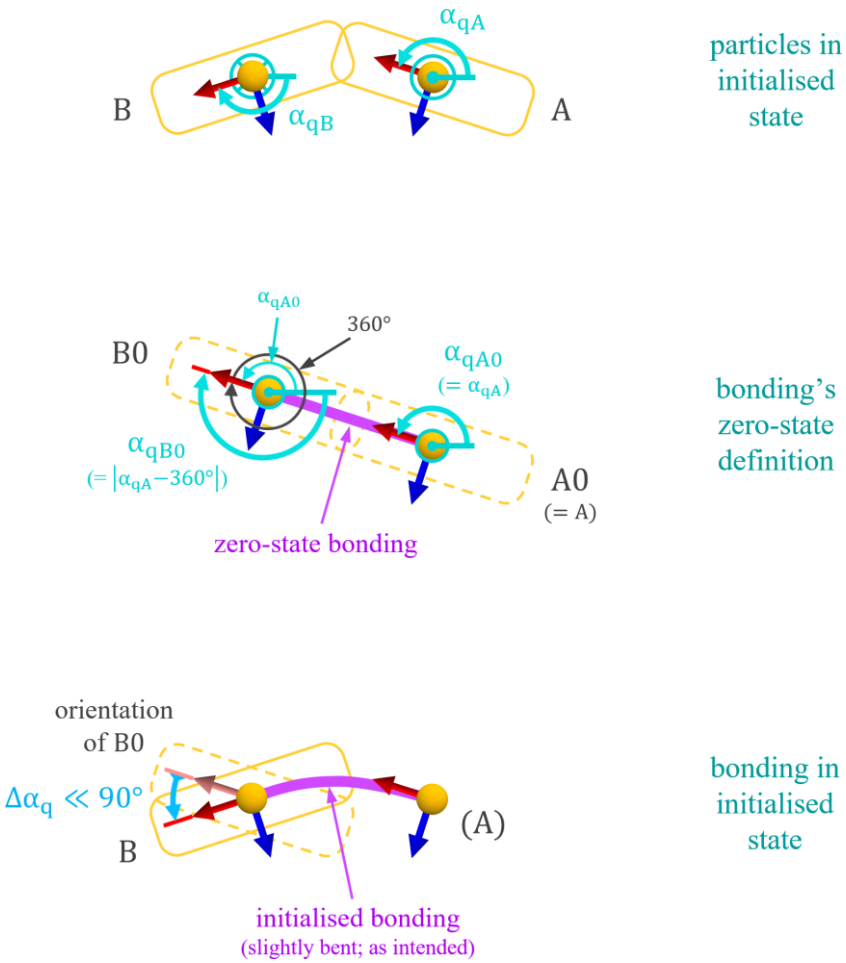

Figure 4-72: Bonding initialisation with considering the somersaulting difference quaternion (by superimposing a full rotation (360°) at B0) – resulting in a slightly pre-deformed (bent) state of the initialised bonding

As illustrated, the zero-state quaternion of the second particle ($\mathbf{q}_{B0}$) is determined by superimposing an additional full rotation to the quaternion of the first particle; specifically by superimposing one full rotation (360°) in the negative rotational direction (relating to the rotation axis of the first particle's quaternion; cf. Figure 4-72, particle A/A0). By applying this principle, the difference quaternion that results (between this resulting quaternion ($\mathbf{q}_{B0}$) and the initialised state quaternion of the second particle ($\mathbf{q}_B$)) is further intended to give a relatively small difference quaternion (indicated with $\Delta\alpha_q \ll 90°$), which is generally intended as corresponding to the relatively small rotational deformation as to be represented by a bonding within a BP belt.

This described operation of superimposing a negative full rotation furthermore equals to negating the quaternion in question. This conformity applies, as the negation of a unit (thus normalised) quaternion gives the alternative form to represent a specific spatial orientation; i.e., changing the "way to reach the spatial orientation" from "the short way around" to "the long way around", and vice versa (cf. Figure 4-72, at B0, the initial quaternion $\mathbf{q}_{\mathrm{A0}}$ and its negated form giving $\mathbf{q}_{\mathrm{B0}}$ as indicated).

(Note: This aspect generally relates to using quaternions in terms of enhanced spatial orientation handling (such as in contrast to Euler angles), as it allows this extended form of orientation representation; and furthermore offers the (already mentioned) operations to apply computations as introduced.)

(Further side note for basic clarification: A negated unit quaternion generally corresponds to the same spatial orientation as its original quaternion, but the "(rotational) way" to reach this orientation is either in the one or in the other rotational direction around the quaternion's rotation axis. Some further details in this context are also addressed in the closing paragraph on quaternion handling in the following section on supplementary considerations. For more details, see also pertinent literature regarding quaternion basics.)

Accordingly, in such special cases, detected as by containing a somersaulting difference quaternion, the zero-state orientation of the second particle is further determined as the negated quaternion of the first particle, which is essentially stated in Figure 4-72 and further covered in the following computational statements.

In conclusion, the determination scheme for the second particle's zero-state quaternion ($\mathbf{q}_{\mathrm{B0}}$) follows from these considerations, as summarised with: If no somersaulting difference quaternion is detected (common case), the quaternion of question is set as equal to the first particle's quaternion (as $\mathbf{q}_{\mathrm{A0}} = \mathbf{q}_{\mathrm{A}}$, as set in Eq. (53)); otherwise (special case), it follows as the negated first particle's quaternion. In computational terms resulting with:

$$\mathbf{q}_{\mathrm{B0}} = \begin{cases} \mathbf{q}_{\mathrm{A}} & \text{if } \mathrm{bIsSmallDiffQ}(\mathbf{q}_{\mathrm{A}}\,,\,\mathbf{q}_{\mathrm{B}}) = \mathrm{true} \\ \mathbf{q}\mathrm{Negate}(\mathbf{q}_{\mathrm{A}}) & \text{otherwise } (\mathrm{bIsSmallDiffQ}(\mathbf{q}_{\mathrm{A}}\,,\,\mathbf{q}_{\mathrm{B}}) = \mathrm{false}) \end{cases} \tag{55}$$

whereby bIsSmallDiffQ() corresponds to a customised function, returning a boolean value (true/false) from comparing two quaternions in terms of their rotational differences, as further outlined in the following considerations regarding quaternion differences. $\mathbf{q}$Negate() represents a standard function to return the negated quaternion of a given quaternion, as addressed before (which in more detail concerns the negation of each entry in the quaternion data)[24].

(Supplementary note: The quaternion negation ($\mathbf{q}$Negate()) in Eq. (55) is basically applied with further fulfilling the condition that the resulting difference quaternion (respectively between this resulting quaternion ($\mathbf{q}_{\mathrm{B0}}$) and the initial state quaternion ($\mathbf{q}_{\mathrm{B}}$)) results as a relatively small quaternion (as fundamentally intended; cf. also Figure 4-66, etc.), which can further be expressed as the condition bIsSmallDiffQ($\mathbf{q}_{\mathrm{B0}}$, $\mathbf{q}_{\mathrm{B}}$) = true.)

The explained computation finally allows the last remaining zero-state data, the orientation of the second particle (B) in quaternion form ($\mathbf{q}_{\mathrm{B0}}$), to be determined, as by specifically considering special cases as described.

Supplementary considerations in terms of quaternion differences

As defined in Chapter 4.2.4.1.3 (and as respectively introduced in Chapter 4.2.3.1.2), the local angular deviations in a prepared belt model are required to be kept relatively low; more specifically, as described by Figure 4-47, this concerns the link/bonding orientations at each point/particle to show either an angular difference of about 90° or correspondingly 180° (with 90° between differently oriented bondings (longitudinal/transverse) and 180° between equally oriented bondings (longitudinal/longitudinal or transverse/transverse)). Conformingly, these aspects are generally evident in all the related previous figures shown, e.g. in Figure 4-69, as distinctive when comparing each adjacent pair of bondings in this regard. Furthermore, as described in Chapter 4.2.4.2.2, the orientation of each particle results basically from its local link/bonding orientations. Therefore, the particle orientation differences, which are of interest for the bonding state computation (as generally dealt with in the previous

[24] three coordinate values forming the rotation axis vector and a rotation-representing value (.W); cf. quaternion basics, and also the following section on supplementary considerations

sections) are basically following from the angular deviations in the original grid structure as provided for conversion.

In order to discuss limits in terms of quaternion differences, as more specifically relating to the previously introduced function bIsSmallDiffQ(), a certain exceptional case of a grid structure – that should actually not occur due to the previously mentioned restrictions – is illustrated in Figure 4-73.

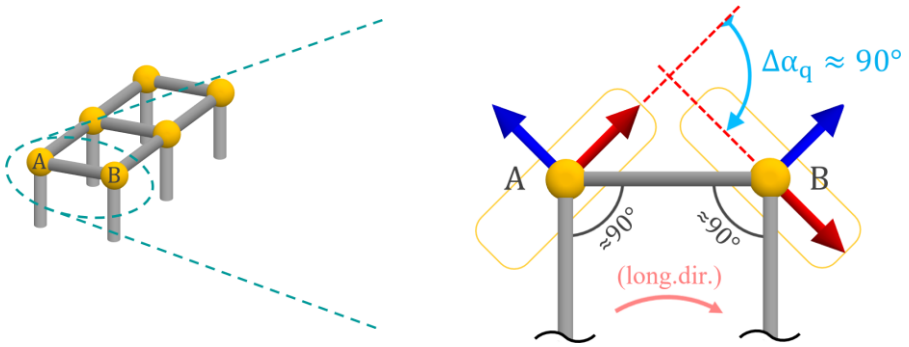

Figure 4-73: Exceptional sharp edge in a grid structure returning an exceedingly large difference quaternion (indicated with $\Delta\alpha_q \approx 90°$)

The figure shows an unintended case in which not only one but two directly adjacent relatively sharp edges occur in the meshed belt model provided, thus in the corresponding grid structure. As illustrated, both edges show an angle of about 90°, which are actually intended to be about 180° according to the aforementioned conditions (as relating to two longitudinally oriented bondings).) As is further evident, this grid structure results in particle orientations determined that show an exceedingly large orientation difference between them. This case is outlined to highlight this occurring quaternion difference (as the orientation difference) in this exceptional case, which explicitly shows an angular difference of about 90°, as illustrated in the figure. In terms of common/special case determination, this orientation difference is principally conceivable to be considered as a (rather high) angular limit (α_{qLimit}). This angular limit consideration also applies similarly to special cases with somersaulting difference quaternions, as illustrated in Figure 4-74. Thereby, with the same exceptional base setup, but this time concerning a somersaulting difference quaternion, thus with the angular difference correspondingly about 270° (resulting as the difference between one full rotation and the just-introduced angular limit (α_{qLimit})).

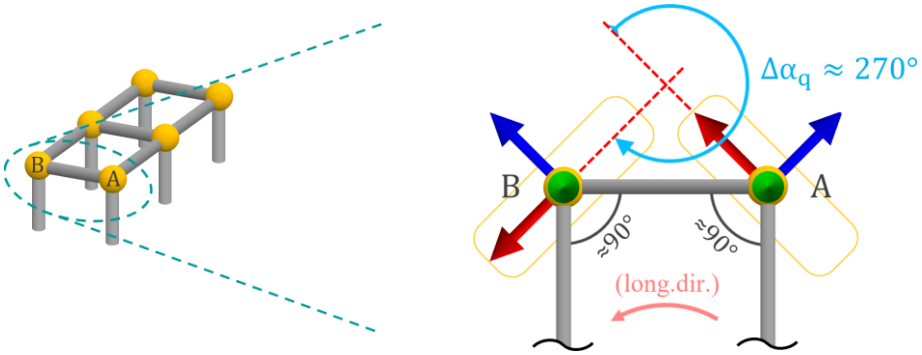

Figure 4-74: Exceptional sharp edge in a grid structure returning an exceedingly large difference quaternion at a special case (somersaulting difference quaternion) (indicated with $\Delta\alpha_q \approx 270°$)

In conclusion, the angular ranges as addressed basically form the condition set for detecting the case resulting from a given angle ($\alpha_{\Delta q}$) of a corresponding (difference) quaternion ($\mathbf{\Delta q}$), consequently with:

If $0° \leq \alpha_{\Delta q} < \alpha_{qLimit}$ common case
(as the cor. Quaternion represents a relatively small quaternion)

Else If $(360° - \alpha_{qLimit}) < \alpha_{\Delta q} < 360$ special case
(as the cor. Quaternion represents a somersaulting quaternion)

Else $(\alpha_{qLimit} \leq \alpha_{\Delta q} \leq (360° - \alpha_{qLimit}))$ unintended exception
(as the cor. Quaternion represents a not intended case)

Condition set (56)

(e.g., with α_{qLimit} set to 90°, or even below, as acc. The previously addressed aspects).

Accordingly, this condition set shows a potential scheme to be implemented in the customised function bIsSmallDiffQ(), specifically to return a boolean value (true/false) from analysing two quaternions (as the provided parameters), more precisely, their difference quaternion (from the first to the second quaternion). After the Condition set (56), a common case is correspondingly detected from a relatively small difference quaternion, thus returning true; with the special case returning false; and the unintended exception further throwing a stop exception, thus aborting the computation process, as an unintended case (with too sharp edges) is detected (more

specifically, this exception consideration refers to a supplementary check of the imported mesh/grid structure). For specific implementation, this function may also be customised/tuned further, such as regarding the conditions/limits for returning true or false.

(More on related quaternion handling: In general terms, a difference quaternion ($\Delta\mathbf{q}$) between two quaternions ($\mathbf{q}_\mathrm{a}$ and $\mathbf{q}_\mathrm{b}$) can be determined with $\Delta\mathbf{q} = \mathbf{q}\mathrm{Normalize}\big(\mathbf{q}\mathrm{Multiply}(\mathbf{q}\mathrm{Inverse}(\mathbf{q}_\mathrm{a}),\, \mathbf{q}_\mathrm{b})\big)$, where $\mathbf{q}\mathrm{Multiply}()$ and $\mathbf{q}\mathrm{Inverse}()$ correspond to functions regarding/returning quaternion data types (multiplication and inverse function; cf. System.Numerics [173]). Further, $\alpha_\mathrm{q} = 2 \cdot \cos^{-1}(\mathbf{q}.\mathrm{W})$ can be used to return the angle (α_q) of a quaternion $\mathbf{q}$ (which is specifically required as a unit (thus normalised) quaternion); with $.\mathrm{W}$ as the value corresponding to the angular rotation of the quaternion. In unit quaternions $.\mathrm{W}$ ranges from -1 to 1, which correspondingly gives angles in the range from 0° to 360° (0 to 2π) around the positive rotation axis vector of the quaternion. Thus, with additionally considering the possibility to invert this rotation axis vector of the quaternion, angular orientations of up to 360° are enabled in both directions, which basically relates to the previously introduced negation of a quaternion (by inversion of the rotational axis, on the one hand, the rotational direction is changed; and by negating the $.\mathrm{W}$ value, on the other hand, the angle is correspondingly changed to the opposite side (with reference to one full rotation, see also Figure 4-72 top-left; and cf. arccos function as applied for determining α_q as stated before). Further details on quaternions can also be found in pertinent literature.)

Excursus: Outlook and theoretical considerations on further adaptions

As mentioned in the previous section, the circumstances that give such special cases with somersaulting difference quaternions basically result from the type of quaternion computation of particle orientations (as presented in the translation section in the previous Chapter 4.2.4.2.2). Theoretically, these initially determined particle quaternions may thus be adapted further in an intermediate step (before the bonding state computation), with the purpose to omit somersaulting difference quaternions in most areas: These adaptions would specifically apply a scheme to the particle quaternions of the particle list, according to which (almost) all difference quaternions at bondings would correspond to a relatively small difference quaternion. Thus, after

this principle, not the zero-state quaternions regarding the bonding initialisation are adapted (as addressed in the previous section regarding the special case handling), but the particle quaternions in the particle list. This scheme is schematically illustrated in Figure 4-75, showing a certain form of an endless arrangement of bonded particles to highlight related effects (also: ref. same orthogonal perspective principles as introduced in the last section).

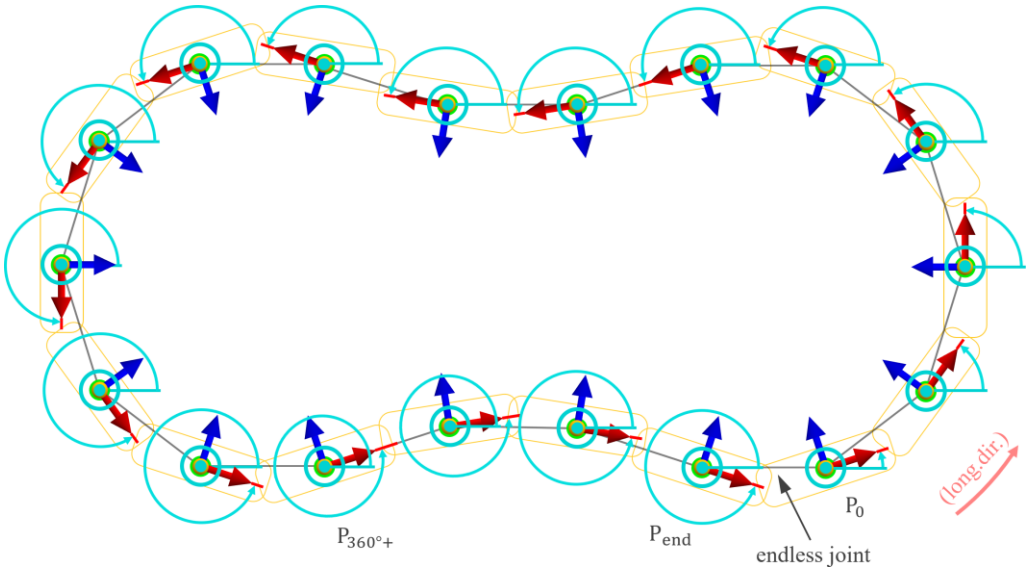

Figure 4-75: Alternative scheme giving small difference quaternions; with two particles showing more than one full rotation as their orientation ($P_{360°+}$), and with the endless joint evident (as resulting a full rotation as the difference quaternion)

As indicated, the particle quaternions are adjusted to fulfil the previous introduced condition of resulting small difference quaternions – in almost every section, as except at endless joints, such as illustrated in the figure as occurring between particle P_0 and P_{end} (cf. principles described in Figure 4-27). Beneficial in this context is that these areas are already known due to the sorted particle list, which allows proper handling of them (by applying the special case determination of $\mathbf{q}_{B0}$, as stated as the second case in Eq. (55)), accordingly only for these bondings that form such endless joints. Moreover, when looking at the figure, it is also evident that quaternions are required to represent rotations of even more than 360° (as indicated explicitly at particle $P_{360°+}$), which exceeds the limit of unit quaternions and which are consequently not applicable anymore. (Side note: Would another full round follow to particle P_{360+}, e.g. when forming a spiral-shaped finite belt, or similar, the angle would correspondingly increase, even up to more than 720°, etc.)

Due to the additional intermediate step for applying this scheme on the determined particle quaternions, which would typically regard the recomputation of a considerable amount of particle data, and further, due to the aspect that unit quaternions (thus normalisation) are not applicable anymore (which basically affects quaternion handling), this approach is not followed further; although it is mentioned for completeness.

As another option, supplementary data adaptation/translation may be applied on the determined zero-state data after their computation (thus, subsequently added after determining the zero-state data with Eq.(52)-(55)), typically with the purpose to bring the already determined zero-state data in a different format; thus, such adaptation/translation is principally not necessarily required. As a fundamental condition for applying such optional adaptations/translation, the generally required relations (in this context especially referring to the determined content per bonding in terms of their inner relative setups) are not to be changed/affected. This means that it is principally possible to relocate/realign each bonding individually, but with the condition to handle each bonding as a complete setup (comprising the quaternion and position data of both bonded particles), respectively. Such a process applied on a general bonding (considered accordingly as a complete setup) is outlined in Figure 4-76, adapting the bonded particle setup A0/B0 into A0'/B0', accordingly without changing their inner-bonding relations/conditions.

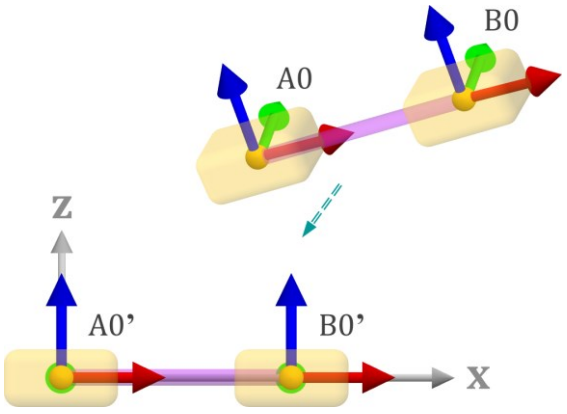

Figure 4-76: Alternative adaptation of relocating and realigning a bonding's zero-state definition (from A0/B0 into A0'/B0'; without affecting the bonding)

This figure further addresses the mentioned purposes, more specifically, the option to apply a certain (and furthermore uniform) scheme to the computed zero-state data:

As indicated in the figure, each bonding may be relocated/realigned to conform to a certain uniform format, according to which each bonding is rotated to coincide along a global coordinate axis (e.g. longitudinal bondings along global x, such as shown, and transverse bondings along global y correspondingly; or similar), and further repositioned to global zero (e.g. with the first particle (A) coinciding with global zero). This scheme outlined would accordingly give a uniform data set, furthermore in a more or less cleaned-up format, in which only the x/y values of the second particle's position data are different from zero, with values further corresponding (uniformly) to the zero-state lengths of the bondings in longitudinal/transverse direction (defined prior to the computation process; cf. Chapter 4.2.4.2.1).

As principally possible but not necessarily required (as mentioned, and as the actual result – the represented BP belt – is not (to be) affected), this approach is not further implemented as an additional module; hence, is in this excursus only mentioned as a further theoretically applicable extension; further to give an outlook on such aspects regarding possible supplementary data adaptation/translation.

4.2.4.3 Additionally applying initial belt velocity

As an extending option, belt velocity can additionally be applied to the determined BP belt. This basically allows to not only initialise the converted BP belt in an almost-final state (as based on the CAD belt geometry provided for conversion) but further to initialise this BP belt in an already running state. For enabling this extended form of initialisation, suitable velocity information is required to be applied to each particle in the BP belt structure.

In this context of BP belt initialisation in a running state (and more specifically: in a longitudinally running state), it is explicitly the translational particle velocity information that is of interest. This can be concluded as each local belt particle in such a longitudinally running BP belt model is primarily required to represent a longitudinal belt movement, which accordingly corresponds to translational velocity. A relatively simple and expedient scheme to apply this form of longitudinal particle velocity for each particle in a respective BP belt is in more detail covered in the following subsection.

Particle velocity determination

From the previously stated condition, that each belt particle is required to represent a longitudinally-oriented belt movement, the translational particle velocity ($\mathbf{v}_\mathrm{p}$) for each particle (of the particle list, as containing the particles of the BP belt including their states) follows with:

$$\mathbf{v}_\mathrm{p} = v_\mathrm{belt}\,\hat{\mathbf{u}} \tag{57}$$

This applies as each particle's u-direction is determined to conform to the local longitudinal direction (cf. Chapter 4.2.4.2.2/Figure 4-55), on which the belt velocity (v_belt), which is optionally defined by the user, is correspondingly applied.

Related notes:

- If no specific belt velocity is defined, no particle velocity is resulting accordingly (thus, returns as $\mathbf{0}$).
- Negative values are also allowed for v_belt, correspondingly inverting the direction in which the BP belt is running at initialisation (in relation to the determined longitudinal direction; cf. Chapter 4.2.4.2.2).
- Concerning finite belts: The additional option to switch the major belt directions (longitudinal with transverse; as introduced in Chapter 4.2.4.1.2) is particularly useful in this context of applying a belt velocity in the longitudinal direction.

Furthermore – as relating to the overall context of this Chapter (4.2), belt initialisation in almost-final state – it is relevant to consider the effects that express as a transient oscillation when applying an initialised BP belt for simulation, as described before in Chapter 4.2.1. During this (commonly rather short) pre-simulation, the respectively initialised BP belt, which in this context is also defined to comprise translational particle velocity information (acc. Eq. (57)), gets formed into its steady-

state[25]. Thereby, imbalances in the particle velocities are compensated locally, resulting each from local conditions, further referring to:

- Transient oscillation of translational velocities (which expresses with typically relatively small, locally varying deviations from the initialised state).
- Transient oscillation of rotational velocities (which results particularly from local conditions in combination with the applied translational velocities). (This forming of rotational velocity without pre-determined values during pre-simulation further indicates that focusing on longitudinal velocity determination is sufficient, as introductory addressed and as further outlined in the considerations given in the following section.)

An exemplary visualisation of translational particle velocities, accordingly applied on a BP belt as determined after the presented scheme (Eq. (57)), is further shown in Figure 4-77 (showing a section of the conventional belt conveyor example from Chapter 5.2). The figure specifically indicates local particle velocities at the initialised (thus computed) state in vector visualisation, further expressing each particle's translational velocity as its direction and its value (correspondingly, showing a consistent velocity value, equal to v_{belt}, at each particle pointing in the computed longitudinal direction).

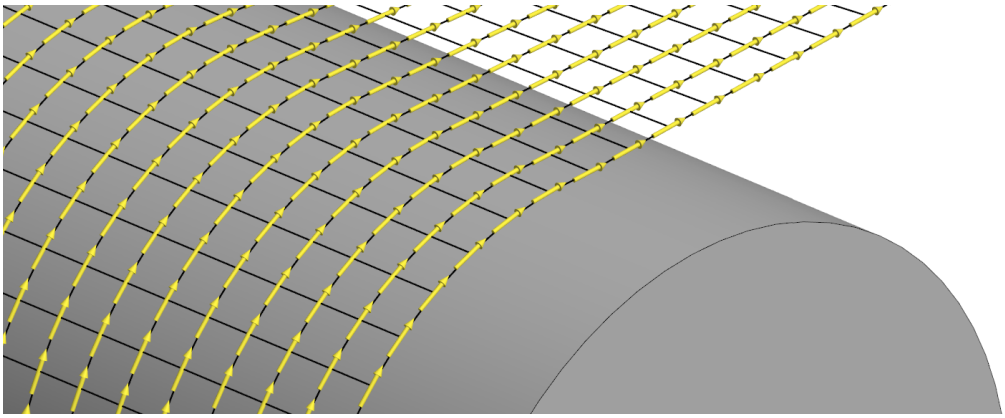

Figure 4-77: Particle velocities applied to the particles of the BP belt, pointing in longitudinal direction, for initialising a running BP belt (with a given belt velocity)

[25] With steady-state especially in context with an already running belt, thus with belt velocity included; in contrast to transient oscillation into an assembled state, which regards non-running belts, thus without belt velocity.

Supplementary considerations regarding rotational particle velocities

As already stated, the application of translational velocity is generally sufficient for applying a (longitudinal) belt velocity to a BP belt. But in addition to that, it is theoretically also possible to determine and further apply a rotational particle velocity, which is fundamentally only relevant to particles in (rather strongly) bent areas – more specifically, bent in respect to the longitudinal direction, such as around pulleys. This generally follows from the commonly known context regarding rotational velocities, as it is in the addressed case of belt particles specifically expressable with: $\mathbf{u}_\mathrm{p} = \boldsymbol{\omega}_\mathrm{p} \times \mathbf{r}_\mathrm{rot}$, in which $\boldsymbol{\omega}_\mathrm{p}$ forms the rotational velocity of the particle of focus, and $\mathbf{r}_\mathrm{rot}$ corresponds to a radius-representing vector, basically indicating the bending around which this particle is moved. This bending is further in relation to the given grid at the particle of focus (in this regard, see also particle state computations in Chapter 4.2.4.2.2). (E.g., around a pulley, this radius would correspond to the distance from the particle to the pulleys centre axis (typically: pulley radius plus half the particle thickness).)

With this context in mind, general areas of typical belt models do not require to consider rotational velocities, as showing no or only minor levels of bending. Even at intended bendings, such as at pulleys, these can commonly also be considered as minor, basically due to the predominance of translatory velocity; and as furthermore, only a relatively minor amount of particles is typically affected (as relatively flat areas commonly predominate over bent areas in common belt applications). (Also, too sharp belt deflections, which relate to relatively sharp edges in a provided belt model, are generally not intended neither supported; cf. Chapter 4.2.4.1.3/Chapter 4.2.3.1.2). Due to these aspects, and as introduced, rotational particle velocity is thus not determined explicitly – furthermore, as it generally results in any case also during pre-simulation, the transient oscillation of an initialised BP belt, as stated before.

(Although not explicitly included in the current version of the presented conversion algorithm (thus, not available in the corresponding software tool BeltConverter), the consideration of such rotational velocities, such as by following the principles described in the paragraph before the previous one, is principally conceivable to be added as another extending option in future adaptations of the algorithm.)

4.2.4.4 DEM data export

In the last essential step of the conversion algorithm, the computed data is brought into the required format to conform to the DEM output data as specified in Chapter 4.2.3.2 (.inp) – and is in this form correspondingly written, thus exported, into the resulting output file for further use. Such an exported output file thus contains the data of the BP belt that is converted from the given CAD belt model according to the before-given modules/steps, comprising:

- CAD data import and preparation (Chapter 4.2.4.1),
- particle and bonding computation (Chapter 4.2.4.2), and
- additionally (optionally) applying initial belt velocity (Chapter 4.2.4.3).

The further use of such an output file specifically implies its import into the respective DEM software environment, thus initialising the BP belt, as already explained in Chapter 4.2.1 regarding the use of a CAD-to-DEM conversion algorithm such as presented. (Corresponding to the INP format, this regards specifically the DEM software ThreeParticle/CAE.) In conclusion, by initialising a converted BP belt via importing the output data file, dynamic belt simulation as intended is fundamentally enabled – explicitly by enabling BP belt initialisation in almost-final, and optionally also in additionally running state.

In the following subsections, the process to form the final output data is correspondingly described. This essentially involves bringing the particle and bonding data from the raw-computed form, as resulting from the computation steps given before, into the specific output data syntax required (INP format).

Basic exporting scheme – transferring particle and bonding data

According to the INP syntax, each particle and bonding is required in a particular single-line string format, as already described in Chapter 4.2.3.2, specifically in Figure 4-27. The computed data, comprising such particles and bondings in raw-computed format, is correspondingly transferred to conform to this type of format, specifically by bringing every particle from the particle list and every bonding from the bonding list into a representative text line with respecting the required syntax.

Figure 4-78 illustrates the scheme for transferring computed particle data into INP syntax.

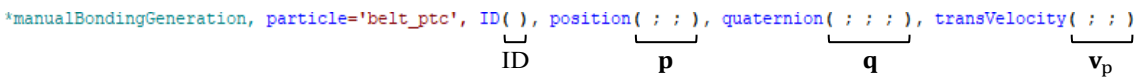

Figure 4-78: Transferring computed particle data into INP syntax

As illustrated, the following assignments are made for each computed particle in the particle list: (with the values to be assigned described in Chapter 4.2.4.2.2/Chapter 4.2.4.3)

- ID: the particle's ID, which equals its number in/from the particle list
- position: the particle's position (**p**)
- quaternion: the particle's spatial orientation (**q**)
- transVelocity: the particle's translational velocity ($\mathbf{v}_p$)

(specifically, with vectors expressed by their three respective vector-forming scalar values (.X; .Y; .Z), and with quaternions expressed by their four respective quaternion-forming scalar values (.X; .Y; .Z; .W).)

Details regarding the particle type property (indicated with belt_ptc) are covered in the next section as of relevance to fibred belt structuring.

Similarly, Figure 4-79 illustrates the scheme for transferring computed bonding data into INP syntax.

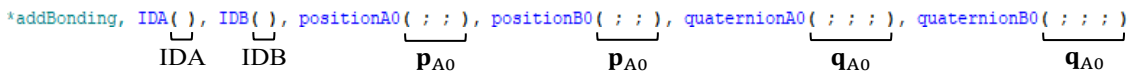

Figure 4-79: Transferring computed bonding data into INP syntax

As illustrated, the following assignments are made for each computed bonding in the bonding list: : (with the values to be assigned described in Chapter 4.2.4.2.3)

- IDA: the first (bonded) particle's ID (referencing to a spec. particle ID)
- IDB: the second (bonded) particle's ID (referencing to a spec. particle ID)
- positionA0: the first particle's zero-state position ($\mathbf{p}_{A0}$)
- positionB0: the second particle's zero-state position ($\mathbf{p}_{B0}$)

- quaternionA0: the first particle's zero-state spatial orientation ($\mathbf{q}_{A0}$)
- quaternionB0: the second particle's zero-state spatial orientation ($\mathbf{q}_{B0}$)

(again, with vectors and quaternions expressed respectively, as explained before.)

These determined INP syntax lines are further accordingly written into the exported output data file. Thereby, a systematic scheme can be applied in order to achieve a clearer file structure and thus improve usability and convenience. This refers to writing the particle lines in a first block, followed by the bonding lines, which can further be blocked into two parts, containing the longitudinally oriented bondings in the one and the transversely oriented bondings in the other. Furthermore, each block itself can also show a systematic structure, such as by containing an ascending order (as referring to the particle ID, essentially resulting when the particle list is processed in ascending order.)

Fibred belt structuring via systematic particle type definition

With the default scheme of applying the same particle type to every particle (belt_ptc; as shown in Figure 4-78), no specific structuring is applied to the BP belt.

To further apply a fibred belt structuring, as in detail explained in Chapter 4.1.2.3, the differentiation of adjacent fibres is required, which is explicitly done by defining such fibres with different particle types. Therefore, each particle type definition is added a fibre numbering index, further indicating to which fibre the respective particle belongs.

For applying an alternating fibre pattern, exactly two particle types (belt_ptc_1 and belt_ptc_2) are required; furthermore, forming a structure with the suffixes as schematically illustrated in Figure 4-80.

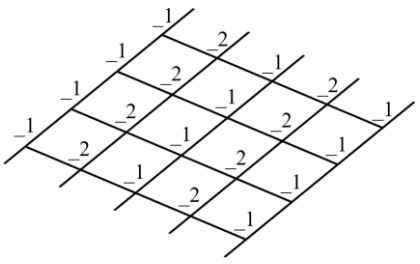

Figure 4-80: Alternating fibres (indicating suffixes following belt_ptc)

Accordingly, a fibre pattern with all individual fibres is resulting when each fibre shows an individual particle type (correspondingly: belt_ptc_1, belt_ptc_2, belt_ptc_3, …), thus forming a structure with the suffixes as indicated in Figure 4-81.

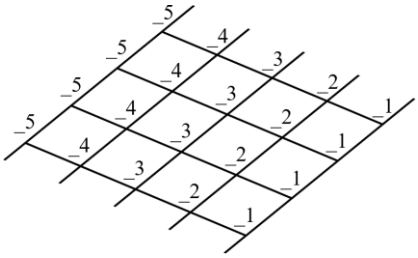

Figure 4-81: Individual (all different) fibres (indicating suffixes following belt_ptc)

The addressed fibre numbering index is trivially determinable due to the systematic numbering scheme initially applied on the grid structure as described in Chapter 4.2.4.1.2 (see specifically Figure 4-30). (In detail, the fibre numbering index (F_{ID}) for each particle follows from a modulo operation (mod), with each particle's ID (P_{ID}) as the dividend, and the number of particles in a (transverse oriented particle) row (n_{pT}) as the divisor. (With n_{pT} obviously also representing the number of fibres.) This determination is specifically expressable with: $F_{ID} = (P_{ID} \bmod n_{pT}) + 1$, where $+1$ is further added to start the fibre numbering at one instead of zero. Furthermore, by determining even/odd, these all-individual-representing indices can further be transferred trivially to represent an alternating fibre pattern.)

Adding supplementary information

In addition to the essential data as covered before, which is fundamentally relevant to enable the initialisation of the computed BP belt, further informational-only data is supplementary written into the created output file, specifically at the beginning, in order to give an overview of the performed conversion process. This informational data comprises two major parts: settings information and conversion-process-related information.

The settings information include which specific settings were made to result in the BP belt data as given by the respective output file; e.g. regarding the zero-state bonding length definitions made (cf. Chapter 4.2.4.2.1); and generally refers to all the settings possible to be made in the GUI of the conversion tool BeltConverter (see

next Chapter 4.2.5, i.e. Figure 4-83). (Furthermore, this information is written in a syntax that allows the reloading of settings from such an output file back into the developed software tool BeltConverter.)

The conversion-process-related information contains some general information (program information, filename of the imported CAD belt model, date) – and essentially gives information about the resulting BP belt, by comprising:

- Belt type (endless or finite)
- Particle-related information
    - Amounts (total and in longitudinal/transverse direction)
    - Dimensions (min./max. x/y/z)
    - IDs (first/last particle ID)
- Bonding-related information
    - Amounts (total and in longitudinal/transverse direction)
    - Lengths (avg./min./max., in longitudinal/transverse direction)
    - Longitudinal lengths in sum (as the belt length; at edges/in the middle)

Thus, this information gives insights into relevant characteristics of the converted BP belt. Furthermore, it is essential that such informational data is written to the output file in the appropriate command line format, as further shown in Figure 4-82 in the next section.

Resulting output file

Figure 4-82 gives an overview of such a resulting DEM output file as created according to the descriptions given before; showing the informational data at the beginning, followed by the major blocks containing the particle and the longitudinal/transverse bonding data. (This shown example corresponds in particular to the conventional belt conveyor application from Chapter 5.2.) Furthermore, as human-readable and thus editable, manual modifications on this data are principally possible, such as regarding changing certain particle types as to create inhomogeneities or also certain forms of belt joints (cf. also Chapter 4.1.2.3).

Figure 4-82: Exported INP file containing the computed BP belt data in a structured/blocked form

As ultimately containing the converted BP belt data, such an output file forms the final result of applying the presented conversion algorithm.

Thus, this conversion algorithm, comprising the essential modules given in the preceding chapters, fundamentally enables the initialisation of a BP belt in an almost-final state, furthermore optionally also in an already running state, and therefore forms a core element of the developed methodology as presented in this thesis.

4.2.5 BeltConverter

The presented conversion algorithm is implemented into a software program, BeltConverter [94], that correspondingly includes the essential modules/computations as described in the previous Chapter 4.2.4 as its core modules. (Details regarding the implementation in software-related terms were already stated in Chapter 4.2.2.4.2.) Moreover, to allow convenient use, more specifically regarding performing belt conversion processes as introduced, this software program is also added a graphical user interface (GUI). This GUI is shown in Figure 4-83, representing the developed software tool to allow CAD-to-DEM belt conversion according to the principles/schemes as presented in this methodology/thesis.

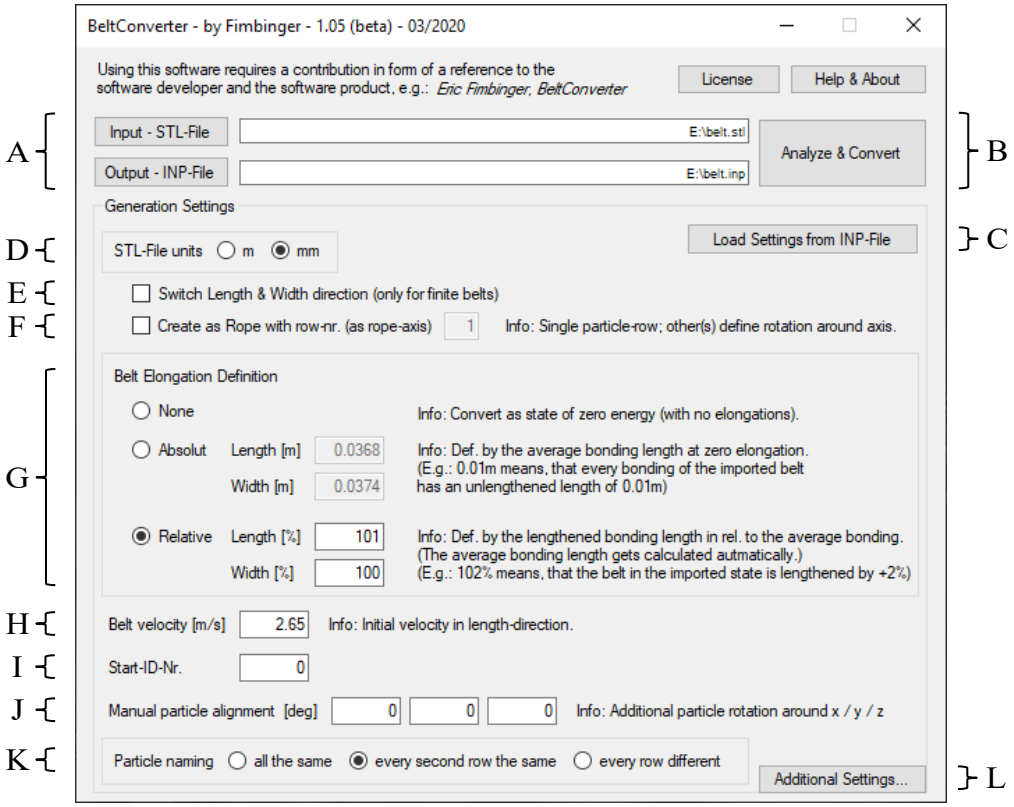

Figure 4-83: GUI of the developed software tool BeltConverter

As evident, this GUI allows users to perform the introduced belt conversion in an intuitive and user-friendly way. The shown main form therefore contains several elements, which are explained in more detail below[26]. (Note: Most of these elements further refer to aspects already covered within the previous chapters; corresponding references are thus given respectively.)

A – File handling

The file handling section regards the location of the STL input file to be loaded, and the INP output file to be exported as a result of a conversion process. In this context, relevant aspects concerning the associated data are in detail given in Chapter 4.2.3; such as specifying the STL input file (in ASCII encoded STL format), containing a quadrilateral-meshed middle surface model of the belt, furthermore fulfilling geometrical conditions, such as with no large angular deviations and no sharp edges. The INP output file, on the other hand, is specified to result in INP (ThreeParticle/CAE keyword file) file format, which also shows human-readable content, as in previous chapters described.

Specific module parts that relate to this file-regarding context are especially Chapter 4.2.4.1.1 (translation of data), concerning the loaded STL input file, and Chapter 4.2.4.4 (DEM data export), regarding the writing of computed data into the INP output file. (Side note: Drag-and-drop of files is supported for more convenient usage.)

B/C – Starting a conversion process / regarding settings in general

Via the respective button (B), a conversion process can be started, which in this context correspondingly relates to the underlying conversion algorithm – with its essential modules as covered in Chapter 4.2.4. Thereby, the specific settings made in the container below are accordingly respected (D and following). In the case of a first program start, these settings are set to typical default values. Furthermore, regarding those settings in a whole perspective, those are also written to the output file in a specific comment-line format as described in Chapter 4.2.4.4, in the DEM data export module. This concerns two purposes: giving information on which settings were

[26] The basic purpose of several elements is also indicated in the GUI, such as in additional info blocks next to certain input fields.

made to result in the BP belt data that is included in a respective output file, and furthermore, allowing to reload these settings from such an output file (C) (where, again, drag-and-drop is also supported for more convenience). Also, when a conversion process is started, the made settings are additionally stored in the Microsoft Windows Registry [174] to enable reloading of them when the program is restarted.

D – Units

As described in Chapter 4.2.3.1.3, STL data does not explicitly contain unit information. The settings option to change the units in which a belt model is provided in a given STL file to either meter (m) or millimetre (mm) addresses this aspect. This option is particularly added, as millimetre models are relatively common (and its implementation into the algorithm is rather trivial, as regarding the inclusion of a corresponding scaling factor (1/1000, for bringing millimetre to metre values) in the import module (Chapter 4.2.4.1).) Principally, separate scaling can be applied prior to loading the STL file in order to bring the content of a certain STL file into metre format (as is basically required for the output data format (inp); cf. Chapter 4.2.3.2).

E – Direction switching

The check box to switch length and width directions regards explicitly finite belt models, as each of the two pairs of opposite belt edges is in principle able to represent the longitudinal belt direction. This direction switching is typically activated as a reaction from the user when the initial conversion of a specific belt model returns a BP belt with inverted direction characteristics. As shown in Chapter 4.2.4.1.2, these characteristics relate to the numbering scheme of particles (which more specifically corresponds to their IDs), which indicates determined directions. Thus, this scheme is accordingly changed when such direction switching is activated, as already introduced in the beforementioned chapter, and as schematically further illustrated in Figure 4-84. (Note: Setting the directions as it is intended is particularly relevant, e.g. in terms of the subsequently described definitions, as regarding elongation states (G), belt velocity (which follows the longitudinal direction) (H), or fibred structuring (K).)

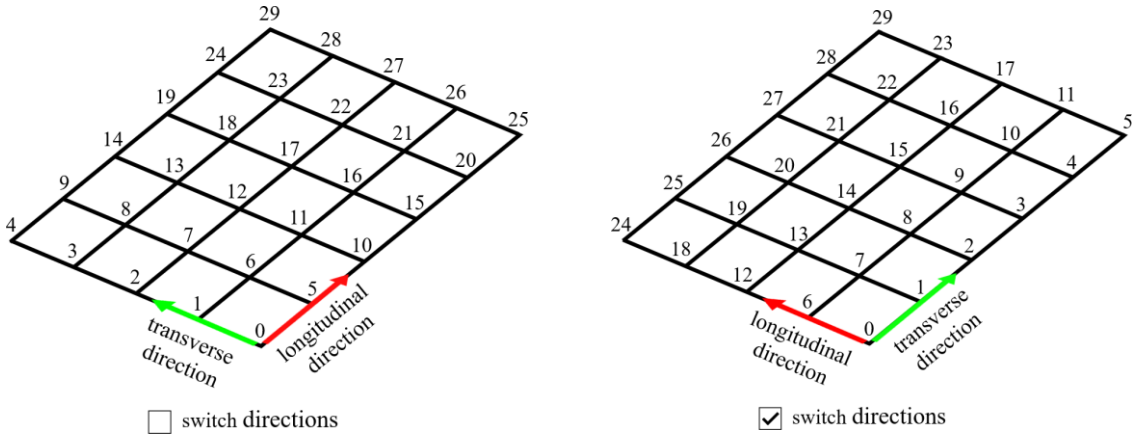

Figure 4-84: Effect of direction switching

F – Rope conversion

As an additional extension, a rope creation feature is further implemented in the software tool. By activating this feature, a single fibre is created as the resulting bonded-particle structure (referred to as BP rope). The number of this fibre is set by the user (ref. rope axis). (In terms of fibred structuring, see also Chapter 4.1.2.3; and also the section on fibred belt structuring in Chapter 4.2.4.4.) Such a BP rope is correspondingly following a specific three-dimensional course, as given by the CAD geometry – also including rotations around its axis, as resulting from the transversely oriented grid-links in the initial model. From this context derives that it is sufficient that the CAD model provided for conversion contains only a single-line quad structure, thus with a width of only one quad in the transverse direction, as illustrated in Figure 4-85 (top). In this figure, a BP rope conversion from CAD data is illustrated with one specific fibre set as the rope axis (as indicated in the middle figure); correspondingly, the transverse grid-links, pointing to the second fibre, are responsible for the rotational orientation of the BP rope around its axis (with the final BP rope resulting as shown on the bottom). (Note: If the other (or with more than two fibres, generally any other) fibre is meant to form the rope axis, this other fibre must accordingly be set as the rope axis number. And, regarding unintended longitudinal/transverse directions, see the respective section on direction switching given before.)

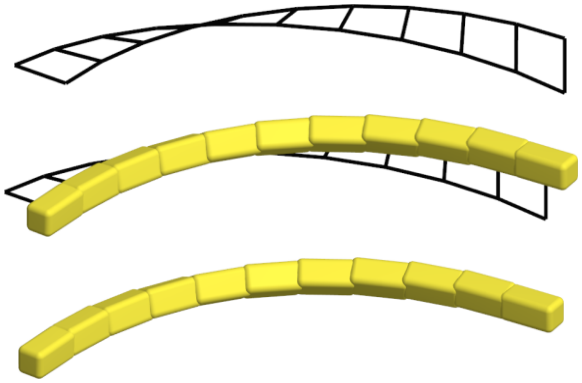

Figure 4-85: Conversion with the option to give a BP rope (pre-deformed BP fibre)

It is important to note that such BP ropes conform to the same principles as BP belts, such as especially in terms of their initialisation (as further referring to deformed/elongated state or velocity definition, etc., which are thus also concerning to such BP ropes).

(Further note regarding adaptations towards rope-like structures: As such BP ropes generally relate to bonded-particle fibres, as described in the basics in Chapter 3.1.2.2.1, there are typically further considerations to be made, such as using different types of particle geometries (for example, using cylindrical or capsule-shaped particles).)

The applications for which such a BP rope conversion may apply reach from typical fibre-related applications, as shown in the basics chapter mentioned above (in this regard comprising part-related as well as handled-material-related models), further to complex structures made from/with such fibres, for example, braided/woven or similar entangled structures.

G – Elongation states (zero-bonding-lengths)

The settings for belt elongation relate to the state in which the converted BP belt is initialised – specifically in terms of initialised pre-deformation (see Chapter 4.2.2.2). For defining such a pre-deformation state, the respective zero-bonding-lengths (in both major directions, longitudinal and transverse) are required to be set, which can be made either via using absolute or alternatively relative values as covered in more detail in Chapter 4.2.4.2.1 (see also the informative description next to the two re-

spective options in the GUI, as shown in Figure 4-83). (In general outline, these values define a zero-state into which a pre-deformed-initialised belt is attempting to deform.)

The additional alternative option to define no specific pre-deformation state results consequently in a BP belt being initialised without certain pre-deformation information, which thus attempts to stay in this initialised form. (Note: This option allows application for certain non-flat objects to be initialised, such as non-flat but deformable wall objects, e.g. shields, or also specific cylindrical objects, e.g. tubes or bellows, etc.)

H – Belt velocity

By setting a belt velocity unequal to zero, a running BP belt can be initialised – as typically applicable for skipping a more extensive start-up process of a belt system. Thereby, each particle in the initialised BP belt is correspondingly applied an additional initial velocity. Further details in this regard are also covered in Chapter 4.2.4.3.

(Relevant notes: As regarding common belt systems, the belt velocity explicitly relates to the longitudinal direction (for direction switching, see previous section E). Furthermore, the direction can also be inverted, as negative values are allowed.)

I – Starting ID

The starting ID option adds an offset to the IDs of the particles in the BP belt (generally following from the numbering scheme as introduced in Chapter 4.2.4.1.2). Such an offset is particularly useful to prevent multiple particles from being assigned the same ID, which would occur if other pre-defined particles are already in the simulation. Such other pre-existing particles may occur due to:

- bulk particles already in the simulation,
- parts that are represented by (complex) particles, such as idlers (cf. smooth-surfaced cylinders in Chapter 4.4), and
- other initialised BP belts, which correspondingly contain a multitude of particles (e.g. see the example of the sandwich conveyor in Chapter 5.4, which contains two BP belts in one simulation setup).

J – Superimposed particle orientation

An extending option allows to additionally rotate the zero-state orientation of the belt particles used. This is specifically relevant when using particle geometries that require a certain non-default alignment at zero-state (with default referring to coincide with x,y,z, as basically illustrated in Figure 4-65 on the left).

This regards, for example, the previously addressed BP ropes (F), when intended to contain cylindrical particles oriented with their cylinder axes in the longitudinal direction: As a cylindrical particle would initially be oriented with its cylinder axis in the y-direction, but the longitudinal (rope) axis actually corresponds to the x-axis (cf. u-direction in the reference given before), an additional rotation of 90° around the z-axis is correspondingly required – which relates to this addressed superimposed particle rotation.

K – Fibred structuring

The structuring of BP belts with a fibred setup was introduced and accordingly described in Chapter 4.1.2.3 – regarding its implementation and also its purpose. Further corresponding details were also addressed in the last module of the conversion algorithm, DEM data export, in Chapter 4.2.4.4. According to the descriptions made in these chapters, fibred structuring fundamentally requires a BP belt to be made from different particle types – which also refers to the three different options available to be set for a conversion process: (in the GUI, Figure 4-83, K, from left to right)

- without specific fibre structuring (all particles of the same type),
- with alternating fibres (every second particle of the same type),
- with all different fibres (every particle type of a different type),

(with particle type differences only regarding the transverse direction, as particle types within each fibre, thus in longitudinal direction, are required to be consistent).

L – Additional settings

The additional settings regard more specific computational/numerical aspects, such as in terms of numerical data handling, e.g. regarding accuracy (rounding) of values, etc.

4.3 Illustration & Verification

In this supplementary chapter, the initialisation of BP belts according to the presented methodology is illustrated; thus, specifically regarding BP belts initialised in pre-deformed states, as regarding the belt initialisation method described in Chapter 4.2 – further with BP belts correspondingly modelled, comprising a structural belt setup as introduced in Chapter 4.1.

In this course, a verification principle, specifically regarding such pre-deformed-initialised BP belts in terms of belt-like behaviour as intended, is also introduced. In particular, this principle refers to the fundamental characteristics that a pre-deformed initialised BP belt is required to deform into its state-of-rest when applied in a simulation in which no external loads or boundaries are affecting the deforming of the belt. Aspects in these terms were already explicitly stated in Chapter 4.2.2.2 and were further also dealt with in Chapter 4.2.4.2.1. Thereby, the (undeformed) zero-state of a BP belt was described as showing a perfectly flat rectangular particle arrangement (with bonding lengths correspondingly equal to defined zero-bonding-lengths); and with this mentioned state generally referring to the belt modelling principles given in Chapter 4.1. These deformed-to-undeformed conditions were explicitly introduced as an underlying basis for the developed conversion algorithm/process.

As already presented, such as specifically with Figure 4-18 and Figure 4-19 (in Chapter 4.2.2.2), the two forms of state-of-rest into which an initialised BP belt is required to deform/relax – when correctly initialised – are:

- perfectly flat rectangular – regarding finite BP belts (cf. Figure 4-18), and
- perfectly circular-cylindrical – regarding endless BP belts (cf. Figure 4-19).

Consequently, a generally initialised BP belt (typically with a complex pre-deformed belt geometry) can be proven as suitable in this essential regard by fulfilling this described required condition to deform/relax into the respective state-of-rest as intended. (For this reason, the principle introduced is further referred to as relaxation-into-state-of-rest principle.)

In the following subsection, a few relatively simple belt geometries – accordingly converted and initialised as BP belts – are analysed in this regard of deforming/relaxing into their state-of-rest. Similarly, this is also applied on rather large, hence

application-oriented, belt models in the subsection following after; particularly with reference to the exemplary applications later shown in Chapter 5. Also, the developed conversion algorithm/process (and thus specifically the developed software tool BeltConverter presented in the previous chapter) can be evaluated in this context as well, as concludingly outlined in the last subsection.

In the demonstrations presented in the following, certain distorted (pre-deformed) belt geometries are analysed regarding the introduced verification principle of deforming/relaxing into a correct state-of-rest (relaxation-into-state-of-rest). Therefore, those belt geometries are converted into BP belts, which are further initialised and simulated accordingly without additional loads or boundaries. In these performed simulations, the BP belts each deform into their state-of-rest, resulting from the relaxation process of the pre-deformed initialised bondings (cf. also Chapter 4.2.4.2.3, section bonding state computation). For each specifically analysed belt geometry given in the following, a BP belt's initialised (thus converted) form is shown at first, with its resulting final form, as the state-of-rest into which the respective BP belt oscillates during the described (relaxation) simulation, correspondingly shown at last; (additionally, with a deformation-process-illustrating state shown in the middle).

The addressed final state-of-rest can be analysed in two terms: regarding the bondings and regarding the particles. Thereby, the bondings are required to show a uniform, rectangular grid structure (see Chapters 4.1.2.1/4.2.2.2/4.2.4.2.1), and the particles are required to show appropriate orientations (see Chapters 4.1.1.3/4.2.4.2.2). In this regard, the particles are generally required to follow a uniform pattern, generally giving a smooth surface. More specifically, the particles are required to be oriented as corresponding to a particle arrangement in either a rectangular or cylindrical pattern (ref. flat or endless belts). (These described aspects are also clearly evident when looking at the BP belt's state-of-rest shown in the following figures, each on the right.)

If a BP belt deforms/relaxes correctly, according to the above-mentioned aspects, thus showing a final state-of-rest geometry as required/intended and as described, proof can consequently be stated (ref. relaxation-into-state-of-rest).

Simple/illustrative belt geometries

Figure 4-86 and Figure 4-87[27] show a case of a relatively small finite BP belt, initialised in a flat-distorted form with relatively large angular grid deviations (20° distorted in relation to perfect rectangles, also including an elongated bonding state along the short edge).[28] As can be seen from the figures on the right, the resulting state-of-rest, into which this finite BP belt deforms/relaxes, shows a correct geometry: a perfectly flat shape with an undistorted rectangular bonding grid.

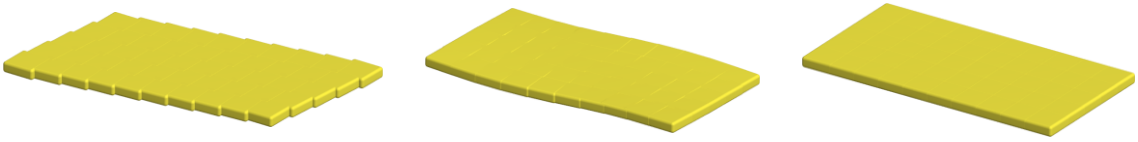

Figure 4-86: Relaxation of a finite flat-distorted BP belt

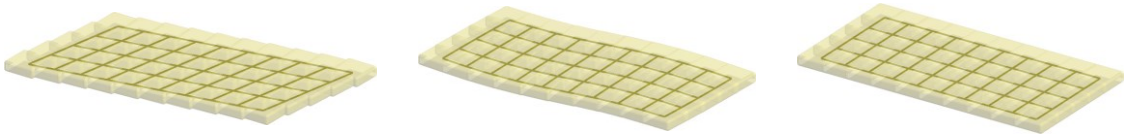

Figure 4-87: Relaxation of a finite flat-distorted BP belt (bonding grid)

In Figure 4-88/Figure 4-89, a different deformation state of a finite BP belt is considered; in this case, pre-deformed in terms of bending as showing a u-shaped geometry. Again, the resulting state-of-rest, into which this pre-deformed BP belt correctly deforms/relaxes, is shown in the figures on the right.

[27] The two associated figures illustrate the addressed case first in full particle visualisation and then in bonding visualisation with transparent particles. This also applies to the following cases.

[28] Note: For scope-extending reasons, the belt model is oriented in a general spatial orientation, i.e. with its grid structure not (necessarily) parallel to a main plane of the global coordinate system. This general orientation aspect also applies to the following cases correspondingly.

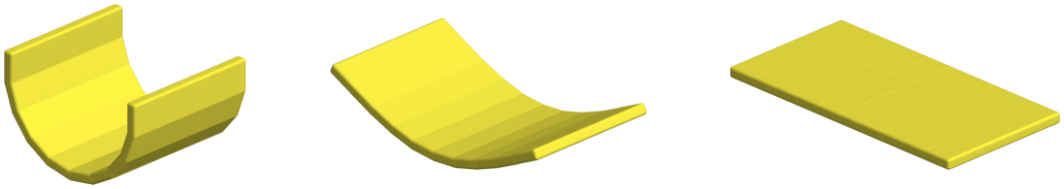

Figure 4-88: Relaxation of a finite u-deformed BP belt

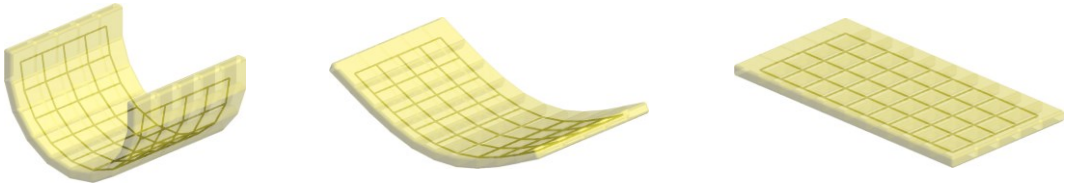

Figure 4-89: Relaxation of a finite u-deformed BP belt (bonding grid)

Another finite BP belt, specifically with an initialised pre-deformed state that combines the two previous ones, is further shown in Figure 4-90/Figure 4-91. Again, the state-of-rest that is reached shows a correct result.

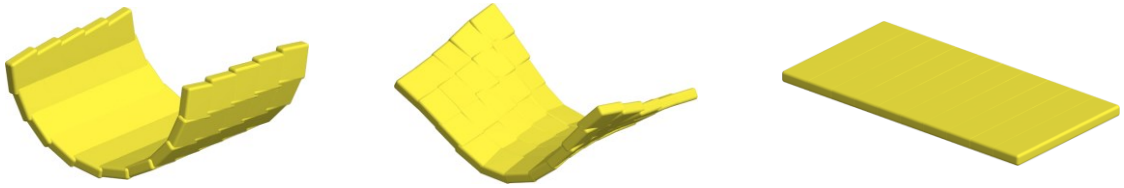

Figure 4-90: Relaxation of a finite u-deformed and distorted BP belt

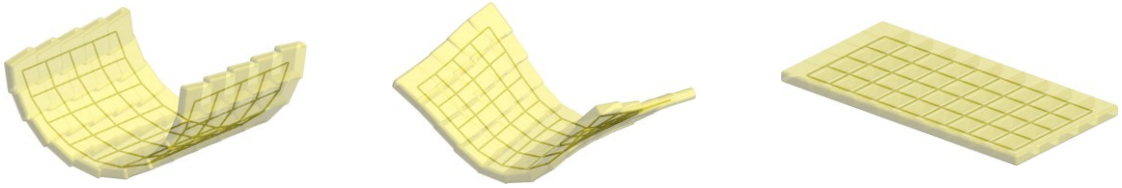

Figure 4-91: Relaxation of a finite u-deformed and distorted BP belt (bonding grid)

Besides these shown examples of finite belts, the deformation/relaxation of an endless BP belt is illustrated in Figure 4-92/Figure 4-93. This endless BP belt is specifically initialised in an elliptically pre-deformed state, furthermore containing an irregular distorted grid structure, further with locally-varying elongation states (as can be seen in the figures on the left). As evident from the figures on the right, the resulting state-of-rest, into which this endless BP belt correspondingly deforms/relaxes, shows a correct geometry: a perfectly circular-cylindrical ring with an undistorted rectangular bonding grid.

Figure 4-92: Relaxation of an endless elliptically distorted BP belt

Figure 4-93: Relaxation of an endless elliptically distorted BP belt (bonding grid)

On a closer look, the bondings in the circumferential direction (ref. longitudinal direction) still contain (bending) stresses, due to which the BP belt would further deform/relax into a perfectly flat geometry when cut open – which is further demonstrated in Figure 4-94/Figure 4-95, particularly regarding a subsequent opening of the endless BP belt from above. As distinctive, the opening of such an endless BP belt results in a finite BP belt with its respective behaviour (cf. u-shape finite belt illustrated previously, Figure 4-88/Figure 4-89). (Further aspects in this regard were also already introduced before, in Chapter 3.2.1 and Chapter 4.2.2.2.)

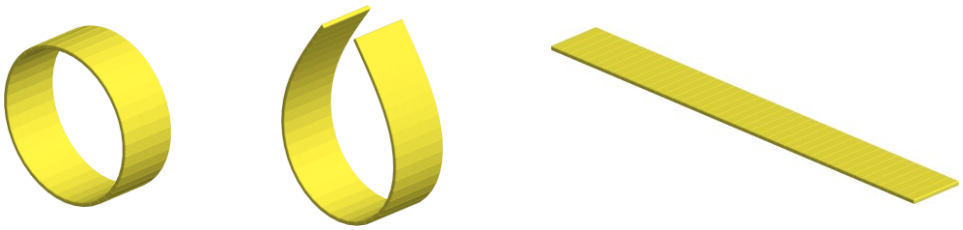

Figure 4-94: Relaxation of the ring-shaped BP belt when cut-open

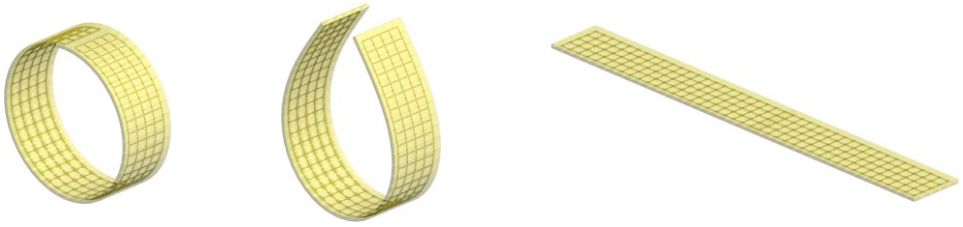

Figure 4-95: Relaxation of the ring-shaped BP belt when cut-open (bonding grid)

Application-related belt geometries

The relaxation-into-state-of-rest principle, introduced before and explained with the previously illustrated relatively simple cases of BP belts, is further applied on application-related, and thus typically relatively complex BP belt geometries – specifically relating to some of the exemplary applications from Chapter 5. As corresponding to such particular applications, the initialised BP belts, as shown in the following, each present an almost-final state geometry that conforms to a respective belt system design. In this regard, appropriately modelled and prepared CAD belt models are each applied for a CAD-to-DEM conversion process from which each initialised BP belt correspondingly results (see Chapter 4.2).

The following figures show steps of the addressed relaxation process, from the initialisation (left) towards a state-of-rest (right) of a respective BP belt. Thereby, these BP belts are typically[29] allowed to interpenetrate themselves due to deactivated belt particle contact (which refers to particle overlapping characteristics, in detail explained in Chapter 4.1.1.2).

In Figure 4-96, the belt of the conventional belt conveyor system from Chapter 5.2 is applied to deform/relax according to the introduced relaxation-into-state-of-rest principle. The final, and above all, correct state-of-rest, into which this almost-final-state-initialised BP belt deforms/relaxes, is evident (on the right, showing a state-of-rest as required for such an endless BP belt).

Figure 4-96: Relaxation of the BP belt of the conventional belt conveyor system

[29] Except the BP belt regarding the pipe conveyor (Figure 4-98), which allows self-contact between opposite belt edges; see Chapter 4.1.1.2 (specifically Figure 4-3) and also Chapter 5.5.

Furthermore, Figure 4-97 shows this addressed relaxation process of the upper belt of the sandwich conveyor system from Chapter 5.4. Again, the forming of a correct state-of-rest can be noticed.

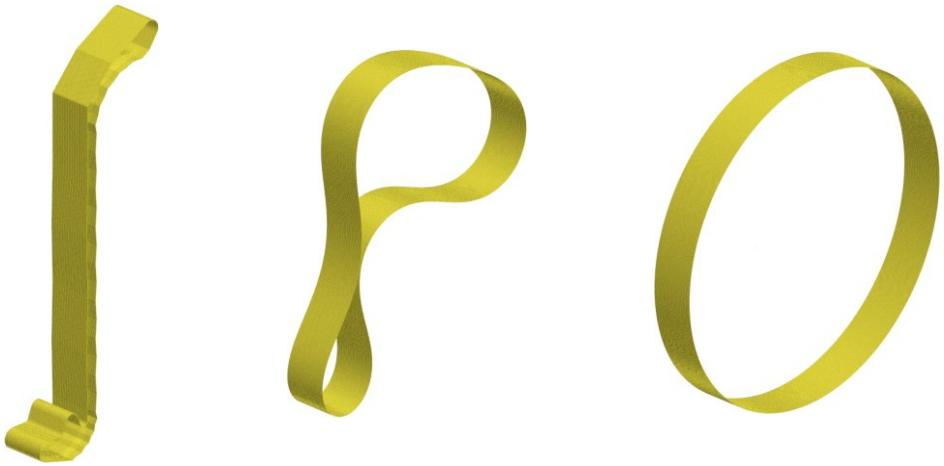

Figure 4-97: Relaxation of the (upper) BP belt of the sandwich conveyor system

As a final illustration of this relaxation-into-state-of-rest principle with application-oriented belt models, the BP belt of the pipe conveyor system from Chapter 5.5 is correspondingly applied, as shown in Figure 4-98 – also with the correct state-of-rest resulting as evident.

Figure 4-98: Relaxation of the BP belt of the pipe conveyor system

Moreover, it is pointed out that this introduced relaxation-into-state-of-rest principle can correspondingly be applied for any BP belt converted from a given (CAD) geometry by using the CAD-to-DEM conversion process presented in Chapter 4.2 (further accordingly relating to Chapter 4.1, as regarding the structural setup of such a converted BP belt).

Proofing the conversion algorithm as suitable

In further conclusion, the presented CAD-to-DEM process with the addressed belt initialisation method in a pre-deformed (almost-final) state, and in this context specifically the developed conversion algorithm/process, thus furthermore the corresponding software program implemented in the software tool BeltConverter, is generally evaluated as suitable/proven. This is furthermore concluded from the introduced relaxation-into-state-of-rest principle returning correct results for several different (and also highly complex) geometries of BP belts[30], which was illustrated in the previous figures, and which was also confirmed in several additional (even more complex and also special-case-forming) geometries that were analysed in this regard.

4.4 Extension: Smooth-surfaced cylinders

The extending method presented in this chapter introduces an enhancing technique by using numerically smooth cylinders in DEM simulation setups, especially for the modelling of cylindrical parts. Accordingly, this method is particularly useful for the modelling of idlers and pulleys in belt (conveyor) systems comprising BP belts, as introduced in the previous chapters. As regarding the modelling of idlers and pulleys, which in addition to the belts also form major system components (as addressed in the basics in Chapter 2.2.2), this method forms an essential extending part of the methodology presented in this thesis, as an enhancing addition to the presented belt model setup and its initialisation (which form the core of this methodology). However, the principles described in the following may also find application in other, not necessarily belt related, setups as well.

In contrast to the conventional belt modelling technique based on rigid belt models (described in Chapter 2.2.3), simulations with dynamic BP belt models require those system components that affect the BP belt's behaviour to be modelled accordingly –

[30] with the specified restrictions considered; see Chapter 4.2.3.1.2/4.2.4.1.3 (e.g. with the CAD belt model corresponding to a finite/endless belt model, further without sharp edges, etc.)

more specifically to allow corresponding interactions with the BP belt (in detail, with its comprising belt particles). This requirement relates especially to the modelling of idlers and pulleys, for which corresponding aspects are described in the following (regarding cylindrically-shaped objects to be used in DEM simulation setups).

The final outcome of the method presented in this chapter, and thus of the developments made respectively, is a supportive software program, PartConverter [95], whose functionalities are explicitly presented in Chapter 4.4.3, and by means of which also further essential and general method-related aspects regarding the use of smooth-surface cylinders are accordingly described.

4.4.1 Smooth instead of common triangulated cylinders

As described in the DEM basics in Chapter 2.1.2.5, in the section relating to parts, system components in DEM simulation setups are typically represented as triangulated parts (commonly via import of STL files). The surfaces that are represented on such triangulated parts are consequently formed by a multitude of triangular elements, which – particularly regarding curved/complex surfaces – correspondingly results in an approximated form of the part's original shape. Furthermore, due to this triangulation, edges result on curved (originally smooth) surfaces. To address these issues, the resolution of a triangulated surface can be increased by reducing the triangle size – which in turn leads to an increase of the number of triangular surfaces (which has a negative impact in terms of contact handling and accordingly on the computation in total). In this regard, a compromise for an adequate resolution must be made, as the number of triangles and their corresponding edges influence the simulation in terms of computational effort, stability and accuracy. (cf. Fimbinger [88])

Especially in terms of BP belt simulations, cylindrical parts that represent idlers and pulleys pose problematic effects when modelled according to these introduced principles with triangulated surfaces. An obvious problematic effect, in addition to the aspects addressed above, corresponds to the polygonal effect that results on such a triangulated cylinder. (A finer resolution, which would be beneficial in terms of this effect, on the other hand, results with smaller and typically relatively long and narrow triangles, which are again influencing the stability and furthermore the overall simu-

lation process unfavourably.) Figure 4-100 shows several examples of different triangulation schemes generally conceivable for approximating a cylindrical part, further highlighting the mentioned characteristic of comprising relatively long and narrow triangles. The original (CAD) cylinder part that corresponds to these triangulated cylinder-representing DEM parts is further shown in Figure 4-99.

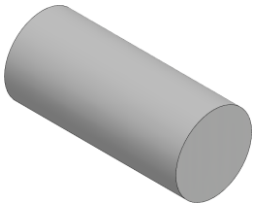

Figure 4-99: Original CAD cylinder part to be represented

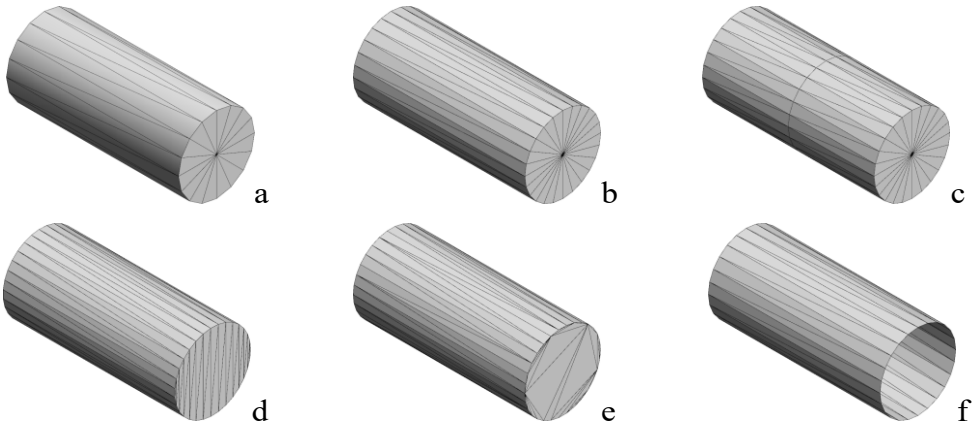

a … with 16 triangulated rectangles
b … with 24 triangulated rectangles
c … with 2 times 24 triang. rectangles
d … different form of top/bottom triangulation
e … unstructured top/bottom triangulation
f … no top/bottom surface (no voluminous part)

Figure 4-100: Representing the cylinder by using various triangulation schemes

As also already addressed in Chapter 2.1.2.5 (section on parts), modern DEM software, in this specific case regarding ThreeParticle/CAE, further supports the use of several mathematically primitive shapes – especially also including primitive cylinders, which promise to be particularly advantageous in this respective regard of idler/pulley modelling as featuring a continuous, thus smooth surface. Especially in combination with BP belts, where the particles of the belt model are required to get in contact with those idlers and pulleys, this method is promising to be exceptionally suitable

Overall, such primitive cylindrical shapes can further also be used in relation to the two fundamental object types regarding a DEM simulation setup (as of ThreeParticle/CAE):

- obviously, in the form of cylindrical parts (see also Chapter 2.1.2.5, parts),
- but also in the form of cylindrical particles (see also Chapter 2.1.2.1).

Both those types are illustrated in Figure 4-101, also relating to the cylindrical part to be represented as introduced before.

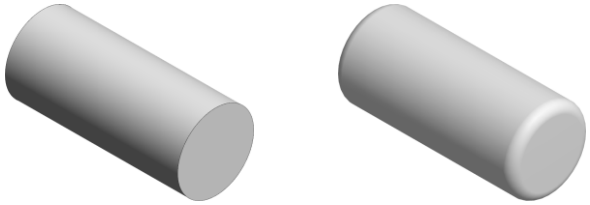

Figure 4-101: Representing the cylinder by using a cylindrical part (left) / a cylindrical particle (optionally with rounded edges) (right) – both based on a primitive shape (primitive cylinder)

As clearly evident, the surface (particularly the circumferential surface) of both these model types show a smooth continuous surface, which is generally beneficial regarding the problematic aspects beforementioned in terms of triangulated cylinders. Both introduced types (parts and particles) are generally feasible to represent cylindrical parts in DEM simulation setups, with their individual characteristics/differences described further below in the subchapter after next (Chapter 4.4.1.2).

4.4.1.1 Implementing smooth cylinders / necessity for a supportive tool

Fundamentally, the specific implementation of smooth cylinders (as parts/particles) into a DEM simulation setup generally requires extensive manual definitions to be made, which particularly regards not only the cylinders dimensions (radius/length) but especially their individual positions and spatial orientations. This specific aspect is further associated with a disproportionately high modelling effort, especially for large (belt/conveyor) systems with many, and especially complexly arranged idlers/pulleys, which is further the reason why this form of modelling using primitive-cylindrically shaped parts/particles is usually not applied for such applications.

In order to address this issue of manual cylinder definition, an algorithm was developed specifically to support this modelling of complex system setups made from a large number of primitive-cylindrically shaped parts/particles; which basically corresponds to typical belt (conveyor) systems as further also required in context with the presented BP belt simulation. As specifically implemented in the software program PartConverter – as a supportive tool allowing convenient and intuitive use, as further shown in Chapter 4.4.3 – this algorithm is described in an overview in the following Chapter 4.4.2.2, as fundamentally representing the core of the conversion process. In a short anticipatory outline: This addressed algorithm/process basically detects cylindrical objects (parts) within a given CAD model and translates/converts this information into DEM readable data. This resulting DEM data thus contains these cylindrical objects in the form of smooth (primitive) cylinders, further allowing their initialisation in a DEM simulation setup accordingly for further use, such as typically in DEM simulations with BP belts. (This process is also referred to as part conversion as it allows cylindrical CAD parts to be converted into primitive cylindrical DEM parts/particles.)

4.4.1.2 Characteristics of cylindrical parts / cylindrical particles

Generally, both types – parts and particles – allow essential cylindrical-part-representing characteristics to be set, such as comprising:

- Dimensions (radius and length)
- Position and spatial orientation
- Interactions regarding the general contact handling (with a BP belt)
- Further behaviour, such as related to specific aspects in context with:
    - Resistance (friction/damping)
    - Mass (moment of inertia)

(The following descriptions specifically relate to ThreeParticle/CAE as the DEM software program of focus.)

As generally revealed by their nature, cylindrical parts are meant to be the standard means of choice to represent smooth cylinders in DEM simulation setups. However, it is also meant that such parts are only used in smaller quantities (basically, as each part only initialises as a single instance; cf. program characteristics of

ThreeParticle/CAE). In contrast to that, particles allow multiple instances to be initialised.[31] Correspondingly, it is possible to place (initialise) a certain type of cylindrical particle multiple times, as to represent a large number of idlers (accordingly of the same type; with the same dimensions, interaction model, etc.). This multi-instancing of such a defined particle type is particularly useful in computational terms.

Furthermore, and explicitly for such cylindrical particles, rounded edges are optionally possible to be defined, as already illustrated in Figure 4-101 on the right. This option may come useful for cylinders at which contact can occur on their edges (with the purpose to influence the simulation advantageously, as particle contacts with such numerically rounded instead of sharp edges typically act positively, as in terms of stability; cf. also cuboidal (belt) particles with rounded edges described in Chapter 4.1.1.3).

On the other hand, cylindrical particles, in contrast to cylindrical parts, do not allow enhanced part-only features, such as applying multibody dynamics (MBD), as introduced in the basics within Chapter 2.1.2.6.2. (Such a specific MBD setup is further shown in the exemplary application of the round hay baler system in Chapter 5.6, correspondingly modelled with using cylindrical parts.)

Regarding the application of movements: this is generally possible for both – parts and particles – specifically due to a recent update in these terms. In this context, it needs to be considered that defined particle movements apply for each instance of this particle type correspondingly.

Summarising conclusion

Cylindrical parts may typically be used to model cylindrical system components that occur in minor numbers, such as more specifically relating to pulleys or certain individual idlers (such as more-or-less unique guiding idlers, etc.), which correspondingly occur singly or in very small numbers. Also, such cylindrical parts are required when belonging to MBD setups.

[31] which is a fundamental characteristic of particles in DEM simulations, basically regarding the generation of a multitude of particles of the same type; cf. basics in Chapter 2.1.2.1/2.1.2.4

For other system components that consequently occur in larger quantities, as it is common for idlers (see also Chapter 2.2.2.2), the modelling of cylindrical particles is suitable.

Furthermore, cylinders with rounded edges also require the modelling of particles, which specifically regards applications in which contacts at such cylinder edges (with a BP belt) are to be considered in advanced form. (General note: In typical belt (conveyor) applications, such belt-cylinder-edge-contacts are generally not intended to occur (those are intended to be omitted, as for belt wear reasons; probably except for certain unconventional exceptional cases). In this regard of typical belt-idler/pulley-contact, see also Chapter 2.2.2, generally illustrating this as mentioned.)

Overall, the use of smooth cylinders generally contributes as a major enhancement to the developed methodology in total, as a further method in addition to the directly BP belt related methods (modelling a BP belt in general and its initialisation in almost-final state; cf. Chapter 4.1 and Chapter 4.2), and is thus also included as such an extending method into the framework of the methodology presented in this thesis.

4.4.2 Essentials of the developed software tool for cylindrical part conversion

In the following, essentials of the software tool PartConverter, specifically developed to allow convenient initialisation of relatively large numbers of smooth (primitive) cylindrical parts/particles – especially in complex arrangements – into DEM simulation setups, are presented. This supportive tool is further also described in terms of its usage via its GUI in the following Chapter 4.4.3.

The major issue which is addressed by this developed tool was previously already outlined in Chapter 4.4.1, highlighting a disproportionally high modelling effort required for conventional, thus manual placing/defining of such cylindrical parts/particles in DEM simulation setups, particularly in context with belt (conveyor) systems. This effort results as such systems commonly contain a relatively large amount of furthermore typically complex-arranged cylindrical parts (idlers/pulleys), which are correspondingly each required to be manually placed/defined (in terms of their individual position, spatial orientation, dimensions, etc.).

As also outlined specifically in Chapter 4.4.1.1, this tool is based on using a CAD file containing the essential cylindrical data, specifically multiple 3D geometries, further to be translated/converted into a DEM data file that ultimately allows the initialisation of them as smooth cylindrical parts/particles – accordingly considering their individual characteristics.

Major details – regarding the prerequisites of this CAD file, the steps underlying the conversion process to determine the cylindrical parts/particles, as well as the resulting DEM data that is exported at the end of this process – are outlined in the following subsections. Further additional aspects/features that are also implemented in the developed tool are subsequently addressed in the descriptions regarding the final resulting software tool as presented with its GUI in the subsequent Chapter 4.4.3.

4.4.2.1 Regarding the CAD input data

Similar to the CAD belt model data in terms of BP belt initialisation in almost-final state, as covered in Chapter 4.2, the required CAD cylinder model data is typically also available from the corresponding CAD design process, as derivable from common 3D CAD system models.

Regarding the data format of this CAD file, Standard ACIS Text (SAT) [227] was evaluated as useful as specifically capable of containing multiple cylindrical geometries as individual parts in one single file – with these cylinders furthermore smooth/primitive (which forms a fundamental prerequisite, and which contrasts to triangulated data as when using STL files; cf. Chapter 4.2.3.1.3). Furthermore, this proposed SAT file format is also a commonly supported CAD export format; thus, relatively easy to be achieved (even if a direct export is not possible, converting such as via a different exchange format using an alternative software is generally feasible). A specific SAT format supported by the developed software tool PartConverter is SAT Out Version 7.0 as exported from Autodesk Inventor [9].

Such a cylinder-containing CAD data file is fundamentally required to be prepared according to the following principles in order to allow conversion into DEM cylinders, as introduced in the next subsection. In this regard, such data is explicitly re-

quired to contain each cylinder as an individual part, further representing an assembly of a multitude of cylindrical parts.[32] In this cylindrical-parts-only assembly, those cylinders can be placed individually, as common, but furthermore also as multiple instances and therefore also in patterned form as well (relating specifically to patterns of idlers along the conveyor line, which is thus allowed/supported). Furthermore, each cylindrical part is required to contain only one single perfectly shaped cylinder element – formed only by its mantle and its two parallel and equally sized circular surfaces that form the top and bottom of the cylinder. Thus, rounded edges or any additional elements (such as additional surfaces inside, as forming a hollow-cylinder, etc.) are accordingly not to be included. These modelling principles resulting in a corresponding SAT file are fundamental, as the detection algorithm (outlined in the following section) detects such perfectly shaped single cylinders only.

Such assemblies containing perfectly cylindrically shaped parts are further shown in Chapter 5 as relating to various exemplary applications, for example, in Figure 5-12 on the left.

4.4.2.2 The conversion process in an overview / cylinder data determination

As already mentioned, the conversion process starts by detecting each cylindrical part that contains one single perfectly shaped cylinder geometry. (In this specific regard, the introduced SAT file is particularly convenient.[33])

From this detection, each part's cylinder axis results from the two midpoints on the top and bottom circles, and the cylinder radius follows correspondingly from the circle radius (radii). (Additionally, further data such as original part names and part colour information are also derivable from an STL data file provided; see also corresponding sections in the subsequent Chapter 4.4.3.)

Accordingly, a list results that contains each detected cylinder with its respective information. This list is furthermore sorted, with the radius as the first order and the length as the second order.

---

[32] I.e., multiple cylindrical elements modelled within one part are consequently not allowed.

[33] With cylinders given as special cases of truncated cone objects, resulting with/by two equally sized circles

Some trivial computations are furthermore required, especially regarding bringing the detected axis data (detected as two points, more specifically two 3D vectors) into a corresponding format (further relating to the DEM output file; see next subsection). In this context, each cylinder is considered as follows:

- The axis (as the difference vector between these two axis points) is translated into its scalar value, which gives the length of the cylinder of focus;
- The midpoint of the axis (i.e., between the two axis points) gives the position as a 3D vector of the cylinder of focus;
- The spatial orientation of the axis (again, as the difference vector between the two axis points) is determined, which gives the cylinders' orientation specifically as Euler angles.

(Note regarding spatial orientations of cylindrical parts/particles: This addressed spatial orientation determination generally relates to the principles described in Chapter 4.2.4.2.2, in the section on the translation of spatial orientation; but as cylindrical objects do not necessarily require an additional orientation around their cylinder axis to be defined, only one rotational step (ref. to the referenced chapter) is required in order to determine the quaternion of question accordingly. Furthermore, quaternion to Euler angles translation regards a common method and is accordingly provided by/described in pertinent literature. And generally, the use of Euler angles is the base form for aligning parts (and also particles) in a spatial orientation, which is fundamentally sufficient for this purpose, and above all required for particle orientation definition (see following subsection on DEM output data). This is in contrast to BP belt initialisation, for which such Euler angles are not sufficient, and quaternions are thus required.)

In summary, each cylinder in the sorted list is detected with its:

- radius (scalar),
- length (scalar),
- position (vector),
- orientation (Euler angles),
- and some supplementary data (original part name, colour in RGB[34]).

[34] common red green blue colour model

This determined data is correspondingly exported in DEM data format, as covered in the next subsection.

4.4.2.3 Regarding the DEM output data

According to the same aspects and principles already described in the context of BP belt initialisation, ThreeParticle/CAE input data format (inp; as specifically introduced in Chapter 4.2.3.2 and as accordingly used in Chapter 4.2.4.4) is set as the output data file format into which the determined cylinder data is brought.

The details regarding the relevant keywords, such as to add and define cylindrical parts (*addCylinder and *setCylinder), as well as to add, define and initialise instances of cylindrical parts (*addParticles, *setParticles and *manualGeneration), are not explicitly described further as their details can be found in the Keywords Guide [12] corresponding to ThreeParticle/CAE.

However, a differentiation principle regarding either exporting a cylinder as a cylindrical part or as a cylindrical particle is already worth mentioning, which is in more detail covered in the next Chapter 4.4.3, as outlined by means of the respective settings available to be made in the GUI of the developed software tool PartConverter (see specifically section E).

In this regard, and basically similar to the structured INP file for exported BP belts (as illustrated in Figure 4-82), the cylindrical parts and the cylindrical particles are blocked in two consecutive sections within the INP file; comprising the particles in the first block and the parts in the second. Additionally, due to the sorted cylinder list in terms of their size, those exported data shows the cylinders in a correspondingly sorted order.

Additionally, and also similar to the created BP belt (INP) file described in Chapter 4.2.4.4, supplementary information is also added at the beginning of the exported INP file containing cylindrical data. In this informational block, also comparable to BP belt INP files, settings followed by conversion information is written; with the conversion information summarising details about the numbers and dimensions of the determined cylinders and whether those are created as parts or particles.

Insights into an INP file containing such cylindrical objects (parts/particles) are given in Figure 4-102, furthermore highlighting the well-structured (blocked and ascending sorted) contents (with this shown data specifically relating to the exemplary application of the pipe conveyor system shown in Chapter 5.5).

Figure 4-102: Exported INP file containing the computed cylindrical parts/particles in a structured/blocked form

A resulting INP file containing cylindrical parts/particles (thus as smooth cylinders) can further be imported into the DEM software environment (of ThreeParticle/CAE) to initialise those parts/particles accordingly to the given CAD file; thus, correspondingly omitting complex manual implementation procedures, and therefore significantly enhancing the modelling efficiency by reducing the efforts in these terms to a minor level – whilst enabling the use of smooth-surfaced cylinders and the advantages associated with it.

4.4.3 PartConverter

The introduced process to enable the initialisation/implementation of smooth cylinders (as cylindrical parts/particles) into DEM simulation setups based on prepared CAD files (as described in the chapter before (Chapter 4.4.2.1)) is implemented into a software program, PartConverter [95]. This software program is moreover added a GUI to allow convenient use, and more specifically, to allow enhanced, easy-to-use, and above all, fast/instant conversion of CAD cylinder parts into respective DEM cylinder parts/particles as smooth-surfaced cylinders (made from primitive cylindrical shapes, and therefore without triangulated surfaces; cf. Chapter 4.4.1). This GUI of the software program is shown in Figure 4-103, by means of which several additionally implemented features are explained below. The fundamental essentials, such as particularly the determination of required cylinder data from given CAD data (which correspondingly forms the core of this presented program), were already described in the previous Chapter 4.4.2.

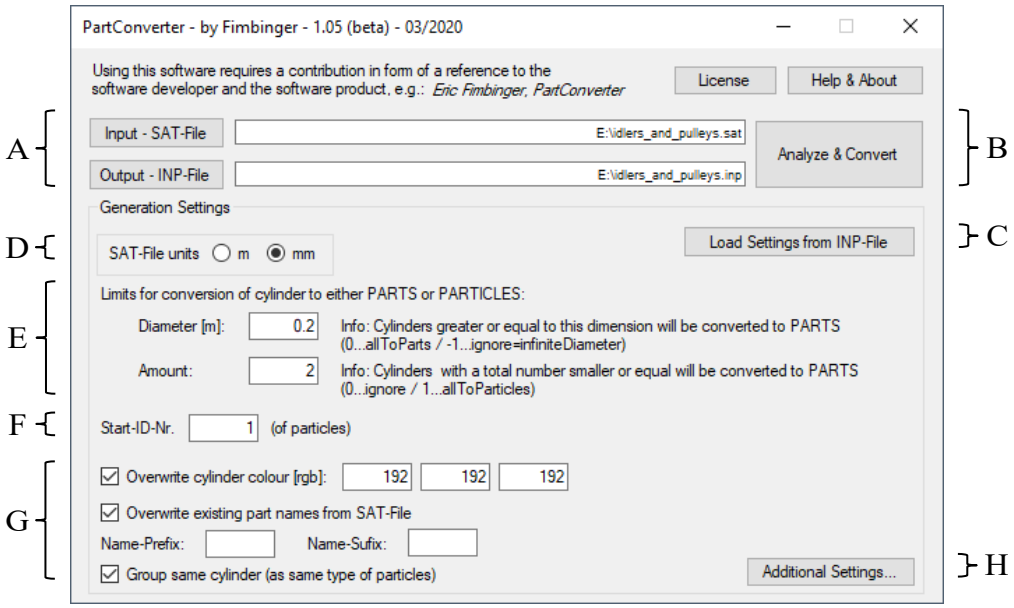

Figure 4-103: GUI of the developed software tool PartConverter

This presented GUI allows users to perform the introduced cylindrical part conversion in an intuitive and user-friendly way. As evident, the major appearance and thus the general usability via the GUI of the tool PartConverter further relates to the previously presented tool for belt conversion, BeltConverter, explained in Chapter 4.2.5 and shown explicitly in Figure 4-83.

The main form of the developed software tool PartConverter, as illustrated in Figure 4-103, contains elements that allow several settings to be made for cylindrical part conversion processes, which are explained in more detail below (with basic purposes as also already indicated/outlined in the GUI itself).

A-D – File handling / starting / settings in general / units

The first main elements – regarding file handling (A), starting a conversion process (B), settings in general (C), and also units of the input (SAT) file (D) – fundamentally correspond to their equivalents in the previously presented software tool BeltConverter. Therefore, the descriptions as already given in this regard in Chapter 4.2.5 further also apply in a respective form[35] to the corresponding elements embedded in the tool PartConverter.

E – Conditions to return either parts or particles

As described in Chapter 4.4.1, the cylindrical geometries given within a CAD data file can either be converted to be initialised as cylindrical parts or also as cylindrical particles. The addressed aspects further describe the use of cylindrical parts for cylinders that occur in relatively low numbers, such as typical for pulleys. Based on this general conclusion, two criteria are implemented that can further be set to allow a certain form of differentiation of cylinders into either parts or particles. This relatively simple differentiation scheme forms as follows:

Two limit values are allowed to be set – regarding the diameter of a particle and further the amount, how often a specific cylinder geometry (with the same dimensions) occurs. These two limits specifically address the differentiation between idlers and pulleys, as generally described in the basics of belt conveyor systems in Chapter 2.2.2.2, according to which pulleys are, on the one hand, typically larger in diameter than idlers, and on the other hand, idlers typically occur in relatively large numbers, thus more often than pulleys. These two aspects are further transferred into the criteria forming the differentiation scheme addressed:

[35] such as concerning SAT input files (instead of STL)

- if a certain cylinder is equal or larger in diameter than the defined diameter limit, it is considered as a part (thus: larger cylinders result as parts / smaller as particles),
- and additionally, if a certain cylinder geometry (with a specific dimension) occurs in a quantity that is equal or smaller than the defined amount limit, all cylinders with this respective dimension are considered as parts (thus: cylinders occurring relatively often result as particles / rather unique cylinders correspondingly as parts).

(Whereby the second criteria, the amount consideration, is weighted higher, thus as overriding the diameter criteria; i.e., if the first criterion gives a part and the second a particle, a particle finally results.)

To address special cases, such as to return all cylinders as parts or also as particles only, specific boundary values can further be set (as also mentioned in the GUI, next to the input boxes):

- setting the diameter limit to 0 returns all cylinders as parts
- setting the diameter limit to -1 ignores this first criterion (equals to infinite diameter)
- setting the amount limit to 1 returns all cylinders as particles (as can be concluded from the descriptions above)
- setting the amount limit to 0 ignores this second criterion

F – Starting ID

Similar to the elements A-D, this concerns similar aspects as for BP belts. Setting a starting ID is furthermore explicit relevant to cylindrical particles, as particles are required to be applied an individual particle ID each. The start ID with which the first cylindrical particle is assigned can be set to a certain value, especially to omit ID collisions (double definitions of particle IDs) with other particles in a simulation setup (e.g. the particles of a BP belt).

G – Further settings: colouring / naming / single/multiple particle instances

The colouring of cylindrical parts is supported to be either derived from the given CAD data file; or, alternatively, a customised colour specified with RGB values can also be set.

Furthermore, the cylinder names can be set as the original part names, as derived from the CAD data file, but can also be overridden, whereby a meaningful naming scheme is applied, which reveals the height and also the radius (and regarding parts also the instance number) of each cylinder.

In addition, a certain pre- or suffix can also be added to each cylinders' name. (This option may be used in larger systems as to group cylinders, or also in certain special cases, as when multiple converted INP files are intended to be used/initialised, more specifically when those contain identical cylinder dimensions (to omit cylinder name conflicts).)

Per default, cylindrical particles are meant to be initialised in a grouped form, which relates to initialisation in multiple instances (according to which a certain cylindrical particle is defined once with multiple instances of it initialised; which further relates to the general characteristics in terms of using particles instead of parts, as addressed in Chapter 4.4.1.2). Optionally, this grouping may be suppressed in certain special cases, such as when individual cylindrical particles with the same cylinder dimensions are required to be defined with different properties, e.g. with individual movement conditions. (Resultingly, each particle is defined individually and also initialised only once; thus, similar to parts – further to be used when particles are explicitly required, such as due to their edge-rounding capabilities, which is not supported with parts; see also next section).

H – Additional settings

Besides additional settings in numerical terms, which are generally similar to the ones for the software tool BeltConverter, as described in Chapter 4.2.5 in the corresponding section (L) (thus, generally regarding accuracy settings, such as the rounding of numerical values), also supplementary general settings are added/enabled to be adjusted. These are embedded in the respective GUI-extending subform, as shown in Figure 4-104.

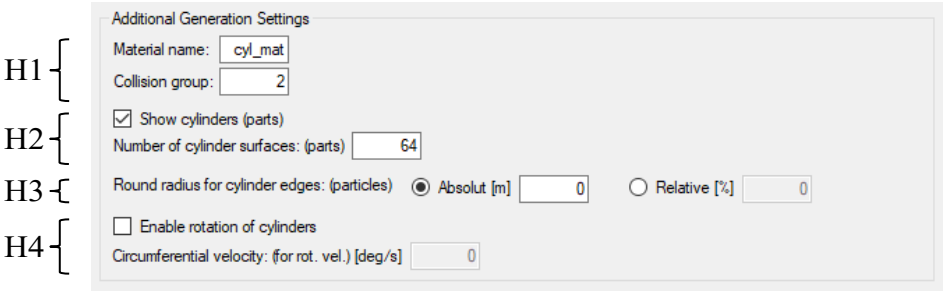

Figure 4-104: Additional settings for cylindrical part conversion

The additional settings possible to be made in this shown subform further regard: (with default values as shown)

H1: Material and collision group assignment (parts and particles). (Regarding collision groups: The contact between cylinders is per default deactivated via a corresponding collision group definition which is written into the resulting INP file; see Figure 4-102. If this contact-off condition is explicitly not intended, this respective collision group definition is to be removed accordingly.)

H2: Appearance options (explicit for cylindrical parts) – including the visibility (shown/hidden) and the number of rectangular surfaces each cylindrical part is visualised with (which only affects the visualisation, not the actual interactional behaviour, which is accordingly considered as numerically smooth). (Note regarding visibility: Hiding cylindrical parts may be used when total system structures are additionally imported for visualisation-only purposes, and especially when those visualising structures contain the cylindrical parts as well, which are already initialised as smooth cylinders, further to avoid them from being shown double.)

H3: Option to set rounded cylinder edges (explicit for cylindrical particles; see Chapter 4.4.1.2) – which is implemented to be set either with an absolute radius (thus equal for each cylinder) or with relative radii (thus individual, as relating to each cylinder's respective radius; e.g., when set to 100% a capsule-like shape would result).

H4: Options regarding rotational capabilities of cylinders. Thereby, the first option concerns the cylinders to be either locked or unlocked in terms of rotational capabilities around their cylinder axes – which further relates to the two basic approaches of either using fully locked or rotatable cylinders as described in more detail in the following Chapter 4.4.4. The aspects described in this context in the respective sections

of this following chapter are of utmost importance to be considered. (From these descriptions, it is furthermore evident why this option is embedded as an additional setting which is per default set to fully locked cylinders; specifically, as the more complex modelling method with using rotatable cylinders forms a comprehensive extending option). The additional option that is only available with rotatable cylinders further regards the possibility to include initial (rotational) velocities, specifically by setting a circumferential velocity from which each cylindrical part/particle's rotational velocity is resulting (trivially via considering their individual cylinder radii). Especially in terms of adding such an initial velocity, further aspects need to be considered, as given in the corresponding section in the next Chapter 4.4.4, which further outlines why this seemingly handy option is not necessarily required to be set – and, correspondingly, the use of this specific extending setting is particularly intended for comprehensive/exceptional applications.

4.4.4 Supplementary aspects/considerations

In order to use the initialised cylindrical parts/particles properly, as for representing certain idler/pulley-system characteristics, further definitions are additionally required to be made to the simulation model – generally depending on the actual scope of the simulation and the specific purposes that are intended.

Furthermore, combinations of the addressed approaches and modelling aspects given in the following are allowed in general, such as using locked cylinders (following subsection) for certain idlers whilst using rotatable cylinders (subsection after next) for certain pulleys or for cylinders relating to MBD (last subsection), etc.

Simple approach of using fully locked cylinders

Setting the addressed cylindrical parts/particles as fully locked – in terms of translation as well as rotation – forms a basic and relatively simple approach, which may be applied specifically if comprehensive idler/pulley effects are not required to be included and are thus of a minor level, more or less neglected in terms of detailed consideration. As consequently also rotations around cylinder axes are locked, certain effects, specifically relating to contact with a BP belt, are required to be included

in the respective interaction model properly – which may also be set to (almost) frictionless behaviour if the aforementioned aspect of minor idler/pulley consideration applies, and the respective cylinders are accordingly only modelled to form/guide a BP belt without further purpose (such as referring to mass-related effects, as covered in the following approach of using rotatable cylinders).

Driven cylinders, as in more detail addressed in the corresponding section following, furthermore require a corresponding (non-frictionless) interaction model; evidently, as to allow a BP belt to be driven by such cylinders.

Enhanced approach with (dynamically) rotatable cylinders

Extending the previous approach of fully locked cylinders by enabling them to rotate around their axes (deactivating this specific locked condition to allow rotation around the respective cylinder axis) forms a more enhanced approach, which accordingly requires more detailed aspects to be considered and further definitions to be made.

A fundamental aspect that is to be considered is that these addressed axes of question regard

- a cylindrical part's local z-axis, and
- a cylindrical particle's local y-axis,

as resulting from the specifications of the DEM software program of focus, ThreeParticle/CAE. Thus, when the required rotation capabilities are enabled, definitions regarding these respective axes are added/adjusted – more specifically, by:

- adding 6DoF[36] to each respective part, further with all its DoFs locked except rotation around z (thus, with translational x,y,z and rotational x,y locked), and
- unlocking the (per default set as locked) particle definitions regarding rotation around y.

Furthermore, as such rotatable cylinders show dynamic behaviour, corresponding mass-related properties are required to be set accordingly – in particular, the mass moment of inertia around each cylinder's axis. These definitions are fundamental to

[36] six degrees of freedom; see also Chapter 2.1.2.6.2

be set manually after the conversion process / initialisation of the cylinders – individually for each part/particle in order to represent the behaviour of a certain type of idler/pulley.[37]

In terms of cylindrical parts, this mass moment of inertia definition is relatively trivial to be set by adjusting the corresponding properties in the 6DoF settings accordingly. (Note: The other mass-related aspects generally show no influence (in common cases; as except when MBD applies, see following section in that regard), but in order to pass the feasibility check to start the simulation, values in this context are additionally required (such as by defining a certain mass, and also mass moments of inertia around x and y; whereby these values, as stated, show actually no influence).)

In terms of cylindrical particles, on the other hand, two different options may apply to achieve a specific mass moment of inertia:

- either via adjusting the density of the material assigned to a certain particle type, as this affects the mass moment of inertia (of an as a solid cylinder considered cylindrical particle),
- or via manually overriding the mass moment of inertia of a cylindrical particle, which is possible by changing the particle type to a compound particle containing the respective cylindrical shape – as such compound particles allow a manual definition of mass-related properties (which is not allowed for primitive-shaped particles per se).

(General note: It is to be considered that the contact characteristics between cylinders and BP belt particles are required to be defined accordingly (referring to considering frictional characteristics) in order to allow dynamic interactions, especially in context with the enabled rotational behaviour of the cylinders.)

Another topic that is generally also made possible to be addressed closer from using rotatable cylinders regards characteristics in terms of rotational resistance/friction or damping behaviour. In this regard, ThreeParticle/CAE allows the definition of a rotational damping factor by using keywords (rotDamping), which basically addresses

[37] Such mass-related values are typically either available from respective documents associated with the idlers/pulleys intended to be represented or can also be derived alternatively from corresponding CAD models.

this aspect in a rather simple form (see also the Keywords Guide [12]). In order to integrate more specific/complex models in these terms, it is furthermore also possible to set up such by using the API[38] and integrate them accordingly (for example, to apply a particular resistance behaviour model for idlers/pulleys; in this regard of using the API, see also the API Guide [10]).

Regarding initialising the cylinders with rotational velocities[39]

Fundamentally, it is crucial to consider that the rotational directions of cylinders are not explicitly determined in the conversion process[40], which is thus required to be further evaluated/set accordingly after the conversion process – more specifically, by checking each cylinder's rotational direction with respect to the total system. This is proposed to be done conveniently via import into DEM software and visualisation of rotational velocities. If a cylinder is defined with rotational direction opposite as intended, inversion of this respective cylinder's rotational velocity is easy to be made (via negation of the respective rotational velocity value). A convenient method for this purpose is furthermore proposed: by splitting the resulting INP file into two parts, with the first part containing not-to-be-inverted cylinders and the second part containing the rest, thus the cylinders for which inversion is required. An inversion of all the rotational velocities in this second part is then relatively easy to be applied (such as via using common find/replace features available in typical text editors, e.g. Notepad++ [118]). Resultingly, both parts contain rotational velocities as it is intended, resolving the addressed issue.

Generally, this implemented option to include initial rotational velocities based on a given circumferential velocity indicates particular usefulness in combination with initialising an already running BP belt (see Chapter 4.2, and especially Chapter 4.2.4.3), whereby the circumferential velocity correspondingly relates to the BP belt's translational velocity (belt velocity). By using this option, it is consequently

[38] Application Programming Interface; for programming user-defined plugins

[39] specifically via defining a circumferential velocity (see previous Chapter 4.4.3, section H(4))

[40] as provided CAD data, containing only cylindrical geometries (cf. Chapter 4.4.2.1), does not give additional information on rotational directions; adaptations towards adding such were considered and evaluated in principle, but were not further followed/included, as the relatively simple and thus convenient method described in this section presents to be useful in this context.

possible to initialise already running (rotating) cylindrical system components in addition to the already running BP belt. (Which particularly addresses rotational acceleration effects of those cylinders, further relating to specific mass-related behaviour to be defined correspondingly (in this regard, see also the previous section on rotatable cylinders.)

However, this effort can also be omitted entirely by initialising cylindrical parts/particles without a specific rotational velocity and using the pre-simulation of the BP belt (transient oscillation process; see Chapter 4.2.1) to accelerate these cylindrical components correspondingly via belt-cylinder-contacts. In this regard, another convenient method is also proposed: by using reduced mass-related values (mass moments of inertia) for the cylindrical parts, specifically set only during the pre-simulation.[41] This would correspondingly affect the acceleration of cylinders, further to reach their final rotational velocities, in a beneficial form.

Due to these aspects (as rotational velocities must be evaluated/manually inverted, and as the method by using adjusted mass-related values in the pre-simulation proposes a relatively simple and promising approach), this option of adding rotational velocities is thus implemented to be used as described for comprehensive/exceptional applications.

Rotational movements and MBD setups

Another more general but fundamental consideration regards driven pulleys (or principally also driven idlers), for which the respective cylinders are correspondingly applied a rotational movement – either in the common form of typical part/particle movements, but also with using virtual movements[42] (explicitly applicable to cylindrical parts). In this regard, the virtual movement specifically relates to the use of fully locked cylinders (see section before the previous one).

Translational movements, for example, for belt tensioning purposes, are also applicable in equivalent form (as, e.g., applied in the application shown in Chapter 5.7, in

[41] Due to reduced mass-related values, higher rotational damping (see previous section on rotatable cylinders) would typically be beneficial (for reasons of numerical stability).

[42] which conforms to a rotational form of the virtual translational movement (as used for the modelling of moving belts according to the rigid belt modelling technique, described in Chapter 2.2.3.)

which the BP belt is tensioned until its breakage by using such a translational pulley movement).

Furthermore, if a system shows an MBD setup, appropriate definitions (such as joints, constraints, or also further mass-related properties) are required to be made to the respective cylindrical parts (as particles do not allow such an MBD use; cf. Chapter 4.4.1.2). As is furthermore obvious, such MBD setups cannot be used with fully locked cylinders. (Additionally, see also the round hay baler system given in the examples in Chapter 5.6, which contains such an MBD setup.)

Chapter 5

Exemplary Applications

The simulation examples shown in this chapter are applied specifically to illustrate the broad spectrum of enabled capabilities and the overall potential of the developed methodology for belt simulation presented in this thesis.

After the introductory chapter, which covers basic relevant information (applicable to each example shown in the following; e.g., regarding a summarising workflow overview, hardware/software aspects, etc.), six selected applications as simulation examples are presented in this matter of demonstrating the belt simulation methodology – primarily by giving insights into relevant modelling/simulation/analyses aspects, characteristics, and capabilities with illustrative figures.

5.1 Overview and relevant information

The following informative contents relate to the subsequently shown simulation examples/applications in general.

Fundamentally, the applications covered in the simulation examples relate to practise/industry-related belt (conveyor) systems already introduced as relevant to dynamic belt simulation in Chapter 2.2.5. Accordingly, these examples also show cer-

tain aspects in these related terms (referring to the overall necessity to consider dynamic belt behaviour for such specific applications/simulations, as generally described in Chapter 2.2.4), and are thus focused on comprising dynamically deformable belt models with corresponding interactional behaviour (which furthermore specifically refers to the developed methodology covered in Chapter 4; for an overview on applying this methodology on these exemplary applications, see also the next Chapter 5.1.1).

Furthermore, each simulation example regards specific modelling aspects/characteristics, which are explicitly stated at the beginning of each respective chapter. Similarly, several different analysis capabilities are also highlighted.

The examples/applications are further ordered in ascending form in respect to their level of complexity, particularly in terms of belt (system) behaviour to be considered/modelled/simulated.

Also, further insights into the simulation examples shown in the following have already been given in several prior publications, as accordingly referenced (cf. also Chapter 1.5).

In several following figures, the common rainbow colouring scheme[43] is used to indicate various characteristics (as stated in the corresponding captions, e.g. particle velocities, bonding deformations, etc.).

5.1.1 Overview for applying the methodology

Applying the developed methodology is principally based on the descriptions given in Chapter 4. In a short reviewing summary, this refers to:

- Belt model characteristics, as referring to details of the structural belt setup – presented in Chapter 4.1 (which specifically regards the modelling of a BP belt, i.e. with cuboidal particles in a rectangular bonding arrangement, furthermore applied an adjusted bonding model to allow belt-typical flexibility, or also a fibred structure as to enable anisotropic belt behaviour, etc.);

[43] as common: relatively low to relatively high with colours from blue (over green, yellow) to red

- Belt initialisation, specifically to initialise a certain BP belt in a given (pre-deformed) geometry, accordingly following the almost-final state initialisation principle – presented in Chapter 4.2 (which specifically regards using the developed software tool BeltConverter to convert a given CAD belt model into a corresponding BP belt, which can further also be evaluated according to the principles described in Chapter 4.3);
- Using smooth-surfaced cylinders – presented in Chapter 4.4 (as an extending method for the initialisation of numerically smooth cylindrical parts/particles, as to represent pulleys/idlers specifically interacting with particles of a BP belt; furthermore by using the developed software tool PartConverter as introduced).

Furthermore, the related workflow for using the developed methodology is based on the descriptions given in the chapters mentioned above – which is additionally also summarised in the following overview:

As a general prerequisite, a 3D CAD model of the belt system intended to be applied for dynamic belt simulation is required as a basis, or otherwise, required to be set up (in at least a reduced form).

1. General system considerations and preparations

1.1. Identifying/specifying relevant properties and assumptions,
especially regarding the BP belt setup intended to be used, and thereby specifically its dimension-related characteristics (such as particle size and overlap, further relating to the required/applied grid dimensions, which are fundamentally relevant for the following step). (These characteristics are further related to the BP belt's resolution; thus, the number of particles and bondings with which a certain BP belt is ultimately formed.)
Relevant chapters in this regard are Chapter 4.1.1 (particles), Chapter 4.1.2 (bondings), and also Chapter 4.2.4.2.1 (grid dimension definition).

1.2. CAD preparation of the belt(s),
according to the definitions given in Chapter 4.2.3.1. (Which regards deriving a mid-surface model of the belt(s) in quadrilateral-meshed form, whereby the applied mesh represents the bonding network that is intended; further respecting the introduced restrictions, and finally providing one continuous belt model each within a CAD file in ASCII encoded STL format.)

1.3. CAD preparation of belt-relevant (typically cylindrical) components,
referring to system components that are interacting with the belt(s), and which are thus required to be modelled/imported in the DEM environment.
Especially for idlers and pulleys, the aforementioned method to use smooth-surfaced cylinders is proposed, for which preparations are required to be made according to the descriptions given in Chapter 4.4.2.1 (which specifically regards providing idlers/pulleys as perfectly cylindrically shaped parts in an SAT assembly file).
(Also, DEM-common part modelling (acc. Chapter 2.1.2.5) can be used, such as proposed for other belt-relevant parts with non-cylindrical shape; cf. the impact bed in the conventional belt conveyor application in Chapter 5.2.)

1.4. Optionally: Preparing additional visualising CAD models,
only for visualisation purposes to indicate the total system structure, such as applied for the sandwich conveyor application in Chapter 5.4.

2. Using the developed software tools for conversion from CAD to DEM data

2.1. BeltConverter,
as described in Chapter 4.2.5.

2.2. PartConverter,
as described in Chapter 4.4.3.

3. Setting up the DEM simulation and importing the converted DEM data

3.1. Preparing the DEM setup,
as before importing the converted BP belt(s), the belt particles must be defined according to the particle types in the created INP file ("belt_ptc", or "belt_ptc_1", "belt_ptc_2", …, if in fibred structure); see Chapter 4.2.4.4.
Similar, before importing converted cylinders (as cylindrical parts/particles), their assigned material must be defined as well (which is per default set to "cyl_mat"); see Chapter 4.4.3.

3.2. Initialising the DEM models,
via importing the (INP) keyword files created from the conversion processes (as the BP belt(s) and idlers/pulleys; following from steps 2.1 and 2.2); and furthermore, if applicable, also importing other system parts (cf. step 1.3); or even further, also importing additional visualising models (cf. step 1.4)

3.3. Defining further DEM setup details,

as required to perform the simulation as intended, which typically regards common DEM modelling aspects as introduced in the basics in Chapter 2.1.2, such as concerning the definition of gravity, interactional/material-related properties, bulk particles and their generation, but furthermore also part movements such as typical for driven pulleys, details regarding multibody dynamics (MBD), etc.

4. **If of interest: performing a test-simulation for evaluation purposes,**

   for example, according to the relaxation-into-state-of-rest principle, as introduced in Chapter 4.3 (with a belt in isolated form; i.e., with disabled and hidden or even removed system parts, further with deactivated gravity, etc.).

5. **Performing the pre-simulation – the transient oscillation into steady-state,**

   as described in Chapter 4.2.1; by performing the relatively short (almost to a minimum reduced) pre-simulation in which the belt system oscillates into its final (steady/stable) state as it is intended for the actual simulation of interest that correspondingly follows.

6. **Performing the simulation that is of interest,**

   which typically includes applying a bulk material (particle) flow to be processed from the belt system, or further also various system adjustments/operations, such as controlling pulley movements. Such specific simulations are shown in the following exemplary applications.

This outlined methodology workflow can be seen as the general basis for the simulations of the exemplary applications following.

5.1.2 Hardware/software

The computing time details given for each simulation example relate specifically to the hardware details as follows. Subsequently, associated/used software is listed.

5.1.2.1 Hardware

The presented simulations were performed on a typical desktop workstation using the CPU[44] Intel® Core™ i7-4770K Processor [122] of the 4th Generation Intel® Core™ i7 Processors, comprising four cores at 3.50 GHz base frequency – which was released in 2013, further intended for desktops; hence, by now, rather below average standards, especially for simulation purposes. From this perspective: The results achieved with this non-high-end hardware furthermore highlight positive efficiency aspects in computational terms and further the overall potential thus revealed by the presented methodology. Especially in simulation-effort-related terms, with particular reference to practice/industry-related use, the methodology proves that supercomputers are not a basic requirement to perform this kind of belt simulation.

5.1.2.2 Software

In accordance with the methodology presented in Chapter 4, the simulations shown are set up, performed, and furthermore also analysed with ThreeParticle/CAE [17].

Furthermore, the developed software tools, as a major outcome of the methodology presented, are applied – regarding the initialisation of BP belts (in almost-final state; BeltConverter [94], see Chapter 4.2.5) and the initialisation of cylindrical parts (as smooth-surfaced cylinders; PartConverter [95], see Chapter 4.4.3). (Another supplementary software tool (ParticleGenerator [99]) is further applied explicitly in the hay baler application in Chapter 5.6, as developed to enable dense-packed generation of flexible fibres as bonded-particles (cf. also fibre-model-related content in Chapter 3.1.2.2.1)).

In addition, a text editor (more specifically Notepad++ [118], further with a User Defined Language corresponding to the keyword syntax of ThreeParticle/CAE enabled) is used as a supportive tool allowing convenient adjusting of simulation setups with keywords, and especially of relevant INP files (see Chapter 4.2.3.2; cf. also Keywords Guide [12]).

[44] Central Processing Unit (processor)

5.2 Conventional belt conveyor

In the following figures, the application of the developed methodology is illustrated as applied on a relatively short conventional belt conveyor system. An overview of the DEM simulation setup of this system is given in Figure 5-1, showing the simulation-relevant structure comprising the therefore required elements (representing major components of such common belt conveyor systems as introduced in the respective basics in Chapter 2.2.2, and as especially shown in Figure 2-13): [45]

- the belt (yellow) as the central element of the system,
- the idlers/idler stations (smaller grey cylindrical parts), forming
  - a troughed belt in the carry (upper) strand, and
  - a flat belt in the return (lower) strand,
- the two pulleys (larger grey cylindrical parts; with the head pulley driven),
- the bulk material particles (green), which are loaded on the belt in the feeding area, and which are discharged over the head pulley (on the right).[46]

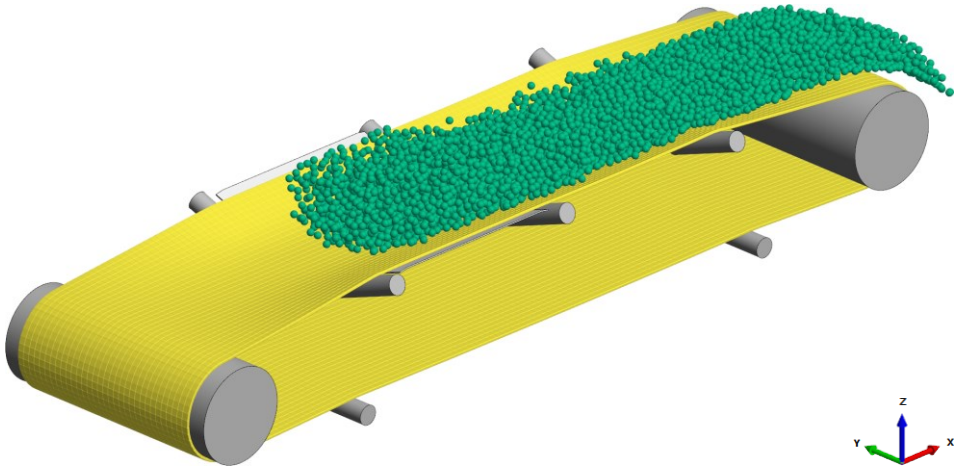

Figure 5-1: The DEM setup of the conventional belt conveyor system applied for dynamic belt simulation, already in operation, showing bulk material particles conveyed on the BP belt

[45] Several details regarding this belt conveyor system were already given previously, such as especially in Figure 4-24, illustrating the BP belt modelling procedure according to the presented methodology. Furthermore, this representative belt conveyor also corresponds to the system shown in the context of rigid belt modelling (in Chapter 2.2.3) and in the general belt initialisation approaches (in Chapter 3.2).

[46] This basic colouring scheme generally also applies to the examples presented in the following chapters.

This specific belt conveyor example also comprises an additional impact bed, which is placed underneath the belt in the feeding area. Furthermore, as illustrated in Figure 5-2, the conveyor system is inclined so that the bulk material is conveyed upwards (with an inclination angle of 7°, modelled by a respectively set gravity direction).

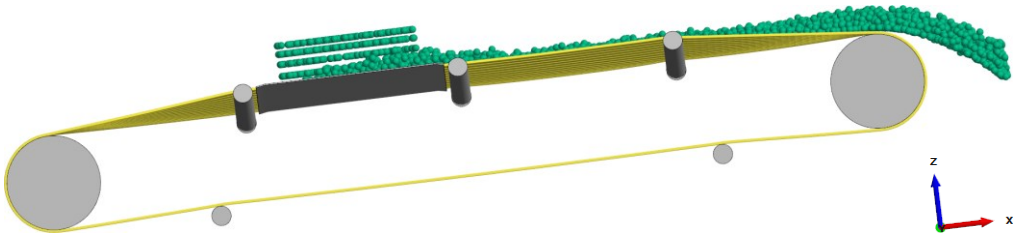

Figure 5-2: Side view of the belt conveyor system illustrating its inclination

A summary of relevant data regarding the performed simulation of this example is given in Table 5-1, especially revealing required computational efforts (of about 17 minutes computation time required per second simulated time at full operation).

System overview

Conveyor length [m]	5.0
Belt length (assembled) [m]	10.9
Belt width [m]	1.2
Conveying/belt velocity	2.65

Amount of DEM elements

BP belt particles	9 400
BP belt bondings	18 500
Bulk material particles at full operation	6 300
Interacting idlers/pulleys	13

Simulation/computation effort*	Simulated time [s]	Computation time [h]
Filling	1.5	0.25
Full operation	7.0	2.0
Total	8.5	2.25

(approximated/rounded values) (*: using an Intel® Core™ i7-4770K; see also Chapter 5.1.2.1)

Table 5-1: Conventional belt conveyor – system and simulation summary

After performing the simulation, various analysis options are possible, as shown and outlined by means of the following figures.

Figure 5-3 illustrates the belt sag at full operation of the system, highlighted via visualisation of local belt deformations, which are basically influenced by:

- the bulk material particles (i.e. loads on the belt due to the bulk material),
- the BP belt (as consisting of particles; i.e. due to the belt's own mass),
- the belt tensioning, and
- the belt-to-idler/component interactions.

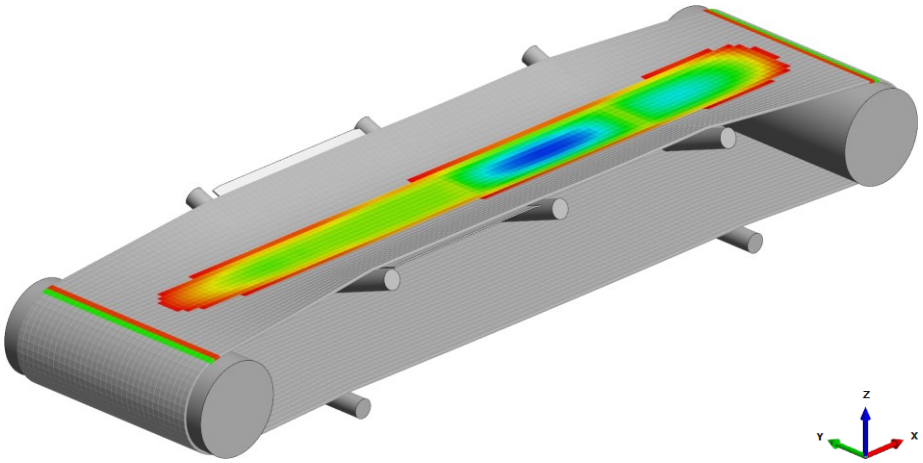

Figure 5-3: Belt sag, indicated via the z-position of belt particles

Another insight into this effect is shown in a cross-sectional side view in Figure 5-4, in which the addressed belt sag is furthermore evident (as in the sections without belt support, e.g. between the two shown idlers, further indicated in blue).

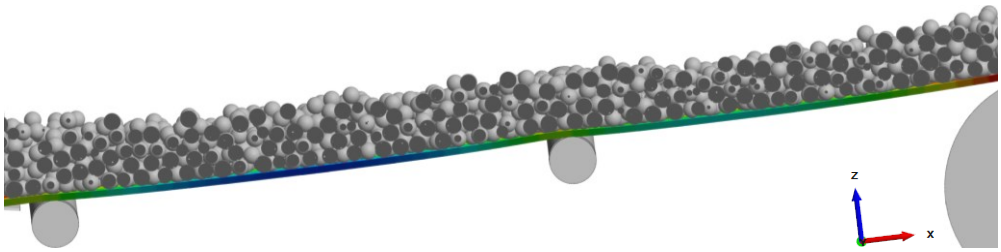

Figure 5-4: Belt sag, indicated via the z-position of belt particles; in cross-sectional side view (with the driven pulley on the right)

As a retroactive effect from the belt deforming under the bulk material load, the bulk material particles express relative (inner-bulk) particle movements whilst conveying (due to their transportation on the dynamically deforming belt surface).[47] This effect

[47] Bulk material rolling/milling and separation are typical physical effects further associated with such inner-bulk movements.

is illustrated in Figure 5-5 by showing the raising and lowering of bulk material particles at the section of an idler station in the cross-sectional side-view (with the raising of the bulk material particles shown just before reaching the idler, indicated in red on the idler's left side, and with their lowering shown just after going over this idler, further indicated in blue). Additionally, the bulk material flow in this section is illustrated in vector visualisation of the bulk material particles, as shown on the right.

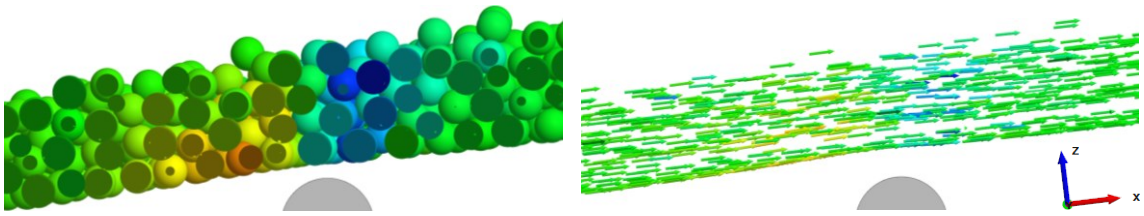

Figure 5-5: Inner movements of bulk material particles on the BP belt (at the idler station before the head pulley), indicated via translational particle velocities in z-direction (in cross-sectional side view; and also in vector visualisation, highlighting particle directions, shown on the right)

In the next two analyses, the focus is set on the bonding structure of the BP belt, which is shown in Figure 5-6, indicating the longitudinal and the transverse bondings in different colours (as the belt is modelled using alternating fibres; cf. Chapter 4.1.2.3).

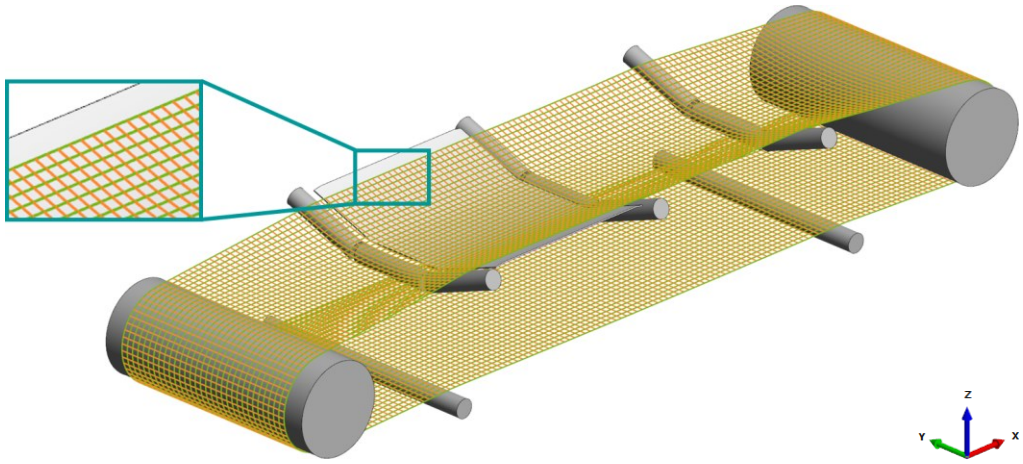

Figure 5-6: Bonding structure underlying the BP belt, with the detailed view showing the longitudinal and the transverse bondings (green and orange)

Longitudinal bondings can be analysed in isolated form, such as to illustrate diverging belt elongations as shown in Figure 5-7, which specifically gives insights into

local bonding elongations occurring during operation (which furthermore corresponds to local belt tensioning and further also to local axial stresses occurring in the belt). Especially the increase of the belt's elongation/tension along its run through the system is revealed from this analysis, as the belt shows relatively low tensioned bondings just after the head pulley (on the right; indicated in blue), which are successively increasing (due to various resistances) along the belt's run towards the upper side of the head pulley (on the top right; indicated in green). Also evident are the higher tensioned belt edges in areas where the belt is formed from flat to troughed and vice versa (indicated in orange/red).

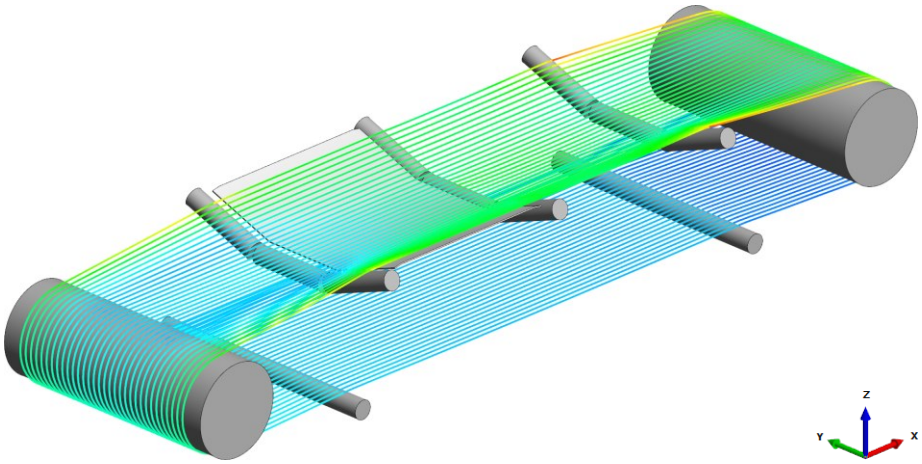

Figure 5-7: Elongational deformations of the BP belt in the longitudinal direction, indicated via translational bonding deformations

Transverse bondings can also be analysed in isolated form, as shown in Figure 5-8, in which these bondings are analysed regarding their rotational deformations. As this form of analysis further provides information on the level of local bending deformation of the belt, those areas in which the belt is bent to certain degrees can be highlighted; such as shown in the figure, in which it is revealed that the belt is bent stronger (respectively in the transverse direction) in troughed sections which are supported by idlers or the impact bed, particularly where this support causes a strong deflection of the belt (as indicated in orange/red).

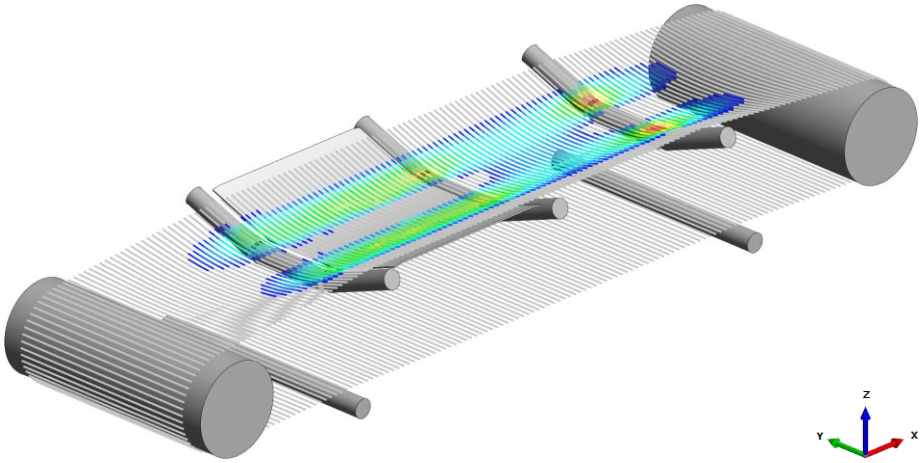

Figure 5-8: Bending deformations of the BP belt in the transverse direction, indicated via rotational bonding deformations

5.3 Belt turnover station

The belt turnover station applied for dynamic belt simulation illustrates the use of a BP belt without bulk material particles but with idlers interacting with the belt. [48] A general introduction into belt turnovers was already given in Chapter 3.1.1.1, in which specifically the use of (uncoupled) FEM simulation was discussed. The methodology presented in this thesis, which in contrast to this FEM-based approach bases on the DEM (by using a BP belt), presents an ideally suited alternative for this purpose, as it is illustrated in Figure 5-9.

In this mentioned figure, the DEM simulation setup at the section of a belt turnover station is illustrated on top, furthermore indicating the alternating-fibred structure of the BP belt (which is illustrated with the yellow/orange coloured belt particles indicating the two different fibres, and which moreover helps to visualise the turnover process). In this application, the belt runs from left to right. Below this illustrated simulation setup, two analyses of the BP belt regarding its bonding structure are

[48] The shown example of the turnover station was initially published by Fimbinger in 2019 (in the brochure of the Chair of Mining Engineering (...) at the University of Leoben 2019) [85].

shown: on the one hand, in the longitudinal, and on the other hand, in the transverse direction (as basically similar to the principles described at the end of the previous exemplary application of the conventional belt conveyor in Chapter 5.2), indicating differences in local belt elongations/tensions (shown in the middle) and in rotational deformations (i.e. belt bending; shown on the bottom).

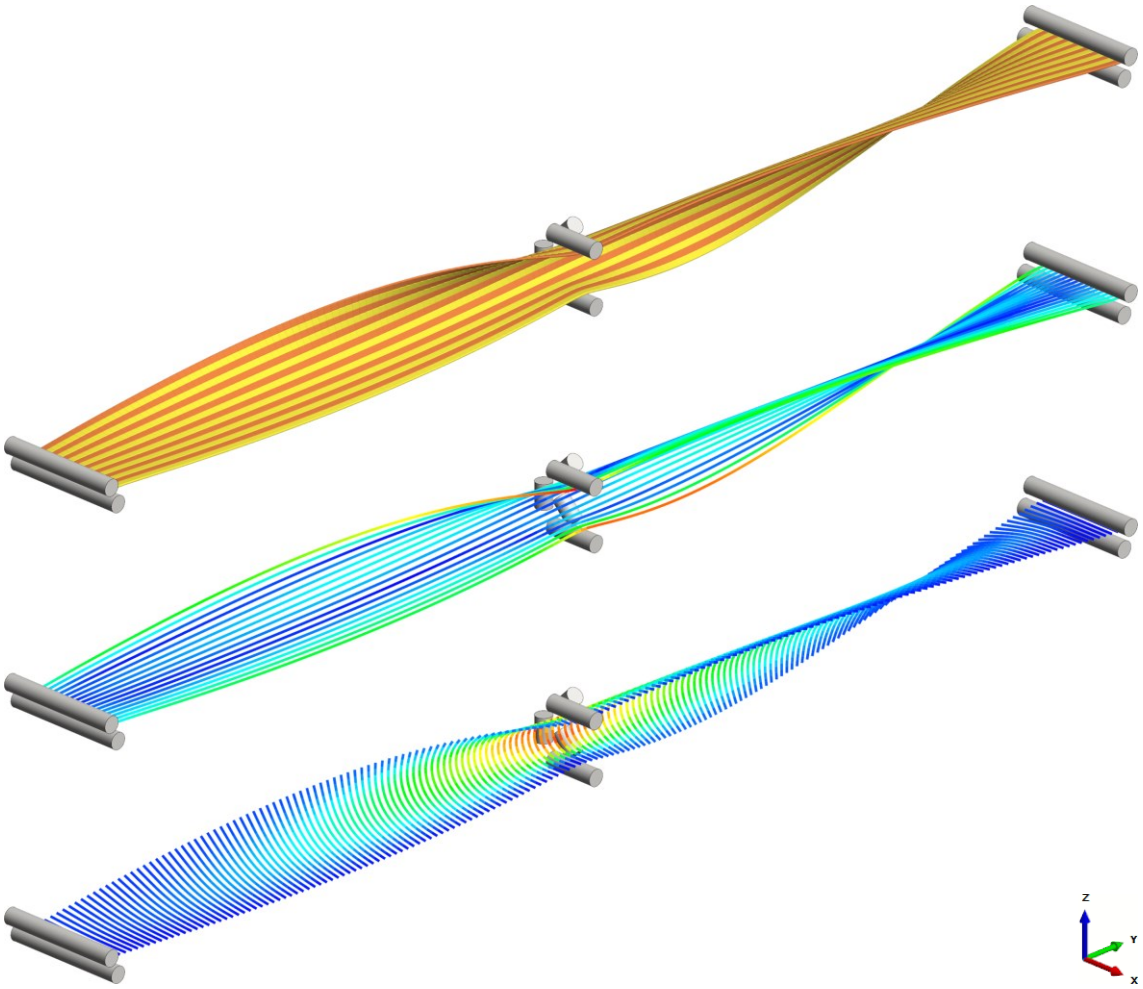

Figure 5-9: The DEM setup of the belt turnover applied for dynamic belt simulation (top), with analyses of the BP belt: elongational deformations in longitudinal direction, indicated via translational bonding deformations (middle), and bending deformations in transverse direction, indicated via rotational bonding deformations (bottom)

In more detail, this simulation comprises a finite BP belt, which is pulled through the turnover section. Therefore, this BP belt is modelled longer than the actual turnover section; and it is initialised with its right end aligned with the pulleys on the right side of the system. During the simulation, the belt is pulled through the system with a constant velocity applied at both ends of the belt (to maintain the belt's intended

tension). After a relatively short transient oscillation of the BP belt, a steady-state can be achieved, which can be analysed, as shown in the figure outlined before.

Table 5-2 further gives a summary of relevant data for the performed simulation.

System overview

Length of the turnover section [m]	10.0
Belt length (finite belt) [m]	13.5
Belt width [m]	0.8
Belt velocity [m/s]	2.0

Amount of DEM elements

BP belt particles	3 600
BP belt bondings	6 900
Interacting idlers/pulleys	9

Simulation/computation effort*	Simulated time [s]	Computation time [h]
Initial forming stage	0.75	0.25
Operation	0.75	0.25
Total	1.5	0.5

(approximated/rounded values) (*: using an Intel® Core™ i7-4770K; see also Chapter 5.1.2.1)

Table 5-2: Belt turnover – system and simulation summary

As an alternative, and especially to model an endless running belt turnover station with a BP belt, using an endless Möbius instead of the finite belt geometry would also be suitable (as described in Chapter 4.2.3.1.1/as shown in Figure 4-20).

5.4 Sandwich conveyor

As a particular characteristic, the application of the methodology on a sandwich conveyor comprises two BP belts that are required to contact each other. Relevant basics of such sandwich conveyor systems were already explained in Chapter 2.2.5.1. [49]

[49] The shown example of the sandwich conveyor was initially published by Fimbinger in 2019 (NAFEMS 2019, Quebec City/ICBMH 2019, Gold Coast) [88, 97, 86, 98], and was further shown/discussed in later publications (see also Chapter 1.5); further details/insights can accordingly be found in these publications.

The general system overview of the sandwich conveyor applied for dynamic belt simulation is shown in Figure 5-10, showing the full DEM simulation setup (also with a visualising system structure included) on the left, and an inside-view into the system with the upper belt hidden on the right, thus showing the bulk material flow (in green) as transported between the two belts (upper belt in darker, lower belt in brighter yellow).

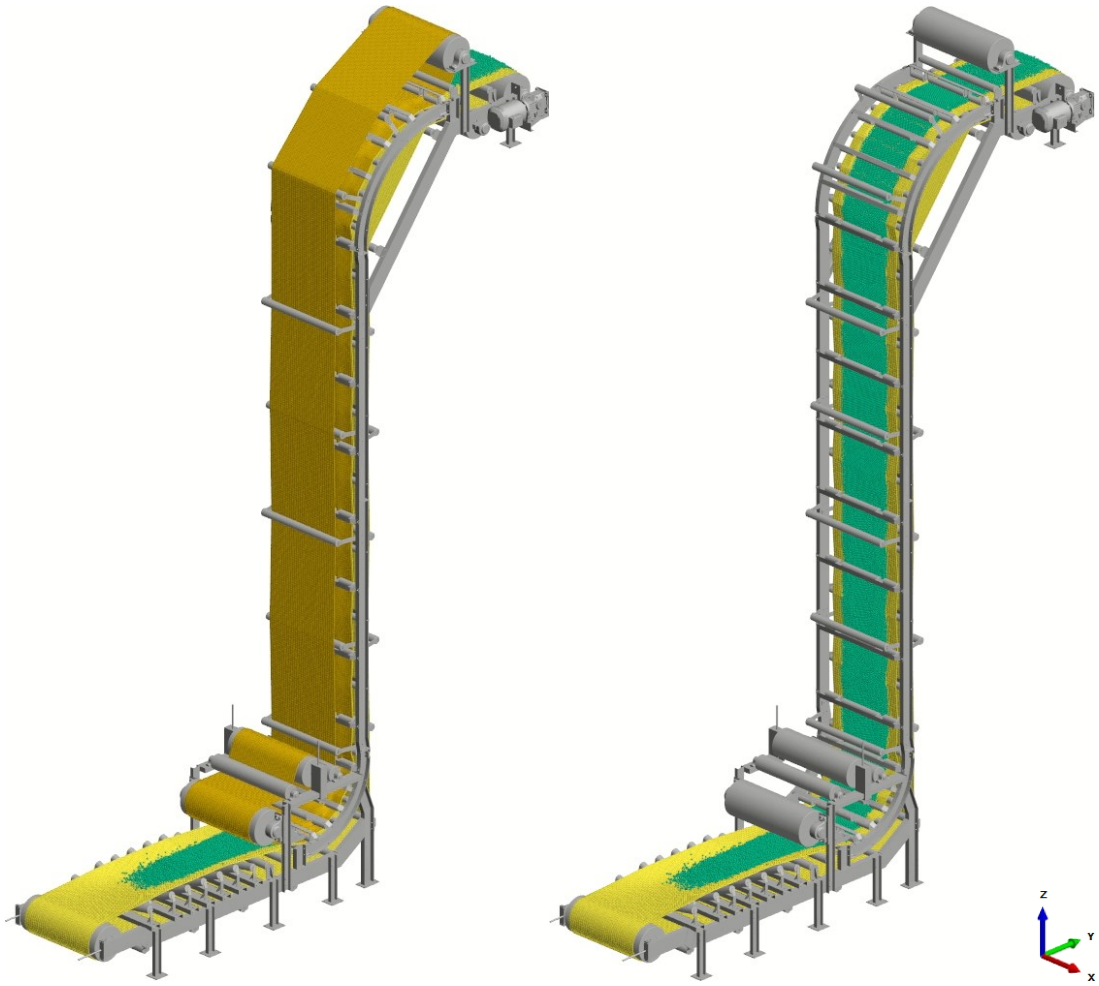

Figure 5-10: The DEM setup of the sandwich conveyor system applied for dynamic belt simulation, already in operation showing bulk material particles conveyed between the two belts (with the upper belt in hidden view on the right, showing the vertical bulk material flow)

The components/element groups of this simulation setup are separately illustrated: in Figure 5-11, showing the two BP belts, and in Figure 5-12, showing the cylindrical system components modelled to interact with these BP belts (on the right) and the

visualising system structure (which does not influence the actual simulation, but serves the purpose of system visualisation).

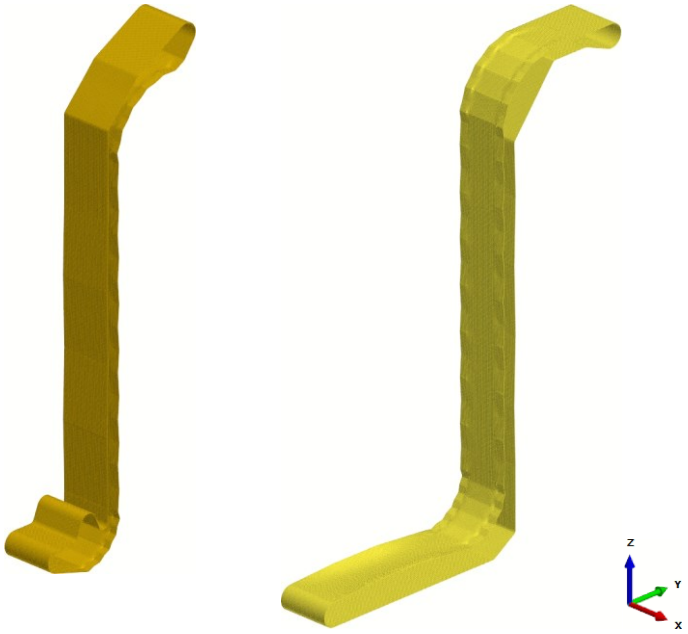

Figure 5-11: The two BP belts of the sandwich conveyor

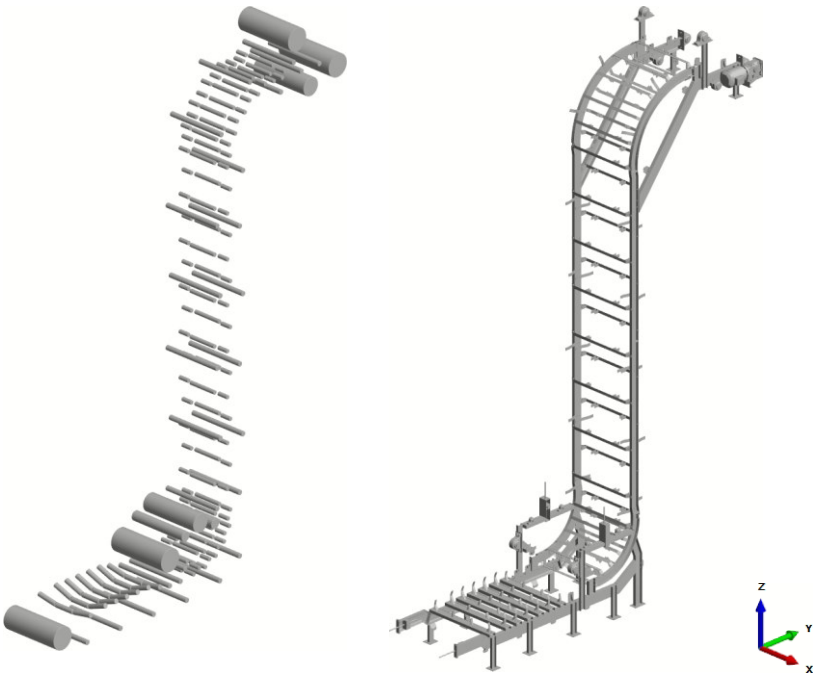

Figure 5-12: Cylindrical system components (idlers/pulleys) on the left; and further system components for visualisation purposes only on the right

A summary of the relevant data regarding the performed simulation of this sandwich conveyor is given in Table 5-3.

System overview	
Conveying height [m]	10.0
Belt length, lower belt (assembled) [m]	35.4
Belt length, upper belt (assembled) [m]	27.1
Belt widths [m]	1.2
Conveying/belt velocity [m/s]	2.1

Amount of DEM elements	
BP belt particles (sum of both belts)	68 100
BP belt bondings (sum of both belts)	134 300
Bulk material particles at full operation	50 000
Interacting idlers/pulleys	166

Simulation/computation effort*	Simulated time [s]	Computation time [h]
Pre-simulation and initial idle mode	1	0.5
Filling	11	9.0
Full operation	2	2.0
Total	14	11.5

(approximated/rounded values) (*: using an Intel® Core™ i7-4770K; see also Chapter 5.1.2.1)

Table 5-3: Sandwich conveyor – system and simulation summary

Figure 5-13 gives insights into the conveyor system during its operation, showing the deformation of the two belts as evident in two different cross-sectional views.

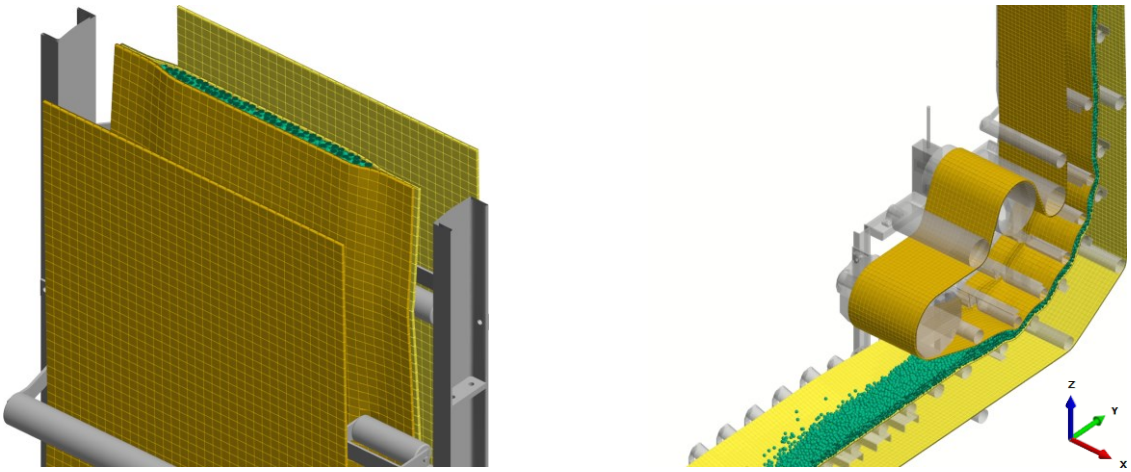

Figure 5-13: Cross-sectional views; showing the conveyor cross-section formed by the bulk material particles resulting from interactions with the two BP belts (left), and the vertical curve after the feeding point where the belts (with bulk material within) are guided by a series of idlers from horizontal into vertical conveying direction

Furthermore, the visualisation of particle velocities of the bulk material particles, as shown in Figure 5-14, allows an analysis of bulk material flow characteristics; in this shown case, highlighting inhomogeneities in certain areas, thereby more specifically revealing accumulating bulk material particles at the intake section (in the area where the bulk material particles are drawn between the two belts, at the beginning of the bottom curve), and further also indicating back-flowing material in certain sections, such ass at the beginning of the top curve, as it is shown in detail in the zoomed-in view of this section.

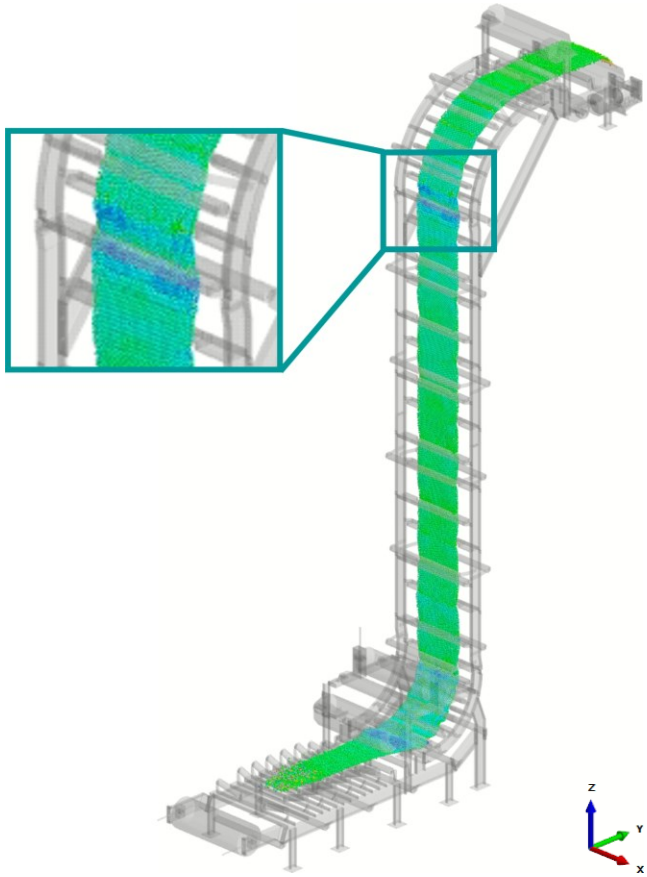

Figure 5-14: Bulk material flow characteristics indicated via translational particle velocities, highlighting differences/inhomogeneities in certain areas (as at the curve sections; further revealing back-flowing bulk material particles as in the section shown in the detailed view)

5.5 Pipe conveyor

As a particular characteristic, the application of the presented methodology on a pipe conveyor system requires the BP belt to allow self-contact (as according to the principles already given in Chapter 4.1.1.2). Relevant basics of such pipe conveyor systems were already explained in Chapter 2.2.5.2. [50]

Figure 5-15 shows the pipe conveyor applied for dynamic belt simulation in operation, with the bulk material (green) conveyed within the pipe-formed belt (yellow).

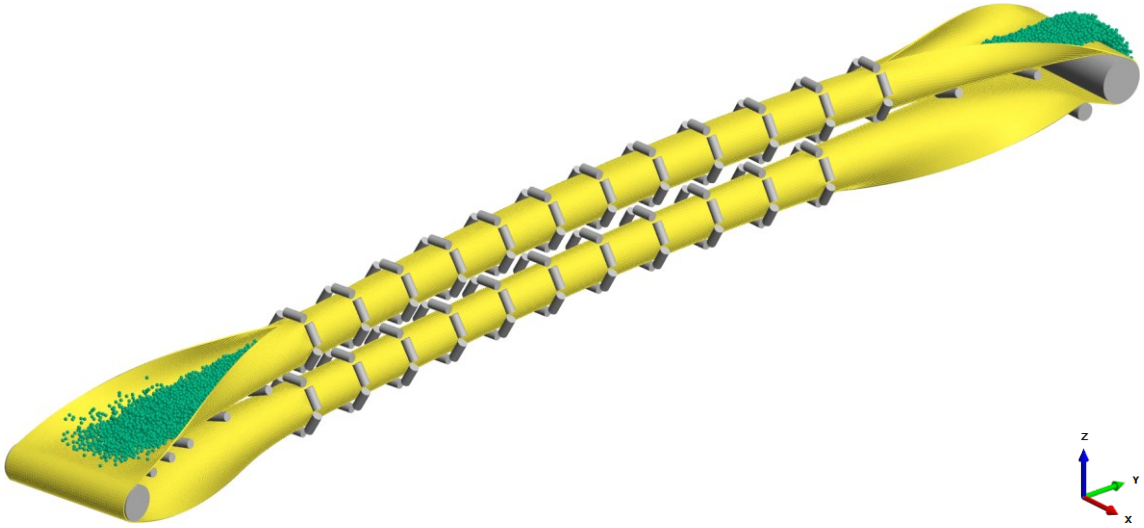

Figure 5-15: The DEM setup of the pipe conveyor system applied for dynamic belt simulation, already in operation showing bulk material particles conveyed within the pipe-formed BP belt

The conveyor line furthermore follows a slightly curved track, as illustrated in Figure 5-16 (with an angle of 10° between the left and right pulley axes).

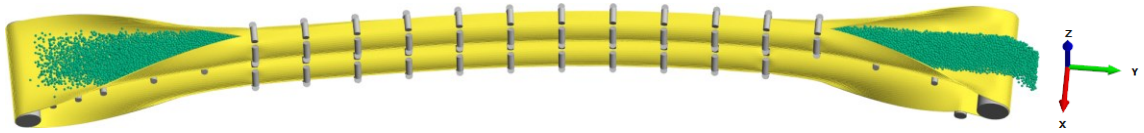

Figure 5-16: Side view of the pipe conveyor system from diagonal-top showing the slightly curved conveyor line

[50] The shown pipe conveyor example was initially published by Fimbinger in 2018 (Conference on Bulk Material Handling (Fachtagung Schüttgutfördertechnik) 2018, Garching) [82, 93], and was also shown in later publications (cf. Chapter 1.5); further details/insights can accordingly be found in these publications.

The setup of the BP belt using contact groups to allow belt self contact at its edges is illustrated in Figure 5-17, indicating the three applied contact groups in different colours. (This setup basically relates to the principles already described in Chapter 4.1.1.2, particularly regarding Figure 4-3.)

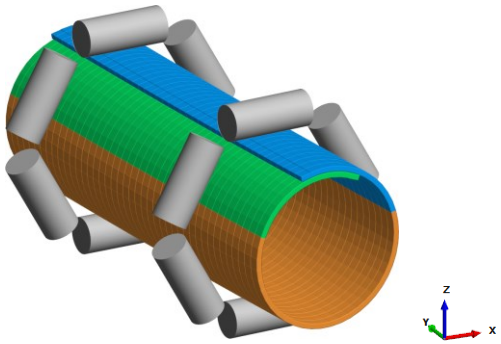

Figure 5-17: Cross-sectional view of the BP belt in the carry (upper) strand; colours indicating contact groups, which are applied to enable belt self contact at the edge areas for pipe forming as shown (with contact between green and blue enabled)

Table 5-4 summarises the relevant data for the simulation and computation of this pipe conveyor system as shown.

System overview

Conveyor length [m]	19.5
Belt length (assembled) [m]	40.0
Belt width [m]	2.0
Pipe diameter [m]	0.55
Conveying/belt velocity [m/s]	2.1

Amount of DEM elements

BP belt particles	50 700
BP belt bondings	100 400
Bulk material particles at full operation	25 000
Interacting idlers/pulleys	161

Simulation/computation effort*	Simulated time [s]	Computation time [h]
Pre-simulation and initial idle mode	1.0	0.5
Filling	8.75	4.5
Full operation	4.0	2.0
Emptying	8.75	4.5
Empty/idle operation	1.5	0.5
Total	24.0	12.0

(approximated/rounded values) (*: using an Intel® Core™ i7-4770K; see also Chapter 5.1.2.1)

Table 5-4: Pipe conveyor – system and simulation summary

Figure 5-18 illustrates the belt sag occurring between idler stations in the carry (upper) strand.

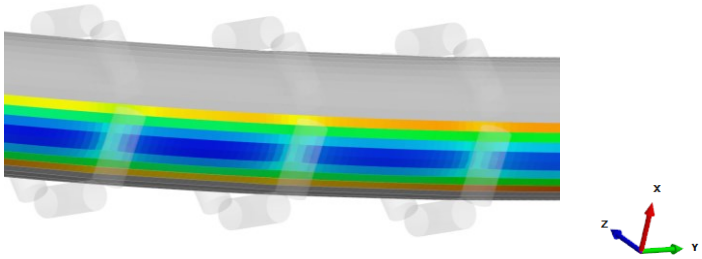

Figure 5-18: Belt sag between idler stations in the carry strand, indicated via the z-position of belt particles (view from diagonal-bottom) during full operation

Due to this shown deformability of the BP belt, similar inner-bulk movement effects as already addressed in the example of the conventional belt conveyor (in Chapter 5.2, and as made visible in Figure 5-5) also occur in this application of the pipe conveyor. Those effects are further visualised in Figure 5-19, highlighting appearing differences in the bulk material particle velocities, which are again especially evident at idler stations, such as shown in the detailed view.

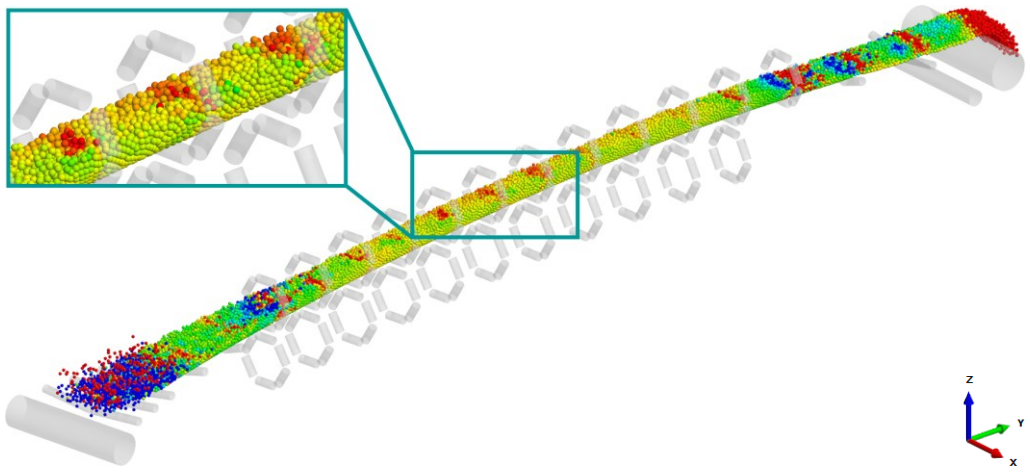

Figure 5-19: Bulk material movement characteristics occurring due to the deformed BP belt, indicated via particle velocities – especially highlighted at idler stations

A further analysis option that reveals these effects associated with inner-bulk movements is the visualisation of the kinetic energy of bulk material particles, as shown in Figure 5-20. In this figure, only bulk material particles above a certain level of kinetic energy are shown. This level is therefore set slightly above the kinetic energy

of bulk material particles in common motion (which corresponds to the kinetic energy apparent from the intended conveying velocity).

This analysis reveals the effect that bulk material particles show an increase of kinetic energy shortly after going through an idler station (see figure). This effect refers to energy inducements into the bulk material basically enabled due to the deformation capabilities of the BP belt; and as the bulk material particles are slightly compressed when going through an idler station, as this compression is again released after these particles pass the idler station and which expresses as the illustrated increase in kinetic energy (which is further dissipated relatively quickly due to friction and damping between particles).

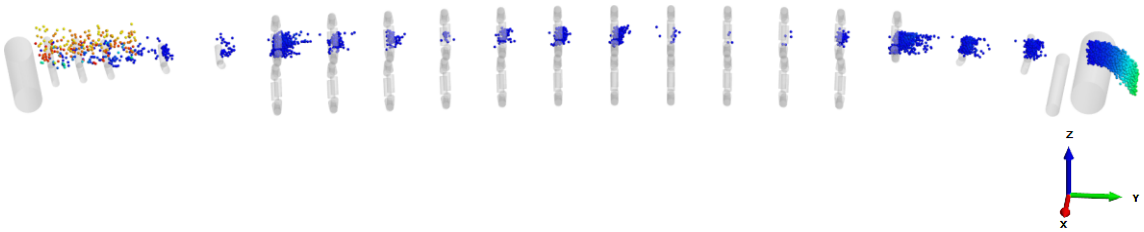

Figure 5-20: View from diagonal-top with bulk material particles below a minimum level of kinetic energy hidden, highlighting a kinetic energy increase of bulk material particles at idler stations

Furthermore, an analysis of the longitudinal bonding elongations shown in Figure 5-21 shows belt elongation/tension effects, especially revealing the differences between the outer and the inner side of the curved conveyor section evident, with the outer belt fibres tensioned stronger than the inner ones.

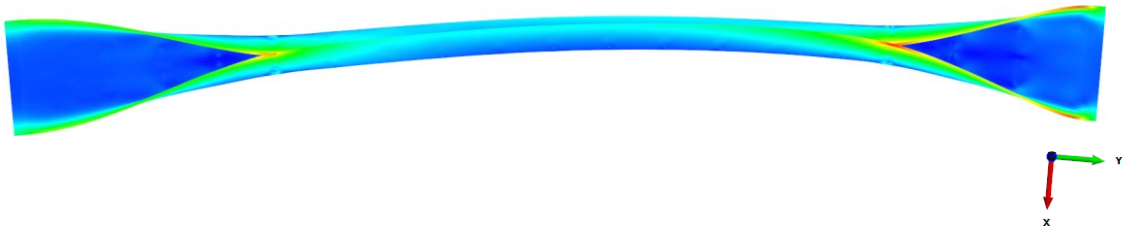

Figure 5-21: Elongational deformations in the longitudinal direction, indicated via translational bonding deformations (especially showing differences at the curve)

5.6 Belt system of a round hay baler

As a particular characteristic, the application of the methodology on such a belt system of a round hay baler comprises multibody dynamics (MBD) for considering/enabling the idler system as a complex-interacting, dynamic system – interacting with the BP belt and thus further with the baled hay/straw-representing particles (in the following termed stalk material particles), which are gathered/baled by this system. In Chapter 2.2.5.5, relevant basics regarding the belt systems used in round hay balers are generally explained. [51]

The principle setup of a BP belt assembled in a hay baler is illustrated in the overview shown in Figure 5-22; showing the BP belt in isolated view – at rest (on the left) and during operation (on the right, further also illustrating the belt's deformation during the baling process).

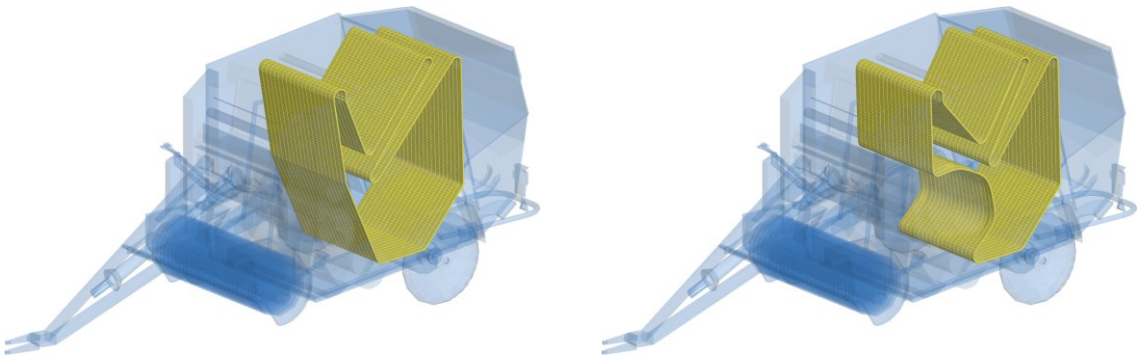

Figure 5-22: The belt visualised within a round hay baler, showing the BP belt at rest (undeformed; left) and in operation/during baling (deformed; right) [90]

Since the increasing amount of baled stalk material particles disproportionally affects the computation time negatively, the simulation up to larger bale diameters (as shown in the figures following) is performed with a partial-section model of the full system. Therefore, the simulation setup is reduced to a one-eight width of the full system (with boundaries defined correspondingly), representing a cut-out middle-section of the complete system, as illustrated in Figure 5-23.

[51] The shown application of the hay baler belt system was initially presented by Fimbinger in 2020 (SimuLand 2020) [90]; further details/insights can accordingly be found in this publication.

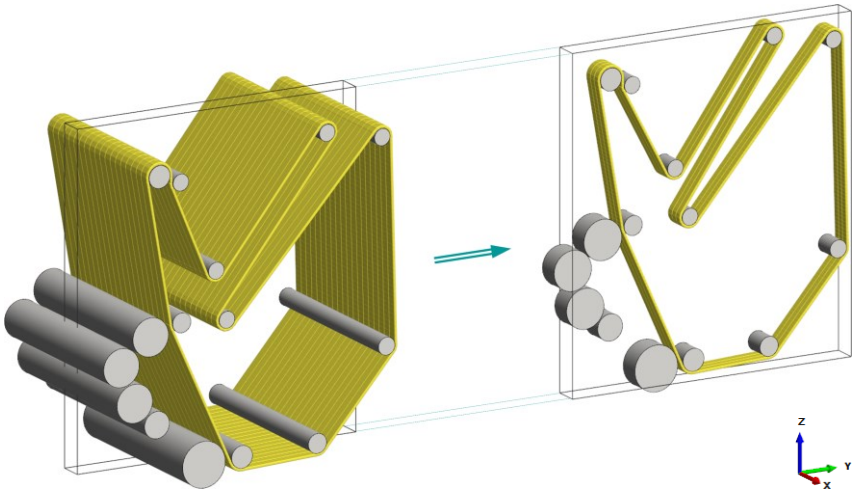

Figure 5-23: The DEM setup of the belt system of the round hay baler applied for dynamic belt simulation; the complete system (left) and the reduced partial-section model (right)

In Figure 5-24, the multibody dynamic setup applied to the idler system is visualised, with the symbols shown in green illustrating MBD elements as follows:

- the cross-points indicating markers
- the two triangles with the circular symbol on top indicating fixed pivot points,
- the solid lines indicating fixed-distance connections of markers (thus forming two rocker arms, each rotatable around its pivot point), and
- the dashed line indicating a tensioning element (tensioned spring-damper).

Furthermore, the idlers are each rotatable around their cylinder axes; and the idler on the top left is driven, thus driving the belt during the baler's operation (in the clock-wise direction).

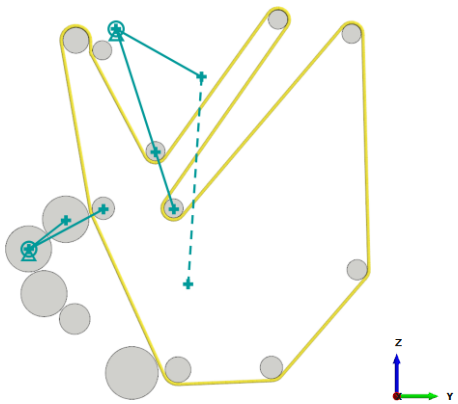

Figure 5-24: The MBD setup of the idler system of the round hay baler, enabling certain idlers to interact dynamically (symbols illustrating MBD marker/joints)

This setup allows an enhanced dynamic interaction of the idlers with the dynamically deformable BP belt, especially expressed during the system's operation, as illustrated in Figure 5-25, showing the baling process and thus the dynamics of the idler system.

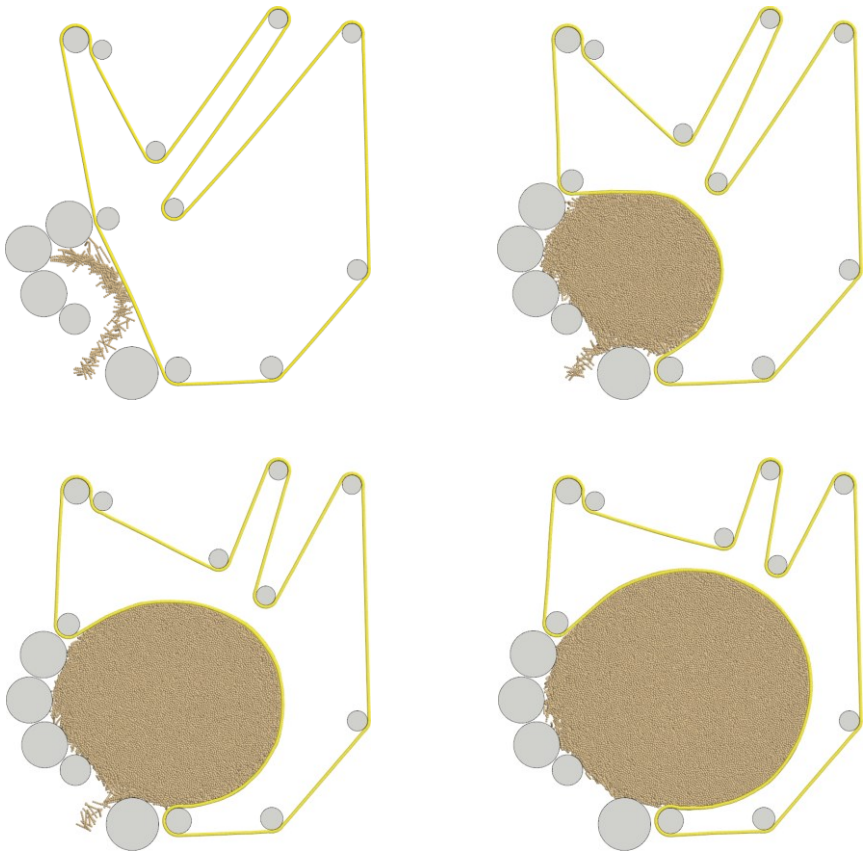

Figure 5-25: Steps of the baling process (from top left to bottom right); with the belt tensioning/ buffering system (top-right idlers) dynamically yielding belt, thus allowing the bale to increase

Besides the forming of the bale, these steps furthermore illustrate the movements of the idlers due to their interactions with the BP belt, and thus furthermore due to the increase of the bale: On the one hand, showing the yielding of the BP belt from the belt tensioning/buffering system that is formed by the upper rocker arm (and more specifically by the four idlers in the top-right section of the system, which guide the BP belt in a zig-zag line, its length decreasing dynamically as the baling process progresses (thus yielding buffered belt length)), and on the other hand, showing the deflection of the lower rocker arm on the left side of the system, which rotates counterclockwise with the two idlers connected to it.

Additionally, the baled stalk material particles are modelled as complex-acting (deformable/flexible) bonded-particle fibres, set up according to the principles described

in the approaches in Chapter 3.1.2.2.1 (as particularly illustrated in Figure 3-16/Figure 3-17; with each stalk modelled as a fibre consisting of linear arranged bonded particles, as principally recognisable on closer inspection of certain figures shown subsequently, e.g. Figure 5-26.). Moreover, a software tool (ParticleGenerator [99]) was developed and applied that specifically enables the generation of dense-packed bonded particle fibres (to implement a dense-packed generation of stalk material particles at the intake of the hay baler system as also evident in the shown figures).[52]

A summary of the relevant data regarding the performed simulation of this hay baler system is given in Table 5-5, in which especially the disproportional increase of required computation time (set in relation to the simulated time) is evident, which is attributable to the increasing number of particles and bondings of the baled material.

System overview

Belt length (assembled) [m]	8.1
Belt width (1/8-section model) [m]	0.125
Conveying/belt velocity (average) [m/s]	3.0

Amount of DEM elements

BP belt particles	1 200
BP belt bondings	2 000
Baled material particles (in the full bale)	120 600
Baled material bondings (in the full bale)	107 200
Interacting idlers/pulleys	15

Simulation/computation effort*	Simulated time [s]	Computation time [h]
Pre-simulation and initial idle mode	1.0	0.1
Filling up to 1/4 (volume)	4.5	1.9
Filling up to 2/4 (volume)	4.5	4.5
Filling up to 3/4 (volume)	4.5	6.5
Filling up to 4/4 (volume)	4.5	12.5
Operation without filling (full bale turning)	1.0	4.5
Total	20.0	30.0

(approximated/rounded values) (*: using an Intel® Core™ i7-4770K; see also Chapter 5.1.2.1)

Table 5-5: Belt system of the round hay baler – system and simulation summary

In the following figures, several analysis capabilities regarding this simulated system of the round hay baler using a dynamically interacting BP belt are illustrated.

[52] This software tool was furthermore developed to enable dense-packed bonded-particle fibre generation for any DEM simulation, and is further outlined in the respective publication by Fimbinger (2020) [90].

Figure 5-26 illustrates the belt elongation, thus highlighting the increase of belt tension along the belt run (starting with the lowest tension after and ending with the highest tension before the driven pulley on the top left side of the system).

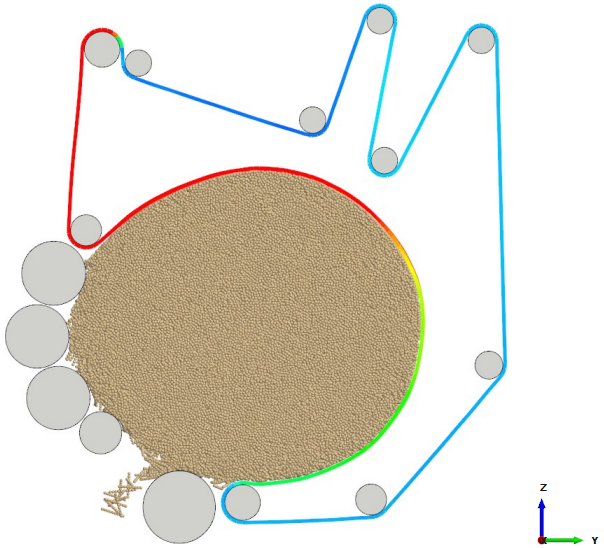

Figure 5-26: Elongational deformations of the BP belt, indicated via translational bonding deformations, highlighting the increase of belt tension along the belt run

In Figure 5-27, the particle velocities are illustrated at the beginning of the bale-forming, showing the formation of a circular movement of the baled particles, which further form the centre of the bale (illustrated in vector visualisation).

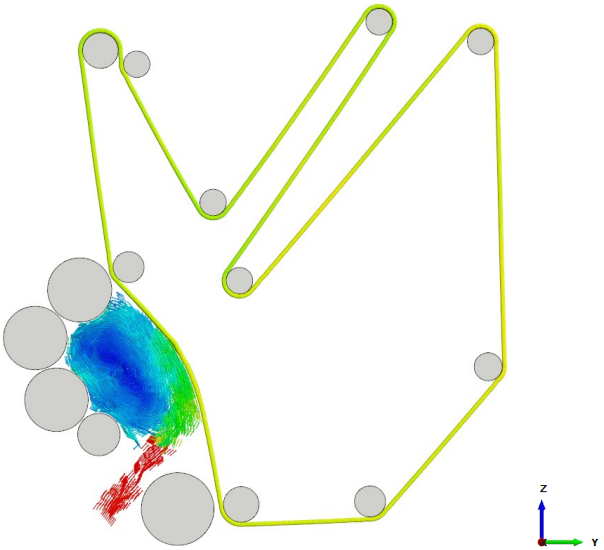

Figure 5-27: Baling process dynamics, indicated via particle velocities (shown at the beginning of the bale-forming)

Figure 5-28 shows the bale's composition in terms of earliest to latest picked up/baled material (indicated via the particle ID), and Figure 5-29 illustrates further capabilities in terms of load-analyses of the baled structure, such as by illustrating compressive effects on the particles forming the bale.

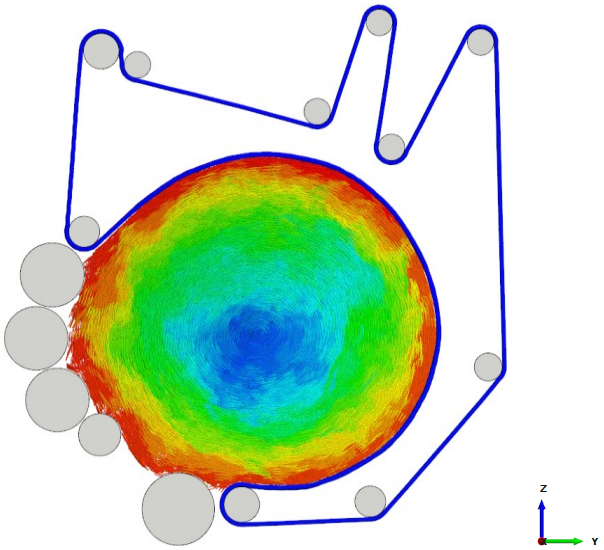

Figure 5-28: Inner setup of the bale in terms of the time of material intake, indicated via the particle IDs (early particles in blue, latest particles in red)

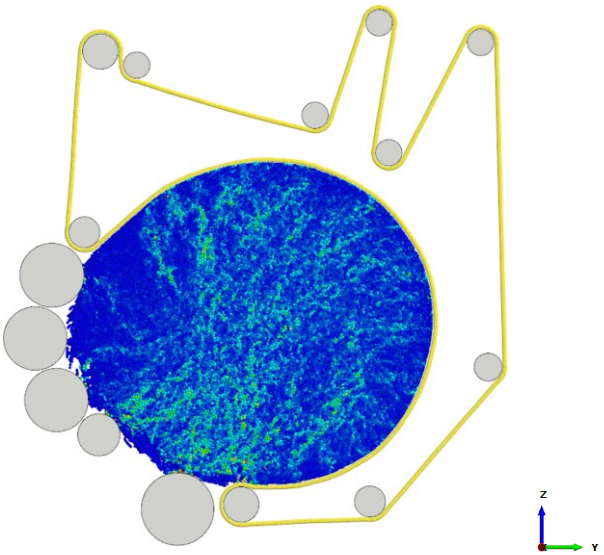

Figure 5-29: Compressive effects on the bulk material baled, indicated via compressive forces on bulk material particles

5.7 Belt breakage

In this exemplary application, an enhanced capability that allows belt breakage is implemented into the BP belt of a belt conveyor system. Therefore, a relatively simple flat belt conveyor system is set up, as shown in an overview in Figure 5-30 on top (showing a typical operating state, such as conveying bulk material from left to right). To induce belt breakage, the BP belt in this system is continuously tensioned via a constant movement of the left pulley, which successively increases the belt tension until a critical tensioning/stress level in the bondings of the BP belt is reached/exceeded, and the belt breaks accordingly (correspondingly, this critical level represents the belt breakage criterion). This breakage, or more specifically a time step shortly after it occurs, is also illustrated in the figure (at the bottom), with the breakage area evident in the middle of the conveyor system. [53]

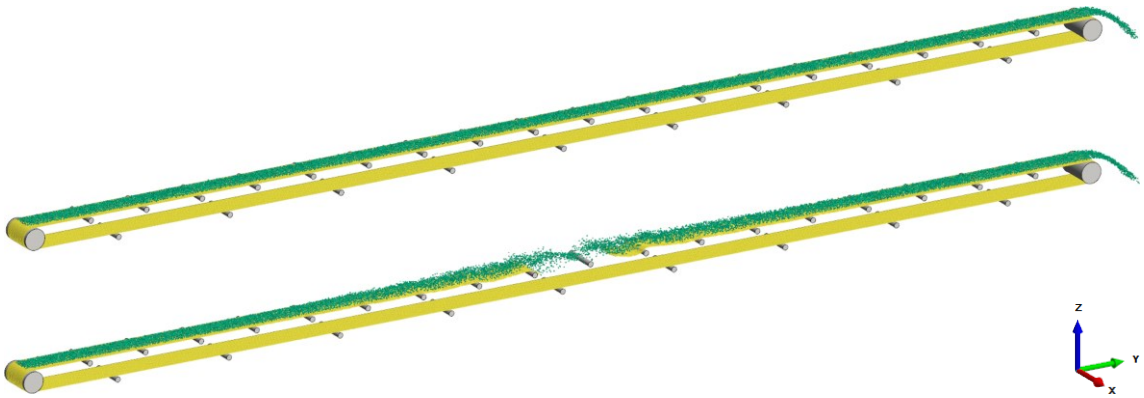

Figure 5-30: The DEM setup of the flat belt conveyor system applied for dynamic belt simulation extended to allow belt breakage; the system during typical operation (top), further tensioned via pulley movement (of the left pulley) until the breakage of the BP belt (bottom)

Side notes on this shown DEM simulation setup: To reduce pre-simulation effort, an already fully-filled conveyor system, thus in full operation, is initialised, for which the bulk material particles are initialised on the BP belt with their initial velocity equal to the belt velocity. Furthermore, to reduce dynamic effects associated with common bulk material particle loading on a BP belt at a feeding point (such as their

[53] Further work related to this shown application of belt breakage was also published by Markut in 2020 [167], which applied the presented belt simulation methodology for his Master's thesis, furthermore in cooperation with/under supervision of Fimbinger; details/insights are accordingly provided in this referenced thesis.

acceleration by the BP belt), the bulk material particles in this application are loaded on the BP belt at the left pulley in an already accelerated form (specifically with their velocities equal to the belt velocity in the carry strand; thus, additional dynamic effects from common loading of bulk material particles onto the BP belt are suppressed.

The addressed belt breakage capability is implemented into the BP belt at a selected belt section, as highlighted in Figure 5-31. As generally related to the principles addressed in Chapter 4.1.2.3, this breakage section is modelled explicitly by changing the belt particle types of two adjacent particle rows, as indicated in the figure, which further gives a row of parallel (longitudinally oriented) bondings between them. These specific bondings are further applied with the aforementioned breakage criteria, thus enabling the capability of BP belt breakage to occur in this specified section (whilst every other bonding in the BP belt is set without the capability to break).

This modelling technique allows controlling the BP belt's breakage in terms of the location at which it is intended to occur. In this context, the breakage section's progression along the conveyor line (due to the BP belt's movement associated with the system's operation) must also be taken into account. In the shown example, the breakage was intended to occur approximately in the middle of the conveyor system, which was achieved by modelling the breakage section with a defined offset before the actual middle position of the conveyor. This offset was further determined via the belt velocity and the time to reach the breakage criterion in the BP belt (theoretically), which furthermore stands in context with the velocity of the pulley that increasingly tensions the belt and with the BP belt's initialised pre-deformation state.

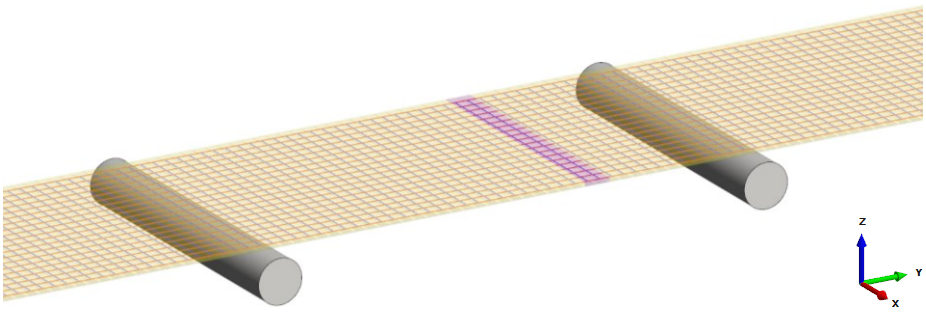

Figure 5-31: The section at which the BP belt is intended to break (highlighted in the middle), modelled with two rows of individual particles giving a row of parallel bondings for which a breakage criterion is set

Table 5-6 summarises relevant data for the simulation and computation of this system illustrating belt breakage. The simulation comprises a tensioning phase until the breakage of the BP belt is reached and a short period following the breakage. From the beginning of the breakage, the save interval (of saved time steps) is required to be reduced in order to allow proper analysis during this phase (which is furthermore the main reason that the computational effort is slightly increased during this second phase of the simulation). Moreover notable is the methodology-related positive aspect/effect that the pre-simulation phase at the very beginning of the simulation (during which the system oscillates from the almost-final into final steady-state) is significantly reduced to a minor level, especially compared to the conventional technique of assembling the belt after initialisation in state-of-rest (cf. Chapter 3.2.1), and furthermore filling it with bulk material particles before performing the actual breakage simulation that is of interest.

System overview

Conveyor length (initially) [m]	19.4
Belt length (assembled; initially) [m]	39.2
Belt width [m]	0.5
Conveying/belt velocity [m/s]	2.6

Amount of DEM elements

BP belt particles	31 400
BP belt bondings	61 300
Bulk material particles at full operation	14 500
Interacting idlers/pulleys	29

Simulation/computation effort*	Simulated time [s]	Computation time [h]
Operation before breakage	1.6	1.2
Operation from breakage	0.1	0.1
Total	1.7	1.3

(approximated/rounded values) (*: using an Intel® Core™ i7-4770K; see also Chapter 5.1.2.1)

Table 5-6: Conveyor system for belt breakage – system and simulation summary

Ultimately, the effects of a breaking BP belt is illustrated in Figure 5-32, particularly showing the release of the energy that corresponds initially to the belt's pre-tensioning, and which expresses as kinetic energy affecting/accelerating the belt (particles), the bulk material (particles), and furthermore also the idlers.

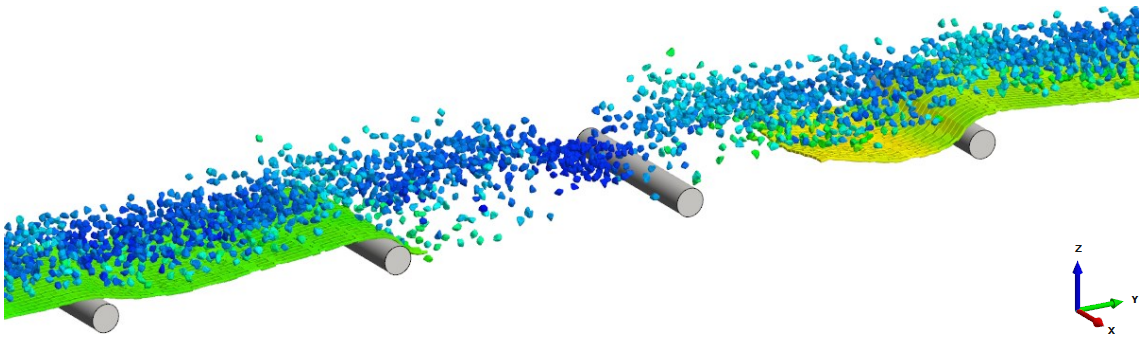

Figure 5-32: The dynamic effects shortly after the BP belt breaks, indicated via particle velocities (bulk and belt); also showing interactions between the BP belt and bulk material particles, as well as the BP belt and idlers

Besides the BP belt itself, especially the bulk material, and furthermore also the idlers – as set up as dynamically interacting components (thus correspondingly comprising mass (inertia) characteristics) – are furthermore influencing the result/behaviour that is revealed by such a belt breakage simulation as shown.

Concluding remark on the examples presented

These representative examples shown before distinctly demonstrated the application of the methodology for dynamic belt simulation presented in this thesis.

Besides insights into various modelling details, such as regarding the use of fibred BP belts or moveable (MBD) idler systems, also computation-related details were stated, which particularly revealed beneficial aspects of using the presented methodology, such as especially the BP belt initialisation in almost-final state, as pre-simulation phases resulted as significantly minor for each simulation example.

In addition, the comprehensive overview given in terms of system analysis methods showed a broad range of enhanced analysis opportunities that are enabled explicitly by the application of this presented belt simulation methodology.

More application potentials of the presented methodology, also beyond the so-far covered scope, are outlined in the outlook following in the next chapter.

Chapter 6

Outlook

To provide a structured overview of the following outlook, potential follow-up work associated with the presented methodology is categorised into five major groups, which relate to different perspectives considered:

- Developer's perspective: Development of additional advancements and methods that further extend the methodology
- Calibration-related perspective: Performing parameter determinations of specifically given types of belts, and also possible development of methods for this purpose
- Engineer's perspective: Application of the methodology on various types of belt systems, further with the purpose to achieve insights into specific systems (virtual prototyping)
- Innovative perspective: Applying/adopting the methodology or certain parts of it to other areas outside of the scope covered in this thesis
- Software developer's perspective: Implementation of developed algorithms by third-party software developers

The following sections describe the outlook in the order of the bullet points mentioned above.

Advancements and methods

Two selected advancements/methods with significant potential for enhancing the presented methodology are outlined in the following.

The first of these potential enhancements concern the initialisation of bulk material particles to form a bulk material flow in motion. With a corresponding initialisation method, it would be possible to not only initialise an already running belt conveyor system (as with the BP belt initialised in almost-final state with additional belt velocity applied) but an already running and also filled conveyor system, thus a system in (almost) operating state. General approaches for this purpose were principally already dealt with, such as also addressed in previous publications (e.g. Fimbinger (2019) [86]) and as basically also applied in the simulation setup for the simulation of belt breakage (Chapter 5.7). However, a supportive method allowing convenient initialisation of already moving bulk material particles would be beneficial (e.g., based on using a CAD model containing a bulk material volume representing geometry).

The second potential enhancement regards modelling additional elements to a converted BP belt, such as to extend the belt model to represent a cleated belt. This is principally possible with manual adaptations, specifically by replacing belt particles within a converted BP belt (e.g. the particles along a transverse row, as to achieve a transversely oriented cleat) with specific cleat-representing particles. Such cleat-representing particles can be made as compound particles, with the initial cuboid as the base element, to which another cleat-representing cuboid is added (i.e. forming a T-shaped compound of two cuboids).

Several further developments may also relate to extending DEM model adaptations, such as regarding particle contact or bonding behaviour, e.g. the implementation of a specifically adopted bonding breakage model for belt breakage simulations.

Parameter determination

In order to depict a specific type of physical belt that is intended to be represented as a digitally modelled BP belt, another major follow-up relates accordingly to the determination/calibration of the parameters that define such a BP belt’s behaviour.

Several aspects in this regard were already outlined previously in corresponding sections of the presented thesis, such as specifically in Chapter 4.1.1.4, regarding particle-related parameters, and in Chapter 4.1.2.4, regarding bonding-related parameters.

Virtual prototyping

The general intention of the methodology provided is its application on belt systems to allow their virtual analysis, especially by enabling the dynamically interacting/deforming BP belt as introduced.

This relates, for example, to virtual prototype analyses of novel and especially complex belt conveyor systems, furthermore to design studies for comparing different system variants in terms of certain effects, or also for optimisation purposes as in terms of particular effects (e.g. to (re)position belt-guiding idlers beneficially).

Application for alternative purposes

Several alternatives for applying the presented methodology were already addressed throughout this thesis, such as regarding the modelling of BP ropes, as addressed in Chapter 4.2.5, section F, which returns only a single bonded particle fibre from a BP belt conversion (a BP rope), correspondingly in a pre-deformed state. This further relates to applications with deformable (and furthermore pre-deformed) ropes/cords/cables, etc., and further to the modelling of complex woven structures (e.g. to set up fences/nets or similar structures by using such BP ropes).

Nets and similar open-surface structures were initially introduced in basic modelling approaches in Chapter 3.1.2.3.2, for which bonded-particle modelling was described as already well-established. For such applications, especially the initialisation method (almost-final state initialisation) shows potential benefits, as generally allowing the initialisation of such bonded-particle structures in complex shapes, also with considering pre-deformations correspondingly (i.e., relating to the capability of almost-final state initialisation of BP nets). In this context, a relatively simple principle for transforming a BP belt into an open-structured model is proposed: By (systematically) deleting specific particles from a converted BP belt model, this initially closed-structured model can be turned into an open-structured bonded-particle setup, further for representing a (rectangular) net.

Furthermore, the presented method of CAD-to-DEM conversion principally also suggests application on various other components than belts, which would further extend the applicational spectrum of the introduced conversion method fundamentally (and which generally also relates to the modelling of structures related to continuous mechanics by using the proposed approaches of the presented methodology).

Relatively trivial applications with models differing from conventionally intended belt structures were already addressed in terms of conversion/initialisation without including a pre-deformation state in Chapter 4.2.5, section G (e.g. regarding shields, tubes, bellows, etc.). Accordingly, it is generally also possible to use the developed software tool to convert objects of belt-like form (i.e. finite/endless geometries) into bonded-particle structures without additional pre-deformation conditions included.

Moreover, combining more than one belt-like sub-elements into a unified bonded-particle structure is principally also possible, specifically by merging the sub-elements after their individual conversion (from CAD to BP models). Therefore, the individual BP models (each created by using the software tool BeltConverter) are merged by adding bondings to connect those models to form one large BP model. If no additional pre-deformations are required to be included, the creation of these additional bondings only requires the IDs of each two opposing particles to be bonded. A simple example for such a combined setup is a box or a box-shaped bag, which would be modelled by four outer sides and one bottom, converted each as a BP model, and which are further connected at the edges to result in a closed box. Due to the bonded-particle setup, such a model then allows reactions/deformations when filled with particles or also due to other loads (e.g. during its handling).

Implementation of the algorithms by third-party software developers

A further increase in the convenience of using the methodology would be the availability of the presented algorithm(s), thus their associated capabilities, directly within DEM simulation software. This specifically addresses the conversion algorithm to create a BP belt from a respective CAD model (STL file) and further the algorithm to create cylindrical primitives (parts/particles) from another respective CAD model (SAT file). With this perspective already in mind, the relevant numerics are provided in this thesis with a corresponding level of detail.

Chapter 7

Summary & Conclusion

This thesis presented a methodology for enabling dynamically interacting belt models in Discrete Element Method (DEM) simulations, opposed to conventional DEM simulations with belts modelled as rigid surfaces.

Basics of the DEM and of belt conveyor systems, particularly with respect to systems related to dynamic belt behaviour, were given at the beginning, followed by a comprehensive elaboration on general approaches for modelling dynamically interactive/flexible (i.e. dynamically deformable) belt-like objects for DEM simulation applications. These general modelling approaches were further supplemented by principles for initialising and assembling deformable belt models into specific DEM simulation setups. Based on these considerations, the approaches that fundamentally form the basis of the present methodology were specified:

- DEM-based belt modelling using a bonded-particle belt model (BP belt), and
- belt initialisation in almost-final state; i.e. initialising a BP belt in a pre-deformed state – with a shape approximated to the assembled form of a belt, as estimated to occur within a specific system – generally with the intention to omit complex, and above all, effortful (virtual) processes for assembling such belt models into DEM simulation setups (pre-simulation).

As forming the core elements of the developed methodology, these two areas (structural belt setup and belt initialisation) were accordingly described in detail.

The structural belt setup presented the modelling systematics for setting up BP belts in general. Thereby, such belt models were defined as consisting of a single layer of rectangularly arranged, cuboidal-shaped bonded (belt) particles with rounded edges, further with inner-belt contacts deactivated, thus allowing these belt particles to overlap without contact effects resulting between them. This setup was specifically introduced to allow the representation of a smoothened belt surface. Furthermore, inner-belt contacts were also specified to support adaptations as to enable specific belt-self-contact, such as for pipe-forming of the belt in pipe conveyor systems. The bondings connecting the belt particles were defined using an enhanced bonding model, specifically for representing belt-typical flexibility characteristics (stiff at tension whilst flexible at bending), and also, modelling of anisotropic/inhomogeneous belt characteristics were made possible by using fibred BP belt structuring (enabling the definition of varying bondings within a BP belt).

For belt initialisation, more precisely for almost-final state BP belt initialisation, a developed algorithm that enables CAD-to-DEM belt conversion was presented. To allow convenient use, this algorithm was further implemented into a software tool, BeltConverter. The addressed CAD-to-DEM belt conversion describes the conversion of a given CAD belt into a DEM (BP) belt model, with the CAD belt model (as an STL file) providing a certain belt geometry intended to be initialised as a BP belt; thus, typically representing a specific near-assembled belt shape. The developed conversion algorithm accordingly considers and includes pre-deformation information so that a correspondingly pre-deformed BP belt is computed in the shape of the provided CAD belt model. Moreover, the definition of specific belt pre-tensioning and adding of initial belt velocity was implemented to be considered/included. Ultimately, the computed BP belt is exported in INP data format, allowing the initialisation of the BP belt into a specific simulation setup of a belt system; further, enabling dynamic belt simulation with an accordingly pre-deformed and already running BP belt.

The developed conversion algorithm was described in detail, with the general intention to enable its reproduction or also use/adaption of certain parts.

The main essential modules of this algorithm for CAD-to-DEM belt conversion were described as basically comprising: import and preparation of CAD data, computation

of particle and bonding states, applying additional initial belt velocity, and export as further usable DEM data (INP file).

Furthermore, the usage of the developed software tool BeltConverter was explained; moreover, including several enhancing options/features that were additionally developed, such as allowing BP rope conversion.

With relation to these two core parts of the methodology (structural setup and almost-final initialisation of BP belts), relaxation-simulation examples were performed, which generally proofed BP belt initialisation successfully, as those examples each illustrated a correct relaxation of a specifically (complex-shaped) initialised BP belt into a corresponding state-of-rest.

In addition to the two core parts, a further methodology-extending method for using smooth-surfaced cylinders was also introduced. This extending method explains the use of numerically smooth parts/particles for cylindrical components, such as idlers or pulleys, which is thus particularly beneficial for belt (conveyor) system simulation with BP belt models that interact with those components accordingly. The use of such numerically smooth cylinders, generally represented as mathematical primitive cylinders, supplants the use of triangulated cylinders for such system components, thus manifesting significant benefits. To support the process of modelling such smooth-surfaced cylinders in DEM simulation setups, especially in larger quantities, a software tool, PartConverter, for the conversion of CAD models containing cylindrical geometries (i.e. representing idlers/pulleys; provided via an assembly (SAT) file) into corresponding DEM data (INP file, allowing initialisation of those provided geometries as (smooth-surfaced) cylindrical parts/particles) was developed and presented.

The effectiveness of the methodology developed was underlined by several different exemplary, industry-relating applications for dynamic belt simulation, covering: a conventional belt conveyor, a belt turnover station, a sandwich conveyor, a pipe conveyor, the belt system of a round hay baler, and belt breakage.

These exemplary applications particularly highlighted the benefits associated with the methodology, such as in terms of enabling convenient modelling or in terms of

the computational efforts required, and ultimately revealed the methodology's favourable suitability for DEM simulations with dynamically interacting/deformable belt models.

The developed methodology proved several advantages, especially in terms of:

- modelling, simulation, and analysis of belt-like objects as dynamically deformable/interacting models in DEM simulations,
- enabling dynamic belt simulation for application-oriented, i.e., relatively complex and furthermore relatively large/application-scaled, belt systems,
- reducing related efforts significantly, as basically associated with:
    - using a BP belt (thus staying within the DEM simulation environment, which is generally positive in terms of modelling and software/solver-related aspects, in terms of usability in general, and which furthermore revealed positive results in terms of computational efforts required,
    - using belt initialisation in almost-final state (which significantly reduces pre-simulation efforts, generally to almost imperceptible levels),
    - using smooth-surfaced cylinders (which positively affects computational efforts),
    - using the developed software tools, BeltConverter and PartConverter, as supportive tools for the modelling of DEM simulation setups with dynamically deformable belt models as BP belts.

In final conclusion, the developed methodology presented in this thesis is not only very promising for application in the development of belt conveyors systems using DEM simulation comprising dynamically interacting/deformable belt models, but also for applications far beyond this scope of conveyor belts.

Directories

Abbreviations

1/2/3D	one/two/three-dimensional
6DoF	six degrees of freedom
ASCII	American Standard Code for Information Interchange
BP	bonded-particle
BP belt	bonded-particle belt (model)
BPM	bonded-particle model
CAD	computer-aided design
CAE	computer-aided engineering
cf.	compare (to) (confer)
DE	discrete elements (particles)
DEM	Discrete Element Method (also Distinct Element Method)
dir.	direction(s)
e.g.	for example (exempli gratia)
Eq.	Equation(s)
FDEM	Finite-Discrete Element Method
FEA	Finite Element Analysis
FEM	Finite Element Method
GUI	graphical user interface
i.e.	which means/in other words (id est)
INP	ThreeParticle/CAE input (file format)

long.	longitudinal
MBD	multibody dynamics
MD	Molecular Dynamics
PFEM	Particle Finite Element Method
ref.	referring (to)
RGB	red green blue (colour model)
rlt.	relating (to)
SAT	ACIS Standard Text (file format)
SPH	Smoothed-Particle Hydrodynamics
STL	Standard Triangle/Tessellation Language (file format)
TBBM	Timoshenko beam bond model
transv.	transverse
XDEM	a specific extended form of the DEM

List of References

[1] 3D SYSTEMS, INC. StereoLithography Interface Specification.:. 1988.

[2] 3D SYSTEMS, INC. StereoLithography Interface Specification.:. 1989.

[3] AI, J., J.-F. CHEN, J.M. ROTTER, and J.Y. OOI, *Assessment of rolling resistance models in discrete element simulations. . Powder Technology.* 2011.:206, 269-282. Available from: doi:10.1016/j.powtec.2010.09.030

[4] ALDER, B.J., and T.E. WAINWRIGHT, *Studies in Molecular Dynamics. I. General Method. . The Journal of Chemical Physics.* 1959.:31, 459-466. Available from: doi:10.1063/1.1730376

[5] ANDRÉ, D., I. IORDANOFF, J. CHARLES, and J. NÉAUPORT, *Discrete element method to simulate continuous material by using the cohesive beam model. . Computer Methods in Applied Mechanics and Engineering.* 2012.:213-216, 113-125. Available from: doi:10.1016/j.cma.2011.12.002

[6] ANSYS, INC. Ansys [software]. Version 2020 R1. 2020.Available from: https://www.ansys.com/

[7] ANSYS, INC. Ansys Mechanical [software]. Version 2020 R1. 2020.Available from: https://www.ansys.com/products/structures/ansys-mechanical

[8] ÅSTRÖM, J.A., and H.J. HERRMANN, *Fragmentation of grains in a two-dimensional packing. . The European Physical Journal B.* 1998.:5, 551-554. Available from: doi:10.1007/s100510050476

[9] AUTODESK. Inventor [software]. Version 2020. 2020.Available from: https://www.autodesk.de/products/inventor

[10] BECKER, Alexander. API Guide.*(ThreeParticle Simulation).* ThreeParticle 2019 R4.0.:. 2019.

[11] BECKER, Alexander. Examples Overview.*(ThreeParticle Simulation).* ThreeParticle 2019 R4.0.:. 2019.

[12] BECKER, Alexander. Keywords Guide.*(ThreeParticle Simulation).* ThreeParticle 2019 R4.0.:. 2019.

[13] BECKER, Alexander. User Guide.*(ThreeParticle Simulation).* ThreeParticle 2019 R4.0.:. 2019.

[14] BECKER, Alexander. *Training - Discrete Element Method. ThreeParticle Simulation.* Presentation/training documents module 2. Villach, Austria, 2020.

[15] BECKER, Alexander. *Training - Introduction to ThreeParticle/CAE. ThreeParticle Simulation.* Presentation/training documents module 1. Villach, Austria, 2020.

[16] BECKER, Alexander and Eric FIMBINGER. Development study/workshop for advancements in DEM.*(An adapted bonding model - development and implementation in ThreeParticle/CAE).* (documented in corresponding notes/e-mail).:. 17 March 2017.

[17] BECKER 3D GMBH. ThreeParticle/CAE [software]. Version 2019 R4.1.0 (RC). 2020.Available from: http://becker3d.com/

[18] BELYTSCHKO, T., and S.P. XIAO, *Coupling Methods for Continuum Model with Molecular Model. . International Journal for Multiscale Computational Engineering.* 2003.:1, 12. Available from: doi:10.1615/IntJMultComPEng.v1.i1.100

[19] BEN-ARI, Moti. A Tutorial on Euler Angles and Quaternions.. Version 2.0.1.:. 2017.

[20] BENVENUTI, Luca. *Particle Simulation with Rocky DEM. CADFEM GmbH - Part 1.* Weimar, 2018. 15th Weimar Optimization and Stochastic Days 2018 (WOST 2018) - Infoday.

[21] BERGSTRÖM, Per. *Modelling Mechanics of Fibre Network using Discrete Element Method.* Dissertation. Sundsvall, Sweden, 2018.

[22] BERTRAND, D., F. NICOT, P. GOTTELAND, and S. LAMBERT, *Discrete element method (DEM) numerical modeling of double-twisted hexagonal mesh. . Canadian Geotechnical Journal.* 2008.:45, 1104-1117. Available from: doi:10.1139/T08-036

[23] BEUMER GROUP GMBH & CO. KG. *Pipe Conveyor* [online]. *Transport for Linz AG* [viewed 31 May 2019].Available from: www.beumergroup.com/en/pipe-conveyor/references/power-industry/alternative-fuel-handling

[24] BIALOWAS, Jakob. *Parameterfindung zur Simulation eines Fördergurtes mit Hilfe der Diskreten Elemente Methode.* Bachelor thesis. Leoben, Austria, 2017.

[25] BIERWISCH, C., R. SCHUBERT, T. KRAFT, and C. DEHNING. Discrete and finite element co-simulations.*(Modelling approach and application perspectives). PARTEC 2016. International Congress on Particle Technology.* Nuremberg, Germany: Düsseldorf VDI Verlag GmbH, 2016.

[26] BIERWISCH, Claas. *Numerical Simulations of Granular Flow and Filling.* Dissertation. Freiburg (Breisgau), Germany, 2009.

[27] BOURRIER, F., F. KNEIB, B. CHAREYRE, and T. FOURCAUD, *Discrete modeling of granular soils reinforcement by plant roots. . Ecological Engineering.* 2013.:61, 646-657. Available from: doi:10.1016/j.ecoleng.2013.05.002

[28] BROWN, N.J., J.-F. CHEN, and J.Y. OOI, *A bond model for DEM simulation of cementitious materials and deformable structures. . Granular Matter.* 2014.:16, 299-311. Available from: doi:10.1007/s10035-014-0494-4

[29] BROWN, Nicholas J., John P. MORRISSEY, Jin Y. OOI, and Jian-Fei CHEN. EDEM Contact Model: Timoshenko Beam Bond Model.:. 2015.

[30] CASTRO-FILGUEIRA, U., L.R. ALEJANO, J. ARZÚA, and D.M. IVARS, *Sensitivity Analysis of the Micro-Parameters Used in a PFC Analysis Towards the Mechanical Properties of Rocks. . Procedia Engineering.* 2017.:191, 488-495. Available from: doi:10.1016/j.proeng.2017.05.208

[31] CHEN, Jian. *Discrete Element Method for 3D Simulations of Mechanical Systems of Non-Spherical Granular Materials.* Dissertation. Chofu, Japan, 2012.

[32] CHENG, J., T. REN, Z. ZHANG, D. LIU, and X. JIN, *A Dynamic Model of Inertia Cone Crusher Using the Discrete Element Method and Multi-Body Dynamics Coupling. . Minerals.* 2020.:10, 862. Available from: doi:10.3390/min10100862

[33] CONTINENTAL AG. *Closed-Trough Conveyor Belts Ensure Energy-Efficient and Low-Dust Coal Transport in China.* (Press Release: 2019-05-29). Hanover, Germany, 8 Oct. 2020.

[34] CONTINENTAL AG. *Plylon Plus* [online]. *Textile Conveyor Belts* [viewed 17 June 2021].Available from: https://www.continental-industry.com/en/solutions/conveyor-belt-systems/material-handling/textile-conveyor-belts/products/product-range/plylon-plus-belts

[35] CONTITECH TRANSPORTBANDSYSTEME GMBH (PART OF CONTINENTAL AG) (ContiTech). *Fördergurte Berechnungen:*5. Auflage. Hannover, Germany: Continental AG, 2013.

[36] CONTITECH TRANSPORTBANDSYSTEME GMBH (PART OF CONTINENTAL AG) (ContiTech). SICON®.*(Enclosed Belt Conveyor System).* (Brochure).:. 2014 [viewed 10 September 2020].Available from: https://www.continental-industry.com/getmedia/ceea3769-6b32-4853-917d-bd7c8f1fbce7/CBG6238-En-Sicon.pdf

[37] CONTITECH TRANSPORTBANDSYSTEME GMBH (PART OF CONTINENTAL AG) (ContiTech). *Pouch Conveyor Belts* [online]. *Clean, safe and able to negotiate curves of up to 180°* [viewed 9 October 2020].Available from: https://www.continental-industry.com/en/solutions/conveyor-belt-systems/material-handling/enclosed-conveyor-belts/products/product-range/pouch-conveyor-belts

[38] CONVEYOR EQUIPMENT MANUFACTURERS ASSOCIATION (CEMA). *Belt Conveyors for Bulk Materials. The Voice of the Conveyor Industry of the Americas:*Seventh edition. Naples, Florida, USA: Conveyor Equipment Manufacturers Association, 2014. ISBN 978-1-891171-44-4.

[39] COUCH, Brian. *A Coupled Model for Material Flexure Resistance in Belt Conveyor Systems.* Dissertation. Callaghan, NSW, Australia, 2016.

[40] CR WILLCOCKS. *New Holland Roll-Belt 180 Round Baler* [online] [viewed 12 October 2020].Available from: https://www.crwillcocks.co.uk/agriculture/new-agriculture/harvest-machinery/round-balers/new-holland-roll-belt-180-round-baler

[41] CREMONESI, M., A. FRANCI, S. IDELSOHN, and E. OÑATE, *A State of the Art Review of the Particle Finite Element Method (PFEM). . Archives of Computational Methods in Engineering.* 2020.:27, 1709-1735. Available from: doi:10.1007/s11831-020-09468-4

[42] CUNDALL, P.A., and R.D. HART, *Numerical modelling of discontinua. . Engineering Computations.* 1992.:9, 101-113. Available from: doi:10.1108/eb023851

[43] CUNDALL, P.A., and O.D.L. STRACK, *A discrete numerical model for granular assemblies. . Géotechnique.* 1979.:29, 47-65. Available from: doi:10.1680/geot.1979.29.1.47

[44] DASSAULT SYSTEMES, SIMULIA, ABAQUS INC. Abaqus [software]. Version 2020. 2020.Available from: https://www.3ds.com/products-services/simulia/products/abaqus/

[45] DAU, F., J. GIRARDOT, and B.D. LE, *A Promising Way to Model Damage in Composite and Dry Fabrics Using a Discrete Element Method (DEM). . Applied Mechanics and Materials.* 2016.:828, 119-136. Available from: doi:10.4028/www.scientific.net/AMM.828.119

[46] DCS COMPUTING AND CFDEMRESEARCH. LIGGGHTS [software]. Version 3.8.0. 2017.Available from: https://www.cfdem.com/liggghtsr-open-source-discrete-element-method-particle-simulation-code

[47] DE BONO, J., and G. MCDOWELL, *Particle breakage criteria in discrete-element modelling. . Géotechnique.* 2016.:66, 1014-1027. Available from: doi:10.1680/jgeot.15.P.280

[48] DE BONO, J., G. MCDOWELL, and D. WANATOWSKI, *Discrete element modelling of a flexible membrane for triaxial testing of granular material at high pressures. . Géotechnique Letters.* 2012.:2, 199-203. Available from: doi:10.1680/geolett.12.00040

[49] DEL COZ DÍAZ, J.J., P.J. GARCÍA NIETO, J.A. VILÁN VILÁN, A. MARTÍN RODRÍGUEZ, J.R. PRADO TAMARGO, and A. LOZANO MARTÍNEZ-LUENGAS, *Non-linear analysis and warping of tubular pipe conveyors by the finite element method. . Mathematical and Computer Modelling.* 2007.:46, 95-108. Available from: doi:10.1016/j.mcm.2006.12.034

[50] DEM SOLUTIONS LTD. Theory Reference Guide.*(EDEM)*:. 2014.

[51] DEM SOLUTIONS LTD. EDEM [software]. Version 2019. 2018.Available from: https://www.edemsimulation.com/

[52] DI RENZO, A., and F.P. DI MAIO, *An improved integral non-linear model for the contact of particles in distinct element simulations. . Chemical Engineering Science.* 2005.:60, 1303-1312. Available from: doi:10.1016/j.ces.2004.10.004

[53] DIN 22101:2011-12, *Stetigförderer - Gurtförderer für Schüttgüter - Grundlagen für die Berechnung und Auslegung. (Continuous conveyors - Belt conveyors for loose bulk materials - Basis for calculation and dimensioning).* Berlin, Germany. *Beuth Verlag GmbH. Available from:* https://www.beuth.de/de/norm/din-22101/145598666

[54] DIN 315:2016-12, *Mechanische Verbindungselemente - Flügelmuttern - Runde Flügelform. (Fasteners - Wing nuts - Rounded wings).* Berlin, Germany. *Beuth Verlag GmbH. Available from:* https://www.beuth.de/de/norm/din-315/263644532

[55] DIN 6799:2017-06, *Sicherungsscheiben (Haltescheiben) für Wellen. (Retaining washers for shafts).* Berlin, Germany. *Beuth Verlag GmbH. Available from:* https://www.beuth.de/de/norm/din-6799/272887976

[56] DIN EN ISO 4762:2004-06, *Zylinderschrauben mit Innensechskant. (Hexagon socket head cap screws).* Berlin, Germany. *Beuth Verlag GmbH. Available from:* https://www.beuth.de/de/norm/din-en-iso-4762/68034695

[57] DONZE, F., V. RICHEFEU, and S.-A. MAGNIER. Advances in discrete element method applied to soil, rock and concrete mechanics.. *Electronic Journal of Geotechnical Engineering.* 2009.:8,

[58] DOS SANTOS, J.A. High angle conveying the vital (missing) link to IPCC systems.. *Australian Bulk Handling Review – ABHR.* 2013.:18 No 4, 44-53.

[59] DOS SANTOS, J.A., and E.M. FRIZZELL. Evolution of sandwich belt high-angle conveyors.. *CIM Bulletin.* 1983.:76, 51-66.

[60] DOS SANTOS INTERNATIONAL. The Cost/Value of High Angle Conveying.:. 2016.

[61] DOUBRAVA INDUSTRIEANLAGENBAU GMBH (PART OF CHRISTOF INDUSTRIES). Doppelgurtförderer.*(Double Belt Conveyor).* (Brochure).:. 2016 [viewed 10 August 2020].Available from: https://www.christof.com/wp-content/uploads/2016/06/doubrava_Doppelgurtfoerderer.pdf

[62] DOUBRAVA INDUSTRIEANLAGENBAU GMBH (PART OF CHRISTOF INDUSTRIES). *Double Belt Conveyors* [online] [viewed 8 October 2020].Available from: https://www.doubrava.at/en/conveying-technology/components/double-belt-conveyors/

[63] DRATT, M., and A. KATTERFELD, *Coupling of FEM and DEM simulations to consider dynamic deformations under particle load. . Granular Matter.* 2017.:19:49. Available from: doi:10.1007/s10035-017-0728-3

[64] DRATT, M., A. KATTERFELD, and C. WHEELER. Determination of the bulk flexure resistance via coupled FEM-DEM simulation.. *International Conference for Conveying and Handling of Particulate Solids (CHoPS2015).* Tel Aviv, Israel, 2015.

[65] DRATT, Mathias. *Kopplung von FEM- und DEM-Simulationen zur Analyse der Gut-Bauteil-Interaktion in der Fördertechnik.* Dissertation:1. Auflage. Magdeburg: Logisch GmbH, Magdeburg, 2016. ISBN 978-3-930385-97-3.

[66] DRÖTTBOOM, Marcel. Rulmeca: Improved Line of Conveyor Belt Idlers with new Frame Design.. News from industry. *bulk-online.* :. 3 April 2019 [viewed 18 June 2021].Available from: https://news.bulk-online.com/news-english/rulmeca-improved-line-of-conveyor-belt-idlers-with-new-frame-design.html#comments

[67] DUNLOP. *Conveyor Belt Technique. Design and Calculation,* 2014.

[68] DYNA ENGINEERING. *Idler Sets* [online] [viewed 18 June 2021].Available from: https://www.dynaeng.com.au/dyna/product/idler-sets/

[69] EFFEINDZOUROU, A., B. CHAREYRE, K. THOENI, A. GIACOMINI, and F. KNEIB, *Modelling of deformable structures in the general framework of the discrete element method. . Geotextiles and Geomembranes.* 2016.:44, 143-156. Available from: doi:10.1016/j.geotexmem.2015.07.015

[70] EFFEINDZOUROU, A., K. THOENI, A. GIACOMINI, and C. WENDELER, *Efficient discrete modelling of composite structures for rockfall protection. . Computers and Geotechnics.* 2017.:87, 99-114. Available from: doi:10.1016/j.compgeo.2017.02.005

[71] EFFEINDZOUROU, Anna Makouala. *Numerical investigation of the energy absorption capacity of rockfall protection measures for underground portals.* Dissertation. Callaghan, NSW, Australia, 2016.

[72] ÉLECTRICITÉ DE FRANCE (EDF). Code_Aster [software]. Version 14.4. 2019.Available from: https://www.code-aster.org/

[73] ELISHAKOFF, I., *Who developed the so-called Timoshenko beam theory? . Mathematics and Mechanics of Solids.* 2020.:25, 97-116. Available from: doi:10.1177/1081286519856931

[74] ESI ITI GMBH. SimulationX [software]. Version 4.1. 2019.Available from: https://www.simulationx.com/

[75] ESI ITI GMBH. *Simulating Belt Conveyor Systems* [online]. SimulationX [viewed 8 September 2020].Available from: https://www.simulationx.com/industries/applications/belt-conveyor-systems.html

[76] ESSS. Rocky [software]. Version 4.3. 2019.Available from: https://rocky.esss.co/

[77] FEDORKO, G., and V. IVANČO, *Analysis of Force Ratios in Conveyor Belt of Classic Belt Conveyor. . Procedia Engineering.* 2012.:48, 123-128. Available from: doi:10.1016/j.proeng.2012.09.494

[78] FEDORKO, G., V. IVANČO, V. MOLNÁR, and N. HUSÁKOVÁ, *Simulation of Interaction of a Pipe Conveyor Belt with Moulding Rolls. . Procedia Engineering.* 2012.:48, 129-134. Available from: doi:10.1016/j.proeng.2012.09.495

[79] FEDORKO, G., and V. MOLNAR, *Design of a calculation fem model of the test static stand of pipe conveyor for analysis of contact forces. . Advances in Science and Technology Research Journal.* 2017.:11, 220-225. Available from: doi:10.12913/22998624/71268

[80] FEECO INTERNATIONAL. Conveyor Systems.. (Brochure).:. 2019 [viewed 10 December 2020].Available from: https://feeco.com/download/6099/

[81] FENNER DUNLOP. Enerka Becker® System.*(Closed Conveyor).* (Brochure).:. 2005 [viewed 10 September 2020].

[82] FIMBINGER, E. Fördergurtsimulation - Entwicklungen und Anwendung der Methodik zur Simulation von Fördergurten mittels der DEM.. In: Johannes Fottner, Willibald A. Günthner, André Katterfeld, and Friedrich Krause, eds. *23. Fachtagung Schüttgutfördertechnik 2018 : Tagungsbericht. Herausgegeben als Begleitband zur gleichnamigen Fachtagung am Lehrstuhl für Fördertechnik Materialfluss Logistik der Technischen Universität München in Garching.* Garching: fml - Lehrstuhl für Fördertechnik Materialfluss Logistik Fakultät für Maschinenwesen Technische Universität München, 2018. ISBN 978-3-941702-95-0, pp. 19-42.

[83] FIMBINGER, E., *Fördertechnik digitalisieren und virtualisieren. .* 3D-Simulation. *Schüttgut.* 2018.:24, 22-24.Available from: https://www.process.vogel.de/foerdertechnik-digitalisieren-und-virtualisieren-a-782154/

[84] FIMBINGER, E. Simulation von Fördergurten mittels der DEM.. In: Oliver Langefeld, ed. *8. Kolloquium Fördertechnik im Bergbau : Tagungsband.* Clausthal-Zellerfeld, Germany: Papierflieger Verlag GmbH, 2018. ISBN 978-3-86948-621-5, pp. 121-133.

[85] FIMBINGER, E. Belt Turnover Simulation.*(Applying the developed belt simulation methodology to analyse the behaviour of conveyor belts in belt turnover stations.). Chair of Mining Engineering, Mineral Economics and Conveying Technology. Research, Innovation and Education - Service for the Industry.* Brochure. Leoben, 2019, p. 34.

[86] FIMBINGER, E. Dynamic Conveyor Belt Simulation using the Discrete Element Method.. In: Mark Jones, ed. *13th International Conference on Bulk Materials Storage, Handling and Transportation ICBMH 2019 : Conference Proceedings.* 9-11 July 2019. Barton, ACT, Australia: The Institution of Engineers Australia, 2019. ISBN 978-1-925627-29-9, (enclosed pdf).

[87] FIMBINGER, E. Dynamische DEM-Gurtsimulation und deren Anwendung für Förderanlagen.. In: Günter Busse, ed. *15. Fachtagung Gurtförderer und deren Elemente: mit Exkursion DMT Brandversuchsanlage.* Tagung Nr. H040035249. Essen, Germany: Haus der Technik e.V. (hdt), 2019, 9.1-9.15.

[88] FIMBINGER, E. Methodology for the Simulation of Conveyor Belts Using the Discrete Element Method.. *NAFEMS World Congress 2019 : Summary of Proceedings. A World of Engineering Simulation.* Québec City, Canada: NAFEMS, 2019. ISBN 978-1-910643-52-5, 94-95 (enclosed pdf NWC19-235).

[89] FIMBINGER, E. Numerical Simulation in Conveying Technology.. *Rema Tip Top International Sales Meeting with in-house exhibition.* Munich, Germany: Rema Tip Top, 2019.

[90] FIMBINGER, E. Methodik zur Simulation dynamischer Gurtsysteme an Rundballenpressen mittels der DEM.. *1. Tagung SIMULAND 2020. Simulation landtechnischer Prozesse.* Düsseldorf, Germany: Jahr, Andreas; Batos, Andrej, 2020. ISBN 978-3-941334-30-4, pp. 93-117.

[91] FIMBINGER, E., *Berücksichtigung verformbarer Fördergurte in DEM-Simulationen. . BHM (Berg- und Hüttenmännische Monatshefte).* 2021.:166, 82-94. Available from: doi:10.1007/s00501-021-01078-2

[92] FIMBINGER, Eric. *Simulation von Fördergurten mittels der DEM.* Presentation. Clausthal-Zellerfeld, Germany, 31 Jan. 2018. 8. Kolloquium Fördertechnik im Bergbau.

[93] FIMBINGER, Eric. *Fördergurtsimulation - Entwicklungen und Anwendung der Methodik zur Simulation von Fördergurten mittels der DEM.* Presentation. Garching, Germany, 19 Sep. 2018. 23. Fachtagung Schüttgutfördertechnik 2018.

[94] FIMBINGER, Eric. BeltConverter [software]. Version v1.03 beta. 2019.Available from: https://github.com/Fimbinger/BeltConverter

[95] FIMBINGER, Eric. PartConverter [software]. Version v1.03 beta. 2019.Available from: https://github.com/Fimbinger/PartConverter

[96] FIMBINGER, Eric. *Dynamische DEM-Gurtsimulation und deren Anwendung für Förderanlagen.* Presentation. Essen, Germany, 13 Mar. 2019. 15. Fachtagung Gurtförderer und deren Elemente.

[97] FIMBINGER, Eric. *Methodology for the Simulation of Conveyor Belts Using the Discrete Element Method.* Presentation in the Session: 3H Discrete Element Method 1. Québec City, Canada, 18 Jun. 2019. NAFEMS World Congress 2019.

[98] FIMBINGER, Eric. *Dynamic Conveyor Belt Simulation using the Discrete Element Method.* Presentation in the Session: Belt Conveying - Design. Gold Coast, Queensland, Australia, 9 Jul. 2019. 13th ICBMH 2019 (International Conference on Bulk Materials Storage, Handling and Transportation).

[99] FIMBINGER, Eric. ParticleGenerator [software]. Version v1.04 beta. 2020.Available from: https://github.com/Fimbinger/ParticleGenerator

[100] FIMBINGER, Eric. *Discrete Element Belts and Their Initialisation in Almost-Final State.* Presentation in the Mini-Symposium: Particle-Based Methods (DEM; PFEM; SPH; MPM; MPSI and others), MS114. Virtual Congress, 11 Jan. 2021.

14th WCCM&ECCOMAS2020 (World Congress on Computational Mechanics & European Congress on Computational Methods in Applied Sciences and Engineering).

[101] FRAUNHOFER IWM. SimPARTIX [software]. 2020.Available from: https://www.simpartix.com/

[102] FRAUNHOFER SCAI. MpCCI [software]. 2020.Available from: https://www.mpcci.de/

[103] FRAUNHOFER SCAI AND FRAUNHOFER IWM. *Struktur-Struktur-Interaktion mit reversibel elastischen Strukturen* [online]. Reversibel-elastische Strukturen [viewed 11 June 2021].Available from: https://www.scai.fraunhofer.de/de/geschaeftsfelder/meshfree-multiscale-methods/coupled-particle-and-finite-element-simulations/applications/struktur-struktur-interaktion-mit-reversibel-elastischen-struktu.html

[104] GEUZAINE, C., and J.-F. REMACLE, *Gmsh. (A 3-D finite element mesh generator with built-in pre- and post-processing facilities). International Journal for Numerical Methods in Engineering.* 2009.:79, 1309-1331. Available from: doi:10.1002/nme.2579

[105] GHASEMI, M.A., and S.R. FALAHATGAR, *Discrete element simulation of damage evolution in coatings. . Granular Matter.* 2020.:22. Available from: doi:10.1007/s10035-020-0997-0

[106] GINGOLD, R.A., and J.J. MONAGHAN, *Smoothed particle hydrodynamics: theory and application to non-spherical stars. . Monthly Notices of the Royal Astronomical Society.* 1977.:181, 375-389. Available from: doi:10.1093/mnras/181.3.375

[107] GITHUB, INC. *GitHub* [online]. *The world's leading software development platform - GitHub.* Built for developers [viewed 12 August 2020].Available from: https://github.com/

[108] GOODYEAR BELTING PTY. LTD, GOODYEAR TIRE AND RUBBER COMPANY (Goodyear). *Handbook of Conveyor & Elevator Belting.* Akron, OH, USA: Goodyear Tire and Rubber Company, 1975. OCLC 4152041.

[109] GOODYEAR RUBBER PRODUCTS - LLC | CONVEYOR BELT DIVISION (Goodyear). *Flexsteel Steel Cable Belt* [online] [viewed 17 June 2021].Available from: https://goodyearbelting.com/topuses/Flexsteel-Steel-Cable-Belt.aspx

[110] GOODYEAR RUBBER PRODUCTS INC. (Goodyear). *Conveyor Belts* [online] [viewed 17 June 2021].Available from: https://www.goodyearrubberproducts.com/top-100-products/Conveyor-Belts/Conveyor-Belts.asp

[111] GUO, Y., C. WASSGREN, B. HANCOCK, W. KETTERHAGEN, and J. CURTIS, *Validation and time step determination of discrete element modeling of flexible fibers. . Powder Technology.* 2013.:249, 386-395. Available from: doi:10.1016/j.powtec.2013.09.007

[112] GUPTA, V., X. SUN, W. XU, H. SARV, and H. FARZAN, *A discrete element method-based approach to predict the breakage of coal. . Advanced Powder Technology.* 2017.:28, 2665-2677. Available from: doi:10.1016/j.apt.2017.07.019

[113] HAGENMULLER, P., G. CHAMBON, and M. NAAIM, *Microstructure-based modeling of snow mechanics: a discrete element approach. . The Cryosphere.* 2015.:9, 1969-1982. Available from: doi:10.5194/tc-9-1969-2015

[114] HAN, K., D. PERIĆ, A. CROOK, and D. OWEN, *A combined finite/discrete element simulation of shot peening processes – Part I: studies on 2D interaction laws. . Engineering Computations.* 2000.:17, 593-620. Available from: doi:10.1108/02644400010339798

[115] HAN, K., D. PERIĆ, D. OWEN, and J. YU, *A combined finite/discrete element simulation of shot peening processes – Part II: 3D interaction laws. . Engineering Computations.* 2000.:17, 680-702. Available from: doi:10.1108/02644400010340615

[116] HASTIE, D., P. WYPYCH, and A. GRIMA. The Current State and Future Requirements of Continuous Haulage Systems for Underground Gateroad Development.. *The International Materials Handling Conference and Exhibition - BELTCON 17. Cutting edge technology promoting the excellence of belt conveying.* Johannesburg, South Africa, 2013.

[117] HERTZ, H., *Über die Berührung fester elastischer Körper. . Journal für die reine und angewandte Mathematik.* 1882.:1882, 156-171. Available from: doi:10.1515/crll.1882.92.156

[118] HO, Don. Notepad++ [software]. Version v8. 2021.Available from: https://notepad-plus-plus.org/

[119] HÖTTE, S. Pipe Belts – Advantages, Challenges and Applications.. In: Mark Jones, ed. *13th International Conference on Bulk Materials Storage, Handling and Transportation ICBMH 2019 : Conference Proceedings.* 9-11 July 2019. Barton, ACT, Australia: The Institution of Engineers Australia, 2019. ISBN 978-1-925627-29-9, (enclosed pdf).

[120] ILIC, D., and C. WHEELER, *Measurement and simulation of the bulk solid load on a conveyor belt during transportation. . Powder Technology.* 2017.:307, 190-202. Available from: doi:10.1016/j.powtec.2016.11.020

[121] INPARTIK. Pasimodo [software].Available from: http://www.inpartik.de/

[122] INTEL CORP. *Intel® Core™ i7-4770K Processor* [online]. *Product Specifications* [viewed 17 August 2021].Available from: https://ark.intel.com/content/www/us/en/ark/products/75123/intel-core-i7-4770k-processor-8m-cache-up-to-3-90-ghz.html

[123] IRAZÁBAL, J., S. LATORRE, F. SALAZAR, M.Á. CELIGUETA, and E. OÑATE. Numerical modelling with discrete elements of rockfall protection systems.. *PARTICLES 2017 - V International Conference on Particle-Based Methods. Fundamentals and Applications.* Hannover, Germany: CIMNE, 2017.

[124] ISO 15236-1:2016-10, *Steel cord conveyor belts - Part 1: Design, dimensions and mechanical requirements for conveyor belts for general use. Available from:* https://www.iso.org/standard/70276.html

[125] ISO 251:2012-10, *Conveyor belts with textile carcass - Widths and lengths. Available from:* https://www.iso.org/standard/61040.html

[126] ISO 703:2017-01, *Conveyor belts - Transverse flexibility (troughability) - Test method. Available from:* https://www.iso.org/standard/71643.html

[127] ISO/IEC 646:1991, *Information technology - ISO 7-bit coded character set for information interchange. Available from:* https://www.iso.org/standard/4777.html

[128] ITASCA. PFC (Particle Flow Code) Version 5.0.:,

[129] ITASCA CONSULTING GROUP, INC. (Itasca). PFC2D Manual.:. 2004.

[130] ITASCA CONSULTING GROUP, INC. (Itasca). FLAC3D [software]. Version 6.00. 2020.Available from: https://www.itascacg.com/software/pfc

[131] ITASCA CONSULTING GROUP, INC. (Itasca). *FLAC3D Integration into PFC3D* [online]. New in PFC 6.0 [viewed 8 September 2020].Available from: https://www.itascacg.com/software/flac3d-integration-into-pfc3d

[132] ITASCA CONSULTING GROUP, INC. (Itasca). PFC3D [software]. Version 6.00. 2020.Available from: https://www.itascacg.com/software/flac3d

[133] ITASCA CONSULTING GROUP, INC. (Itasca). *Distinct Element Method in PFC* [online]. *Discontinuous versus Continuous Models* [viewed 16 February 2021].Available from: https://www.itascacg.com/software/distinct-element-method

[134] JEBAHI, Mohamed, Damien ANDRÉ, Inigo TERREROS, and Ivan IORDANOFF. *Discrete element method to model 3D continuous materials.* London, UK: John Wiley & Sons, Inc, 2015. Discrete element model and simulation of continuous materials behavior set. volume 1. 9781119103042.

[135] JENIKE & JOHANSON. *Transfer Chutes* [online]. Conceptual & Functional Engineering [viewed 8 March 2021].Available from: https://jenike.com/services/conceptual-functional-engineering/transfer-chutes/

[136] JENSEN, A., K.A. FRASER, and G. LAIRD. Improving the Precision of Discrete Element Simulations through Calibration Models.. *13th International LS-DYNA User Conference 2014,* 2014.

[137] JOHN DEERE (DEERE & COMPANY). *Hay & Forage Equipment* [online] [viewed 12 October 2020].Available from: https://www.deere.com/en/hay-forage/baling/

[138] JOHNSON, K.L., K. KENDALL, and A.D. ROBERTS, *Surface energy and the contact of elastic solids. . Proceedings of the Royal Society of London. A. Mathematical and Physical Sciences.* 1971.:324, 301-313. Available from: doi:10.1098/rspa.1971.0141

[139] KARAJAN, N., J. WANG, Z. HAN, H. TENG, C.T. WU, W. HU, Y. GUO, and K.A. FRASER. Particle Methods in LS-DYNA.. *13. LS-DYNA Forum 2014.* Bamberg, Germany, 2014.

[140] KATTERFELD, A., M. DRATT, and C. WHEELER. Prediction of the Conveyor Belt Deflection by the Use of Coupled FEM-DEM Simulations.. *Bulk Solids Handling.* 2010.:30, 380-384.

[141] KATTERFELD, A., T. GROGER, M. HACHMANN, and G. BECKER. Usage of DEM Simulations for the Development of a New Chute Design in Underground Mining.. In: Peter Wypych, ed. *Conference proceedings / 6th Int. Conf. for Conveying and Handling of Particulate Solids (CHoPS). 10th Int. Conf. on Bulk Materials Storage, Handling & Transportation (ICBMH) ; 3 - 7 August 2009, Brisbane, QLD, Australia.* Barton, ACT, Australia: Engineers Australia, 2009. 9780858259065, pp. 90-95.

[142] KEMPER, S., T. LANG, and L. FRERICHS, *Der überlagerte Schnitt im Scheibenmähwerk – Ergebnisse aus Feldversuchen und Simulation. .* 171–175 Seiten / LANDTECHNIK, Bd. 69 Nr. 4 (2014) / LANDTECHNIK, Bd. 69 Nr. 4 (2014). 2014.:. Available from: doi:10.15150/LT.2014.570

[143] KESSLER, F., K. GRABNER, and K.-J. GRIMMER. "bico-TEC" - A New Type of Belt Conveyor with Horizontal Curves.. *Bulk Solids Handling.* 1993.:13, 741-747.

[144] KHAZAELI, S., and S. HAJ-ZAMANI. A Coupled Extended-Finite-Discrete Element Method: On the Different Contact Schemes between Continua and Discontinua.. *World Academy of Science, Engineering and Technology, International Journal of Geological and Environmental Engineering.* 2016.:10, 261-268.

[145] KOCKARA, S., T. HALIC, C. BAYRAK, K. IQBAL, and R.A. ROWE, *Contact Detection Algorithms. . Journal of Computers.* 2009.:4. Available from: doi:10.4304/jcp.4.10.1053-1063

[146] KOVÁCS, Á., and G. KERÉNYI. Modeling Of Corn Ears By Discrete Element Method (DEM).. In: Zita Zoltay-Paprika, Péter Horák, Kata Váradi, Péter Tamás Zwierczyk, Ágnes Vidovics-Dancs, and János Péter Rádics, eds. *Proceedings, 31st European Conference on Modelling and Simulation ECMS 2017. May 23rd-May 26th, 2017, Budapest, Hungary.* Europe: European Council for Modelling and Simulation, 2017. 9780993244049, pp. 355-361.

[147] KOVÁCS, Á., and P.T. ZWIERCZYK. Coupled DEM-FEM Simulation On Maize Harvesting.. In: Lars Nolle, Alexandra Burger, Christoph Tholen, Jens Werner, and Jens Wellhausen, eds. *Proceedings, 32nd European Conference on Modelling and Simulation ECMS 2018. May 22nd-May 25th, 2018, Wilhelmshaven, Germany.* Europe: European Council for Modelling and Simulation, 2018. 9780993244063, pp. 405-411.

[148] KRAUSE, F., A. KATTERFELD, F. KESSLER, L. OVERMEYER, M. ten HOMPEL, K.-H. WEHKING, and W.A. GÜNTHNER. Stetigförderer.. In: Karl-Heinrich Grote, Beate Bender, Dietmar Göhlich, and Heinrich Dubbel, eds. *Dubbel - Taschenbuch für den Maschinenbau.* Berlin: Springer Vieweg, 2018. ISBN 978-3-662-54804-2, pp. 1736-1764.

[149] KRUGGEL-EMDEN, H., S. WIRTZ, and V. SCHERER, *Applicable Contact Force Models for the Discrete Element Method: The Single Particle Perspective. . Journal of Pressure Vessel Technology.* 2009.:131. Available from: doi:10.1115/1.3040682

[150] KUHN, M.R., *A flexible boundary for three-dimensional dem particle assemblies. . Engineering Computations.* 1995.:12, 175-183. Available from: doi:10.1108/02644409510799541

[151] KUHN S.A.S. *Round balers* [online] [viewed 12 October 2020].Available from: https://www.kuhn.com/com_en/range/balers/round-balers.html

[152] KUWAGI, K., H. TAKEDA, and M. HORIO. The similar particle assembly (SPA) model: an approach to large-scale discrete element (DEM)simulation.. In: Umberto Arena, ed. *Fluidization XI : Proceedings of the 11th International Conference on Fluidization. Present and future for fluidization engineering.* Brooklyn, NY, XVI, 853 S: Engineering Conference International (ECI), 2004. 0918902525, pp. 243-250.

[153] LABUSCHAGNE, A., N. VAN RENSBURG, and A.J. VAN DER MERWE, *Comparison of linear beam theories. . Mathematical and Computer Modelling.* 2009.:49, 20-30. Available from: doi:10.1016/j.mcm.2008.06.006

[154] LAMBERT, P., A. CHAU, A. DELCHAMBRE, and S. RÉGNIER, *Comparison between two capillary forces models. . Langmuir.* 2008.:24, 3157-3163. Available from: doi:10.1021/la7036444

[155] LANGSTON, P., A.R. KENNEDY, and H. CONSTANTIN, *Discrete element modelling of flexible fibre packing. . Computational Materials Science.* 2015.:96, 108-116. Available from: doi:10.1016/j.commatsci.2014.09.007

[156] LEI, Z., and M. ZANG, *An approach to combining 3D discrete and finite element methods based on penalty function method. . Computational Mechanics.* 2010.:46, 609-619. Available from: doi:10.1007/s00466-010-0502-4

[157] LEMMON, R. Local Stresses in Belt Turnovers in Conveyor Belt.. *SME Annual Meeting 2002. Bulk Material Handling by Conveyor Belt IV.* Littleton, CO, USA: SME, 2002. ISBN 978-9990919240.

[158] LEMMON, R. Belt Turnover Design Using Finite Element Analysis.. *Beltcon 15,* 2009.

[159] LISJAK, A., and G. GRASSELLI, *A review of discrete modeling techniques for fracturing processes in discontinuous rock masses. . Journal of Rock Mechanics and Geotechnical Engineering.* 2014.:6, 301-314. Available from: doi:10.1016/j.jrmge.2013.12.007

[160] LIVERMORE SOFTWARE TECHNOLOGY CORPORATION (LSTC). LS-DYNA [software]. Version R7.1.1. 2014.Available from: http://www.lstc.com/

[161] LOMMEN, S., D. SCHOTT, and G. LODEWIJKS, *DEM speedup: Stiffness effects on behavior of bulk material. . Particuology.* 2014.:12, 107-112. Available from: doi:10.1016/j.partic.2013.03.006

[162] LORENTZ, Julien. *Etude de la capacité de dissipation sous impact d'une structure sandwich de protection contre les chutes de blocs rocheux.* Dissertation. Grenoble, France, 2007.

[163] LORIG, L.J., and P.A. CUNDALL. Modeling of Reinforced Concrete Using the Distinct Element Method.. In: Surendra P. Shah, ed. *Fracture of concrete and rock. SEM-RILEM international conference, June 17 - 19, 1987, Houston, Texas, USA.* New York, Berlin, Heidelberg, London, Paris, Tokyo: Springer, 1989. 978-0-387-96880-3, pp. 276-287.

[164] LUCY, L.B., *A numerical approach to the testing of the fission hypothesis. . The Astronomical Journal.* 1977.:82, 1013. Available from: doi:10.1086/112164

[165] MAOR, E. Das Möbiusband.. In: Eli Maor, ed. *Dem Unendlichen auf der Spur.* Basel, s.l.: Birkhäuser Basel, 1989. 978-3-0348-6146-5, pp. 168-178.

[166] MARIGO, M., and E.H. STITT, *Discrete Element Method (DEM) for Industrial Applications: Comments on Calibration and Validation for the Modelling of Cylindrical Pellets. . KONA Powder and Particle Journal.* 2015.:32, 236-252. Available from: doi:10.14356/kona.2015016

[167] MARKUT, Thomas. *Fördergurtfangsystem.* Master thesis. Leoben, Austria, 2020.

[168] MASSACHUSETTS INSTITUTE OF TECHNOLOGY (MIT). *Discrete element method* [online]. Abaqus documentation [viewed 15 February 2021].Available from: https://abaqus-docs.mit.edu/2017/English/SIMACAEANLRefMap/simaanl-cdemanalysis.htm

[169] MASSEY FERGUSON (BRAND OF AGCO S.A.S.). *Balers* [online] [viewed 12 October 2020].Available from: http://int.masseyferguson.com/balers.aspx

[170] MATUTTIS, Hans-Georg and Jian CHEN. *Understanding the Discrete Element Method. Simulation of Non-Spherical Particles for Granular and Multi-body Systems.* Hoboken: Wiley, 2014. 9781118567210.

[171] MAU, Hans, inventor. Schlauchartig verformbares, kurvengängiges Förderband.*(Deutsches Wirtschaftspatent)*. Appl: 11 September 1952. Patentschrift Nr. 7712.

[172] MICROSOFT. .NET Framework [software].Available from: https://dotnet.microsoft.com/

[173] MICROSOFT. *System.Numerics Namespace* [online]. Documentation [viewed 4 July 2021].Available from: https://docs.microsoft.com/en-us/dotnet/api/system.numerics

[174] MICROSOFT. *Registry* [online]. Documentation [viewed 5 August 2021].Available from: https://docs.microsoft.com/en-us/windows/win32/sysinfo/registry

[175] MIKAMI, T., H. KAMIYA, and M. HORIO, *Numerical simulation of cohesive powder behavior in a fluidized bed. . Chemical Engineering Science.* 1998.:53, 1927-1940. Available from: doi:10.1016/S0009-2509(97)00325-4

[176] MINDLIN, R. Compliance of Elastic Bodies in Contact.. *Journal of Applied Mechanics - Transactions of the ASME.* 1949.:16, 259-268.

[177] MINDLIN, R., and H. DERESIEWICZ. Elastic Spheres in Contact under Varying Oblique Force.. *Journal of Applied Mechanics - Transactions of the ASME.* 1953.:20, 327-344.

[178] MORDSTEIN, W. The behavior of conveyor belts with turnovers in the bottom run of conveyor systems.. *Deutsche Hebe- und Fordertechnik.* 1961.:7, 25-31.

[179] MORDSTEIN, Walter, inventor. Arrangement For Inverting The Sides Of Belts In Endless Conveyors And The Like.*(US Patent).* US 3,139,970.

[180] MSC.SOFTWARE CORPORATION. Adams [software]. Version 2019. 2019.Available from: https://www.mscsoftware.com/de/product/adams

[181] MUNJIZA, A., D. OWEN, and N. BICANIC, *A combined finite-discrete element method in transient dynamics of fracturing solids. . Engineering Computations.* 1995.:12, 145-174. Available from: doi:10.1108/02644409510799532

[182] MUNJIZA, A., H. SMOLJANOVIĆ, N. ŽIVALJIĆ, A. MIHANOVIC, V. DIVIĆ, I. UZELAC, Ž. NIKOLIĆ, I. BALIĆ, and B. TROGRLIĆ, *Structural applications of the combined finite–discrete element method. . Computational Particle Mechanics.* 2020.:7, 1029-1046. Available from: doi:10.1007/s40571-019-00286-5

[183] MUNJIZA, Ante. *The combined finite-discrete element method.* Chichester, West Sussex, UK: John Wiley & Sons, Ltd, 2004. 0-470-84199-0.

[184] NAKASHIMA, H., and A. OIDA, *Algorithm and implementation of soil–tire contact analysis code based on dynamic FE–DE method. . Journal of Terramechanics.* 2004.:41, 127-137. Available from: doi:10.1016/j.jterra.2004.02.002

[185] NEW HOLLAND AGRICULTURE (A BRAND OF CNH INDUSTRIAL). Roll-Belt.*(Roll-Belt 150 | Roll-Belt 180).* (Brochure).:. 2016 [viewed 10 December 2020].Available from: https://agriculture.newholland.com/eu/en-uk/about-us/buying-services/before-purchase/download-a-brochure?series=BIGBALER%20HIGH%20DENSITY

[186] NEW HOLLAND AGRICULTURE (A BRAND OF CNH INDUSTRIAL). *Agricultural & Farm Machinery - by New Holland Agriculture* [online] [viewed 12 October 2020].Available from: https://agriculture.newholland.com/eu/en-uk

[187] NEW HOLLAND BELGIUM N.V., ed. UNDERHILL, Kenneth, and WHITE, Dennis, inventors. Tension control system for round bale forming apparatus.*(European Patent).* EP 0 954 960 A1.

[188] NORDELL, L. K. and Z. P. CIOZDA. Transient belt stresses during starting and stopping: elastic response simulated by finite element methods.. *Bulk Solids Handling.* :4, pp. 93-98.

[189] OBERMAYR, M., K. DRESSLER, C. VRETTOS, and P. EBERHARD, *A bonded-particle model for cemented sand. . Computers and Geotechnics.* 2013.:49, 299-313. Available from: doi:10.1016/j.compgeo.2012.09.001

[190] OÑATE, E., and J. ROJEK, *Combination of discrete element and finite element methods for dynamic analysis of geomechanics problems. . Computer Methods in Applied Mechanics and Engineering.* 2004.:193, 3087-3128. Available from: doi:10.1016/j.cma.2003.12.056

[191] O'SULLIVAN, C., and J.D. BRAY, *Selecting a suitable time step for discrete element simulations that use the central difference time integration scheme. . Engineering Computations.* 2004.:21, 278-303. Available from: doi:10.1108/02644400410519794

[192] O'SULLIVAN, Catherine. *Particulate Discrete Element Modelling. A Geomechanics Perspective:*1st Edition. London, UK: Spon Press (Taylor & Francis), 2011. Applied geotechnics. 978-0415490368.

[193] OVERLAND CONVEYOR CO., INC. *Pipe Conveyors* [online] [viewed 8 October 2020].Available from: http://www.overlandconveyor.com/consulting/conveyor-consulting-services/pipe-conveyor.aspx

[194] OWEN, D., and Y.T. FENG, *Parallelised finite/discrete element simulation of multi-fracturing solids and discrete systems. . Engineering Computations.* 2001.:18, 557-576. Available from: doi:10.1108/02644400110387154

[195] OWEN, D.R.J., Y.T. FENG, J. YU, and D. PERIĆ. Finite/Discrete Element Analysis of Multi-fracture and Multi-contact Phenomena.. In: José M. L. M. Palma, Jack Dongarra, and Vicente Hernández, eds. *Vector and Parallel Processing - VECPAR 2000. 4th International Conference Porto, Portugal, June 21-23, 2000 Selected Papers and Invited Talks.* Berlin, Heidelberg: Springer, 2001. ISBN 978-3-540-41999-0, pp. 483-505.

[196] PATWA, A., R.K. AMBROSE, and M. CASADA, *Discrete element method as an approach to model the wheat milling process. . Powder Technology.* 2016.:302, 350-356. Available from: doi:10.1016/j.powtec.2016.08.052

[197] PENG, L., H. FENG, Z. WANG, H. WANG, H. YANG, and H. HUANG, *Screening Mechanism and Properties of a Cantilevered Vibrating Sieve for Particles Processing. . Applied Sciences.* 2019.:9, 4911. Available from: doi:10.3390/app9224911

[198] PETERS, B., X. BESSERON, A. ESTUPINAN, A. MAHMOUDI, and M. MOHSENI, *A Discrete/Continuous Numerical Approach to Multi-physics. . IFAC-PapersOnLine.* 2015.:48, 645-650. Available from: doi:10.1016/j.ifacol.2015.05.141

[199] PETRINIC, Nikica. *Aspects of Discrete Element Modelling Involving Facet-to-facet Contact Detection and Interaction.* Dissertation. Wales, UK, 1996.

[200] PICCIOTTO, Davide, Glenn LONGWELL, and RAVINDRA AGLAVE. Role of physics-based simulation in engineering for consumer products and cosmetics.:. 2020.

[201] PIETSCH, M., and C. WHEELER. Innovative Conveying System (ICS).*(An overview of a New Bulk Conveying Technology). In:* Mark Jones, ed. *9th International Conference on Bulk Materials Storage, Handling and Transportation ICBMH 2007.* 9-11 October 2007, 2007.

[202] POTYONDY, D.O. A Flat-Jointed Bonded-Particle Material for Hard Rock.. In: Antonio Bobet, ed. *46th US Rock Mechanics/Geomechanics Symposium 2012.* Red Hook, NY, USA: Curran Associates, Inc., 2012. ISBN 9781622765140, pp. 1510-1519.

[203] POTYONDY, D.O., and P.A. CUNDALL, *A bonded-particle model for rock. . International Journal of Rock Mechanics and Mining Sciences.* 2004.:41, 1329-1364. Available from: doi:10.1016/j.ijrmms.2004.09.011

[204] POWDER/BULK SOLIDS. *Jenike & Johanson Inc.* [online]. Engineering Solutions for Powder & Bulk Solids Handling [viewed 17 March 2021].Available from: https://directory.powderbulksolids.com/jenike-johanson-inc

[205] PREVITALI, M., M.O. CIANTIA, S. SPADEA, R.P. CASTELLANZA, and G.B. CROSTA. Discrete element modeling of compound rockfall fence nets.. *IACMAG2020,* 2020, pp. 1-8.

[206] PYTHON SOFTWARE FOUNDATION. Python [software]. Version 3.8.X. 2020.Available from: https://www.python.org/

[207] RABINOVICH, Y.I., M.S. ESAYANUR, and B.M. MOUDGIL, *Capillary forces between two spheres with a fixed volume liquid bridge: theory and experiment. . Langmuir.* 2005.:21, 10992-10997. Available from: doi:10.1021/la0517639

[208] RAYLEIGH, *On Waves Propagated along the Plane Surface of an Elastic Solid. . Proceedings of the London Mathematical Society.* 1885.:s1-17, 4-11. Available from: doi:10.1112/plms/s1-17.1.4

[209] REMA TIP TOP. DBP Conveyor Belting Portfolio.:. 2016 [viewed 17 June 2021].

[210] RENČÍN, Lukáš. *Quality assessment pressing pick-up balers.* Diploma thesis. Brno, Czech Republic, 2015.

[211] ROCKY DEM. *ESSS releases new version of Rocky DEM software* - [online] [viewed 9 June 2021].Available from: https://rocky.esss.co/new/esss-releases-new-version-of-rocky-dem-software/

[212] ROCKY DEM. *Calibrating material density to match your representative and not your actual PSD* [online] [viewed 16 June 2021].Available from: https://rocky.esss.co/blog/calibrating-material-density-to-match-your-representative-and-not-your-actual-psd/

[213] ROCKY DEM. *Efficient and accelerated process development in the agricultural industry using Rocky DEM* [online] [viewed 9 June 2021].Available from: https://rocky.esss.co/blog/efficient-agricultural-equipment-development-using-rocky-dem/

[214] ROCKY DEM. *From pet hair to barley: discover how Rocky's fiber model expands the types of problems that DEM can now solve* [online] [viewed 27 May 2021].Available from: https://rocky.esss.co/blog/rocky-dem-fiber-model/

[215] ROCKY DEM. *Agriculture Equipment - Rocky DEM* [online] [viewed 9 June 2021].Available from: https://rocky.esss.co/industries/agriculture-equipment/

[216] ROCKY DEM, INC. Rocky and Ansys.*(Rocky DEM. Next Generation DEM Particle Simulator).* Product Info Flyer.:. 2018 [viewed 29 July 2020].

[217] RULMECA HOLDING S.P.A (Rulmeca). *Rulmeca* [online] [viewed 18 June 2021].Available from: https://www.rulmeca.com/

[218] SADRMANESH, V., and Y. CHEN, *Simulation of tensile behavior of plant fibers using the Discrete Element Method (DEM). . Composites Part A: Applied Science and Manufacturing.* 2018.:114, 196-203. Available from: doi:10.1016/j.compositesa.2018.08.023

[219] SAKAI, M., and S. KOSHIZUKA, *Large-scale discrete element modeling in pneumatic conveying. . Chemical Engineering Science.* 2009.:64, 533-539. Available from: doi:10.1016/j.ces.2008.10.003

[220] SARKAR, Saurabh. *How to Apply Rocky DEM to Generate More Accurate Structural Analysis* [online] [viewed 29 July 2020].Available from: https://www.ansys.com/blog/rocky-dem-structural-analysis

[221] SCHILLING, O., M. WESTERWALD, and J. WIEDENROTH. ABAQUS FE Analysis of a Pipe Conveyor Using Solids with Embedded Truss Elements and Shells with Rebar Layers.:. 2007.

[222] *Sempertrans Conveyor Belt Solutions GmbH* [viewed 18 June 2021].Available from: https://www.sempertrans.com/

[223] SHEN, J., C. WHEELER, D. ILIC, and J. CHEN, *Application of open source FEM and DEM simulations for dynamic belt deflection modelling. . Powder Technology.* 2019.:357, 171-185. Available from: doi:10.1016/j.powtec.2019.08.068

[224] SHEN, J., C. WHEELER, J. O'SHEA, and D. ILIC, *Investigation of the dynamic deflection of conveyor belts via experimental and modelling methods. . Measurement.* 2018.:127, 210-220. Available from: doi:10.1016/j.measurement.2018.05.091

[225] SIEMENS PLM SOFTWARE. Simcenter STAR-CCM+ [software]. 2020 [accessed 28 July 2020].Available from: https://www.plm.automation.siemens.com/global/en/products/simcenter/STAR-CCM.html

[226] SMILAUER, Vaclav, Emanuele CATALANO, Bruno CHAREYRE, Sergei DOROFEENKO, Jerome DURIEZ, Nolan DYCK, Jan ELIAS, Burak ER, Alexander EULITZ, Anton GLADKY, Ning GUO, Christian JAKOB, Francois KNEIB, Janek KOZICKI, Donia MARZOUGUI, Raphael MAURIN, Chiara MODENESE, Luc SCHOLTES, Luc SIBILLE, Janek STRANSKY, Thomas SWEIJEN, Klaus THOENI, and Chao YUAN. *Yade Documentation 2Nd Ed:* Zenodo, 2015.

[227] SPATIAL CORP. (PART OF DASSAULT SYSTEMES). *SAT File Format* [online] [viewed 11 August 2021].Available from: https://www.spatial.com/resources/glossary/sat-file-type

[228] STARCLEAN (MEMBER OF SCHULTE STRATHAUS / PART OF FESS GROUP). Heroes of Spillage Control.. (Brochure).:. 2020 [viewed 10 September 2020].

[229] STARCLEAN (MEMBER OF SCHULTE STRATHAUS / PART OF FESS GROUP). *Safebelt® Closed Conveyor System* [online] [viewed 9 October 2020].Available from: https://www.starclean-solutions.de/en/products/safebelt-closed-conveyor-system.html

[230] STRAND7 PTY LTD. Strand7 [software]. 2020.Available from: https://www.strand7.com/

[231] TAKRAF GMBH (PART OF TENOVA S.P.A.). Pipe Conveyors.*(Optimal Solutions for Specialised Handling).* (Brochure).:. 2017 [viewed 10 August 2020].Available from: https://www.tenova.com/fileadmin/user_upload/takraf_pages/About_us/Brochure_Downloads/TAKRAF_Pipe_Conveyors_eng.pdf

[232] TAKRAF GMBH (PART OF TENOVA S.P.A.). *Tube Conveyors* [online] [viewed 8 October 2020].Available from: https://www.tenova.com/product/tube-conveyors/

[233] TAVARES, L.M., F.P. ANDRÉ, A. POTAPOV, and C. MALISKA, *Adapting a breakage model to discrete elements using polyhedral particles. . Powder Technology.* 2020.:362, 208-220. Available from: doi:10.1016/j.powtec.2019.12.007

[234] TECHNISCHE UNIVERSITÄT MÜNCHEN (TUM). *Volumenstrom (volume flow rate)* [online]. *Logistikkompendium.* TUM Wiki [viewed 18 March 2021].Available from: https://wiki.tum.de/display/logistikkompendium/Volumenstrom

[235] TENEK, L.T., and J. ARGYRIS. A brief history of FEM.. In: Lazarus Teneketzis Tenek and John Argyris, eds. *Finite Element Analysis for Composite Structures.* Dordrecht: Springer, 1998. ISBN 978-90-481-4975-9, pp. 17-25.

[236] TERRA NOVA TECHNOLOGIES, INC. (TNT). *Kisladag* [online] [viewed 12 October 2020].Available from: https://www.tntinc.com/casestudy/kisladag

[237] THOENI, K., A. EFFEINDZOUROU, B. CHAREYRE, and A. GIACOMINI, *Discrete Modelling of Soil-Inclusion Problems. . Applied Mechanics and Materials.* 2016.:846, 397-402. Available from: doi:10.4028/www.scientific.net/AMM.846.397

[238] THOENI, K., A. GIACOMINI, C. LAMBERT, S.W. SLOAN, and J.P. CARTER, *A 3D discrete element modelling approach for rockfall analysis with drapery systems. . International Journal of Rock Mechanics and Mining Sciences.* 2014.:68, 107-119. Available from: doi:10.1016/j.ijrmms.2014.02.008

[239] THOENI, K., C. LAMBERT, A. GIACOMINI, and S.W. SLOAN. Discrete modelling of a rockfall protective system.. In: E. Oñate and D. R. J. Owen, eds. *Particle-based methods II. Fundamentals and applications : proceedings of the II International Conference on Particle-Based Methods Fundamentals and Applications (Particles 2011) : Barcelona, Spain, 26-28 October 2011.* Barcelona: International Center for Numerical Methods in Engineering, 2011. 9788489925670, pp. 24-32.

[240] TIMOSHENKO, S.P., *LXVI. On the correction for shear of the differential equation for transverse vibrations of prismatic bars. . The London, Edinburgh, and Dublin Philosophical Magazine and Journal of Science.* 1921.:41, 744-746. Available from: doi:10.1080/14786442108636264

[241] TIMOSHENKO, S.P., *X. On the transverse vibrations of bars of uniform cross-section. . The London, Edinburgh, and Dublin Philosophical Magazine and Journal of Science.* 1922.:43, 125-131. Available from: doi:10.1080/14786442208633855

[242] TSUJI, Y., T. TANAKA, and T. ISHIDA, *Lagrangian numerical simulation of plug flow of cohesionless particles in a horizontal pipe. . Powder Technology.* 1992.:71, 239-250. Available from: doi:10.1016/0032-5910(92)88030-L

[243] UBACH, P.A., F. ARRUFAT, L. RING, R. GANDIKOTA, F. ZÁRATE, and E. OÑATE, *Application of an enhanced discrete element method to oil and gas drilling processes. . Computational Particle Mechanics.* 2016.:3, 29-41. Available from: doi:10.1007/s40571-015-0080-5

[244] UNIVERSITY OF STUTTGART. *Pasimodo - Showroom* [online]. *Institute of Engineering and Computational Mechanics* [viewed 16 June 2021].Available from: http://info.itm.uni-stuttgart.de/research/particle_fluid/particle_fluid_de_anim.php

[245] VHV ANLAGENBAU GMBH. Innovative steep incline conveying technology.. (Brochure).:. 2009 [viewed 8 October 2020].Available from: https://www.vhv-anlagenbau.de/vhv2020/wp-content/uploads/2019/08/Steilfoerdertechnik_EN-1.pdf

[246] VHV ANLAGENBAU GMBH. *Steep incline conveyor* [online]. *Space-saving and innovative* [viewed 8 October 2020].Available from: https://www.vhv-anlagenbau.de/en/steilfoerderer/

[247] VON MISES, R.E. Mechanik der festen Körper im plastisch-deformablen Zustand.. *Nachrichten von der Gesellschaft der Wissenschaften zu Göttingen. Mathematisch-physikalische Klasse, aus dem Jahre 1913.* 1913.:, 582-592.

[248] WACONIA MANUFACTURING INC. *Tripper Discharges for Overhead Belt Conveyors* [online] [viewed 12 October 2020].Available from: https://www.powderbulksolids.com/mechanical-conveying/tripper-discharges-overhead-belt-conveyors

[249] WANG, M., *A scale-invariant bonded particle model for simulating large deformation and failure of continua. . Computers and Geotechnics.* 2020.:126, 103735. Available from: doi:10.1016/j.compgeo.2020.103735

[250] WANG, M., Y.T. FENG, Y. WANG, and T.T. ZHAO, *Periodic boundary conditions of discrete element method-lattice Boltzmann method for fluid-particle coupling. . Granular Matter.* 2017.:19. Available from: doi:10.1007/s10035-017-0733-6

[251] WANG, Q., H. MAO, and Q. LI, *Modelling and simulation of the grain threshing process based on the discrete element method. . Computers and Electronics in Agriculture.* 2020.:178, 105790. Available from: doi:10.1016/j.compag.2020.105790

[252] WEATHERLEY, Dion Kent. ESyS-Particle.*(An introduction to scripting DEM simulations)*:,

[253] WEIGERT, T., and S. RIPPERGER, *Calculation of the Liquid Bridge Volume and Bulk Saturation from the Half-filling Angle. . Particle & Particle Systems Characterization.* 1999.:16, 238-242. Available from: doi:10.1002/(SICI)1521-4117(199910)16:5<238::AID-PPSC238>3.0.CO;2-E

[254] WELLMANN, Christian. *A Two-Scale Model of Granular Materials Using a Coupled DE-FE Approach.* Dissertation. Hannover, Germany: Peter Wriggers, 2011. ISBN 978-3-941302-02-0.

[255] WHEELER, Craig. *Analysis of the main resistances of belt conveyors.* Dissertation. Callaghan, NSW, Australia, 2003.

[256] WOLFF, M., V. SALIKOV, S. ANTONYUK, S. HEINRICH, and G.A. SCHNEIDER, *Three-dimensional discrete element modeling of micromechanical bending tests of ceramic–polymer composite materials. . Powder Technology.* 2013.:248, 77-83. Available from: doi:10.1016/j.powtec.2013.07.009

[257] WRIGGERS, P., and B. AVCI. Discrete Element Methods: Basics and Applications in Engineering.. In: Riva, Laura de Lorenzis, and Alexander Düster, eds. *Modeling in Engineering Using Innovative Numerical Methods for Solids and Fluids.* Cham: Springer International Publishing, 2020. 978-3-030-37517-1, pp. 1-30.

[258] YAN, C., and X. HE. Model and Dynamic Simulation of Belt Conveyor.. *2010 International Conference on Intelligent System Design and Engineering Application (ISDEA 2010). Changsha, Hunan, China, 13 - 14 October 2010 ; [proceedings.* Piscataway, NJ: IEEE, 2010. 978-1-4244-8333-4, pp. 949-951.

[259] YANG, G., H. ALKOTAMI, and S. LEI, *Discrete Element Simulation of Orthogonal Machining of Soda-Lime Glass with Seed Cracks. . Journal of Manufacturing and Materials Processing.* 2020.:4, 5. Available from: doi:10.3390/jmmp4010005

[260] YEOM, S.B., E.-S. HA, M.-S. KIM, S.H. JEONG, S.-J. HWANG, and H. DU CHOI, *Application of the Discrete Element Method for Manufacturing Process Simulation in the Pharmaceutical Industry. . Pharmaceutics.* 2019.:11. Available from: doi:10.3390/pharmaceutics11080414

[261] ZAMIRALOVA, Maria Eduardovna. *Design aspects of pipe belt conveyors.* Dissertation. Delft, The Netherlands: Delft University of Technology, 2017.

[262] ZANG, M., W. GAO, and Z. LEI, *A contact algorithm for 3D discrete and finite element contact problems based on penalty function method. . Computational Mechanics.* 2011.:48, 541-550. Available from: doi:10.1007/s00466-011-0606-5

[263] ZHANG, Y. A Finite Element Analysis on the Troughed Belt Turnover.. *SME Annual Conference & Expo 2017. Creating value in a cyclical environment.* Red Hook, NY, USA: Curran Associates, Inc., 2017. ISBN 978-1510836471.

[264] ZHANG, Yijun. *A Finite Element Analysis on the Troughed Belt Turnover.* Technical Session. Denver, CO, USA, 2017. Society for Mining, Metallurgy & Exploration Annual Conference.

[265] ZHENG, Q.J., M.H. XU, K.W. CHU, R.H. PAN, and A.B. YU, *A coupled FEM/DEM model for pipe conveyor systems: Analysis of the contact forces on belt. . Powder Technology.* 2017.:314, 480-489. Available from: doi:10.1016/j.powtec.2016.09.070

[266] ZHU, Z.-H., J.-H. YIN, J.-Q. QIN, and D.-Y. TAN, *A new discrete element model for simulating a flexible ring net barrier under rockfall impact comparing with large-scale physical model test data. . Computers and Geotechnics.* 2019.:116, 103208. Available from: doi:10.1016/j.compgeo.2019.103208